Investigating nephronophthisis using a novel murine and cell model.

Ann Marie Hynes

A thesis submitted for the Degree of Doctor of Philosophy

Institute of Genetic Medicine,

Newcastle University,

September 2013

Abstract

Nephronophthisis (NPHP) is a major cause of pediatric renal failure. Currently there is little understanding of the aetiology of the disease. In order to identify the molecular events leading to NPHP, we have created a novel mutant mouse strain containing a truncating mutation in the *Cep290* gene.

Patients with mutations in *CEP290* present with a ciliopathy phenotype that includes retinal dystrophy, cerebellum defects and NPHP. Characterisation of $Cep290^{LacZ/LacZ}$ mice confirms that they display all the features of the human condition. Microarray analysis of newborn kidney tissue was used to explore initiating events leading to NPHP.

Ciliopathies have recently been associated with either disrupted Wingless integrated (Wnt) or sonic hedgehog (Shh) signaling. We show that mutant kidneys display abnormal Shh signaling in the absence of Wnt signaling abnormalities. Primary cell cultures of collecting duct (CDT) cells (isolated from $Cep290^{LacZ/LacZ}$ mice and wild-type litter mates crossed with the “immorto” mouse) were established and characterised.

CDT cells expressed the mineral corticoid receptor (MR) and the epithelial sodium channel (ENaC) alpha subunit. The CDT cell lines formed epithelial layers and formed tubules when maintained in 3D culture media. $Cep290^{LacZ/LacZ}$ CDT cells displayed ciliogenesis abnormalities as well as abnormal spheroids with loss of lumen when grown in 3D culture. Pharmacological activation of Shh signaling (purmorphamine) partially rescues the spheroid and ciliogenesis defects in $Cep290^{LacZ/LacZ}$ CDT cells.

This implicates abnormal Shh signaling in the onset of NPHP and suggests that targeted treatment of Shh antagonists have therapeutic potential.

Dedication

In loving memory of my Mam.

I’ve missed you every day

Acknowledgements

Firstly and most importantly, I would like to thank my two supervisors Dr. Colin Miles and Dr. John Sayer for their expert guidance, support, help and supervision during my PhD. I would also like to thank Professor Nicholas Simmons for his many interesting ideas and my internal assessors Professor Judith Goodship and Dr. Simon Bamforth for your helpful advice.
I would also like to thank my collaborators; Dr. Rachel, H. Giles, who assisted with analysis on 3D cultures, Dr. Matthew Bashton, who carried out the data analysis on the microarray data, Dr. Kath White, Ms Tracey Davey and Caroline Miller who assisted with the electron microscopy images and Dr. Pete Thelwall who assisted with analysis on brain MRI scanning.

A special thank you to, Dr. Lorraine Eley, for all the technical advice, written advice and finally for the relentless encouragement to get this thesis finished. A huge thank you to the willing volunteers who proof read various chapters of my thesis, including Dr. Roslyn Jane Simms, Dr. Georgina Carr and Dr. Kevin Gillinder. Thank you to all the members of the kidney/muscle/endocrine lab for all your support, friendship and enabling me to borrow labs supplies/equipment when I had run out. Also a big thank you to Holly Anderson who kindly let me film her so I would know how to transfer a western blot on my own.

Special thanks to Dr. Adya Misra and Amy-Leigh Johnson for all your moral support and encouragement. A big thanks to my life time friends Claire Feeney and Claire Burns back at home in Ireland who have supported me through everything life has thrown at me, I'm grateful to have such wonderful friends.

I would like to thank all my family who have marked their calendars and will be lighting their candles for me on the day of my viva. Special thanks to my dad for your continuous support. I would also especially like to thank my big brother Cathal who I know is always there for me, listening to my problems and giving me support and encouragement when I needed it most.

Finally I would like to thank my partner Dean Hallam for your constant support, wonderful meals, looking after me when I was unwell and for your invaluable expertise in the final formatting of my thesis.

Table of Contents

List of Tables

List of Figures

List of Abbreviations

ADPKD	Autosomal dominant polycystic kidney disease
Ag	Antigen
APC	Adenomatous polyposis coli
AQP	Aquaporin
ARPKD	Autosomal recessive polycystic kidney disease
BBS	Bardet Biedl syndrome
cAMP	Cyclic adenosine monophosphate
cDNA	Complementary deoxyribonucleic acid
CDT	Collecting duct tubule
Cep290	Centrosomal protein 290
CGN	Cerebellar granule neurons
CGN	Cerebellar granule neurons
CK1	Casein kinase 1
Cl-	Chloride
Co	Cortex
CPK	Congenital polycystic kidneys
DAPI	4', 6- diamidino-2-phenylindole
dATP	Deoxyadenosine triphsophate
DAVID	Databse for annotation visualisation and integrated discovery
DBA	Dolicos Biflorus Agglutinin
dCTP	Deoxycytidine triphosphate
DEPC	Diethylpyrocarbonate
dGTP	Deoxyguanosine triphosphate
DMEM	Dulbecco's modified eagle media
DNA	Deoxyribonucleic acid
dNTP	Deoxyribonuclotide triphosphate
DPX	Di-N-Butyle Phthalate in Xylene
DTT	Dithiothreitol
dTTP	Deoxythymidine triphosphate
DVl	Dishevelled
ECL	Enhanced chemi lumescent
EDTA	Ethylene diamine tetra acetic acid
ENaC	Epithelial sodium channel
ERK	Extracellular signal-regulated kinases
FL	Full length
GCL	Ganglion cell layer
GCP	Granule Cell progenitors
GFR	Glomerular filtration rate
Gli3A	Gli3 activator
Gli3R	Gli3 repressor
H+E	Haematoxylin and Eosin
HCL	Hydrogen chloride
HPI-4	Hedgehog pathway inhibitor 4
HRP	Horseradish peroxidise
hTERT-RPE	human immortalized retinal pigmented epithelial
IFN	Interferon
IFN-Y	Interferon gamma
IFT	Intraflagellar transport
IMCD3	Inner medullary collecting duct 3 cells
INL	Inner nuclear layer
IPL	Inner plexiform layer
JATD	Jeune asphyxiating thoracic dystrophy
JBTS	Joubert syndrome
KAP3	Kinesin associated protein 3
KID	Kinase inducible domain
LCA	Leber congenital amaurosis
LEF	lymphocyte enhancer binding factor
LRP5/6	Lipoprotein receptor related protein complex 5/6
MAPK	Mitogen-activated protein kinases
Me	Medulla

MEFs	Mouse embryonic fibroblasts
Miox	Myoinositol oxygenase
MIQUE	Minimum information for publication of quantitative real-time PCR experiments
MKS	Meckel Gruber syndrome
MR	Mineral corticoid receptor
mTOR	mammalian target of rapamycin
NCBI	National centre for biotechnology
NLS-BP	Bipartite nuclear localisation signal
NPHP	Nephronophthisis
OFDS	Orofacial digital syndrome
ONL	Outer nuclear layer
OPL	Outer plexiform layer
PCA	Principal Component analysis
PCM1	Pericentriolar material 1
PCR	Polymerase chain reaction
PKD	Polycystic kidney disease
PL	Photoreceptor layer
PPAR-y	Peroxisome proliferator activated receptor gamma form.
PPAR-Y	Peroxisome proliferator activated receptor
Pur	Purmorphamine
Pvalb	Paravalbumin
qPCR	Quantitative polymerase chain reaction
RAAS	Renin angiotensin aldosterone system
RD	Retinal degeneration
Ren1	Renin
RFLP	Restriction fragment length polymorphism
RNA	Ribonucleic acid
RPE	Retinal pigmented epithelium
RPGR	Retinitis pigmentosa GTPase regulator
RT	Reverse transcription
RTK	Receptor tyrosine kinase
SDS	Sodium Dodecyl Sulphate
SEM	Scanning Electron Microscopy
Shh	Sonic hedgehog pathway
SIGR	Sanger institute gene trap resource
SL	Short length
SLC	Solute carriers
SLS	Senior Løken syndrome
SMC	Structural maintenance of chromosomes
SV40	Simian vacuolating virus
T	Large Tumour
TBST	Tris buffered saline and tween
TCF	T cell factor
TEM	Transmission Electron Microscopy
TEMPO	Tolvaptan phase 3 efficiancy and safety study in ADPKD
Tff2	Treffoil factor 2
TM	Tropomyosin domains
TMS	Trichrome Masson Staining
V2	Vasopressin 2
Wnt	Wingless in *Drosophila*
X gal	5-bromo-4-chloro-indolyl-β-galactopyranoside
β-gal	β-galactosidase
β-Trcp	β-transduction repeat containing protein

Chapter 1 Introduction

1.1 Polycystic Kidney Disease (PKD)

Polycystic kidney disease is usually an inherited disorder characterised by cyst initiation and expansion of the renal tubules, it can also be acquired at end stage renal failure (Dell 2011). The disease can be inherited in two forms; autosomal dominant (AD) and autosomal recessive (AR) (Halvorson, Bremmer et al. 2010).

1.2 Autosomal Dominant Polycystic Kidney Disease (ADPKD)

ADPKD has a worldwide prevalence of 1:400 to 1:1,000 (Torres and Harris 2009) with renal failure occurring by the fifth/sixth decade of life (Chapman 2008). In the U.K., ADPKD accounts for 9.6% of all adults requiring dialysis/transplantation (Byrne, Steenkamp et al. 2010). There are 2 causal genes (*PKD1* and *PKD2*) that when mutated result in ADPKD (Torres and Harris 2009). The ADPKD mutation database http://pkdb.mayo.edu/ currently lists 619 known *PKD1* pathogenic mutations compared to 129 known *PKD2* pathogenic mutations. 85-90% of ADPKD cases result from *PKD1* mutations and the other 10-15% from *PKD2* mutations (Mochizuki, Tsuchiya et al. 2013). Mutations in *PKD1* tend to lead to more severe disease than mutations in *PKD2* due to cyst development occurring at an early age in patients with *PKD1* mutations (Torres and Harris 2009). The clinical effect of mutations in both *PKD1* and *PKD2* are highly variable, even within families (Rossetti and Harris 2007).

ADPKD was first described over 200 years ago and since then has been considered an untreatable condition (Chang and Ong 2013). Recently however results from the Tolvaptan Phase 3 Efficacy and Safety Study in ADPKD (TEMPO 3:4) trials have demonstrated that the cystic disease and loss of renal function can be slowed in humans (Torres, Chapman et al. 2012). The identification of the molecular mechanisms associated with ADPKD in the kidney, will lead to the translation of new ADPKD treatments which will aim to reduce the expansion of renal cysts. Extra renal manifestations can also occur in patients with ADPKD which include, polycystic liver disease, intracranial aneurisms (Rossetti and Harris 2007), mitral valve disease (Pirson 2010), pancreatic cysts and colonic diverticulae (Kumar, Adeva et al. 2006).

1.3 Autosomal Recessive Polycystic Kidney Disease (ARPKD)

ARPKD has traditionally been referred to as the “juvenile” form of PKD (Dell 2011). In contrast to the relatively frequent ADPKD, the incidence of ARPKD is much rarer and is approximately 1 in 20,000 (Torres and Harris 2009; Dell 2011). ARPKD is caused by mutations in the *PKHD1* gene (Zerres, Mucher et al. 1994). The Polycystic Kidney and Hepatic Disease 1 (*PKHD1)* gene is one of the largest human genes characterised to date containing 86 exons (Onuchic, Furu et al. 2002). *PKHD1* mutations are often unique to single families, highly variable and seem to be found scattered across the exons of the gene (Blyth and Ockenden 1971; Bergmann, Senderek et al. 2004). ARPKD, like ADPKD, also presents with extra renal manifestations which include congenital hepatic fibrosis (Ward, Hogan et al. 2002), pulmonary hypoplasia, characteristic facial and spine and limb abnormalities (Harris and Torres 2009).

1.4 Pleiotropic PKD disorders.

The protein products of the genes mutated in both ADPKD and ARPKD are localised to the primary cilium of renal cells linking PKD to a common pathophysiology (Nauli, Alenghat et al. 2003; Harris and Rossetti 2004; Dell 2011). New advances in research have identified other pleiotropic PKD disorders which include nephronophthisis (NPHP), Senior-Loken syndrome (SLS), Joubert syndrome (JBTS), Meckel syndrome (MKS), Bardet-Biedel syndrome (BBS) and orofacial digital syndrome (OFDS). Collectively these forms of PKD are now well established as “ciliopathies” as the protein products of the genes mutated in these disorders are localised to the centrosome/basal body of the primary cilium (Harris and Torres 2009).

1.5 NPHP

NPHP is the most common cause of end-stage renal disease in the first 30 years of life (Hildebrandt and Zhou 2007). The initial symptoms of NPHP include polyuria, polydipsia, and a decreased urinary concentrating ability (Gusmano, Ghiggeri et al. 1998; Salomon, Saunier et al. 2009).

The renal histology of NPHP consists of cortico-medullary cysts, tubular atrophy with thickened or thinned tubular basement membrane and interstitial fibrosis. Patients with NPHP have normal or small sized kidneys, in marked contrast to patients with ADPKD and ARPKD where kidneys are enlarged up to 10 fold (Zollinger, Mihatsch et al. 1980; Waldherr, Lennert et al. 1982; Wolf and Hildebrandt 2011).

Currently there are 20 genes known to cause NPHP (Table 1.1). The list of *NPHP* genes has continued to grow since the identification of the first *NPHP* gene 16 years ago (Hildebrandt, Otto et al. 1997; Saunier, Calado et al. 1997). 10-15% of patients with NPHP have extra renal manifestations including retinal degeneration, JBTS and liver fibrosis (Wolf and Hildebrandt 2011).

Table 1.1 lists the known *NPHP* and *JBTS* genes. Numerous patients with *NPHP* mutations also have extra renal characteristics (for example retinal degeneration (RD) or JBTS). This information is highlighted in table 1.1 to emphasize that it is very common to see RD and JBTS in association with NPHP. Interestingly 50% of patients with JBTS have a mutation in the *CEP290/NPHP6* gene (Valente, Brancati et al. 2013). The known *JBTS* genes are also listed in Table 1.1.

Despite 20 known genetic causes of NPHP (Table1.1), to date approximately 60% of patients with NPHP do not have a detectable mutation in any of the coding regions of these known genes (Halbritter, Porath et al. 2013). Therefore this list of known genes will more than likely continue to grow.

Nephronophthisis (20 Known Genes)					Joubert Syndrome (20 Known Genes)				
Official Gene Symbol	**Other known gene symbols**	**NPHP Reference**	**Extra renal manifestations also observed in patients include**	**Extra organ Reference**	**Official Gene Symbol**	**Other known gene symbols**	**JBTS Reference**	**Other organ manifestations also seen in patients include;**	**Extra Organ Reference**
NPHP1	*JBTS4*	(Hildebrandt, Otto et al. 1997; Saunier, Calado et al. 1997)	(A) Tapeto-RD (B) Joubert syndrome	(A) (Caridi, Murer et al. 1998) (B) (Parisi, Bennett et al. 2004)	*JBTS1*	*INPP5E*	(Saar, Al-Gazali et al. 1999; Bielas, Silhavy et al. 2009)	RD and retina coloboma,	(Travaglini, Brancati et al. 2013)
NPHP2	*INVS*	(Otto, Schermer et al. 2003)	*Situs inversus,* Ventricular septal defect (VSD)	(Tory, Rousset-Rouviere et al. 2009)	*CORS2*	*JBTS2/ TMEM216*	(Valente, Logan et al. 2010)	NPHP, ocular motor apraxia, developmental delay	(Valente, Salpietro et al. 2003)
NPHP3	*MKS7*	(Olbrich, Fliegauf et al. 2003)	(A) SLS (B) embryonic lethal, MKS, *situs inversus*, Choroid plexus cysts, Dandy-Walker malformation (C) VSD	(A) (Omran, Sasmaz et al. 2002) (B) (Bergmann, Fliegauf et al. 2008) (C) (Tory, Rousset-Rouviere et al. 2009)	*AHI1*	*JBTS3 ORF1*	(Dixon-Salazar, Silhavy et al. 2004; Ferland, Eyaid et al. 2004; Lagier-Tourenne, Boltshauser et al. 2004)	Nystagmus, hypotonia (A) RD, no verbal communtication NPHP	(A) (Lagier-Tourenne, Boltshauser et al. 2004)
NPHP4		(A) (Mollet, Salomon et al. 2002)	(A) Cogan syndrome (B) SLS	(B) (Otto, Hoefele et al. 2002)	*NPHP1*	*JBTS4*	(Parisi, Bennett et al. 2004)	See *NPHP1* for extra organ information	
IQCB1	*NPHP5*	(Otto, Loeys et al. 2005)	SLS	-	*CEP290*	*JBTS5*	(Sayer, Otto et al. 2006)	See *NPHP6* for extra organ information	
CEP290	*JBTS5, MKS4, BBS14, NPHP6*	(A) (Sayer, Otto et al. 2006)	(A) Tapeto-RD; congenital amaurosis (bilateral); cerebellar vermis aplasia	-	*TMEM67*	*JBTS6 / MKS3*	(Baala, Romano et al. 2007)	See *NPHP11* for extra organ information	
GLIS2	*NPHP7*	(Attanasio, Uhlenhaut et al. 2007)	-	-	*RPGRIP1L*	*JBTS7/ NPHP8*	(Arts, Doherty et al. 2007; Delous, Baala et al. 2007)	See *NPHP8* for extra organ information	
RPGRIP1L	*JBTS7, MKS5, NPHP8*	(A) (Delous, Baala et al. 2007)	(A) Cerebella ataxia, mental retardation, oculomotor apraxia, nystagmus, retinitis pigmentosa (B) Ocular coloboma	(B) (Wolf, Saunier et al. 2007)	*ARL13B*	*JBTS8*	(A) (Cantagrel, Silhavy et al. 2008)	(A) encephalocele, retinopathy (B) NPHP	(B) (Otto, Ramaswami et al. 2011)
NEK8	*NPHP9*	(A) (Otto, Trapp et al. 2008)	(A) Retinis pigmentosa (B) Renal-hepatic and pancreatic dysplasia	(B) (Frank, Habbig et al. 2013)	*CC2D2A*	*JBTS9*	(A) (Gorden, Arts et al. 2008; Tallila, Jakkula et al. 2008)	(A) RD, nystagmus, liver fibrosis, encephalocele (B) (MKS), PKD, polydactyly	(B) (Tallila, Jakkula et al. 2008)
SDCCAG8	*BBS16, NPHP10*	(Otto, Hurd et al. 2010)	RD, mental retardation, hypogenitalism, peripheral neuropathy, obesity.	-	*OFD1*	*CXORF5/ JBTS10*	(A) (Rakkolainen, Ala-Mello et al. 2002)	(A) Facial dysmorphism, cleft palate, tooth aplasia, tongue abnormalities, PKD, mental retardation (B) polydactyly low set ears+ (A features)	(B) (Coene, Roepman et al. 2009)
TMEM67	*JBTS6, MKS3, NPHP11*	(Otto, Tory et al. 2009) and JBTS	Liver fibrosis, RD, mental retardation.		*TTC21B*	*JBTS11/ NPHP12*	(Davis, Zhang et al. 2011)	See *NPHP12* for extra organ information	
TTC21B	*JBTS11, NPHP12, IFT139*	(Davis, Zhang et al. 2011)	JATD		*KIF7*	*JBTS12*	(Dafinger, Liebau et al. 2011)	Polydactyly, facial dysmorphism, mental retardation, retinal coloboma	(Dafinger, Liebau et al. 2011)
WDR19	*NPHP13*	(Bredrup, Saunier et al. 2011)	Retinitis pigmentosa. Short 2nd and 5th toes and fingers.		*TCTN1*	*JBTS13*	(Garcia-Gonzalo, Corbit et al. 2011)	bilateral frontotemporal pachygyria	-
AHI1	*JBTS3*	(Utsch, Sayer et al. 2006)	RD, Joubert syndrome	(Dixon-Salazar, Silhavy et al. 2004; Ferland, Eyaid et al. 2004)	*TMEM237*	*JBTS14*	(Huang, Szymanska et al. 2011)	PKD, coloboma, cleft palate, encephalocele, hydrocephaly, polydactyly, liver fibrosis, ventricular septal defect	-
ATXN10		(A) (Sang, Miller et al. 2011)	(A) Cerebral atrophy, seizures and liver fibrosis.	-	*CEP41*	*JBTS15*	(Lee, Silhavy et al. 2012)	Leukoma, liver abnormalities, polydactyly, growth hormone deficiency, micropenis	-
ZNF423	*NPHP14 JBTS19*	(Chaki, Airik et al. 2012)	Cerebellar vermis hypoplasia, *situs inversus*, breathing abnormalities, LCA and RD	-	*TMEM138*		(Lee, Silhavy et al. 2012)	PKD, RD, polydactyly, oculomotor apraxia, coloboma	
CEP164	*NPHP15*	(Chaki, Airik et al. 2012)	RD, LCA, nystagmus, cerebellar vermis hypoplasia, facial dysmorphism, developmental delay, polydactyly, obesity		*C5ORF42*	*JBTS17*	(Srour, Schwartzentruber et al. 2012)	Developmental delay, limb abnormality, oculomotor apraxia, breathing abnormalities	-
ANKS6		(Hoff, Halbritter et al. 2013)	N/A	N/A	*TCTN2*		(Sang, Miller et al. 2011)	Nystagmus, muscle hypotonia	-
NPHP-like	*XPNPEP3*	(O'Toole, Liu et al. 2010)	Cardiomyopathy, muscle fatigue, hearing loss, tremors		*TCTN3*	*JBTS18*	(Thomas, Legendre et al. 2012) and RD	Polydactyly, oral abnormalities, PKD, bile duct proliferation of the liver, ventricular septal defects, horseshoe kidneys, cleft palate, bowing of long bones	-
	SLC41A1	(Hurd, Otto et al. 2013)	Bronchiectasis,frequent episodes of fever, coughing and respiratory infections since 1 month old. Inflamatory infiltrates in lungs	Hurd, Otto et al. 2013	*ZNF423*	*JBTS19/ NPHP14*	(Chaki, Airik et al. 2012)	Cerebellar vermis hypoplasia, situs inversus, breathing abnormalities, LCA and RD	-
					TMEM231	*JBTS20*	(Srour, Hamdan et al. 2012) and RD	Oculomotor apraxia, breathing abnormalities, limb abnormalities, RD+ PKD	-

Table 1.1 List of known genes mutated in NPHP and JBTS.

List of known *NPHP* and *JBTS* genes. The other organ manifestations found in patients with either NPHP or JBTS are also recorded along with the reference citing the other organ manifestations. (JATD) Jeune asphyxiating thoracic dystrophy; LCA Leber congenital amaurosis, RD Retinal Degeneration

Note (A) highlights the reference that corresponds to the extra organ manifestations (Also highlighted by A) identified in a study investigating patients with mutations in a particular *NPHP/JBTS* gene. If another study identified other extra organ defects from mutations in the same *NPHP/JBTS* gene (B) highlights the reference and the type of extra organ manifestations identified in that study.

1.6 Clinical effect of *NPHP* genetic mutations

NPHP1 mutations accounts for 20-25% of patients with NPHP (Hildebrandt, Attanasio et al. 2009)*.* Nonsense mutations and small deleted sections in the *NPHP1* gene can present with a cystic kidney phenotype alone (Hildebrandt, Otto et al. 1997) but large deletions of the *NPHP1* gene may cause a SLS (Caridi, Murer et al. 1998) or JBTS phenotype (Parisi, Bennett et al. 2004). Mutations in *NPHP2* cause “infantile” NPHP (Otto, Schermer et al. 2003). Infantile NPHP slightly differs from juvenile NPHP as there is moderate renal enlargement, cortical microcysts and cystic Bowman’s spaces with no tubular basement membrane disruptions (Simms, Eley et al. 2009).

NPHP3 mutations are associated with SLS as well as NPHP (Omran, Sasmaz et al. 2002). In 2005 *NPHP4* was found “localized to the primary cilia in epithelial tubular cells suggesting that nephrocystin proteins may play a role in ciliary function” (Mollet, Silbermann et al. 2005). *NPHP4* expression was also detected at the centrosomes of dividing cells and close to the actin cytoskeleton (Mollet, Silbermann et al. 2005). From the study by Mollet and Silbermann in 2005 the relationship between the pathogenesis of NPHP and the function of primary cilia was further considered (Hildebrandt and Otto 2005) and is still being investigated to this day.

A number of different phenotypes have been observed in patients with mutations in either the *NPHP* and/or the *JBTS* genes (Table 1.1).

1.7 *NPHP6* mutations

Intriguingly *NPHP6* mutations (also known as *CEP290* which it will be called from herein) have been found in patients with a multitude of disorders which include BBS (Leitch, Zaghloul et al. 2008), JBTS (Sayer, Otto et al. 2006), LCA (den Hollander, Roepman et al. 2008), MKS (Baala, Romano et al. 2007) and SLS (Valente, Silhavy et al. 2006). *CEP290* is the most intriguing gene of all *NPHP* genes because of the collection of disorders associated with it.

So far 128 *CEP290* mutations have been identified according to the *CEP290* database. The majority of *CEP290* mutations identified in patients are truncating mutations. 48 mutations were reported as truncating mutations, 40 nonsense mutations, 29 unknown (the affects are unknown at this time from base pair substitutions but are predicted pathogenic) and 3 are reported as in-frame deletions http://medgen.ugent.be/cep290base/overview.php . The database links phenotypes to detailed mutation information. In addition the database also includes variants in other genes which interact with *CEP290* variants providing links to genetic modifier loci associated with clinical manifestations (Coppieters, Lefever et al. 2010).

1.8 Current *Nphp* mouse models

Animal models are required to understand more about the molecular mechanisms of NPHP. In order to identify potential target drug treatments animal models are necessary as there are currently no therapeutic therapies available to treat the cyst pathology for patients with NPHP (Nagao, Kugita et al. 2012). Table 1.2 details a list of mouse models with a mutation in one of the known *Nphp* genes.

Mouse Models with mutations in the *Nphp* genes				
Official Gene Symbol	**Mouse Model**	**Information on Mouse model**	**Phenotype**	**Reference**
Nphp1	*Nphp1*$^{del20/del20}$	Targeted null exon 20	Sterile males	(Jiang, Chiou et al. 2008)
Nphp2	*Inv/Inv*	47kb deletion removing exons 3-11 of *INVS*	Renal cysts, enlarged kidney *Situs inversus* (Die after P6)	(Morgan, Turnpenny et al. 1998)
Nphp3	*(A) Pcy* (B1) *Nphp3*$^{Ko/Pcy}$ (B2) *Nphp3*$^{Ko/Ko}$	Exon12 T1841G (spontaneous mutation) (A) Hypomorphic *Nphp3* allele = cysts (B2) Null allele = situs inversus, congenital heart defects and embryonic lethality in mice	(A) Renal cysts at 2 weeks (B1) Extensive renal cysts at 4 weeks	(A) (Omran, Haffner et al. 2001); (Olbrich, Fliegauf et al. 2003); (Gattone, Wang et al. 2003) (B) (Bergmann, Fliegauf et al. 2008)
Nphp4	*Nphp4*$^{nmf192/nmf192}$	Nonsense mutation exon 4 of *NPHP4*	Retinal degeneration by 9 weeks old. Males are sterile	(Won, Marin de Evsikova et al. 2011)
Iqcb1	-	-	-	-
Cep290	*Rd16/Rd16* (B) *Cep290*$^{-/-}$ (C) *Rd16Nrl*$^{-/-}$	In-frame deletion of 897bp (exons35-39) in the *Cep290* gene (B) Floxed region (containing exons 36 and 37 of 52 exons) *Cep290* mice lack the full length cep290 protein (data not shown) (C) crossed *Rd16* mouse with *Nrl* mouse. *Nrl* is associated with retinitis pigmentosa	Retinal degeneration from P19/ Loss of Olfactory function (B) *Cep290*$^{-/-}$ mice present with a midline fusion defect and retinal degeneration (C) Retained cone photoreceptors disproportionate cone function loss	(Chang, Khanna et al. 2006)/ (McEwen, Koenekoop et al. 2007) (B) (Lancaster, Gopal et al. 2011) (C) (Cideciyan, Rachel et al. 2011) (D) Nrl mice origninated from (Mears, Kondo et al. 2001)
Glis2	*Glis2*$^{LacZ/LacZ}$	Disrupted *Glis2* at exons 3-5	Renal atrophy and fibrosis from 8 weeks old	(Attanasio, Uhlenhaut et al. 2007)
	Glis2^{mut}	1.5kb region encoding exon 6 of *Glis2* deleted	Renal atrophy reduced life span due to renal failure (Some mice survived to 12 months)	(Kim, Kang et al. 2008)
Rpgrip1l	*Ftm*$^{-/-}$ *(homologous to RPGRIP1L)*	Truncated mutation lacks the last 2 of the 3 Coil-Coiled domains in the *Ftm* gene C2+RID domain	*Ftm*$^{-/-}$ die at birth showing reduced eye size, polydactyly, craniofacial defects and at earlier stages of development *Situs inversus*	(Vierkotten, Dildrop et al. 2007)
	Rpgrip1L$^{-/-}$	In frame deletion (exons 8-17) of the *RPGRIP1L* gene	Exencephaly, deep set eyes cleft lips dilated ventricles, cerebellar hypoplasia and microcystic kidneys and bile duct proliferation (E18+E16.5)	(Delous, Baala et al. 2007)
Nek8	(A) *Jck*$^{-/-}$ (B) *Nek8*$^{-/-}$	(A) Sequence change at bp 1346-1348 results in Gly to Val substitution at aa 448 (B) Targeted null after exon 2	Cystic collecting ducts, Enlarged multinucleated cells, abnormal actin cytoskeleton.(Observed at 6-7 weeks) Survival age not defined (B) Left right asymmetry defects cardiac anomalies and glomerular cysts	(A) (Liu, Lu et al. 2002) (B) (Manning, Sergeev et al. 2013)
Sdccag8	-	-	-	-
Tmem67	(A) *bpck/bpck* (B) *Tmem67-/-*	(A) Spontaneous deletion of *Tmem67* *Tmem67*$^{-/-}$ lack exons 2-3	(A) Hydrocephally at 2 weeks, Polycystic kidneys, death at 3 weeks of age (B) Mice die shortly after birth are severely growth retarded, and have cystic kidneys at E18.5	(A) (Cook, Collin et al. 2009) (B) (Garcia-Gonzalo, Corbit et al. 2011)

Mouse Models with mutations in the *Nphp* genes (Continued)				
Official Gene Symbol	**Mouse Model**	**Information on mouse model**	**Phenotypes**	**Reference**
Ttc21b	*Aln*$^{-/-}$	A→C mutation converts glutamine to proline (highly conserved). Absence of Thm1 protein in *Aln*$^{-/-}$	Pre-axial polydactyly, split and fused ribs, cortically layer abnormalities Defects in eye, brain and neural tube development and craniofacial defects (E10.5 +) some survive until birth but die shortly after.	(Herron, Lu et al. 2002; Tran, Haycraft et al. 2008; Stottmann, Tran et al. 2009)
Wdr19	*Ift144*^{twt} *Ift*^{dmhd}	(WDR19 encodes Ift44) *N-ethyl-N-nitrosourea (ENU)*hypomorphic missense mutation (*Ift*^{dmhd}null allele)	Survive up to birth.Exencephaly Polydactyly, truncated ribs, craniofacial abnormalities	(Ashe, Butterfield et al. 2012)
Ahi1	*Ahi1*$^{-/-}$	Knockout mouse model	Cystic kidneys at 5 months, Retinal degeneration between 2-4 weeks of age, Cerebellar hypoplasia and a vermis-midline fusion defect	(Lancaster, Louie et al. 2009; Louie, Caridi et al. 2010; Lancaster, Gopal et al. 2011)
Atxn10	*Sca10*	Expanded ATTCT repeat in the *ATXN10* gene	Locomotive dysfunction (ataxic gait) died of seizures, neuronal loss survive to 6 months of age	(White, Xia et al. 2012)
Znf423	*Nur12*$^{-/-}$	Knockout mouse model *Znf423* expression deleted	Loss of corpus callosum, reduction of hippocampus and malformation of cerebellum / midline structures	(Alcaraz, Gold et al. 2006)
Cep164	-	-	-	-
Anks6	*Han:SPRD* $^{cy/+}$	Missense mutation	Proximal tubule cysts and expression in the cortex (P36),	(Brown, Bihoreau et al. 2005) (Note Rat Model not mouse)
XPNPEP3	-	-	-	-
SLC41A1	-	-	-	-
Arpkd	*Ift88*$^{Orpk/Orpk}$	A deletion of 2.77kb of genomic DNA at transgene integration site but no exons deleted	Polycystic kidneys, hyperplastic and dysplastic bile ducts liver fibrosis	(Moyer, Lee-Tischler et al. 1994)
	cpk/cpk	Spontaneous mutation	Die at 5 weeks, enlarged cystic kidneys, cysts are grossly visible	(Mandell, Koch et al. 1983)
	Bpk$^{-/-}$	Knockout model	Die at 1 month of age with renal failure and cystic kidney disease. Renal cysts proximal and collecting duct, hyperplasia in the biliary tract	(Nauta, Ozawa et al. 1993)

Table 1.2 List of published mouse models associated with NPHP.
Green highlights JBTS phenotypes seen in NPHP mouse models. Blue highlights retinal degeneration phenotypes seen in NPHP mouse models. ARPKD mouse models are at highlighted at the of the table. If there is more than 1 mouse model for a particular NPHP gene (A) represents the 1st mouse model generated and the phenotype and reference associated with that mouse. (B) represents the 2nd mouse model with a different mutation in the same *nphp* gene, (B) also highlights the phenotype associated with the 2nd mouse model and the reference associated with the 2nd mouse model. (C) represents the 3rd mouse model generated with a different mutation in the same NPHP gene and highlights the phenotype for that particular mouse and the reference for that particular mouse. E10.5, 18.5, 16.6 Embryonic Day 10.5. 18.5 and 16.5. P36, 36 days after the first day of birth and P6 is 6 days after the first day of birth.

1.9 JBTS

NPHP phenotypes may also be observed in patients with JBTS (Table 1.1). Patients with mutations in 16 of the 20 JBTS genes highlighted in Table 1.1 presented with abnormalities which included NPHP. NPHP is the main renal condition associated with JBTS and it occurs in up to 25% of patients with JBTS (Brancati, Dallapiccola et al. 2010).

JBTS was first described in 1968. 4 siblings in a consanguineous family presented with ataxia, developmental delay, oculomotor apraxia and breathing abnormalities (Joubert, Eisenring et al. 1968). Magnetic resonance imaging (MRI) scans of the brain are used to identify the midbrain-hindbrain malformation which appears as a “molar tooth” image in the middle/back of the brain of an affected JBTS individual. Maria and Hoang first described the molar tooth sign in MRI scans of patients with JBTS (Maria, Hoang et al. 1997). The prevalence of JBTS is estimated to be about 1:100,000 worldwide (Parisi, Doherty et al. 2007; Kroes, van Zon et al. 2008). JBTS prognosis is usually dependent on the severity of the other organ manifestations associated with JBTS which includes liver fibrosis or the NPHP phenotype which will eventually lead to liver or kidney failure (Sattar and Gleeson 2011).

JBTS mouse models may be ideal models in understanding the disease course of NPHP and JBTS phenotypes. A list of JBTS mouse models is highlighted in Table 1.3.

The majority of JBTS mouse models are lethal prior to birth or just a few days after (Table 1.3). In order to study the disease course of NPHP, a novel mouse model is required, which displays a NPHP phenotype but is not lethal. Such a mouse model would need to develop cysts at an early time point in development to mimic the childhood disease but would also need to survive in order to be able to test various targeted therapies.

Mouse Models of JBTS				
Official Gene Symbol	**Mouse Model**	**Information on Mouse model**	**Phenotypes**	**Reference**
Jbts1/ Inpp5e	*Inpp5e*$^{\Delta/\Delta}$	Knockout mice	Died at birth, bilateral anophthalmos, postaxial hexadactyly, ceased eye development at optic vesicle stage, cystic kidneys, skeletal abnormalities and cleft palate	(Jacoby, Cox et al. 2009)
Cors2 Jbts2	*Hty*$^{-/-}$	Severe truncation or in-frame deletion identified *C2cd3* ortholog is close to the critical chromosomal region of *JBTS2*	Lethal, neural tube defects, abnormal dorsal-ventral patterning of the spinal cord, *situs inversus*, polydactyly Embryonic lethalithy between E11 and E13	(Hoover, Wynkoop et al. 2008)
Ahi1, Nphp1, Cep290, Tmem67, Rpgrip1l			Table 1.2 for mouse model information / phenotype	
Arl13b	*Hnn*$^{-/-}$	Null allele of *Arl13b*	Defects in neural tube patterning, limbs (polydactyly) and eye defects. Survive until E13.4-E14.5 Cilia half the length of wild type in node	(Caspary, Larkins et al. 2007)
Cc2d2a	*Cc2d2a*$^{-/-}$	Truncation mutation after exon 11	Randomised left-right axes, holoprosencephaly, microphthalmia, embryonic lethal.	(Garcia-Gonzalo, Corbit et al. 2011)
Ofd1	*Ofd1*$^{\Delta 4\text{-}5}$	*Ofd1* exons flanked by *loxP* sites	Craniofacial and limb abnormalities, cleft palate, skeletal defects (newborn autopsy = brain disorganisation, reduced lungs and cystic kidneys. Died at birth	(Ferrante, Zullo et al. 2006; D'Angelo, De Angelis et al. 2012)
Ttc21b			Table 1.2 for mouse model information / phenotype	
Kif7	(A) *Kif7*$^{-/-}$ (B) *Kif7*^{maki}	(A) Loss of *Kif7* function (B) T to C missense substitution disrupting *AluI* restriction site creating a RFLP	(A) Exencephaly, oedema and polydactyly, ceased eye development, hedgehog signalling defects survive until E10.5 (B) Polydactyly, Negative regulation of hedgehog pathway die at end of gestation	(A) (Cheung, Zhang et al. 2009; Liem, He et al. 2009)
Tctn1	*Tctn1*$^{-/-}$	Knockout mouse model of *Tctn1* gene	Required for ciliogenesis E10.5 mutants reduced telencephalon size and holoprosencephaly	(Reiter and Skarnes 2006)
Tmem237	-	-	-	-
Cep41	*Cep41*$^{Gt/Gt}$	Knockout model	Malformed hindbrain, exencephaly, brain hemorrhage, dilated pericardial sac and lethality (Phenotypes observed between E10-E13)	(Lee, Silhavy et al. 2012)
Tmem138	-	-	-	-
C5orf42	-	-	-	-
Tctn2	*Tctn2*$^{-/-}$	Knockout mouse of *Tctn2* gene	Neural tube closure defect, hedgehog signalling defects, cleft palate and polydactyly (embryonic lethal)	(Sang, Miller et al. 2011)
Tctn3	-	-	-	-
Tmem231	*Tmem231*	*Tmem231* Gene disrupted after Intron 1	Embryonic lethal (http://www.mmrrc.org/catalog/sds.php?mmrrc_id=32667/032667.html Note another *Tmem231* knockout mouse model is described in Table 1.6	(Tang, Li et al. 2010)
MRE11	*Mre11*	Hypomorphic mouse	Exclusively cell cycle components observed in oocytes from E17.5 E18 days of gestation in mice (mice lethal)	(Cherry, Adelman et al. 2007) http://flybase.org/reports/FBgn0020270.html

Table 1.3 List of known mouse models associated with JBTS

RFLP Restriction Fragment Length Polymorphism. Blue highlights RD phenotype observed in JBTS mouse models. Yellow highlights cystic kidney phenotype observed in JBTS mouse models. (A) highlights the first mouse model associated with a mutation in the JBTS gene highlighted and (B) highlights the second mouse model with a different mutation in the same gene. The phenotypes and references for each mouse model for that selected gene are highlighted accordingly; as (A) and (B).

1.10 MKS

The vast majority of human MKS cases result in prenatal lethality, usually due to a number of different organ defects including neural tube defects, kidney cysts, microphthalmia, occipital meningoencephalocele, hepatic cysts and postaxial polydactyly (Otto, Tory et al. 2009; Hurd and Hildebrandt 2011; Bergmann 2012). A number of *NPHP* genes are also *MKS* genes which include *NPHP3/MKS7*, *NPHP6/MKS4*, *NPHP8/MKS5* and *NPHP11/MKS3*. MKS phenotypes have been seen in a number of *nphp/jbts* mouse models which include the *Rpgrip1L*$^{-/-}$ mouse model, the *Ift144*^{twt} mouse model, the *Kif7*$^{-/-}$ mouse model and the *Cep41*$^{Gt/Gt}$ mouse model to name a few (See table 1.2 and 1.3 for references).

1.11 BBS

A recent review article described the clinical characteristics of BBS to include "obesity, hypogonadism, retinal degeneration, polydactyly, mental retardation and renal disease; with renal disease being the major cause of mortality in patients with BBS" (Bergmann 2012). Recently the BBS4 protein was found to genetically interact with *CEP290*. Increased body weight and accelerated photoreceptor degeneration was evident in the *Cep290*$^{rd16/rd16}$ mice with an additional loss of *Bbs4* allele when compared to *Cep290*$^{rd16/rd16}$ mice. *Cep290*$^{rd16/+}$*; Bbs4*$^{+/-}$ double heterozygote mice also saw increased body weight when compared to *Cep290*$^{rd16/rd16}$ mice suggesting that *Bbs4* modifier loci are affecting the *Cep290* phenotype (Zhang, Seo et al. 2013).

1.12 Sub cellular location of NPHP and JBTS protein products

Animal models have helped identify the sub cellular location of the current known NPHP and JBTS proteins.

The most recent article describing the sub cellular locations of each of the known NPHP protein products was in 2012 and only 11 of the NPHP genes were discussed (Shiba and Yokoyama 2012), even though there were more than 11 NPHP genes published at this stage. The sub cellular locations of the other 9 NPHP proteins have been identified and are highlighted in Table 1.4.

In 2010 the sub cellular location of JBTS protein products was described in a review article (Lee and Gleeson 2010), however only 5 JBTS protein products were shown, even though there were a number of additional JBTS genes published. Table 1.5 highlights the sub cellular location of each of the JBTS proteins. An updated account of each of the NPHP and JBTS protein products subcellular locations is required for future studies. The subcellular location of the protein products may aid in providing links to disease mechanisms and interacting proteins.

The 20 NPHP and JBTS protein products locations are summarised in table 1.4 and in table 1.5. In total 40 genes were assessed and only 1 of the genes' (*JBTS17/C5ORF42*) sub cellular location is currently unknown (Srour, Hamdan et al. 2012).

NPHP protein products location in relation to the primary cilium		
Gene Symbol	Protein Product Location	Reference
NPHP1/JBTS4	Transition zone, length of the cilium Adherence junctions, focal adhesions, cell-cell	(Hildebrandt and Otto 2005; Fliegauf, Horvath et al. 2006),
NPHP2/ NPHP3/ NPHP9 (B) *NPHP2*	Proximal part of the cilium "Inversin compartment" (B) Cilia, basal body and nucleus, cell-cell junctions	(Shiba, Yamaoka et al. 2009; Shiba, Manning et al. 2010) (B) (Morgan, Eley et al. 2002; Nurnberger, Bacallao et al. 2002)
NPHP4	Transition zone, basal body, centrosome and length of cilium	(Mollet, Silbermann et al. 2005; Winkelbauer, Schafer et al. 2005).
IQCB1/ NPHP5	Length of the primary cilium	(Otto, Loeys et al. 2005
CEP290 / NPHP6	Centrosomal protein, located at the transition zone and co-localises with CC2D2A at the basal body	Andersen, Wilkinson et al. 2003; Sayer, Otto et al. 2006; Gorden, Arts et al. 2008; Tallila, Jakkula et al. 2008; Craige, Tsao et al. 2010)
GLIS2 / NPHP7	Nucleus	(Zhang, Nakanishi et al. 2002)
RPGRIP1L/ NPHP8	Basal body Localises to the (B) centrosome complex with NPHP4 and CEP290 (C) And the transition zone complex with JBTS14	(Arts, Doherty et al. 2007) (B) (Delous, Baala et al. 2007) (C) (Huang, Szymanska et al. 2011)
NEK8/ NPHP9	Centrosomal and ciliary location (B) Inversin compartment (C) Nucleus	(Otto, Trapp et al. 2008), (B) (Shiba, Manning et al. 2010), (C) (Habbig, Bartram et al. 2012)
SDCCAG8/ NPHP10	Centrosome and nuclear foci in hTERT-RPE cells	(Chaki, Airik et al. 2012)
TMEM67/ JBTS6	Transition zone (B) basal body	(Garcia-Gonzalo, Corbit et al. 2011) (B) (Adams, Simms et al. 2012)
TTC21B/ JBTS11	Cilium	(Davis, Zhang et al. 2011)
WDR19/ NPHP13	Cilium	(Efimenko, Blacque et al. 2006)
AHI1/ JBTS3	Mother centriole	(Hsiao, Tong et al. 2009)
ATXN10	Basal body	(Sang, Miller et al. 2011)
ZNF423/ NPHP14	Transition zone as it interacts with CEP290	(Chaki, Airik et al. 2012)
CEP164/ NPHP15	Mother centriole/ distal appendages Also co-localises with NPHP10 and NPHP14 in the nuclear foci	(Chaki, Airik et al. 2012).
ANKS6	Proximal part of the cilium similar to NPHP2,NPHP3 and NPHP9	(Hoff, Halbritter et al. 2013)
SLC41A1	Transporter encodes Na^+/Mg^{2+} exchanger when SLC41A1 expression is inhibited Na^+/Mg^{2+} exchanger expression is also inhibited	(Kolisek, Nestler et al. 2012)
XPNPEP3	Mitochondrial	(O'Toole, Liu et al. 2010)

Table 1.4 Subcellular localisation of NPHP protein products. Subcellular location of the known proteins mutated in NPHP and the connection of the protein products to the primary cilium. (B) and (C) highlight additional studies and the subcellular location of where the NPHP protein product was found in that study. human immortalized retinal pigmented epithelial (hTERT-RPE) cells

JBTS protein products location in relation to the primary cilium			
Gene Symbol		Protein Product Location	Reference
1	*JBST1*	Ciliary axoneme and basal body	(Bielas, Silhavy et al. 2009)
2	*CORS2/ JBTS2*	Colocalises with TCTN1, JBTS5,JBTS6 and TCTN2 to the transition zone	Garcia-Gonzalo, Corbit et al. 2011)
3	*AHI1/ JBTS3*	Table 1.4	
4	*NPHP1/ JBTS4*	Table 1.4	
5	*CEP290/ JBTS5*	Table 1.4	
6	*TMEM67/ JBTS6*	Table 1.4	
7	*RPGRIP1L/ JBTS7/NPHP8*	Table 1.4	
8	*ARL13B/ JBTS8*	Ciliary axoneme	(Blacque, Perens et al. 2005
9	*CC2D2A/ JBTS9*	Basal body Ca^{2+} sensor	(Li, Gerdes et al. 2004) (Noor, Windpassinger et al. 2008)
10	*OFD1/ JBTS10*	Centrosome	(Romio, Wright et al. 2003)
11	*TTC21B/ JBTS11/ NPHP12*	Table 1.4	
12	*KIF7/ JBTS12*	Primary cilium base and translocates to the tip when shh pathway is activated	Liem, He et al. 2009)
13	*TCTN1/ JBTS13*	Colocalises with JBTS2, JBTS5,JBTS6 and TCTN2 to the transition zone	Garcia-Gonzalo, Corbit et al. 2011)
14	*TMEM237/ JBTS14*	Transition zone	(Huang, Szymanska et al. 2011)
15	*CEP41/ JBTS15*	Basal body and primary cilium	(Lee, Silhavy et al. 2012)
16	*TMEM138*	Base of the cilium	(Lee, Silhavy et al. 2012)
17	*C5ORF42/ JBTS17*	Subcellular location currently unknown	(Srour, Schwartzentruber et al. 2012)
18	*TCTN2*	Colocalises with TCTN1, JBTS5,JBTS6 and JBTS13 to the transition zone	Garcia-Gonzalo, Corbit et al. 2011)
19	*TCTN3*	Transition zone	(Thomas, Legendre et al. 2012
20	*TMEM231*	Transition zone and basal body	Chih, Liu et al. 2012)

Table 1.5 Subcellular localisation of JBTS protein products.
Subcellular location of the known proteins mutated in JBTS and the connection of the protein products to the primary cilium

1.13 The primary cilium and NPHP/JBTS protein products

Table 1.4 and Table 1.5 highlight that most of the known protein products associated with *NPHP* and *JBTS* mutations are located in and around the primary cilium which includes the basal body, transition zone and the inversin compartment, with a few of the mutated genes protein products found in the nucleus, adherens junction of the cell and in the mitochondria (*XPNPEP3*). The latest *NPHP*-like gene, *SLC41A1* was identified as a transporter, encoding the Na^{+}/Mg^{2+}exchanger.

Figure 1.1 is a schematic illustration featuring the sub cellular locations for each of the known NPHP and JBTS protein products described in Tables 1.4 and 1.5.

The primary cilium has been described as a membrane bound organelle that projects from the apical surface of the collecting duct tubule into extracellular space and use their surface area to detect environmental cues (Satir, Pedersen et al. 2010) and (Goetz and Anderson 2010). In the kidney, primary cilia are thought to act as mechanosensors and chemosensors, bending in response to fluid flow (Rodat-Despoix and Delmas 2009);(Berbari, O'Connor et al. 2009).

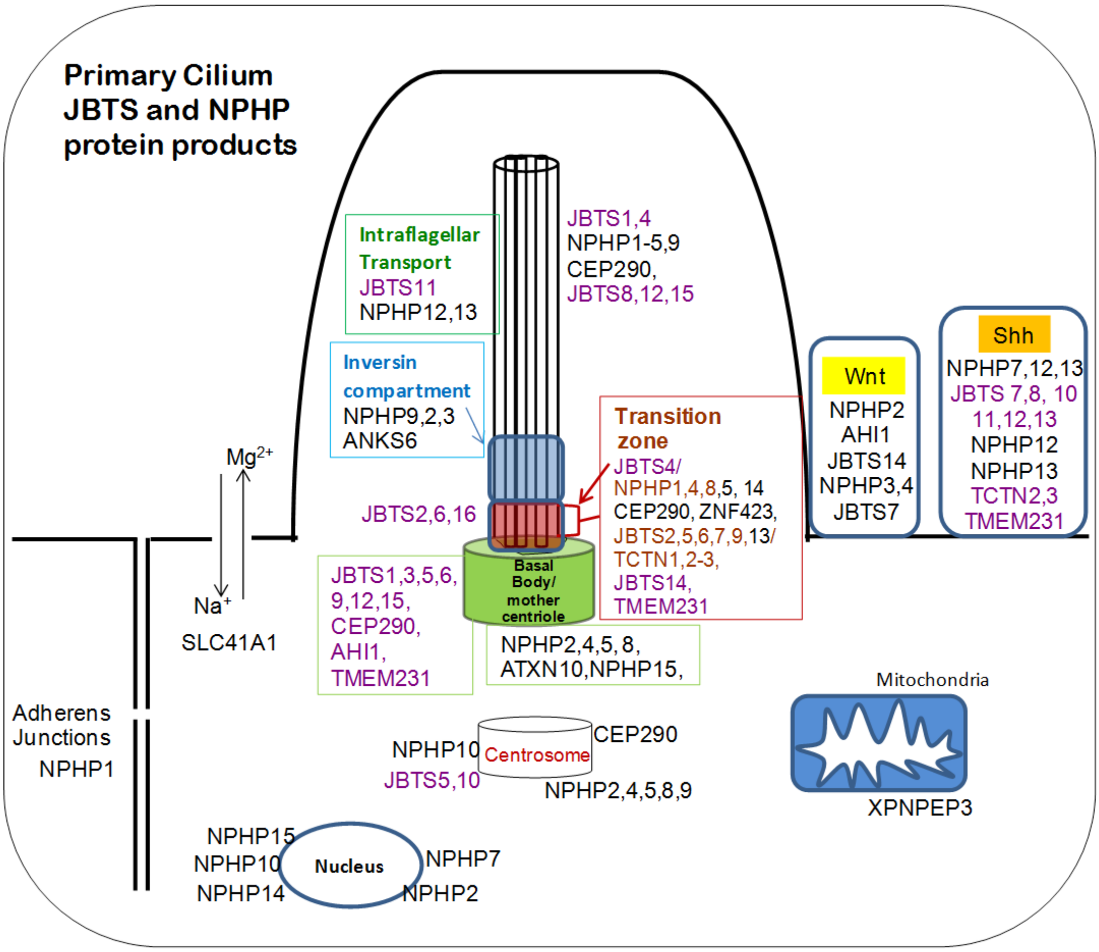

Figure 1.1 Schematic representation of the primary cilium and subcellular locations of the protein products from the known genes mutated in NPHP and JBTS.

An interesting review paper previously discussed the role of cilia in disease summarising “that compromised cilia function/structure can have profound consequences for cellular homeostasis” (Bisgrove and Yost 2006). Cilia assembly occurs in a series of well-organized steps. The first step in ciliogenesis involves the differentiation of the mother centriole into the basal body which in turn generates the transition zone then the axoneme and finally migrates to the apical cell surface (Ishikawa and Marshall 2011; Kim and Dynlacht 2013). The transition zone and the inversin compartment are required for ciliary trafficking through intraflagellar transport (IFT). IFT is required for the assembly and the maintenance of primary cilia (Pazour and Rosenbaum 2002). An example highlighting the importance of IFT proteins maintaining primary cilia assembly in kidneys was identified in a mouse model of ARPKD (the *Tg737* mouse model).

Mice homozygous for a mutation in the *Tg737* gene (which encodes a protein homologous to the IFT88 subunit, previously shown to be required for flagellar assembly in *Chlamydomonas*) developed PKD. Scanning electron microscopy of the kidneys from *Tg737* mutant mice showed abnormal cilia (Pazour, Dickert et al. 2000).

As the majority of the protein products of genes mutated in NPHP/JBTS are located in/around the primary cilium, the integrity of the structure/function of the primary cilium is crucial for maintaining kidney homeostasis. Therefore cilia structure and function should be assessed in each *Nphp* and *Jbts* mouse model created.

It has been hypothesised that "the primary cilium is a sensory organelle, acting as a mechanosensor in the kidney coordinating multiple signalling pathways with nuclear trafficking of some molecules" (Sang, Miller et al. 2011; Bergmann 2012).

1.14 Linking Shh and Wnt signalling with NPHP and JBTS

During the investigation to identify the sub cellular locations of the protein products for each of the known *NPHP* and *JBTS* genes, a link between cilia and defective sonic hedgehog signalling (Shh) and/or Wnt signalling was identified (Figure 1.1,Table 1.6).

Figure 1.1 highlights the NPHP and JBTS protein products (when the genes are mutated) which were found to disturb the normal signalling processes of both the Wnt and the Shh pathways.

NPHP and JBTS mouse model phenotypes were investigated and it was found that the majority of NPHP and JBTS mouse models presented with defects in neural tube patterning which was associated with abnormal Wnt or Shh signalling expression (Table 1.6).

Gene	Hedgehog signalling	Wnt signalling	Reference
Jbts1 ND			
Cors2/ Jbts2	Gli3 disrupted in E10.5 *Hty and C2cd3^GT^* embryos	ND	Hoover, Wynkoop et al. 2008)
Ahi1	Not assessed in the kidney. In the cerebellum of *Ahi1*$^{-/-}$ mice there were no differences in gene expression levels of n-myc, ptch1 and Gli in the *Ahi1*$^{-/-}$ mouse when compared to the wild type mouse	(A)Lef1 expression was down-regulated in 5 month old *Ahi1*$^{-/-}$ kidneys (B) Decreased Wnt reporter activity evident at the site of hemisphere fusion in the developing cerebellum	(A) (Lancaster, Louie et al. 2009) (B) (Lancaster, Gopal et al. 2011)
Jbts4/ ***Nphp1*** ND and *Jbts5/Cep290* ND			
Tmem67/ Jbts6/ ***Nphp11***	Shh expression reduced in *Tmem67*$^{-/-}$ mice. E11.5 floor plate and notochord and the neural tube had short bulbous cilia (Classified as the MKS group)	Increase level of β-catenin expression in the neuroepithelial cell of the fourth ventricle. Protein levels of β-catenin and Dvl-1 also increased in knockout *Tmem67* MEFS. Axin2 decreased in P0 *Tmem67*$^{-/-}$ cortex mice died at birth from neurodevelopmental disorders (Classified as the JBTS group)	(Abdelhamed, Wheway et al. 2013)
Rpgrip1l/ Jbts7/ ***NPHP8***	(B) *Ftm*$^{-/-}$ shows *JBTS7* is necessary for left-right asymmetry patterning of neural tube and limbs and Gli3 activator to Gli3 repressor is disrupted in E11.5 *Ftm*$^{-/-}$ embryos	(A) RPGRIP1L destabilises dishevelled, acts in a complement with **Nphp2** and **Nphp4** to modulate dishevelled stability using co immunoprecipitation experiments	(A) (Mahuzier, Gaude et al. 2012) (B) (Vierkotten, Dildrop et al. 2007)
Arl13b/ Jbts8	*Hnn* mouse model null mutation of *Arl13b* open neural tube die at E14.5. low *ptch1* expression in the ventral to dorsal gradient. cilia are short in the embryonic node at E8.5 (B) *Arl13b* regulates the cilia entry of smoothened	Disrupted *Wnt1* in the posterior of *Hnn* embryo	(Caspary, Larkins et al. 2007) (B) (Larkins, Aviles et al. 2011)
Cc2d2a/ Jbts9	*Cc2d2a*$^{-/-}$ MEFs when treated with SAG showed reduced ciliary localisation.	ND	(Garcia-Gonzalo, Corbit et al. 2011
Jbts10	(A) *Ofd1* deficient mice, Shh expression absent in neural tube, *ptch1* and *Gli1* reduced in ventral neural tube, (C) *Ofd1* deficient embryoid bodies display defects in both the Wnt and Shh signalling pathway. When Shh pathway activated wild type showed a 3 fold increase in *Gli1* and *ptch* expression where as *Ofd1* remained the same. Also Gli3 processing could not be activated when Shh activated its processing remained as the truncated repressor form	(B) *Ofd1*$^{-/-}$ ES cells lack cilia and when Wnt3a was added the ES cells were hyper-responsive to Wnt3a suggesting primary cilium modulates wnt transduction (C) Ofd1 deficient embryoid bodies when activated with Wnt3a showed increased responsiveness to Wnt3a compared to wt using *axin2, c-myc* and *cyclinD1* as *Wnt* target genes.	(A) (Ferrante, Zullo et al. 2006) (B) (Corbit, Shyer et al. 2008) (C) (Hunkapiller, Singla et al. 2011)
Ttc21b/ ***NPHP12***	"*Ttc21b* is required to restrict Shh activity in the mouse forebrain"	Wnt1expression reduced in the diencephalon of aln mutants	(Stottmann, Tran et al. 2009)
Kif7/ Jbts12	Also known as *kif7*. *Kif 7* is a known regulator of shh signalling (Goetz and Anderson 2010) "Kif 7 acts downstream of Smo and upstream of Gli2 and has both negative and positive effects on Shh signalling". (Liem, He et al. 2009). (B) Kif7 also regulates Gli transcription factors	ND	Liem, He et al. 2009) (B) Cheung, Zhang et al. 2009)
Tctn1/ Jbts13	*Tctn1* regulates Shh signalling downstream of smoothened. Shh is not expressed in T*ctn1* mutant neural tube. Gli1 and ptch is reduced in the neural tubes of *tctn1* mutants	ND	(Reiter and Skarnes 2006)
Tmem237/ Jbts14		Tmem237 increased levels of β-catenin observed in *Tmem237* transfected mouse inner medullary collecting duct cells when compared to wt cells	(Huang, Szymanska et al. 2011)
Cep41/ Jbts15-Tmem138/ C5orf42/Jbts17		ND	
Tctn2	Polydactyly and neural tube defects consistent with Shh defects. SAG activation of Shh pathway in MEFS (Shh agonist) resulted in negligible	ND	

	responsiveness compared to wt with a 20 fold increase. *Tctn2*$^{-/-}$ emrbryos had increased expression of Gli3 activator compared to wt. *Tctn2* is important for Gli3 processing.		(Sang, Miller et al. 2011)
Tctn3/ Jbts18	*Tctn3* is necessary for the transduction of Shh pathway as revealed by abnormal Gli3 processing in patient cells. *Tctn3* cells failed to respond to Shh agonist	ND	(Thomas, Legendre et al. 2012)
Tmem231	*Gli1* reduced in *Tmem231* knockout embryos by qRT-PCR. Only 10% of *Tmem231* knockout MEFs contained a primary cilium while 55% wild types contained a primary cilium. Die at E15.5 with severe vascular defects. Phenotypes which are consistent with defective Shh signalling microphthalmia and polydactyly.	ND	(Chih, Liu et al. 2012)
Nphp1	ND	ND	ND
Nphp2	Conflicting results in the *invs/invs* kidney no change observed in wnt pathway (A) in *invs/invs* MEFs β-catenin target genes are upregulated Also See *JBTS7*, *NPHP3* and *NPHP4* as *NPHP2* interacts with these genes resulting in defective Wnt signalling defects.		(A) (Sugiyama, Tsukiyama et al. 2011), (B) (Veland, Montjean et al. 2013)
Nphp3	ND	(A) Interacts with *invs* (*Nphp2*), inhibits Wnt signalling by inhibiting dishevelled, also gastrulation and neurulation defects as well as shortened body axis and dorsal bending in xenopus occured which suggest a role in Wnt pathway. (B) studies in Human embryonic kidney cells suggest that *Nphp3* inhibit the wnt signalling pathway as well	(A) (Bergmann, Fliegauf et al. 2008) (B) (Simons, Gloy et al. 2005)
Nphp4	ND	(A) Inhibits canonical Wnt signalling negatively regulates β-catenin signalling (B) *Nphp4* represses the wnt pathway in zebrafish cloaca and in mammalian kidney cells in culture by interacting with *Invs/Nphp2* and dishevelled regulating dishevelled stability and subcellular localisation	(A) (Borgal, Habbig et al. 2012) (B) (Burckle, Gaude et al. 2011)
Iqcb1	Alias *Nphp5* ND	ND	ND
Cep290	Shh signalling reduced in JS human fetal purkinje cells	ND	(Aguilar, Meunier et al. 2012)
Glis2/ Nphp7	Also known as Glis2 (Gli similar 2), Glis2 is a functional component of Shh signalling. Glis2 is necessary to inhibit the Shh signalling pathway to maintain tubular epithelial phenotype in the adult kidney. *Glis2*$^{LacZ/LacZ}$ mouse model n-myc Downregulated. Glis2 interacts with sufu subjecting it to ubiquitination.	(B) At amino acid 170-193 Glis2 interacts with β-catenin. This region also contains the 1st zinc finger motif of Glis2 and this study suggests that Glis2 functions as a negative regulator of β-catenin/TCF mediated transcription using yeast 2 hybrid screening systems. It was also found that Glis2 represses the Wnt/β-catenin pathway as it represses the human *cyclin D1* gene which is a natural Wnt target gene	(Li, Rauhauser et al. 2011) and (Attanasio, Uhlenhaut et al. 2007) (B) (Kim, Kang et al. 2007)
Rpgrip1l/ NPHP8	See JBTS7 above		
Nek8		*Jck* deficient mice repressed β-catenin expression in the wnt pathway in osteocytes	(Sabbagh, Graciolli et al. 2012)
Sdccag8	ND	ND	ND
Tmem67 / Nphp11 and *Ttc21b/ Nphp12*		See *Jbts6* above and *Jbts11* above	
Wdr19/ Nphp13	*Ift144twt* MEFs did not respond to Shh agonist SAG like the wild type MEFs did by *Ptch1* expression, WISH showed an increase of *Ptch1* expression in whole mount embryos particularly in the facial prominences and limbs	ND	(Ashe, Butterfield et al. 2012)
AHI1	See *Jbts3* above		
Atxn10,Znf423/ Nphp14, *Cep164/Nphp15*, *Anks6. Xpnpep3* and *Slc41a1*		Currently no links to shh or wnt signalling identified-as they have not been investigated	

Table 1.6 Linking NPHP and JBTS mutations to disrupted Wnt and Shh signalling pathways.

Table 1.6 highlights the disrupted Wnt and or Shh signalling pathways previously associated with NPHP and JBTS mouse models or cell lines. ND not discussed/not defined. MEFs (Mouse Embryonic Fibroblasts);Wt (Wild type). Note (B) and (C) represent other studies and the references for those studies, linking either defective Wnt and or Shh signalling pathways with mutations in the same gene.

1.15 Defective Shh/Wnt signalling identified in *Nphp* mouse models

Two of the *Nphp/Jbts* mouse models mentioned in Table 1.6 present with late onset NPHP, the *Ahi1*$^{-/-}$ mouse model and the *Glis2*$^{-/-}$ /*Nphp7*$^{-/-}$ mouse model (Lancaster, Louie et al. 2009; Li, Rauhauser et al. 2011).

The *Ahi1*$^{-/-}$ mouse model showed reduced Wnt signalling in 5 month-old *Ahi1*$^{-/-}$ kidney samples when compared to wild-type mice. Expression levels of the *Lef1* gene (downstream target of the Wnt pathway) was reduced in the *Ahi1*$^{-/-}$ mice therefore suggesting Wnt signalling was reduced (Table 1.6) (Lancaster, Louie et al. 2009).

The *Nphp7* mouse model showed that Glis2 (Gli similar 2), is a functional component of the Shh pathway. Gli transcription genes are activated when the Shh pathway is active. The *Glis2*$^{-/-}$ mouse model identified that “Glis2 interacts with Sufu subjecting it to ubiquitination and therefore affecting the signalling cascades of the Shh pathway”. Sufu is an important for maintaining the balance between Gli activators and repressors. In the absence of *Glis2* Shh activity was increased in the kidney when the organ was fully matured (Li, Rauhauser et al. 2011).

“Hedgehog signalling is crucial during embryogenesis as it controls tissue patterning and cell fate specification” (Ingham and McMahon 2001). In a mouse model of Nphp, *Glis2* was found to be mutated in NPHP type 7 (Attanasio et al., 2007). *Glis2* mice displayed features of NPHP including renal atrophy and prominent fibrosis (Attanasio et al., 2007). Loss of *Glis2* resulted in the up-regulation of genes that promote epithelial to mesenchymal transition, possibly providing an explanation for the fibrosis associated with NPHP and loss of Gli2 also implicates the Shh pathway in the pathogenesis of cystic kidney diseases (Hurd and Hildebrandt 2011).

The *Ahi1*$^{-/-}$ and the *Glis2*$^{-/-}$ mouse models develop kidney cysts when the kidneys are fully matured i.e. when the mice are classified as adults. Currently there are no murine models for the juvenile form of NPHP. Therefore there is a gap in understanding the defected signalling mechanisms associated with juvenile NPHP. Hence a novel mouse model of juvenile NPHP may lead to a new understanding of disease pathogenesis.

1.16 Defective Shh signalling in JBTS/MKS mouse models

Intriguingly 15 of the 40 mutated NPHP/JBTS protein products were associated with disrupted Shh pathway signalling, in comparison to 10 of the mutated NPHP/JBTS protein products associated with Wnt signalling defects (Table 1.6). Neural tube defects were observed in 6 of the 12 genes associated with Shh signalling defects which included mouse models with mutations in the *JBTS6/NPHP11*, *JBTS8*, *JBTS10, JBTS11/NPHP12, JBTS13*, and *TCTN2* genes (Ferrante, Zullo et al. 2006; Reiter and Skarnes 2006; Caspary, Larkins et al. 2007; Vierkotten, Dildrop et al. 2007; Stottmann, Tran et al. 2009; Larkins, Aviles et al. 2011; Sang, Miller et al. 2011; Abdelhamed, Wheway et al. 2013).

There are known specific downstream transcription factors of Shh (Ruiz i Altaba 1997). Ci is a specific downstream factors and correct levels of functioning Ci is required to mediate Shh signalling in flies and in frog embryos. Ci is a family member of the Gli transcription factors (Ruiz i Altaba 1997).

Since the discovery of abnormal Ci functioning in the fly was linked to Shh signalling defects, abnormal Gli processing has been found in NPHP/JBTS murine models associated with developmental defects including neural tube patterning defects and polydactyly (Ferrante, Zullo et al. 2006) and (Hoover, Wynkoop et al. 2008).

The JBTS mouse models with abnormal Gli processing in neural tube patterning and limb morphology include; the *Ftm*$^{-/-}$ mouse model representing mutations in *JBTS6/NPHP11;* the *Tctn1*$^{-/-}$ mouse model representing *JBTS13* mutations, the *Tctn2* mouse model and the *Tmem231*$^{-/-}$ mouse model. These all showed abnormal Gli processing which were linked to Shh signalling defects (Table 1.6).

NPHP/JBTS mutations which have been associated with defective Wnt or Shh signalling have mostly been identified in the developing neural tube, in the brain or MEFs (Table 1.6). However, to date there are no reports of which signalling pathway may be influencing the juvenile form of NPHP associated with known *NPHP/JBTS* genes.

1.17 *CEP290* mutations and *Cep290* animal models

A broad range of ciliopathy phenotypes are caused by *CEP290* mutations (Aguilar, Meunier et al. 2012), therefore a novel *Cep290* mouse model would be an ideal model to study the molecular mechanisms associated with the NPHP/JBTS phenotype caused by mutations in the *Cep290* gene.

The number of identified mutations in the *CEP290* gene is continuously rising and a CEP290 database has been generated to accumulate the mutations in one online resource http://medgen.ugent.be/cep290base/overview.php .The majority of *CEP290* mutations identified in patients are truncating mutations (Coppieters, Lefever et al. 2010) hence a novel mouse model with a truncated mutation in the *Cep290* gene is required.

To date there is only one *Cep290* mouse model described in detail, known as the *Rd16* mouse. In the *Rd16* mouse model a 300 amino acid in-frame deletion of *Cep290* exclusively causes retinal degeneration without any renal or cerebellum involvement, as the splicing mutation affects the eye tissue but not renal tissue (Chang, Khanna et al. 2006; Hildebrandt and Zhou 2007).

Cep290 knockdown experiments in zebrafish resulted in defects of JBTS, comprising of retinal degeneration, cerebellar abnormalities with an abnormal mid-brain to hindbrain malformation associated with hydrocephaly and pronephric cyst formation (Sayer, Otto et al. 2006; Schafer, Putz et al. 2008).

1.18 CEP290 and its sub cellular location in primary cilia

Previous studies have demonstrated that *Cep290* is required for cilium formation and that *Cep290* is located in the transition zone of cultured mouse neural progenitor cells (Aguilar, Meunier et al. 2012), hTERT-RPE1 cells and from Inner medullary collecting duct 3 (IMCD3) cells (Tsang, Bossard et al. 2008; Garcia-Gonzalo, Corbit et al. 2011; Sang, Miller et al. 2011). In the G_0 phase CEP290 was found on both the daughter and mother centriole of the primary cilia assembly in transfected human cells (Tsang, Bossard et al. 2008).

Cep290 expression was previously detected in the connecting cilia of rod cells of the mouse retina (Chang, Khanna et al. 2006; Sayer, Otto et al. 2006) and in olfactory sensory neurons, Cep290 was also found to localise to the dendritic knobs (McEwen, Koenekoop et al. 2007). Hence this suggests that JBTS patients with *CEP290* mutations may be caused by ciliary defects but they have not proven it. There is still no evidence of the exact mechanism (whether ciliary defects and/or signalling through the cilium are involved) that is defective in NPHP patients from *CEP290* mutations.

1.19 CEP290's interacting partners.

In epithelial cells, CEP290 was found to interact with ATF4/CREB2, a transcription factor known to be implicated in cAMP- dependent kidney cyst formation (Sayer, Otto et al. 2006). cAMP pathway is thought to play a role in cell proliferation, stimulating apical chloride secretion and driving the accumulation of cyst fluid in kidney cyst formation in both ADPKD and ARPKD renal epithelia (Calvet and Grantham 2001) and (Sweeney and Avner 2006).

CEP290 interacts with several centrosomal and ciliary proteins (Coppieters, Lefever et al. 2010). Coimmunoprecipitation experiments using mouse or bovine retinal extracts showed that Cep290 is in a complex with dynactin subunits p150^{Glued} and p50- dynamitin, kinesin subunit KIF3A, kinesin-associated protein (KAP3), centriolar components γ-tubulin and pericentrin, centrin, pericentriolar material (PCM1), ninein, chromosomal partition protein (SMC)1, SMC3, retinitis pigmentosa GTPase regulator (RPGR^{0RF15}) and RPGRIP1 (Chang, Khanna et al. 2006).

CEP290 was also found to interact with CP110 (known to suppress ciliogenesis) and it is suggested that CP110's main role in interacting with CEP290 is to keep CEP290 inactive in growing cells until cells are ready to undergo ciliogenesis (Tsang, Bossard et al. 2008). The same study also suggests that CEP290 cooperates with Rab8a (a protein required for ciliary biogenesis to promote ciliogenesis (Yoshimura, Egerer et al. 2007) and (Tsang, Bossard et al. 2008).

CEP290 was also found to specifically interact with CC2D2A at amino acids 703-1130 which contain the coiled-coil domains 4-6 (Gorden, Arts et al. 2008). CC2D2A mutations were found in a subset of JBTS patients. CC2D2A encodes a coiled-coil domain with predicted structural similarity to RPGRIP1L/NPHP8 (Gorden, Arts et al. 2008). Intriguingly CC2D2A mutations can also cause multi-spectrum disorders which include BBS, JBTS, LCA and renal cysts (Arts, Doherty et al. 2007; Delous, Baala et al. 2007; Gorden, Arts et al. 2008). The C-terminal region of CC2D2A is related to the CEP76 protein (Andersen, Wilkinson et al. 2003). This is significant as CEP76 was also found to react with CP110 (Tsang, Spektor et al. 2009) and it was found that CEP76 and CP110 together to suppress cilia assembly (Spektor, Tsang et al. 2007).

Cep290 was found to be recruited to centriolar satellites along with BBS4 by PCM-1 which is required for the organisation of the cytoplasmic microtubule network (Kim, Krishnaswami et al. 2008). Cep290 was also found to bind $RPGR^{ORF15}$ in the *Rd16* mouse leading to aggregation of $RPGR^{ORF15}$ in the inner segments and redistribution of rhodopsin and arresting throughout the plasma membrane (Chang, Khanna et al. 2006). Another example of CEP290 interacting with a protein associated with a ciliopathy disease is NPHP5. NPHP5 was shown to specifically bind to a region of CEP290 encompassing both the coil coiled 3 domains and part of the SMC homology domain (Schafer, Putz et al. 2008). From these examples it is clear that CEP290 is required for ciliogenesis and therefore it is an important gene to investigate using a novel mouse model.

1.20 Expression patterns of CEP290 in human embryonic and fetal tissue

Recently we have shown that CEP290 expression is prominent in the spinal cord, the developing cerebrum, choroid plexus, the developing hindbrain and the retina in human fetal embryos (Cheng, Eley et al. 2012).

CEP290 expression was also observed in the developing renal collecting duct tubules and glomeruli of human fetal embryos (Cheng, Eley et al. 2012) . Therefore mutations in the *CEP290* gene (leading to a loss of CEP290 function) could result in defects in the normal development of collecting duct tubules.

1.21 The normal physiology of collecting duct tubule (CDT) cells are required to aid in understanding disease pathology of NPHP.

Some NPHP phenotypes are characterised by collecting duct cysts (Hildebrandt and Otto 2000) which are hypothesised to arise due to altered fluid and electrolyte transport in the collecting duct (Saigusa, Reichert et al. 2012).

In using animal models and collecting duct tubule (CDT) cell lines derived from these animal models, an insight into understanding the physiological role of the collecting duct tubule in the kidney has been accomplished.

The CDT is the final site of renal regulation of Na^+ and water balance, with the vasopressin responsive aquaporin 2 (AQP2) water channel playing an important role (Rohatgi, Greenberg et al. 2003). AQP2 expression is localised to the apical cell membrane of the collecting duct system in the presence of vasopressin/anti-diuretic hormone (Devuyst, Burrow et al. 1996). Vasopressin binds to the basolateral membrane resulting in intracellular cAMP levels increasing the phosphorylation of AQP2 by cAMP- dependent protein kinase, AQP2 then fuses to the apical membrane causing the cell to be water permeable (Sands, Naruse et al. 1997).

Within the CDT, Na^+ is reabsorbed from the urinary space into principal cells through the apical ENaC where it is pumped out of the cell at the basolateral membrane in exchange for K^+ via the Na^+-K^+-ATPase (Garty and Palmer 1997; Satlin 1999). ENaC aids in maintaining fluid homeostasis and blood pressure under the control of aldosterone (via the RAAS system) acting on the mineralcorticoid receptor (Canessa, Schild et al. 1994; Garty and Palmer 1997).

1.22 ARPKD CDT cell lines previously studied

Numerous ARPKD CDT cell line models have been generated.An example of an ARPKD CDT cell line study involved the generation of conditionally immortalised cells from fetal kidneys diagnosed with ARPKD renal cysts where they showed that Na^+ absorption (through ENaC expression) is increased in the CDT by at least twofold greater than wild type CDT cells (Rohatgi, Greenberg et al. 2003).

In the *orpk* ARPKD mouse model CDT cells were isolated and cultured confirming that Na^+ absorption was up regulated in an ARPKD model (Olteanu, Yoder et al. 2006). Such studies indicate that ENaC mediated sodium absorption is an important ion transport pathway which when disrupted may influence the development of cysts (Zheleznova, Wilson et al. 2011).

1.23 Using animal models to test potential target ADPKD drugs.

From the use of studies determining the physiological state of CDT cysts, a target V2 receptor antagonist drug called OPC-31260, was found to lower renal cAMP and reduce cystogenesis, i.e slow the effect of PKD in three animal models of ADPKD and ARPKD which included the PCK rat (ARPKD) (Gattone, Wang et al. 2003; Wang, Gattone et al. 2005), *pcy* mouse (NPHP3- adolescent NPHP) (Gattone, Wang et al. 2003) and the $Pkd2^{-/tm1Som}$ mouse (ADPKD)(Torres, Wang et al. 2004) as reviewed by (Torres 2004; Nagao, Kugita et al. 2012).

Another V2 receptor antagonist drug the OPC-41061, (a more potent V2 antagonist than the OPC-31260 for humans) was also tested in PCK rats to confirm that this antagonist also lowers renal cAMP and slows the effect of PKD. The conclusion from the OPC-41061 PCK rat study was that OPC-41061 is an effective V2 receptor antagonist as it slows cyst progression in PCK rats and the study suggested that this drug should be used in ADPKD clinical trials (Wang, Gattone et al. 2005).

Peroxisome proliderator-activated receptor (PPAR)- γ agonist are pharmalogical agonists which inhibits growth by causing the cell cycle to arrest, by down regulating the ERK/mTOR pathway and decreasing inflammation and fibrosis by downregulation of TGF-β. PPAR- γ agonists has been found to improve animal models of PKD (Yoshihara, Kurahashi et al. 2011; Nagao and Yamaguchi 2012; Yoshihara, Kugita et al. 2012).

The receptor tyrosine kinase (RTK) pathway when activated stimulates the mitogen-activated protein kinase (MAPK) components, Raf, MEK and ERK which were increased in the number of cyst-lining cells in the kidneys of *Cy* rats (ADPKD) (Nagao, Yamaguchi et al. 2003), *PCK* rats (Nagao, Nishii et al. 2006), *pcy* mice (Omori, Hida et al. 2006) and *jck* (Smith, Bukanov et al. 2006) mice. Treatment with tyrosine kinase inhibitors decreased PKD progression in the *Cy* rat and the *orpk* and *bpk* mouse models (Richards, Sweeney et al. 1998; Sweeney, Chen et al. 2000; Torres, Sweeney et al. 2003).

A somatostatin drug called octreotide (known to inhibit cAMP) was given to PCK rats to inhibit renal cyst growth. The study found that octreotide inhibited cAMP levels and slowed cyst growth. The kidney weight and cyst volume from PCK rats treated with octreotide were reduced, concluding that octreotide is a potential drug for treating ADPKD (Masyuk, Masyuk et al. 2007).

Interestingly by increasing water intake, reduced intracellular cAMP was evident through reduction of plasma levels by vasopression and therefore decreased the progression of PKD in the PCK rat (Nagao, Nishii et al. 2006). Therefore increasing water intake could potentially aid in decreasing the progression of PKD in coherence with other target therapies.

1.24 Treating PKD patients

Currently there are no drugs which are suitable for treating renal cysts in ADPKD, ARPKD and NPHP. Patients with PKD are currently “managed” by controlling blood pressure and cardiovascular management as 40% of PKD patients have high blood pressure http://www.pkdcure.org/research/clinical-trials/blood-pressure.

Rapamycin is a pharmaceutical drug which has been found to inhibit the mTOR pathway (Sabers, Martin et al. 1995). An increase in kidney volume was found in patients treated with rapamycin (Stallone, Infante et al. 2012) (which is also consistent with the decline of GFR when the kidney volume reaches 1500ml (Walz, Budde et al. 2010)). There were also a number of side effects associated with rapamycin treatment which include hyperlipidemia, pneumonia, oral ulcers, and oedema. In higher doses of rapamycin treatment (3ng/ml) a reduction in cyst volume was evident however it was concluded that it does not significantly affect the progression of ADPKD (Stallone, Infante et al. 2012).

Everolimus is another mTOR inhibitor and has been recently used in a clinical trial involving 433 patients with ADPKD. It was found that Everolimus slowed kidney volume but had no effect on the cystic phenotype. There were also a number of side effects associated with the use of everolimus which include leukopenia, thrombocytopenia, hyperlipidemia, increased cholesterol levels and angioedema to name a few, therefore this drug is not suitable for treating ADPKD patients (Walz, Budde et al. 2010). Another 2 clinical trials using a mTOR inhibitor called Sirolimus also found similar results to rapamycin and everolimus treatments confirming that mTOR inhibitors alone are not suitable for treating PKD (Serra, Poster et al. 2010) and (Perico, Antiga et al. 2010).

Octreotide (a somatostatin agonist) was recently used in an ADPKD clinical trial. ADPKD patients treated with octreotide had minimal changes in kidney volume in response to octreotide as well as minimal changes in glomerular filtration rate although they did see a reduction in cyst growth. The adverse side effects included hair loss, diarrohea, abdominal cramps, nausea, vomiting dizziness and headaches. The study concluded that combination therapies would be required and that longer and larger clinical trials would also be required to establish the long term efficacy of octerotide (Hogan, Masyuk et al. 2010).

A phase III clinical trial using Tolvaptan (also known as OPC-41061) in ADPKD patients has recently been completed. Tolvaptan is a vasopressin V2-receptor antagonist (Shiba and Yokoyama 2012). The results of the tolvaptan 3 year clinical trial show a slowed increase in renal volume and decline in renal function (when measuring serum creatinine levels) when compared to a placebo, overall slowing the rate of disease progression. However, there have been adverse side effects of tolvaptan seen in the trial which include elevated liver enzyme levels and events related to aquaresis (excretion of electrolyte-free water) which contributed to a high discontinuation rate (Torres, Chapman et al. 2012).

The results from the clinical trials highlight that other target therapeutic drugs are required in order to manage PKD at an earlier time point in the disease course, in order to give the juvenile NPHP patients a better standard of living. Of note, the patients in the clinical trials above were 18 yrs old and older http://www.pkdcure.org/research/clinical-trials.

Blood pressure maintenance is crucial for slowing the progression of PKD. Currently there are 2 stage 3 clinical trials in the USA recruiting 8-21 yr old patients to test the effect of Statin therapy on PKD disease progression. Statins targets the angiotensin II pathway reducing hypertension (Cadnapaphornchai, George et al. 2011). This is the only drug which is currently and has ever been used in clinical trials for patients younger than 18 yrs of age with PKD. As the clinical trial is still ongoing no results are available as of yet.

As mentioned earlier increased water intake in the PCK rat decreased the progression of PKD. A pilot study was recently carried out in 8 ADPKD patients to determine if increased water intake would reduce PKD progression it is thought that this will aid in slowing the disease however it will not cure the disease (Wang, Creed et al. 2011).

1.25 Aims of this study

Currently there are no suitable therapies for treating juvenile NPHP. Also there are no representative animal models of juvenile NPHP. There are published articles of *Nphp* mouse models with defective Shh and Wnt signalling in the neural tube, MEFs and limb tissue. However these signalling pathways have not been investigated in the early stages of a cystic phenotype in renal tissue of *Nphp* mice.

This study aims to focus on;

1. Generating a novel *Cep290* NPHP mouse model and a CDT cell line model derived from this novel *Cep290* NPHP mouse model.
2. Investigate and resolve if there is defective Shh and or Wnt signalling implicated in the early stages of a cystic phenotype in this novel juvenile NPHP mouse model.
3. To identify abnormalities prior to overt cyst formation; at the earliest stages of disease
4. Provide a novel juvenile CDT cell line and mouse model for potentially testing new target drugs prior to an overt cystic kidney phenotype.

Chapter 2 Materials and Methods

A range of molecular techniques, histological techniques and tissue culture techniques were employed in this study. These techniques were employed in order to characterize a novel *Cep290* mouse model and to investigate possible signaling pathway defects associated with juvenile NPHP. The tissue culture techniques were utilised on a collecting duct tubule cell line isolated from the *Cep290* mice and this cell line was used to test the effects of a potential Shh therapeutic agonist purmorphamine.

2.1 DNA extraction.

Genomic DNA was extracted from mouse ear clips/cell pellets after boiling in a lysis solution at 95°C for 30 min in 100µL of 25mM NaOH;0.2mM ethylene diamine tetra acetic acid (EDTA). The DNA was neutralised using 100µL of 40mM Tris-HCl at pH 5.0. 5µL of DNA was then added to each PCR reaction required.

2.2 Mouse genomic DNA extraction.

Mouse ear clips/cell pellets were lysed in 25mM NaOH/0.2mM EDTA (typical volume 100ul) at 95°C for 30 min. The reaction was neutralised with an equal volume of 40mM Tris-HCl pH 5.0.

2.3 Genotyping, Polymerase Chain Reaction (PCR)

Genotyping was required to distinguish between A) *Cep290* wild type, heterozygous (will have one copy of the wild type and one copy of the mutant DNA) and homozygous animals and B) Immortal (*H-2Kb-tsA58*) wild type and heterozygous animals. DNA extracted from transgenic mice was amplified from Genomic DNA (Table 2.1 for oligonucleotide primers used for genotyping.) The immorto mouse primers used were designed by (Kern and Flucher 2005). The *Cep290* primers were designed using online tools i.e http://frodo.wi.mit.edu/

Gene Name	Forward Oligonucleotide Primer	Reverse Oligonucleotide Primer	Predicted DNA bp length
Cep290 F4	5'-CATGTCTGCCTCCTTTAGTG-3'	*CEP290* R2 5'-GGCCTGCTAAACCTGAAC-3'	Wild type (550bp)
Cep290R5	5'-CATGTCTGCCTCCTTTAGTG-3'	5'-CACTTCACATGGTATTGCTC-3'	Mutant (300bp)
Immorto_wt	5'-GATCTGCCTGAGGTGTTACTTG-3'	5'-GGATGGCATCACTAGTCATGAC-3'	Wild type (509bp)
Immorto_tsA	5'-AGTCCTCACAGTCTGTTCATGATC-3'	5'-GGATGGCATCACTAGTCATGAC-3'	Mutant (300bp)

Table 2.1 Cep290 and Immorto mouse genotyping primers.
Forward and reverse primer pairs for identifying the genotype of *Cep290* and *Immorto* mice. The PCR reactions including annealing temperatures are shown in section 2.3

2.4 PCR protocol

A typical PCR reaction consisted of 50-100ng of DNA, 10pmol of each primer and Taq PCR Mastermix provided by Qiagen (cat # 201443) with a final concentration of 1.5mM $MgCl_2$ and 200µM of each dNTP). Cycling conditions were as follows; 95°C for 3 min, 94°C for 5 s, 57°C for 1 min, 72°C for 1 min for 30 cycles, 72°C for 10 min and a final hold of 4°C. The annealing temperature step of 57°C was adjusted according to the melting temperature of each primer pair. A 4°C hold was required to stabilise the PCR product and to prevent degradation.

2.5 Agarose Gel Electrophoresis

PCR products were analysed using agarose gel electrophoresis. Typically 1X of loading buffer (New England Biolabs cat # B7021S) was added to 50ng of PCR reaction and loaded on a 2% w/v agarose gel (NBS biological Agarose Low EEO cat # NBS-AG500) with 1X TAE. A 2% gel was generally preferred as the products were approximately 200bp-600bp in length. Gel red was added to agarose prior to pouring the gel for casting to visualise the DNA bands. 100 bp ladder (New England Biolabs cat # N3231L) was also included to calculate the size of the DNA bands. DNA bands were sufficiently separated after 60 minutes at 100V.

2.6 Ribosomal Nucleic Acid (RNA) extraction from Tissue.

Whole mouse kidney was isolated and homogenised in 500µl - 3mls TRIzol® reagent (the amount required depended on the size of the tissue) (Invitrogen,Cat# 15596-026) on ice for ~2 min or until the tissue was disrupted. The excess kidney and insoluble material was pelleted following centrifugation at 12,000g for 10 min at 4°C and the supernatant was transferred to a new screw cap tube. For every 1ml of TRIzol used to disperse the tissue, 200µL of chloroform reagent (Sigma, cat # C2432-25ml) was added to the sample followed by vigorous agitation by hand for 10 s. The sample was immediately incubated for 3 min at room temperature followed by centrifugation at 12,000g for 10 minutes at 4°C to separate the organic phase from the aqueous phase. The aqueous phase (the supernatant) was transferred to a new screw cap tube and RNA precipitation occurred by adding 500µL (amount relative to 1 ml of TRIzol used for dispersing tissue) of Isopropanol. This was then incubated at room temperature for 10 min and centrifuged at 12,000g for 10 min at 4°C. The supernatant was removed and the pellet was resuspended in RNAse-free 70% ethanol to remove any excess isopropanol; followed by centrifugation at 7,500g for 5 min at 4°C. The supernatant was removed and the RNA pellet air dried for 20 min. The RNA pellet was re-suspended in 20µL RNAse-free water, aliquoted and stored at -80°C. RNA was quantified (as ng/µL) at an absorbance of 260-280nm using the Nanodrop spectrophotometer ND-1000.

2.7 Illumina Microarray

The Illumina MouseWG-6 v2 Expression BeadChip (Source Bioscience) was critical for studying an unbiased list of genes, their expression levels and their link to the molecular pathways influencing the cystic renal phenotype of this novel *Cep290* mouse model*. "*More than 45,200 transcripts, along with the accessibility of testing six samples simultaneously, are available on a single BeadChip. The BeadChip content is derived from the National Center for Biotechnology Information Reference Sequence (NCBI RefSeq) database (Build 36, Release 22), supplemented with probes derived from the Mouse Exonic Evidence Based Oligonucliotide set as well as exemplar protein-coding sequences described in the RIKEN FANTOM2 database." http://www.illumina.com/products/mousewg_6_expression_beadchip_kits_v2.ilmn

2.7.1 Illumina Microarray sample preparation.

The left kidney from newborn *Cep290*$^{+/+}$ and *Cep290*$^{LacZ/LacZ}$ mice were dissected and RNA was extracted as described in section 2.6 for microarray analysis. Total RNA (measured with the Nanodrop spectrophotometer ND-1000) of 50-500ng in diethylpyrocarbonate (DEPC) treated H_20 with an absorbance of 1.9 or greater at 260-280nm was sent for microarray analysis. The quality control measures utilised by Illumina included the use of spectrophotometry (LSN-X-013) and an agilent bioanalyser (LSN-X-024) which analyses the sensitivity of total RNA in a sample.

2.7.2 Normalisation of Illumina Microarray Data.

The dataset generated from the Illumina MouseWG-6 v2 Expression BeadChip required normalisation to remove non-biological variation between samples and quality control tests (t-tests, fold changes) for differential expression using the Beadstudio analysis programme. A non-biological variation can vary between high back round on an array, low signal or poor stringency. A microarray experiment performance can be achieved by clustering samples using sample clustering (biological replicates from the same cellular origin will cluster together), box plots (a quick way to identify variation within an array- some samples may show abnormally high levels of signal intensities) or scatter plots (an asymmetrical scatter plot may be an indication of a poor quality sample).

2.7.3 Data analysis

Data Analysis and normalisation was kindly provided by Dr. Matthew Bashton from the Bioinformatics Support Unit, Newcastle University. Briefly data analysis was carried out using the R (bioconductor) lumi package with a superior normalisation method. A list of genes was generated from the package with cut-offs adjusted to a p value of 0.05 and a fold change of 1.0

2.8 Reverse Transcription (RT)

Reverse transcription was required to produce cDNA from RNA using Superscript III® reverse transcriptase as per manufacturer's instructions (Invitrogen cat # 18080-044). For each RT reaction 1µL of 10mM dNTPs mix (containing dATP, dCTP, dGTP, and dTTP) and 1µL of 0.1M random hexamers was added to 2µg of RNA. This solution was then incubated at 65°C for 5 minutes to allow annealing of the random primers and immediately returned to ice. The following was then added to the RNA-primer mix;

1. 4µL of 5X first strand buffer (containing 250 mM Tris-HCl [pH 8.3 at room temperature], 375 mM KCl, and 15 mM MgCl2),

2. 1µL of 0.1M DTT (DTT is required for RT and Taq polymerase as it reduces disulfide bonds),

3. 40 Units of RNaseOUT™ (Invitrogen cat # 10777-019) [note RNaseOUT™ inhibits 200ng of RNase A by 50% using cytidine 2´, 3´ cyclic monophosphate (cCMP) as the substrate]

4. 200 units of Superscript III® (Invitrogen cat # 18080044) [note Superscript III® is a purified enzyme from *E.coli* containing a modified gene of Moloney Murine Leukaemia Virus, this enzyme is used to synthesise cDNA of 100bp up to > 12kb from single stranded RNA.

cDNA was then generated using the following cycling conditions; 50°C for 50 min, 70°C for 15 min and cooled to 4°C. The cDNA was then stored and aliquoted at -20°C until required.

2.9 Quantitative PCR (qPCR)

Genes selected for analysis (from the list of genes generated using the lumi R package in section 2.7.3) were quantified using qPCR techniques. Primers were designed across exons before and after the probe sequence obtained from the microarray to remove and residual genomic DNA amplification. The software programme used to design the qPCR primers was http://www.ensembl.org/index.html (to obtain the cDNA sequence of the gene of interest) and http://frodo.wi.mit.edu/ (to design primers around the area of interest).

10µL reactions for qPCR consisted of 1µg of cDNA, RNase free H20, 10µM of forward and reverse primers and 2X of sybergreen solution (Sigma cat # s4438) [sybergreen is a fluorescent dye that binds all double-stranded DNA and detection is monitored by measuring the increase in fluorescence at 494nm throughout the PCR cycle]. The conditions were as follows; 95°C for 15min, 95°C for 30s, then for 39 cycles, 60°C for 30s, 72°C for 30s, 74°C for 10s with a final melt curve incubation consisting of 68°C for 10s up to 99°C for 10s. All primers used for qPCR can be found in Appendix 1. The housekeeping genes chosen were *Gapdh* and *Hprt*. The minimum information for publication of quantitative real-time PCR experiments (MIQE) guidelines were utilised as they were necessary to ensure the minimum set of requirements were adhered to enable other researchers to replicate our findings (Bustin, Benes et al. 2009; Bustin, Beaulieu et al. 2010; Bustin, Benes et al. 2011). RT-PCR was also carried out qualitatively. The PCR cycling conditions for this were as per section 2.3. We used housekeeping genes consisting of *Gapdh* and *Hprt* (as above) to provide normalisation of the cDNA samples. Samples were compared to controls visually (when there were comparable differences by eye).

2.10 Mouse Husbandry.

Cep290 mice were generated using customised ES cell lines obtained from the Sanger Institute Gene Trap Resource (SIGTR). *Cep290*$^{LacZ/+}$ animals were maintained on the C57BL/6J and the129/Ola background (Charles River UK). Litter frequency and back ground generations used can be seen in chapter 3 characteristics of a novel *Cep290* mouse model.

2.11 Tissue preparation for histology

Mouse tissues were dissected and fixed in 4% paraformaldehyde/PBS(PFA) (Sigma cat # 158127) at 4°C for various durations of time depending on the age of the tissue (Table 2.2), the type of tissue sample (liver/eye were stored for 1 week/overnight) and if X-gal staining (10 min) was to be applied on the tissue. Eye samples were not embedded in wax (Section 2.11.2)

Incubation Required	Newborn Kidney/ Eye tissue	2 week old Kidney	1 month old Kidney	6 month old Kidney	1 year old Kidney/Liver	Temperature Required
4% PFA	Overnight	2 nights	3 nights	5 nights	1 week	4°C
PBS wash	5min (3 X)	5min (3 X)	5min (3 X)	5min (3 X)	5min (3 X)	Room Temp
50% EtOH/ddH$_2$0	1h (X2)	2h (x2)	3h (x2)	5h (x2)	5h(x2)	Room Temp
70% EtOH/ddH$_2$0	1h (X2)	2h (x2)	3h (x2)	5h (x2)	5h(x2)	Room Temp
95% EtOH/ddH$_2$0	1h (X2)	2h (x2)	3h (x2)	5h (x2)	5h(x2)	Room Temp
100% EtOH/ddH$_2$0	1 h (X2)	2 h and O/N	3 h and O/N	5 h and O/N	5 h and O/N	Room Temp
100% Histoclear	20min(x2)	20min(x2)	30min(x2)	1h (x2)	1h (x2)	Room Temp
Histoclear * / Wax	30min	40min	40min	1h	1h	Heat at 60-65°C
Wax	30 min(x6)	40 min(x6)	40 min(x6)	1h(x6)	1h (x6)	Heat at 60-65°C

Table 2.2 Paraffin wax embedding protocol for various kidney tissues. All kidney tissues are fixed in 4% PFA for various times depending on the age and size of the tissue. The renal tissues are then processed through a series of EtOH increments with a final immersion in Histoclear before hot paraffin wax is added to start the embedding process. The incubation times for an aged matched kidney are clearly labelled from the 4%PFA stage through to EtOH washes, histoclear incubation and finally wax embedding. * Histoclear was obtained from National Diagnostics cat # HS-200. Samples were then embedded in paraffin in a dispomould (Cell Path cat # GAD 1502 O2A) and left to solidify overnight at 4°C. O/N Overnight.

The renal tissue in paraffin blocks were trimmed and 8μM tissue sections were cut using a microtome (Leica Model # RM 2235) The sections were transferred to a 37°C dd$H_2$0 waterbath where they were stretched out (Thermo Scientific cat # 12638566) and then retrieved for adherence to the superfrost plus slides (VWR 631-0447. The slides were then left at room temperature overnight to remove any residual $H_2$0. Superfrost plus slides have a permanent positive charge which aids in adhesion of the tissue to the slides.

2.11.1 Whole mount X-gal staining.

The *Cep290* gene trap contains a β-galactosidase reporter gene. β-galactosidase expression in various tissues of the *Cep290* mouse can be visualised by X-gal staining. X-gal is a chemical analog of lactose that hydrolyses to the β-galactosidase enzyme. Fixed mouse tissue was permeabilised in 0.1M X-gal wash buffer (containing 0.1M phosphate buffer pH7.3, 0.01% Na-deoxycholate, 0.02% Nonidet-P40 and 2mM $MgCl_2$) for 3x15 minutes. Tissue samples were then stained in X-gal staining solution (10mM postassium-ferrocyanide, 10mM ferricyanide and 1mg/ml X-gal in 0.1M X-gal wash buffer) overnight at 37°C in the dark. X-gal itself is colourless however in the presence of an active form of β-galactosidase and ferrous and ferric ions (which provide the electrons for the dimerisation and oxidation reactions) a stable blue product forms. The pH of the staining and wash solution is critical at pH7.3 to allow penetration of the X-gal solution into the tissue samples. When overnight staining was complete the tissue specimens were washed in 0.1M X-gal wash buffer (3 x 30min washes or until the solution no longer turned yellow from the tissue specimens), fixed in 4% PFA overnight at 4°C and stored at 4°C in PBS. Tissue samples were then processed for paraffin embedding.

2.11.2 OCT embedding

Mouse tissue samples were fixed at 4°C for 1h in 4% PFA and embedded in Optimal cutting temperature media (OCT) (obtained from Thermo Scientific cat # LAMB/OCT) on dry ice for 20-25min. 8μM sections were cut using a cryostat (Microm AG Model # HM560) and mounted on to Superfrost plus slides (VWR 631-0447). The sections were stored at -20°C for short term storage and at -80° with a desiccator (for optimal preservation) inserted into each slide box for long term storage until immunofluorescence staining was required. Prior to immunofluorescene and Haematoxylin and Eosin (H&E) staining OCT sections were brought to room temperature for 1h.

2.12 Histology methods.

2.12.1 Brain MRI Imaging.

As described in section 2.11 *Cep290* brain tissues were fixed in 4% PFA at 4°C for various times depending on the size of the brain tissue (Table 2.2 for times) and then stored in PBS. MRI processing and imaging was carried out by Dr. Pete Thelwall at the Newcastle Magnetic Resonance Centre, Newcastle University. The processing involved immersing fixed mouse brains in a 10% neutral buffered formalin solution containing 10 mM gadoteric acid (Dotarem, Guerbet, Shirley, UK) for a period of at least 4 weeks to allow equilibration of T_1 contrast agent through the brain. Samples were then removed from fixative solution and blotted dry, and immersed in a sealed cylindrical plastic container perfluorotributylamine (a susceptibility-matched solution that does not contribute signal to an MRI image). MRI of brain samples was performed on a 7T horizontal bore preclinical scanner (Varian Inc, Yarnton, United Kingdom) equipped with a 25mm diameter ^{1}H birdcage coil (Rapid Biomedical, Rimpar, Germany). Images were acquired using a T_1-weighted 3D gradient echo sequence (TE = 9.5 ms, TR = 35 ms, FOV = 20.48 × 20.48 × 20.48 mm, acquisition matrix = 512 × 512 × 512) with a resultant isotropic image resolution of 40 µm. 6 averages were acquired, resulting in an acquisition time of 15.3 hours. Multiplanar reformatting of resultant datasets was performed using OsiriX (http://www.osirix-viewer.com/) [OsiriX: An Open-Source Software for Navigating in Multidimensional DICOM Images. J Digit Imaging. 2004 Sep;17(3):205-216] to generate coronal, sagittal and transverse views of brain structure.

2.12.2 Rehydrating kidney tissues embedded in paraffin.

Rehydration of paraffin embedded sections was required prior to histological staining. Slides were sequentially added to 100%, 90%, 70%, 50% EtoH/ddH$_2$0 for 2 min each, with a final wash in ddH$_2$0 for 5 min.

2.12.3 H+E staining and Mounting coverslips.

H+E staining is a widely used stain to identify any structurally abnormalities in a tissue sample. The haematoxylin stains the nuclei a blue purple colour and eosin stains the collagen and cytoplasm red. Slides were immersed in Harris Haematoxylin (Thermo Fisher Scientific cat # Lamb/230-D) for 30 seconds, rinsed in ddH_20 until the ddH_20 ran clear, followed by immersion in 1% Aqueous Eosin (Thermo Fisher scientific cat # Lamb/100-D) for 5min and rinsed again in ddH_20 until ran clear. Tissue sections were then dehydrated through a series of EtoH (30%, 50%, 70%, 90% and 100%) for 2 min each with a final rinse in histoclear for 10min A drop of DPX (A mixture of Distyrene, a plasticizer, and xylene) mountant (VWR cat # 360294H) was added to the sections and a coverslip placed over the top.

2.12.4 Trichrome Masson Staining

Trichome Masson was used to detect collagen fibers in the kidney specimen. Trichome Masson staining was employed as per manufacturer's instructions (Sigma cat # HT15-1KT) to detect abnormalities in the connective tissue of the kidney, particularly to identify fibrosis in the renal tissue of *Cep290*$^{LacZ/LacZ}$ mice. Sections were immersed in haematoxylin for 30s, rinsed in ddH_20 followed by biebrich scarlet acid fusion staining for 5min, rinsed in ddH_20, immersed in 1 part Phosphomolybdic acid solution to 1 part phosphotungstic acid solution, quickly followed by 5min in Aniline blue solution. Slides were then placed in 1% acetic acid solution for 2min subsequently coverslips were mounted with DPX onto the slides.

2.12.5 Sirius Red Staining

Sirius Red was used to detect if fibrosis was evident in newborn kidneys samples by binding to all types of collagen. All stages of this protocol was performed at room temperature. Briefly paraffin wax sections were immersed in xylene for 10 min, 100% EtoH for 2 min, 95% EtoH for 2 min and rinsed in running water for 2 min before washing in 0.1% acetic acid for 2 min. Slides were then incubated in 0.1% Sirius red F3B for 1 h and washed twice in 0.1% acetic acid. Slides were then rapidly dehydrated in 3 washes of 100% EtoH at 2min each and cleared in xylene for 10 min before mounting in Di-N-Butyle Phthalate in Xylene (DPX).

2.12.6 Nuclear Fast Red Staining

X-gal stained tissue was counter stained with- nuclear fast red solution, (Sigma cat # N3020) to distinguish between *LacZ* (blue) expression and nuclei (red) expression. Sections were rehydrated as described in section 2.12.2, immersed in nuclear fast red for 5 min, rinsed in ddH_20, dehydrated and mounted on coverslips as described in section 2.12.3 Microscopy.

2.13 Light Microscopy

All histology staining samples were visualised with a Zeiss Axioplan microscope. Images were stained as .tif files with scale bars burned into each image and stored on a portable 1 tera byte hard drive and on the Newcastle University hard drive system.

2.14 Electron Microscopy Methods

Processing and imaging techniques for both SEM and TEM were provided by;

1. Dr. Kath White and Ms Tracey Davey, EM Research Services, Newcastle University

2. Caroline Miller, Electron Microscopy Centre, IU School of Medicine, Department of Anatomy & Cell Biology, Indianapolis, Indiana.

2.14.1 Scanning Electron Microscopy (SEM)

Kidneys dissected from *Cep290* mice were fixed at 4°C in 2% gluteraldehyde sorensons phosphate buffer solution (provided by Newcastle University EM services). Briefly samples were rinsed in Sorenson's phosphate buffer several times, dehydrated in EtoH solutions (25%, 50%, 75% and 100% - 30 minutes each) with a final dehydration in $C0_2$ in a Baltec Critical point dryer. Specimens were mounted on aluminium stubs with Achesons Silver Dag and dried overnight. A Stereoscan 240 Scanning Electron Microscope was use employed and images were acquired using the Orion6.60.6 software (protocol provided by EM research services, Newcastle University).

2.14.2 Transmission Electron Microscopy (TEM).

Fresh *Cep290* mouse kidney tissues were fixed at 4°C in 2% gluteraldehyde containing 0.1% sodium cacodylate with a secondary fix in 1% Osmium

Tetroxide for 1h at room temperature. Note the fixation (minimum overnight) time-span at 4°C depended on the size of the tissue for both SEM and TEM techniques.

Samples were dehydrated through various acetone solutions, (25%, 50%, 75% and 100% - 30min each) infused with 25% resin in acetone, followed by 50%, 75%, 100% 30min each and a final 100% resin in acetone for embedding at 60°C for 24h.

1µm sections were cut and stained with 1% Toluidine Blue in 1% Borax. Ultrathin sections (70nm) were then cut using a diamond knife on a Leica EM UC7 ultramicrotome. Sections were stretched with chloroform, thus eliminating compression and mounted on Pioloform filmed copper grids.

The grids were examined on a Philips CM 100 Compustage (FEI) Transmission electron microscope and digital images were required using AMT CCD camera (Deben).

2.15 Tubular basement membrane measurements

The tubular basement membrane thickness was determined by taking measurements across three different areas of the tubule to determine a mean tubular basement membrane thickness. Statistical analysis methods (Section 2.30) were then employed to determine the significance of the results.

2.16 Immunofluorescent staining in *Cep290* renal tissue.

Cryosections were fixed in 4% PFA in PBS and then permeabilised with 0.5% triton/PBS (Sigma cat # X-100) for 10min prior blocking then incubated overnight with shaking at a speed of 24rpm in primary antibody diluted in blocking buffer at 4°C. The following day, the tissue specimens were washed in PBS for 20min, three times. Secondary antibody was applied for 1 hour at room temperature. After washing as previously described, nuclei were stained with VectorShield with 4’6-diamidino-2-phenylindole (DAPI) mounting media (Vector Laboratories H-1200). Tissue specimens were visualised with a Zeiss Axioimager 2 with Apotome microscope. The filter sets used are 488nm (FITC) and 594nm (Rhodamine). Antibodies used in this study along with their dilutions can be found in the appendice 2 and 3.

2.17 Breeding *Cep290*: *H-2Kb-tsA58* mice to generate an immortal collecting duct cell lines

The *H-2Kb-tsA58* mouse line, a kind gift from Dr. Helen Arthur was crossed with the *Cep290* mouse (described above) to generate double transgenic *Cep290*$^{LacZ/LacZ}$:: *H-2Kb-tsA58*$^{+/-}$ and *Cep290*$^{+/+}$:: *H-2Kb-tsA58*$^{+/-}$ mice. The transgene in these mice is usually dormant and can only be activated by culturing explanted cells at 33°C. The *tsA58* is activated permanently at 33°C *in vitro* specifically by the *H-2kb* promoter driven by interferon gamma (IFN–γ) within all cells previously expressing *Cep290* under the control of the splice acceptor ribosomal re-entry site driving the *Cep290* gene trap. All transgenic mouse lines were maintained on the inbred C57Bl6/J background (Charles River UK).

All mouse work was performed under a personal licence (PIL No. 60/12787) granted from the Home Office (United 33 Kingdom) in accordance with the guidelines and regulations for the care and use of laboratory animals outlined by the Animals (Scientific Procedures) Act 1986.

2.18 *Cep290* CDT Cell Culture

The *Cep290*$^{LacZ/LacZ}$ ::*H-2Kb-tsA58*$^{+/-}$ collecting duct cell lines were isolated from kidneys of one month old transgenic mice. Kidney samples were removed, sliced using a sterile scalpel and digested with 0.1% collagenase type II (Worthington Biochemical corportation cat # 41H12763) (0.5%wt/volume) in 0.1% Bovine serum Albumin (Sigma cat # A2153) for 30min at 37°C. This cell suspension digest was then mixed in 1:1 dilution of (cortical collecting duct) *CDT* media as described by Bens *et al.,*(Bens, Vallet et al. 1999) (outlined in section 2.18.1) and plated onto 6 well plates coated with 10 mg/ml *Dolichos Biflorus* Agglutinin (DBA) (Sigma cat # L-2785) (10µg/ml in 0.1M $NaHC0_3$) overnight at 33°C. DBA specifically binds collecting duct principal and intercalated cells. Unbound cells were removed with gentle washing in fresh culture media added and cells were incubated at 33°C in 5% $C0_2$.

2.18.1 CDT media (Bens, Vallet et al. 1999)

A specialised media was used to maintain CDT cells. This consisted of Dulbecco's modified Eagle's high glucose medium [DMEM] (Invitrogen cat # 41966029) and Ham's F12 (GIBCO cat # 21765029) media 1:1 (vol: vol), 5µg/ml insulin (Sigma, culture grade, cat # I 1882), 50nM dexamethasone (Sigma, culture grade, cat # D 8893), 60nM sodium selenate (Sigma, culture grade, cat # S 9133), 5µg/ml transferrin (Sigma, culture grade, ref: T 1428), 1nM Triiodothyronine (Sigma, culture grade, cat # T 5516), 10ng/ml Epidermal growth factor (EGF) from mouse (Sigma, culture grade, cat # E 4127), 20mM Hepes (GIBCO x100 concentrated, cat # 15630-056), 2mM glutamine (GIBCO cat # 25030024), 2% heat inactivated Fetal calf serum (GIBCO cat # 10106-169), 1% penicillin/Streptomycin (Sigma cat # P4333) and 15µg IFN-γ (Invitrogen Recombinant mouse IFN-γ Cat # PMC4031)

2.18.2 Maintenance of *Cep290* CDT immortal cells

CDT media was changed every 48-72 hrs to replenish the cells with nutrients and IFN-γ and cultures were passaged when approximately 70-80% confluent. Cells were briefly washed in PBS and then incubated in 0.05% trypsin- EDTA with phenol red (Invitrogen, Cat # 25300-- 40054) for 5 min at 33°C to dissociate cells from each other and the flask surface as confirmed by light microscopy. An equal volume of heat inactivated fetal calf serum was added to neutralise the trypsin. Trypsinised cells were then centrifuged at 500xg for 5 min and re-suspended in CDT culture medium for continued growth or in recovery cell culture freezing medium (Life Technologies cat # 12648-010) and stored for long term storage in liquid nitrogen.

2.19 Purmorphamine treatment in *Cep290* CDT cells

Purmorphamine was previously shown to activate the Shh signalling pathway (Wu, Walker et al. 2004). Approximately 25,000 *Cep290* renal collecting duct cells were seeded onto 6 well plates and grown to 80% confluency. *Cep290* collecting duct cells were then subjected to 2µM Purmorphamine/DMSO treatment for 72 hrs (DMSO was used as a negative control) and protein/RNA was then collected for analysis. In order to assess the role of the Shh pathway in *Cep290* cells Gli3 Repressor and Activator levels were examined between wild type and mutant cells (treated and untreated). Samples were compared to controls by visual examination.

2.20 Hedgehog Pathway Inhibitior- 4 (HPI-4) treatment in *Cep290 CDT* cells.

HPI-4 was previously shown to inhibit the hedgehog signalling pathway. *Cep290* cells were treated with HPI-4 using the same dosage and controls as purmorphamine treatment (section 2.19). (Hyman, Firestone et al. 2009)

2.21 Immunofluorescent labelling in *Cep290* CDT cells.

Approximately 25,000 *Cep290* renal collecting duct cells were seeded onto coverslips plated on 6 well plates and grown to 80% confluency. Cells were either fixed in 100% methanol on ice for 3 minutes or in 4% PFA for 10 min at room temperature. Fixed Cells were then blocked in 5% BSA in PBS for 30 minutes at room temperature. Immunofluorescence staining was then carried out as per section 2.16.

2.22 Measuring cilia lengths in *Cep290* CDT cells.

Cep290 collecting duct cells were stained by immunofluorescent techniques as described in 2.21 with mouse acetylated tubulin to highlight cilia present in the cells. Z-stack images were taken using the Zeiss Axioplan. The cilia length was determined by noting the µM slice measurement at the tip of the cilia and at the end of the cilia and subtracting these two figures (where the tip is first in focus to where the end of the cilia is in focus). The significance of this data was assessed by using a student's *t-test* to determine if the length of the cilia was statistically significant between wild type and mutant cells using a prism software programme graph pad http://www.graphpad.com/scientific-software/prism/ .

2.23 3D culturing of *Cep290* CDT cells.

Processing and imaging of *Cep290* collecting duct cell 3D cultures was kindly provided by Dr. Rachel Giles, University Medical Centre Utrecht, Netherlands. 3D cultures require extracellular matrix components (provided by Collagen I solution) and the hormone human growth factor in order to grow as tubular spheroids as described by *Elia & Schwartz, 2009* (Elia and Lippincott-Schwartz

2009). Markers were used to identify adherence and tight junctions of the 3D spheroids. The markers used included; Zona occludens (Zo1) for tight junctions, β-catenin (for adherens junctions) and acetylated tubulin to identify if cilia were protruding in the apical layer of the epithelial cell. Identification of tubule morphology, the 3D cultures were treated as per section 2.19 and section 2.20 (Elia and Lippincott-Schwartz 2009).

2.24 Protein Extraction

2.24.1 Whole cell protein extraction

Cep290 collecting duct cells were grown to confluency on 6 well plates and treated as described in section 2.19 and 2.20 and rinsed in PBS to remove any floating dead cells, media especially BSA. 200µl of protein extraction buffer (90.75M Urea, 0.5M Tris pH 6.8, 20% SDS, 500µL β-mercaptoethanol and 50% glycerol in ddH_20) was added and the cells were removed from the 6 well plate using a cell scrapper for 2min each.

2.24.2 Whole tissue extracts

For whole tissue extracts approximately 1mL (amount changed depending on size of tissue) [similar to section 2.6] protein extraction buffer was added and the tissue was homogenised to disperse the protein from the tissue on ice to reduce heat build up and denaturation. Samples were aliquoted and stored at -20°C until required.

2.25 Western blotting

Western blotting was required to confirm knockdown of the gene trap at the protein level and also to analyse the molecular pathways which may play a role in *Cep290* mutation of Joubert syndrome disorders

2.26 Acrylamide Gel preparation and separation of proteins

Proteins were resolved by electrophoresis on 6%,10%, 12% and 15% polyacrylamide gels; (Table 2.3 for kDa size separation)

Polyacrylamide Gel percentage	Size separation range
6%	50-200 kDa
10%	25-200kDa
12%	20-100kDa
15%	10-50kDa

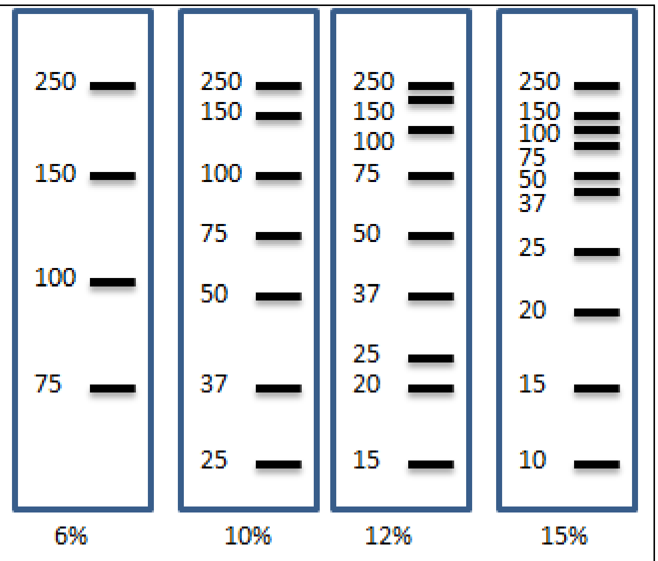

Table 2.3 The protein sizes which resolve on 6%, 10%, 12% and 15% acrylamide percentage gels and a representative image of how the proteins separate on each gel.
The protein sizes which can be resolved on 6%, 10%, 12% and 15% are clearly labelled. The 3rd column on this table is a visual representation of the proteins resolved on 6%, 10% 12% and 15% acrylamide gels. Section 2.26 describes how each % gel was made.

Each acrylamide gel comprises of a resolving gel (1.5M Tris-HCL pH 8.8, 30% Acrylamide mix, 10% sodium dodecyl sulphate (SDS), 10% ammonium per sulphate and 0.003% Tetramethylethylenediamine) and an acrylamide stacking gel (1.5M Tris-HCL pH 6.8, 30% Acrylamide mix, 10% SDS, 10% ammonium per sulphate and 0.003% Tetramethylethylenediamine) with a running buffer of Tris, Glycine and 20% SDS. The protein samples were denatured at 95°C for 5min and then resolved at a constant voltage of 200V until bands of the correct size were resolved. Separation was visualised using a Multi Spectra wide range protein ladder (Thermo scientific cat # 26634).

2.26.1 Transferring an acrylamide gel to a nitrocellulose membrane

The resolved proteins were transferred from the acrylamide gel to a nitrocellulose membrane (sigma N7892). Figure 2.1 for transfer procedure

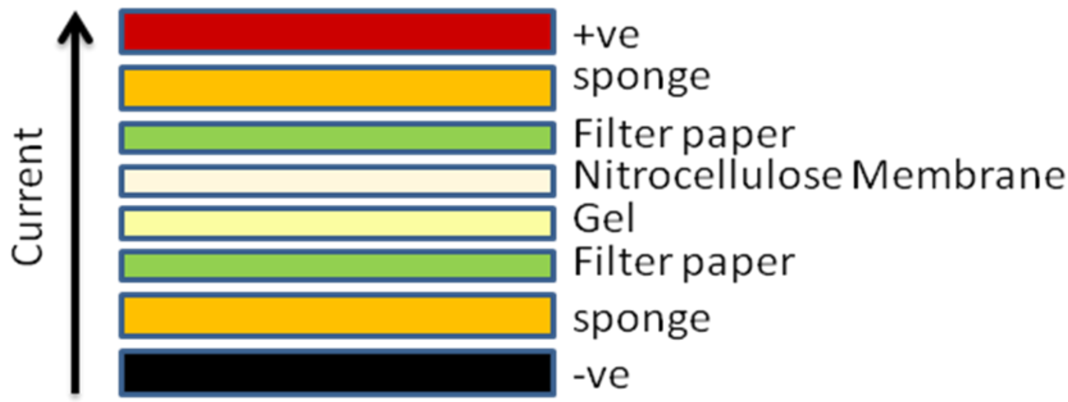

Figure 2.1 Transferring an acrylamide gel to a nitrocellulose membrane. A representative figure of the layers required when transferring your acrylamide gel to a nitrocellulose membrane. The first part of the sandwich is the sponge, a filter paper is placed on top of this, followed by the acrylamide gel, then the nitrocellulose membrane, followed by another filter paper and with a final sponge to complete the sandwich.

The transfer procedure involved immersing 2 sponges, 2 filter papers and a nitrocellulose membrane in ice-cold transfer buffer (25 mM Tris, 192 mM glycine and 10% methanol). The sandwich began with one of the sponges, followed by a filter paper, then the acrylamide gel, a nitrocellulose membrane another filter paper and the final sponge (Figure 2.1). Transfer was carried out at constant current of 350mA for 60min at 4^{o}C.

2.27 Confirming the transfer of proteins to a nitrocellulose membrane

Following transfer the nitrocellulose membrane was immersed in Ponceau (Sigma P7170) (Ponceau is a negatively charged stain which binds to positively charged amino acids of proteins transferred to the nitrocellulose membrane) and rinsed with ddh_20 to remove excess ponceau staining that did not adhere to the proteins on the membrane. The position of the lanes were marked and divided as appropriate depending on the antibody to be detected.

2.28 Detecting a protein of interest on a nitrocellulose membrane

The nitrocellulose membrane blot was blocked (to prevent non specific binding of proteins) in 5% Milk (Marvel original dried skimmed milk) containing a mixture of Tris-Buffered Saline and Tween (TBST) for 1-2 h at room temperature. All antibodies were diluted in the 5% Milk TBST solution and incubated with the membrane whilst shaking at room temperature for 1-2h or at 4°C overnight (Appendix 3 for antibody dilution and incubation conditions). The membrane was then washed 3 times for 15min in TBST at room temperature with shaking of 60 rpm to remove any unbound antibody. A horseradish peroxidase-conjugated (HRP) secondary antibody was then added to the membrane for 1h at room temperature. The membrane was washed in TBST as above to remove any unbound secondary. Enhanced Chemi-Luminescence (ECL) Western blotting detection solution was added to the blot (Thermo Scientific cat # 32109) for 5 minutes, excess detection solution was removed by blotting with paper and the proteins were visualized on an X-ray film. The X-ray film was scanned and saved as a jpeg image.

2.29 Imaging storage and manipulation

Histological and immunofluorescent images were saved as a TIFF file format and scale bars were added to each image when applicable. Adobe Photoshop was employed to stitch a series of images together in the case of whole kidney images when the kidney section was greater than P0.

2.30 Statistical analysis

Student's *t* –test was used to analyse the length of cilia in 2 populations of cells, tubular basement membrane thicknesses between *Cep290*$^{+/+}$ and *Cep290*$^{LacZ/LacZ}$ mice and the urine mean urine output between *Cep290*$^{+/+}$ and *Cep290*$^{LacZ/LacZ}$ mice. Graphs were created using the GraphPad Prism software. The standard error of the mean was also calculated using GraphPad Prism software. All *t*-tests are two-tailed, unpaired mean+/- standard error of the mean.

Chapter 3 Characterisation of a novel *Cep290* mouse model.

3.1 Introduction

The clinical phenotype of *Cep290* pathogenic mutations varies markedly in patients ranging from the embryonic lethal MKS to BBS, JBTS, NPHP and LCA. These ciliopathy phenotypes typically affect the central nervous system, retina, kidneys and liver (Coppieters, Lefever et al. 2010).

Children and adolescents are continuously growing and maturing until they reach sexual maturity. The therapies which are currently being suggested as treatments for ADPKD could cause devastating effects in children and adolescents. The mTOR inhibitor rapamycin for example is a drug which is currently been tested in clinical trials for ADPKD (See chapter 1). In various rat and mouse models of ADPKD rapamycin treatment reduced the size of renal cysts. Rapamycin is a powerful immunosuppressive and has anti-proliferative properties (Tao, Kim et al. 2005; Shillingford, Murcia et al. 2006; Wahl, Serra et al. 2006; Wu, Wahl et al. 2007). The adverse effects this drug may have on children who are still growing and not fully matured could be devastating and therefore limits its use in the paediatric setting.

This chapter investigates the physiological appearance of a novel transgenic NPHP mouse model with a truncated mutation in the *Cep290* gene.

A novel *Cep290* mouse model provides an opportunity to mimic the renal functional decline associated with *NPHP*, assess the molecular mechanisms of renal cystogenesis and evaluate potential therapeutic treatments for the paediatric population suffering with this debilitating form of renal failure.

It is hoped that this study will provide the means of following this NPHP ciliopathy disease in an animal model that is genetically, anatomically and physiologically similar to human juvenile NPHP patients. Given the limitations of studying ciliopathies in juvenile patients, a good mouse model is invaluable in order to reveal targeted treatment approaches using new or existing therapies.

This chapter investigates the phenotypes/genotypes of novel *Cep290* mutant mice (named *Cep290*$^{LacZ/LacZ}$ for this study) and ascertains whether the phenotypes observed are consistent with the patient forms of NPHP/JBTS.

3.2 Aims

1. In order to determine the effect of the gene trap insertion on the murine *Cep290* gene, an analysis to determine the evolutionary conservation of *Cep290* between mice and other model organisms was carried out.

2. In order to confirm the precise location of where the gene trap was inserted in the *Cep290* gene; RT-PCR and DNA genotyping was performed from tissue samples and ear clips were taken to identify *Cep290*$^{+/+}$, *Cep290*$^{LacZ/+}$ and *Cep290*$^{LacZ/LacZ}$ mice.

3. In order to determine expression profiles of Cep290 in *Cep290*$^{LacZ/+}$ mice, *LacZ* staining was utilised. Using *LacZ* staining, the expression of *Cep290* in the cerebellum, retina and renal tissues was determined.

4. In order to determine if there was a true JBTS phenotype occurring in *Cep290*$^{LacZ/LacZ}$ mice; the retina, renal, liver and brain tissues were examined. *Cep290* mice were inbred on a 129/Ola mouse colony and a mixed C57Bl/6J mouse colony. *Cep290* mice were also inbred up to the F_6 generation on the C57Bl/6J mouse strain. The different mouse colonies were employed to determine whether the phenotype was influenced by genetic modifiers.

3.3 CEP290

The human full length amino acid sequence transcript of Cep290 (a 290 kDa centrosomal protein) has 13 putative coiled coiled domains, a region with homology to chromosome segregation, a bipartite nuclear localization signal, six RepA/Rep^{+} protein Kinase inducible domain (KID) motifs, three tropomyosin homology domains (TM) and an ATP/GTP binding site motif A (Sayer, Otto et al. 2006). (Figure 3.1). To determine homology conservation of amino acids clustalW2 http://www.ebi.ac.uk/Tools/msa/clustalw2/ was used to align the mouse full length protein sequence with the human full length protein sequence. From this programme it was determined that the mouse and human full length proteins are 88% homologous. The predicted protein domains of CEP290 are conserved (>80%) across 5 species selected (*M. musculus, R. norvegicus, C. lupus* and *H. sapiens*), Figure 3.2.

The *Cep290* mouse model was generated from ES cells with which contained a “gene trap” from the Sanger institute gene trap library. Sequencing has confirmed that this gene trap is located at intron 24 of the *Cep290* gene. (More detail on the generation of this *Cep290* mouse model will follow in section 3.4). Therefore, given the site of the gene trap, it is predicted that $Cep290^{LacZ/LacZ}$ mice will not carry the SMC homology region the KID domain the bipartite nuclear localization signal (NLS-BP) and the P-loop (Figure 3.1).
SMC is thought to be crucial for maintaining functional chromosomal segregation (Nasmyth and Haering 2005). The KID motifs are also involved in chromosomal segregation and cell cycle regulation (Sayer, Otto et al. 2006) . A disruption of the NLS-BP was also identified in the NPHP2 *INVS* model of cystic kidney disease. End stage renal failure occurred at 14 months of age in patients with mutations disrupting the NLS-BP of NPHP2 (Otto, Schermer et al. 2003). The KID domains mediate multiple cell signalling networks linked to cell growth and differentiation (Locascio and Donoghue 2013). The loss of the KID domain in $Cep290^{LacZ/LacZ}$ mice suggests that cell signalling mediation processes may no longer be functioning.

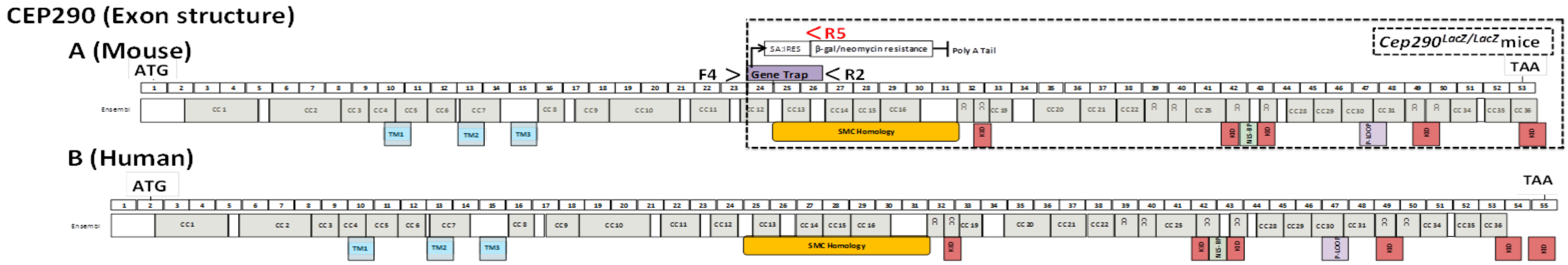

Figure 3.1 Exon structure of (A) mouse and (B) human CEP290 cDNA and protein motif representatives (below exons) shown in relation to the position of the exons coding them.

The human *CEP290* gene measures 93.2kb and extends over 55 exons (Sayer et al., 2006). The CEP290 start codon in humans is located in exon 2 and the last codon is located at exon 55. The *Cep290* mouse start codon is located in exon 1 and the stop codon is located in exon 53. The mouse *Cep290* gene measures 80.6 kb and extends over 54 exons (Ensembl).
CC ,coiled coil domain (yellow); TM, Tropomyosin (blue); KID (red); NLS-BP, bipartite nuclear localisation signal (green); P-loop (purple); Structural maintenance of chromosomes (SMC) homology (Orange)
Human exon structure and protein TM, KID, NLS-BP and P-loop domains adapted from Sayer et al., 2006 and imported in the mouse protein motif accordingly. Coil-coiled domains for both mouse and human protein motifs obtained from Ensembl.
The forward primer sequence (denoted as F4 **>**) was created at the start of exon 23 in the *Cep290* gene. The gene trap was inserted in the intron prior to exon 24 of the *Cep290* gene and thus the *Cep290* gene is terminated after exon 23 in *Cep290*$^{LacZ/LacZ}$ mice due to the poly A tail inserted at the end of the gene trap.
In order to identify *Cep290*$^{LacZ/+}$ and *Cep290*$^{LacZ/LacZ}$ mice a reverse primer was generated to amplify a segment of the gene trap sequence analogous to the β-galactosidase sequence (denoted as **<**R5) the product size for identifying *Cep290*$^{LacZ/LacZ}$ mice is 330bp.
In order to identify *Cep290*$^{+/+}$ animals a reverse primer sequence was created at the start of exon 25 in the *Cep290* sequence (denoted as **<**R2) the product size for identifying *Cep290*$^{+/+}$ mice was in total 550bp. The *Cep290*$^{LacZ/+}$ mice will amplify one copy of the *Cep290*$^{+/+}$ product (550bp product) and one copy of the gene trap primer pair product (300bp) Image of genotyping results can be seen in Figure 3.4 . (See methods section chapter 2 for primer sequences).

A

```
H. SAPIENS          1    MPPNINWKEIMKVDPDDLPRQEELADNLLISLSKVEVNELKSEKQENVIH    50
M. MUSCULUS         1    MPPNIKWKELIKVDPDDLPRQEELADKLLISLSKVEVNELKNEDQENMIH    50
R.NORVEGICUS        1    MPPNIKWKELIKVDPDELPRQEELADKLLISLSKVEVNELKNEDQENMIH    50
C.LUPUS             1    MPPNINWKEIIKVDPDDLPRQEELADNLLVSLSKVEISELKTESQENVIH    50
D.RERIO             1    MPAAADWRLLMGMDPEDLGDEDEKICDLILM---VKPRDLKADDSEKMIQ    47

H. SAPIENS         51    LFRITQSLMKMKAQEVELALEEVEKAGEEQAKFENQLKTKVMKLENELEM   100
M. MUSCULUS        51    LFRITQSLMKMKAQEVELALEEVEKAGEEQAKFENQLKTKVMKLENELEM   100
R. NORVEGICUS      51    LFRITQSLMKMKAQEVELALEEVEKAGEEQAKFENQLKTKVMKLENELEM   100
C.LUPUS            51    LFRITQSLMKMKAQEVELALEEVEKAGEEQAKFENQLKTKVMKLENELEL   100
D.RERIO            48    LFRISQTLLRMKLDEIKCAYEVVDSAGAEQARIENELKAKVLKLESELEM    97

H. SAPIENS        101    AQQSAGGRDTRFLRNEICQLEKQLEQKDRELEDMEKELEKEKKVNEQLAL   150
M. MUSCULUS       101    AQQSAGGRDTRFLRDEIRQLEKQLEQKDRELEDMEKELDKEKKVNEQLAL   150
R. NORVEGICUS     101    AQQSAGGRDTRFLRDEIRQLEKQLEQKDRELEDMEKELDKEKKVNEQLAL   150
C.LUPUS           101    AQQSAGGRDTRFLRDEIRQLEKQLEQKDRELEDMEKELEKEKKVNEQLAL   150
D.RERIO           098    AQRVMGGGDKHFLRDEIRQLESHLERKEKEVTQLEKEMGKERKSNEELAL   147

H. SAPIENS        151    RNEEAENENSKLRRENKRLKKKNEQLCQDIIDYQKQIDSQKETLLSRRGE   200
M. MUSCULUS       151    RNEEAENENSKLRRENKRLKKKNEQLRQDIIDYQKQIDSQKESLLSRRGE   200
R. NORVEGICUS     151    RNEEAENENSKLRRENKRLKKKNEQLRQDIIDYQKQIDSQKESLLSRRGE   200
C.LUPUS           151    RNEEAENENSKLRRENKRLKKKNEQLRQDIIDYQKQIDSQKETLLSRRGE   200
D.RERIO           148    RAEEAEEKNRKLKREIKQLTRKNEQLQQDIEFYRKEAEQRES--LQTKEE   195

H. SAPIENS        201    DSDYRSQLSKKNYELIQYLDEIQTLTEANEKIEVQNQEMRKNLEESVQEM   250
M. MUSCULUS       201    DSDYRSQLSKKNYELVQYLDEIQTLTEANEKIEVQNQEMRKNLEESVQEM   250
R. NORVEGICUS     201    DSDYRSQLSKKNYELVQYLDEIQTLTEANEKIEVQNQEMRKNLEESVQEM   250
C.LUPUS           201    DSDYRSQLSKKNYELVQYLDEIQTLTEANEKIEVQNQEMRKNLEESVQEM   250
D.RERIO           196    SNEIQRRLTKANQQLYQCMEELQHAEDMAANLRSENEHLQKNLEESVKEM   245

H. SAPIENS        251    EKMTDEYNRMKAIVHQTDNVIDQLKKENDHYQLQVQELTDLLKSKNEEDD   300
M. MUSCULUS       251    EKMTDEYNRMKALVHQSDAVMDQIKKENEHYRLQVRELTDLLKAKDEEDD   300
R. NORVEGICUS     251    EKMTDEYNRMKAIVHQTDTVMDQIKKENEHYRLQVRELTDLLKAKDEEDD   300
C.LUPUS           251    EKMTDEYNRMKAIVHQTDNVMDQLKKENDHYRLQVQELTDLLKAKNEEDD   300
D.RERIO           246    EKMTDEYNKMKIAVQQTDAIMDQLRKDRDHAKLQVRELTDQIQARVEEDD   295

H. SAPIENS        301    PIMVAVNAKVEEWKLILSSKDDEIIEYQQMLHNLREKLKNAQLDADKSNV   350
M. MUSCULUS       301    PVMMAVNAKVEEWKLILSSKDDEIIEYQQMLQSLRGKLKNAQLDADKSNI   350
R. NORVEGICUS     301    PVMMAVNAKVEEWKLILSSKDDEIIEYQQMLQSLRGKLKNAQLDADKSNI   350
C.LUPUS           301    PVMAAVNAKVEEWKLILSSKDDEIIEYQQMLHNLREKLKNAQLDADKSNV   350
D.RERIO           296    PVMAAVNAKVEEWKSVLSGKDLEILEYQQMIRDLREKLRTAQMDSDKSNI   345

H. SAPIENS        351    MALQQGIQERDSQIKMLTEQVEQYTKEMEKNTCIIEDLKNELQRNKGAST   400
M. MUSCULUS       351    MALKQGIQERDSQIKMLTEQVEQYTKEMEKNTFIIEDLKNELQKDKGTSN   400
R. NORVEGICUS     351    MALKQGIQERDSQIKMLTEQVEQYTKEMEKNTFIIEDLKNELRKDKGTSN   400
C.LUPUS           351    MALQQGIQERDSQIKMLTEQVEQYTKEMEKNTFIIEDLKNELHRNKGAST   400
D.RERIO           346    IALQQAVQERDNQIKMLSEQVEQYTTEMERNAMLIEELKRPLKKDKGHSS   395

H. SAPIENS        401    LSQQTH-MKIQSTLDILKEKTKEAERTAELAEADAREKDKELVEALKRLK   449
M. MUSCULUS       401    FYQQTHYMKIHSKVQILEEKTKEAERIAELAEADAREKDKELVEALKRLK   450
R. NORVEGICUS     401    IYQQTHYMKIHSKVQILEEKTKEAERTAELAEADAREKDKELVEALKRLK   450
C.LUPUS           401    LSQQTHYMKIQSKVQMLEEKTKEAERTAELAEADAREKDKELVETLKRLK   450
D.RERIO           396    -DHQRRLEDLSAKLQVAERKVLEAQRAAQLAERDARDKDKELNDTLSRIR   444
```

B

```
H. SAPIENS       450   DYESGVYGLEDAVVEIKNCKNQIKIRDREIEILTKEINKLELKISDFLDE   499
M. MUSCULUS      451   DYESGVYGLEDAVIEIKNCKAQIKIRDGEMEVLTKEINKLEMKINDILDE   500
R. NORVEGICUS    451   DYESGVYGLEDAVIEIKNYKAQIKIRDGEIEVLTKEINKLEMKINDVLDE   500
C.LUPUS          451   DYESGVYGLEDAVIEIKNCKNQIKIRDREIEVLTKEINKLELKINDFLDE   500
D.RERIO          445   LYESGTDGLEAAISEIKECKNQIRVRDREIEGMIKEINQLEMKINNLLDE   494

H. SAPIENS       500   NEALRERVGLEPKTMIDLTEFRNSKHLKQQQYRAENQILLKEIESLEEER   549
M. MUSCULUS      501   NEALRERAGLEPKTMIDLTEFRNSKRLKQQQYRAENQVLLKEIESLEEER   550
R. NORVEGICUS    501   NEALRERAGLEPKTMIDLTEFRNSKRVKQQQYRAENQILLKEIESLEEER   550
C.LUPUS          501   NEALRERVGLEPKTMIDLTEFRNSKSLKQQQYRAENQILLKEIESLEEER   550
D.RERIO          495   NEDLRERLGLNPKEELDLSEFRRSKILKQRQYKAENQVLLKEIERLEEER   544

H. SAPIENS       550   LDLKKKIRQMAQERGKRSATSGLTTEDLNLTENISQGDRISERKLDLLSL   599
M. MUSCULUS      551   LDLKRKIRQMAQERGKRNAASGLTIDDLNLSETFSHENKIEGRKLNFMSL   600
R. NORVEGICUS    551   LDLKRKIRQMAQERGKRSAASGLTIDDLNLTETFSHGDKIGERKLNFISF   600
C.LUPUS          551   LDLKKKIRQMAQERGKRAATSGLTMEDLNLTENFSQENKIGERKFDFTSL   600
D.RERIO          545   LELKQRIRALVKDKGVTVVSNSL-------LDNSVEEKPV--RSLRPSSG   585

H. SAPIENS       600   KNMSEAQSKNEFLSRELIEKERDLERSRTVIAKFQNKLKELVEENKQLEE   649
M. MUSCULUS      601   NNMNETQSKNEFLSRELAEKEKDLERSRTVIAKFQSKLKELVEENKQLEE   650
R. NORVEGICUS    601   NNMNETQSKNEFLSRELIEKEKDLERSRTVITKFQNKLKELVEENKQLEE   650
C.LUPUS          601   KNMNEAQSKSEFLSRELTEKERDLERGRTTITKFQNKLKELAEENKQLEE   650
D.RERIO          586   STDDEIKRKNERLQKELSNKEKELELRRSESTQFKAKLNEMLNENKQLEQ   635

H. SAPIENS       650   GMKEILQAIKEMQKDPDVKGGETSLIIPSLERLVNAIESKNAEGIFDASL   699
M. MUSCULUS      651   GMKEILQAIKDMPKDSDVKGGETSLIIPSLERLVNAMESKNAEGIFDASL   700
R. NORVEGICUS    651   GMKEILQAIKDMPKDSDVKGSETSLIIPSLERLVNAMESKNAEGIFDASL   700
C.LUPUS          651   GMKEILQAIKEMQKDPDVKGGETSLIIPSLERLVNAIESKNAEGIFDANL   700
D.RERIO          636   GMKEILQAIQDTQKKTPTSTG---VSIPSLERLVNALEMKYSEGKFDASL   682

H. SAPIENS       700   HLKAQVDQLTGRNEELRQELRESRKEAINYSQQLAKANLKIDHLEKETSL   749
M. MUSCULUS      701   HLKAQVDQLTGRNEELRQELRQSRKEAVNYSQQLVKANLKIDHLEKETDL   750
R. NORVEGICUS    701   HLKAQVDQLTGRNEELRQELRESRKEAVNYSQQLVKANLKIDHLEKETDL   750
C.LUPUS          701   HLKAQVDQLTGRNEELRQELRESRKEAINYSQQLAKANLKIDHLEKETIL   750
D.RERIO          683   HLRTQVDQLTGRNEELRQEMKTAREEAANTLSQLTKANEKIARLESEMES   732

H. SAPIENS       750   LRQSEGSNVVFKGIDLPDGIAPSSASIINSQNEYLIHLLQELENKEKKLK   799
M. MUSCULUS      751   LRQSAGSNVVYKGIDLPDGIAPSSAYIINSQNEYLIHLLQELDNKEKKLK   800
R. NORVEGICUS    751   LRQSSGSNVVYKGIDLPDGIAPSSAYIINSQNEYLIHLLQELDNKEKKLK   800
C.LUPUS          751   LRQSEGSNVVFKGVDLPDGIAPSSANIINSQNEYLIHILQELEYKEKKLK   800
D.RERIO          733   MSKSTGSSIPHKTLALPEEMTPTSAEAINALNEYTVQLLQEIKNKGDSIE   782

H. SAPIENS       800   NLEDSLEDYNRKFAVIRHQQSLLYKEYLSEKETWKTESKTIKEEKRKLED   849
M. MUSCULUS      801   HLEDSLEDYNRKFAVIRHQQSLLYKEYLSEKDIWKTDSEMIREEKRKLED   850
R. NORVEGICUS    801   HLEDSLEDYNRKFAVIRHQQSLLYKEYLSEKDVWKADSEMIKEEKRKLED   850
C.LUPUS          801   NLEESLEDYNRKFAVIRHQQSLLYKEYLSEKETWKTESETVKEEKKKLED   850
D.RERIO          783   QLGSALEEYKRKFAVIRHQQGLLYKEHQSERESWQKERDSFAELKSKLEE   832

H. SAPIENS       850   QVQQDAIKVKEYNNLLNALQMDSDEMKKILAENSRKITVLQVNEKSLIRQ   899
M. MUSCULUS      851   QAEQDAVKVKEYNNLLSALQMDSNEMKKMLSENSRKITVLQVNEKSLIRQ   900
R. NORVEGICUS    851   QAQQDAVKVKEYNNLLNALQMDSNEMKKMLSENSRKITVLQVNEKSLIRQ   900
C.LUPUS          851   QIQQDAIKVKEYNNLLSALQMDSDEMKKTLSENSRKITVLQVNEKSLIRQ   900
D.RERIO          833   QREVDAVKIKEYNHLLETLEKDPSEIRREMAETGRKIVVLRVNEKCLTRR   882
```

Figure 3.2 Amino acid sequence alignments of CEP290 across 5 different species

Panels (A –C); amino acid sequences of Cep290 reference sequences from zebrafish (NP_001161739.1), mouse (NP_666121.2), rat (NP_001129227.1), wolf (XP_539708.2) and human (NP_079390.3) using the ClustalW alignment tool(Sievers, Wilm et al. 2011) prior to where the gene trap is inserted in this novel *Cep290*$^{LacZ/LacZ}$ mouse model.

Gaps in sequence alignments are highlighted by dashes. Dark grey are homologous residues in >80% of aligned sequences between mouse, rat, zebrafish, wolf and humans.

3.4 Generation of a novel *Cep290* mouse model.

As confirmed in section 3.3 the Cep290 amino acid sequence and domain structure is highly homologous across various species. The *Cep290* murine gene is orthologous to the human *CEP290* gene and *Cep290* mutations are associated with a wide range of disorders. Over 128 *CEP290* disease causing mutations have been identified http://medgen.ugent.be/cep290base/overview.php. The vast majority of these *CEP290* mutations identified in patients are truncating mutations (Coppieters, Lefever et al. 2010). A novel *Cep290* mouse model with a truncated mutation in the *Cep290* gene was generated in order to study the phenotypes and molecular mechanisms associated with a truncated mutation occurring after exon 23 in the *Cep290* gene.

Using database searches (http://www.ncbi.nlm.nih.gov/nucgss/), a "gene trap" ES cell line was identified and (DU635568.1, Sanger Institute Gene Trap Library) in which the murine *Cep290* was disrupted at intron 24 (at position 3.308kb on the *Cep290* gene, located by a primer within En-2 intron 1 of the construct) to induce a truncated mutation.

The gene trap contains a *β*-galactosidase and a neomycin reporter gene with a ribosomal re-entry site followed by a poly A tail. The ES cells altered by the gene trap were injected into blastocysts to create chimeric mice. Male chimeras (with 50% 129/Ola<->C57BL/6J) were mated with either 129/Ola (for an inbred *Cep290* mouse strain, because ES cells were 129/Ola) or with C57BL/6J females to generate (firstly a F_1 generation continued on to create up to the F_6 generation) heterozygous mice for the *Cep290*$^{LacZ/LacZ}$ truncated mutation (Figure 3.3).

The heterozygous mice generated (with one copy of this gene trap) were named *Cep290*$^{LacZ/+}$ mice. A combination of 3 oligonucleotide primers was used in order to genotype the mice and distinguish between wild type, heterozygous and homozygous mice. Two of the oligonucleotide primers were located on either side of the insertion site of the gene trap to identify (in the absence of the gene trap) wild type alleles and an internal oligonucelotide primer specific to the gene trap was used to identify insertion of the gene trap sequence (Figure 3.1) for location of primers in relation to the *Cep290* gene. Thus, primers were designed such that in heterozygous animals, two PCR products are amplified (wild type and a copy of the gene trap sequence) and in the homozygote animals, oligonucleotide primers will only amplify the gene trap. (Figure 3.4 panel B).

Cep290$^{LacZ/+}$ mice from both strains were mated to generate *Cep290*$^{LacZ/LacZ}$ mice and the genotypes were confirmed by DNA Genotyping, Reverse Transcriptase-PCR genotyping and Western blotting (Figure 3.4). Once *Cep290*$^{LacZ/LacZ}$ mice were generated the mice were mated with *Cep290*$^{LacZ/+}$ mice to confirm that the mice were not sterile.

On the C57BL/6J genetic background of both the F_2 and the F_6 generations analysed the *Cep290*$^{LacZ/LacZ}$ mice were smaller and presented with a domed shaped head at 4 weeks of age compared to their *Cep290*$^{+/+}$ littermates (Figure 3.4 a).

Primers targeting the mRNA sequence of the *Cep290* gene were also generated (Primers spanned Intron exon boundary of exons 41-42 of the *Cep290* gene). It was observed in the *Cep290*$^{LacZ/LacZ}$ mouse that there was partial expression of the *Cep290* gene downstream of the gene trap suggesting a truncated mutation in *Cep290*$^{LacZ/LacZ}$ mice (Figure 3.4).

Western blot analysis from kidney extracts from 1 month old *Cep290*$^{LacZ/LacZ}$ mice identified that the full length *Cep290* protein expression profile was lost (Figure 3.4), suggesting that any full length protein derived from the truncated mutation is below the limit of detection by western blot. Ensemble have not identified any other mouse *Cep290* transcripts http://www.ensembl.org/index.html .

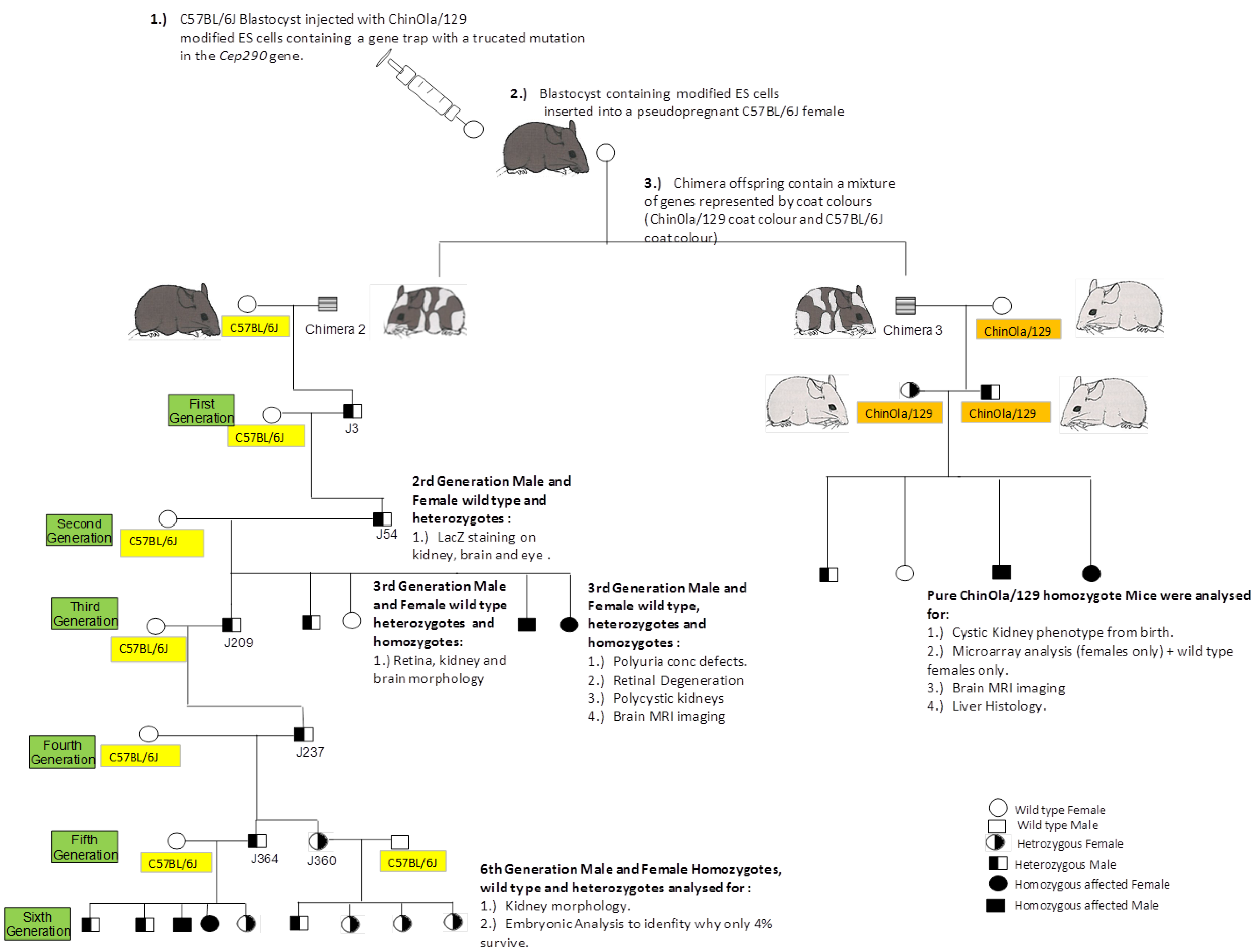

Figure 3.3 Generation of a novel *Cep290* mouse followed by breeding strategies for *Cep290* mice on a C57BL/6J and a 129/Ola backround.
A wild type C57BL/6J female pseudopregnant mouse was injected with a blastocyst containing modified ES cells which had a truncated mutation in the *Cep290* gene. This female gave birth to a chimeric male offspring. The chimeric male offspring was then mated with wild type C57BL/6J females to produce a F_1 generation on the C57BL/6J strain or with the 129/Ola female mouse to generate pure mice heterozygous for the *Cep290* truncated mutation.
In order to study the effects of the *Cep290* mutation on this mouse model the mice are bread to a "purer" generation by breeding a *Cep290*$^{LacZ/+}$ mouse (highlighted in yellow) with a C57BL/6J wild type mouse to eliminate any genetic modifiers. The heterozygous mice were given specific identities (J3 from F_1 generation, J54 from F_2 generation, etc.) by the use of ear clips and cage number identifications to ensure the correct generations were generated. The morphological phenotypes analysed on the C57BL/6J mouse strain are described alongside the F2 generation and the F6 generation of the C57BL/6J mice. The morphology of the pure genetic backround in the 129/Ola mice was also analysed as described above. Mouse images were adapted from (Strachan 2004)

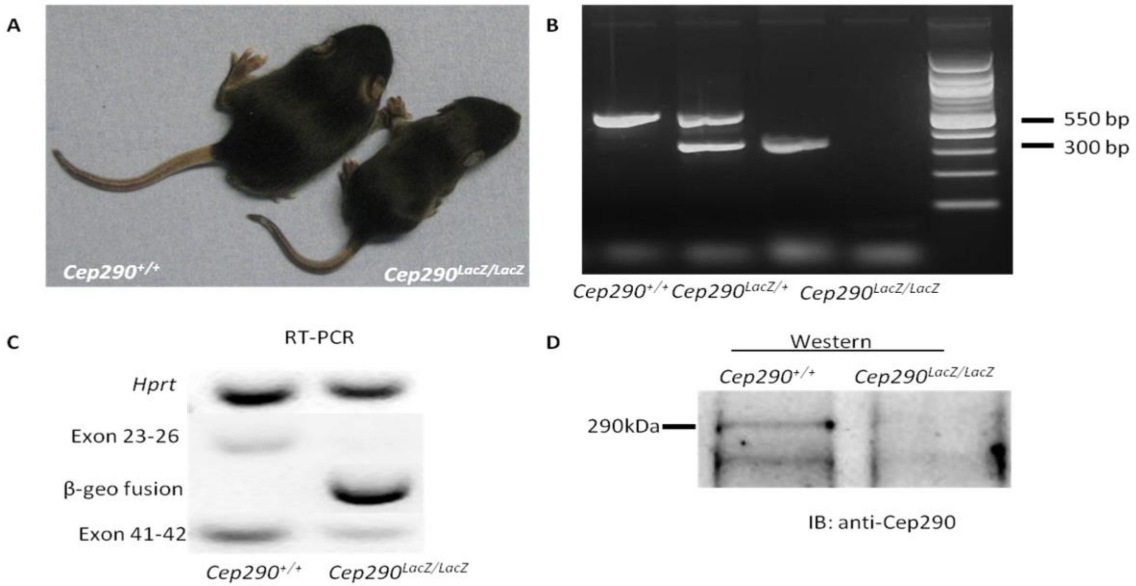

Figure 3.4 The phenotype of *Cep290*$^{LacZ/LacZ}$ animals, genotyping of *Cep290*$^{LacZ/LacZ}$ animals and western blotting of whole kidney protein extracts from *Cep290*$^{LacZ/LacZ}$ animals.

Panel (A). *Cep290*$^{LacZ/LacZ}$ and wild-type litter mates at 1 month of age on the F_3 C57BL/6J generation. *Cep290*$^{LacZ/LacZ}$ mice are smaller and some survive to 12 months of age.

Panel (B) DNA Genotyping PCR of *Cep290* mice. *Cep290*$^{+/+}$ mice amplify a single 550bp product whilst *Cep290*$^{LacZ/LacZ}$ mice amplify a single 300bp product. DNA isolated from *Cep290*$^{LacZ/+}$ mice will amplify both products. (Figure 3.1 shows where the primers were generated in the *Cep290* gene and where the gene trap was inserted in the *Cep290* gene).

Panel (C). RT-PCR analysis of mRNA which amplify exon intron boundarys between exons 23-26 and 41-42 of the *Cep290* gene in *Cep290*$^{+/+}$ and *Cep290*$^{LacZ/LacZ}$ 1 month old kidney samples. There is an absence of product equivalent to exons 23-26 in *Cep290*$^{LacZ/LacZ}$ animals and an insertion of a *β-geo* fusion cassette. mRNA representing exons 41-42 downstream of the gene trap insertion show reduced expression in *Cep290*$^{LacZ/LacZ}$ animals. *Hprt* is shown as a loading control.

Panel (D). The mutation leads to loss of Cep290 protein expression in 1 month old *Cep290*$^{LacZ/LacZ}$ kidneys, as shown by western blotting with a Cep290 antibody.

Mouse Genotype	Mixed /F1+2 gen	129/Ola (99.9%)	F3 gen C57BL/6J	F4 gen C57BL/6J	F5 gen C57BL/6J	F6 gen C57BL/6J	F6 gen embryos E10.5- C57BL/6J
Cep290$^{+/+}$	141	54	2	10	6	14	8
Cep290$^{LacZ/+}$	267	91	3	5	7	25	13
Cep290$^{LacZ/LacZ}$	56	38	0	0	0	2	3
Total	464	183	5	15	13	41	24
Cep290$^{+/+}$ %	30.39	29.51	40.00	66.67	46.15	34.15	33.33
Cep290$^{LacZ/+}$ %	57.54	49.73	60.00	33.33	53.85	60.98	54.17
Cep290$^{LacZ/LacZ}$ %	12.07	20.77	0.00	0.00	0.00	4.88	12.50

Table 3.1 Cohort of C*ep290* mice generated.

Table 3.1 Identifies the total number of mice utilized in this study. Mouse strains (129/Ola or C57BL/6J) were categorized and the generation of each strain studied was recorded. The C57BL/6J *Cep290*$^{LacZ/LacZ}$ strain did not follow Mendelian ratios.A few embryos from the *Cep290*$^{LacZ/LacZ}$ 6th generation on the C57B/6 background were analysed to test for possible developmental implications. Embryo analysis was inconclusive due to the low numbers of *Cep290*$^{LacZ/LacZ}$ embryos available (n=3). The 129/Ola mice mendelian numbers were significantly improved compared to C57B/6J mice. Percentages of each genotype identified for each mouse strain were documented. The Mendelian ratio is 1:2:1 for *Cep290*$^{+/+}$: *Cep290*$^{LacZ/+}$*: Cep290*$^{LacZ/LacZ}$ in the 129/Ola inbred mice.

3.5 Examining CEP290 expression in *Cep290*$^{LacZ/+}$ mice.

In order to examine the expression of *Cep290* in detail, *Cep290*$^{+/+}$ and *Cep290*$^{LacZ/+}$ mice were stained with 5-bromo-4-chloro-indolyl-β-D-galactopyranoside (X-gal) and analysed. In particular we needed to know where the truncated mutation is expressed in these *Cep290* mice. *Cep290*$^{+/+}$ kidney brain and eye tissues samples analysed did not show X-gal expression (Figure 3.5) and therefore this confirms there were no endogenous *β-galactosidase* activity and no background staining occurring.

The X-gal staining in this study prompted the in situ hybridisation studies on human embryonic fetal tissue (Cheng, Eley et al. 2012). In the kidney of the *Cep290*$^{LacZ/+}$ mice there was X-gal expression at the cortical medullary border, consistent with the known cortico-medullary location of cysts in patients with NPHP. Recently we have shown that CEP290 expression is prominent in the brain and spinal cord, the developing cerebrum, choroid plexus and the developing hindbrain in human fetal embryos (Cheng, Eley et al. 2012).

In this study Cep290 expression was observed in the choroid plexus of the brain. The choroid plexus is a highly ciliated structure vital for maintaining sufficient levels of cerebrospinal fluid (Lindvall and Owman 1981). Finally Cep290 expression was also found in the retinal layers of the eye, which is consistent with our findings in human fetal embryos (Cheng, Eley et al. 2012).

In conclusion *β-galactosidase* expression was evident in the kidneys, brain and eye tissues of heterozygous mice (*Cep290*$^{LacZ/+}$) (Figure 3.5). As mentioned above Cep290 expression was evident in the cortio medullary region of the kidney consistent with the known location of cysts in patients with NPHP. In the *Glis2* mouse model (the NPHP7 mouse model) Glis2 expression was evident closer to the medulla region (Figure 3 (C) (Attanasio, Uhlenhaut et al. 2007)). The Glis2 mice shows extensive fibrosis, apoptosis and loss of tubules but there is little evidence of cystogenesis (Attanasio, Uhlenhaut et al. 2007) which is one of the contributing factors of the NPHP phenotype. The Glis2 mouse model is a good example of why additional NPHP mouse models are required as not all NPHP features are in one mouse model.

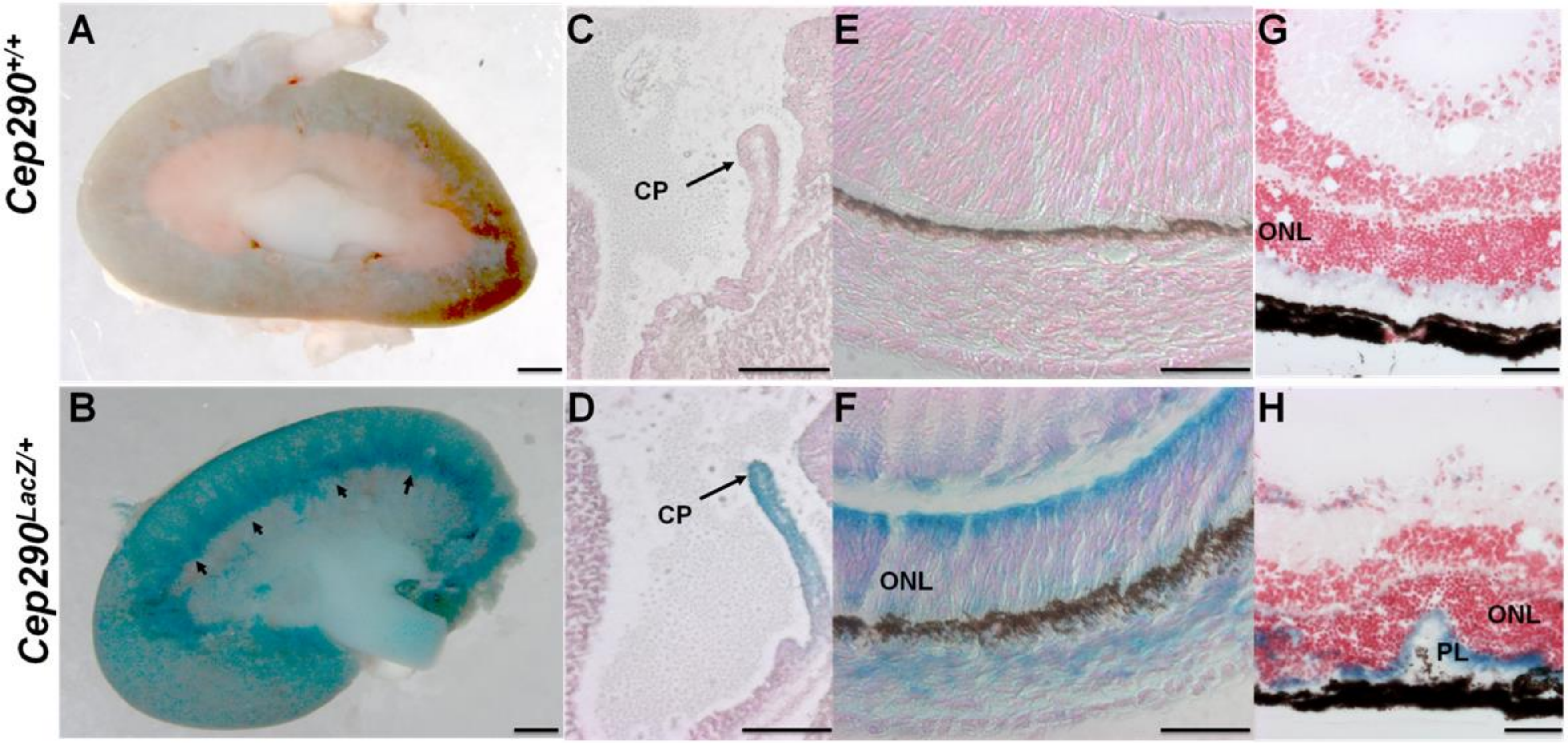

Figure 3.5 Xgal staining in the *Cep29*$^{LacZ/+}$ mouse.
(A-B) Whole mount staining of 6 week old *Cep290*$^{+/+}$ (A) and (B) *Cep290*$^{LacZ/+}$ kidneys. (C-D) *Cep290*$^{+/+}$ and *Cep290*$^{LacZ/+}$ mouse embryos at E16.5, identifying β-galactosidatse expression in the (CP) choroid plexus at the anterior part of the brain. (E-H) LacZ staining is evident in the retinal layers of the *Cep290*$^{LacZ/+}$ mice at E13.5 (F) and 1 month of age (H). (E+G) *Cep290*$^{+/+}$ retinal layers at the same time points. Scale bars (A+B) 1mm (C-H) 50µM.

In order to determine the phenotype of *Cep290*$^{LacZ/LacZ}$ mice on the C57BL/6J mouse strain (F_3 generation) urine analysis, EM analysis, immunohistochemistry and histology techniques were employed. The organs and tissues analysed included the kidney, brain and retina as this is where Cep290 expression was observed when LacZ staining was employed.

3.6 *Cep290*$^{LacZ/LacZ}$ mice develop polyuria at 1 month of age.

In the first decade of life patients who develop NPHP initially present with a urinary concentration defect, following this they typically develop cystic kidney disease and finally progress to end stage renal disease by the second or third decade of life (Salomon, Saunier et al. 2009).

At 1 month of age polyuria was evident in *Cep290*$^{LacZ/LacZ}$ mice compared to their wild type and heterozygous littermates bred on the C57BL/6J strain (Figure 3.6). A 1 month old mouse from the C57BL/6J mouse strain is comparable to a 12 and a half year old human (Flurkey 2007). The comparison of mouse life phase equivalencies to human age equivalents was identified in 2007. The life phases of C57BL/6J mice were analysed which consisted of a cohort of 150 male and 150 female C57BL/6J mice. A survival curve was generated and the maturational rates of both human and mice were compared (Flurkey 2007). This data allows us to infer that a 1 month old mouse is roughly equivalent to an adolescent human.

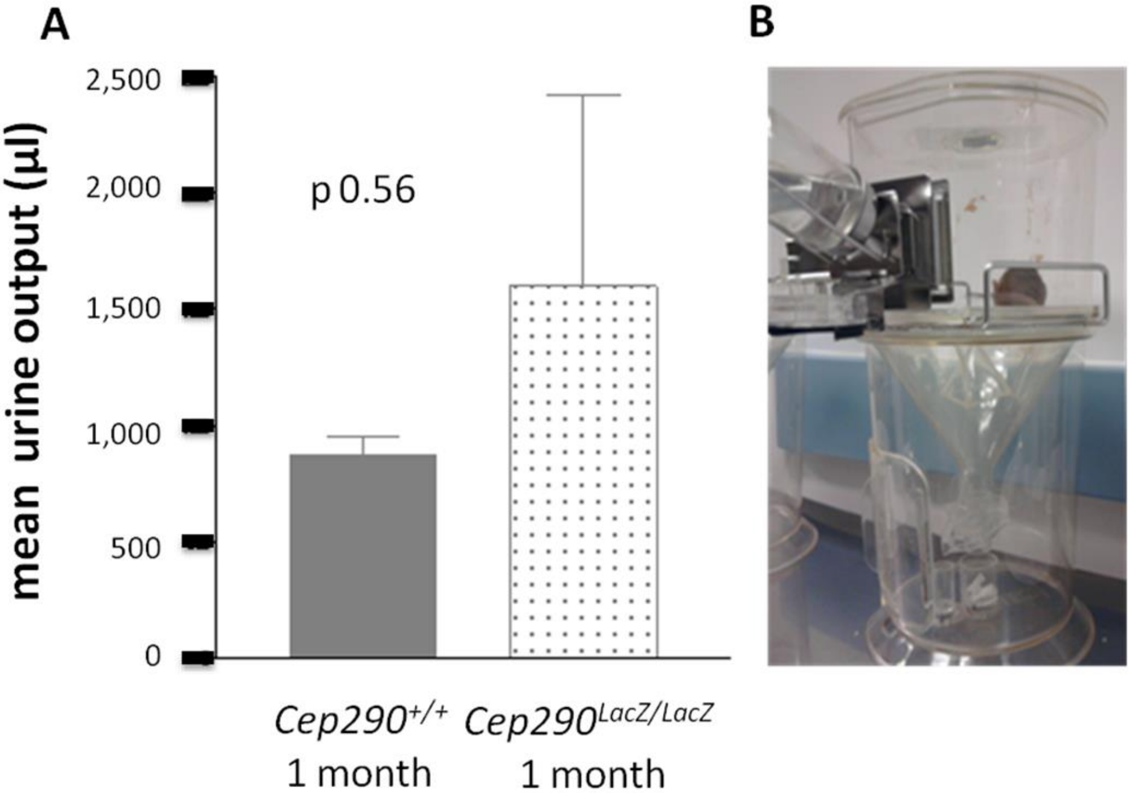

Figure 3.6 *Cep290$^{LacZ/LacZ}$* mice are polyuric at 1 month of age.
Panel A) An increase in urine output is evident in 1 month old *Cep290$^{LacZ/LacZ}$* mice on the C57BL/6J F_3 generation compared to *Cep290$^{LacZ/+}$* and *Cep290$^{+/+}$* mice. The average *Cep290$^{LacZ/LacZ}$* mouse urinated 1.5mls after 24 hours in a metabolic cage compared to littermates which urinated approximately 0.8mls in 24 hours. Panel B image of the metabolic cage utilized in this study. Urine was collected from 3 *Cep290$^{+/+}$* mice and 6 *Cep290$^{LacZ/LacZ}$* mice. Standard deviation of the error of the mean for *Cep290$^{+/+}$* mice was 88.19 and the standard deviation of the error of the mean for *Cep290$^{LacZ/LacZ}$* mice was 781.20. These results are not significant as the p value is 0.56. More experimental repeats would be needed to identify if there is a significance in urine out put as there seems to be a trend when raw data is observed.

A *Cep290$^{LacZ/LacZ}$* mouse from this mixed generation passed approximately 50mls of urine in 24 h and consumed over 32g of $H_2 0$ within the 24 h. This phenomenon occurred in only 1 *Cep290$^{LacZ/LacZ}$* mouse. After this analysis the mouse died at 6 weeks of age, the kidneys were analysed by H+E staining and there was no observable renal damage evident (Appendix 4). This suggests that this mouse was an outlier with a phenotype that was not representative of its littermates. Polyuria occurs in the first decade (approximately 12.5 years of age) of life in patients who go on to develop NPHP (Salomon, Saunier et al. 2009). With more experimental repeats the trend of urine output observed in Figure 3.6 suggests that *Cep290$^{LacZ/LacZ}$* mice may mimic the NPHP patient’s initial symptoms of polyuria.

3.7 Investigating the renal morphology of *Cep290*$^{LacZ/LacZ}$ mice.

Polyuria and loss of concentrating ability is a precursor of NPHP. In addition to polyuria, renal cysts followed by renal failure are prominent features of this disease. Patients may present with problems relating to renal failure which can include fatigue, nausea, growth retardation or anemia (Hildebrandt, Attanasio et al. 2009).

The renal biopsy of NPHP patients may demonstrate collecting duct cysts as well as proximal tubule cysts, glomerular cysts, interstitial fibrosis and tubular basement membrane defects (Hildebrandt, Attanasio et al. 2009).

All three renal manifestations were examined in the *Cep290*$^{+/+}$ and *Cep290*$^{LacZ/LacZ}$ mouse model using various histological techniques. Renal cysts are predominantly characterized by tubular dilatation with increased epithelial cell layer proliferation. Kidney sections from *Cep290*$^{Lacz/LacZ}$ and *Cep290*$^{+/+}$ mice were stained with H+E to assess renal histology. This showed evidence of cysts in the cortex and medulla of 1 month old kidneys (Figure 3.7).

Interstitial fibrosis can be determined using Trichrome Masson staining (TMS) or Sirius red staining techniques. Kidney sections from the *Cep290*$^{+/+}$ and *Cep290*$^{LacZ/LacZ}$ F_3 C57BL/6J generation was analysed for fibrosis using Trichrome masson stain.

Fibrosis was identified as TMS stains the collagen deposition surrounding the cysts are blue colour in the *Cep290*$^{Lacz/LacZ}$ mouse at 2 months old. Collagen deposits are a classic hallmark of fibrosis in histological sections (Figure 3.7).

EM techniques were employed to determine tubular basement membrane defects in the *Cep290*$^{Lacz/LacZ}$ mice. (EM figure 3.11 and 3.12). All three techniques confirmed renal phenotype similar to that seen in NPHP patients (Figure 3.7- 3.8 and Figure 3.11 and Figure 3.12).

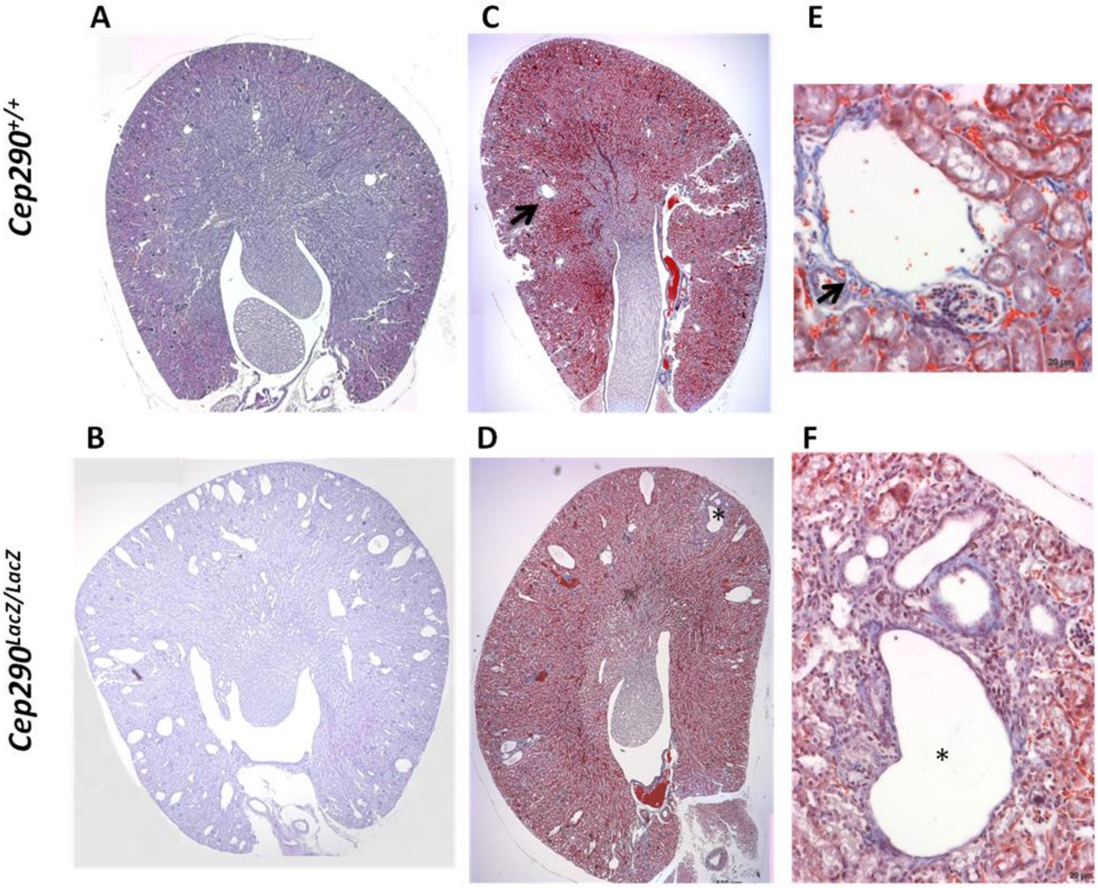

Figure 3.7 Renal cysts evident in *Cep290*$^{LacZ/LacZ}$ mixed strain mice
Panels (A-B) Haematoxylin and Eosin staining on 1 month old *Cep290* kidneys. Trichome Masson staining of *Cep290*$^{+/+}$ and *Cep290*$^{LacZ/LacZ}$ at 2 months (Panel C+D). A simple kidney cyst in *Cep290*$^{+/+}$ 1 month old mouse (E). Magnified image of cyst in the *Cep290*$^{Lacz/LacZ}$ kidney stained with Trichome Masson staining (Panel F). An asterisk highlights a cyst evident in *Cep290*$^{LacZ/LacZ}$ kidneys. Panel (E-F) scale bar 20µm

The *Cep290*$^{LacZ/LacZ}$ kidney tissue was affected with multiple cysts compared to its wild type littermate. Trichome masson staining was used to determine if fibrosis was evident. Collagen deposition was evident (blue staining surrounding cysts) in *Cep290* mice; this is a well known marker for interstitial fibrosis. (Panel F).. The *Cep290*$^{LacZ/LacZ}$ kidney presents with cysts in the cortex and corticomedullary region of the kidney (Figure 3.7). The cysts vary in shape and size however all have an epithelial cell layer surrounding the cyst (hallmark of cyst). This cystic and fibrotic phenotype has been confirmed in10 animals for both *Cep290*$^{+/+}$ and *Cep290*$^{LacZ/LacZ}$ type mice from the C57BL/6J F_3 generation.

Cep290 kidneys at birth (n=2), 1 month (n=6), and 1 year (n=2) were also analysed on the F_3 generation. *Cep290*$^{LacZ/LacZ}$ mice at these time points also have renal cysts. Of the 56 *Cep290*$^{LacZ/LacZ}$ mice born on the F_2-F_3 generation, 11 *Cep290*$^{LacZ/LacZ}$ mice were analysed for histology. 10 of the *Cep290*$^{LacZ/LacZ}$ mice exhibited cysts. Fibrosis was only evident at 2 months of age and later. The renal images from the *Cep290*$^{LacZ/LacZ}$ mice at birth and 1 year are not shown as the cystic nature was variable in mixed crosses.

3.8 Confirming the cellular location of *Cep290*$^{LacZ/LacZ}$ renal cysts

NPHP patients' cysts originate from the dilatation of collecting duct tubules and are predominantly found in the corticomedullary region of the kidney. To address the issue of which nephron segment the *Cep290*$^{LacZ/LacZ}$ mice renal cysts originated from, immunofluorescent staining antibodies were utilised. The antibodies utilised target specifically principal and intercalated cells of the collecting duct tubule in kidney cells.

AQP2 is a member of a family of water channel proteins originally found in the collecting duct of the kidney (Fushimi, Uchida et al. 1993). AQP2 immunofluorecent specific antibodies may be used to identify the apical surface of principal cells of the collecting duct.

ATP6V0A4 is a protein expressed by intercalated cells of the collecting duct and specific antibodies towards ATP6V0A4 can be used to identify these cells.

AQP3 is expressed in the basolateral cell membrane of principal collecting duct cells. Antibodies directed towards these 3 proteins may be used as collecting duct markers, and confirmed that the renal cysts are located in the collecting duct tubules of murine kidney (Figure 3.8).

Every cyst seen in *Cep290*$^{LacZ/LacZ}$ mice were positive for markers of collecting ducts, no other cysts were seen in proximal or distal tubules or the loop of henle. ADPKD cysts are evident in multiple segments of the nephron (Wilson 1997).

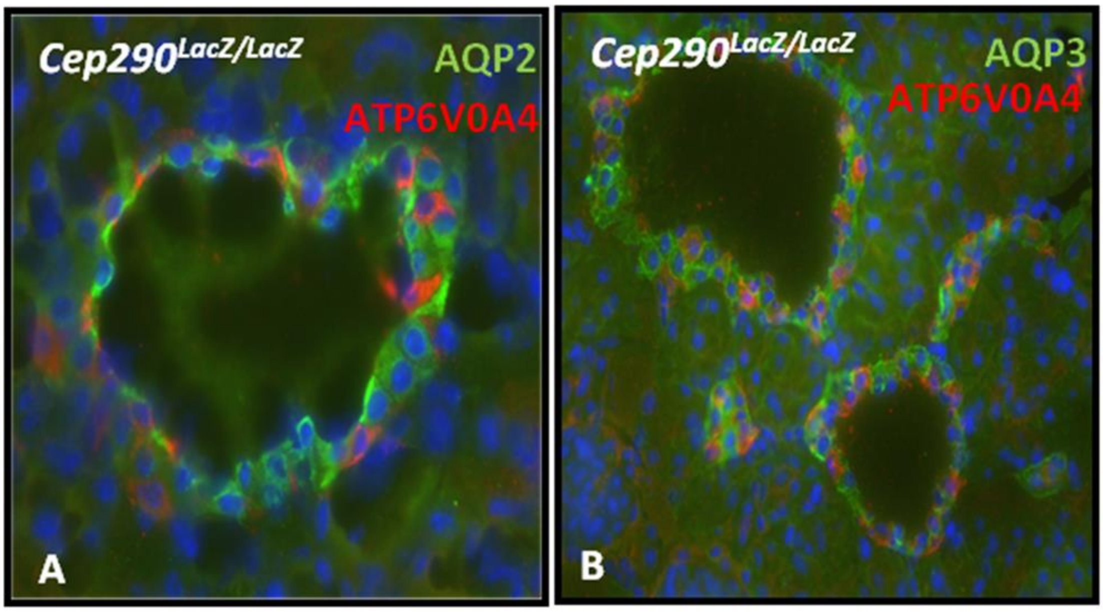

Figure 3.8 ***Cep290*$^{LacZ/LacZ}$ renal cysts are collecting duct in origin**
Immunofluorescent staining of *Cep290*$^{LacZ/LacZ}$ renal cysts. Panel (A) renal section of *Cep290*$^{LacZ/LacZ}$ cysts at 12 weeks. AQP2 (green) stains the apical surface of cells of collecting duct tubules. ATP6V0A4 (Red) stains the intercalated cells of collecting duct tubules. Panel B corresponding section of *Cep290*$^{LacZ/LacZ}$ renal cysts at 12 weeks. AQP3 (green) stains the basolateral layer of collecting duct tubules. Blue = dapi to identify nuclei.

3.9 Are primary cilia evident in *Cep290*$^{LacZ/LacZ}$ collecting duct cysts?

An example of a mouse model with renal cysts occurring early in development was the *Kif3a* mouse model and the cysts in this mouse model lacked primary cilia (Lin, Hiesberger et al. 2003).

Another example of a mouse model with cystic kidneys lacking cilia is the *Ift20* mouse model (Jonassen, San Agustin et al. 2008). The *Ift20* gene is highly expressed in kidneys and is responsible for the assembly and maintenance of cilia assembly. Knockdown of *Ift20* blocks cilia assembly and also reduces the expression of *Pkd2* a well known gene implicated in polycystic kidney disease (Jonassen, San Agustin et al. 2008).

Therefore it was reasonable to investigate whether a loss of cilia was the main determinant of renal cysts in the *Cep290*$^{LacZ/LacZ}$ mouse, hence kidney sections were stained with anti-acetylated tubulin (an antibody that binds to primary cilia, centrioles, mitotic spindles and microtubules) (Piperno and Fuller 1985).

The kidney sections of *Cep290*$^{+/+}$ and *Cep290*$^{LacZ/LacZ}$ were analysed. Within the *Cep290*$^{LacZ/LacZ}$ cystic epithelia, primary cilia were clearly evident, although it was not possible to determine whether or not there was a reduction in the number of cilia (Figure 3.9).

SEM and TEM were employed to identify if there was a loss of cilia in renal cysts. Collecting duct cysts were primarily identified by SEM analysis and acetylated tubulin staining and it was confirmed that cilia were present after both sets of analysis (Figure 3.9 and 3.10). This set of data therefore confirms that in the renal tubule cysts of *Cep290*$^{LacZ/LacZ}$ cilia were not completely absent.

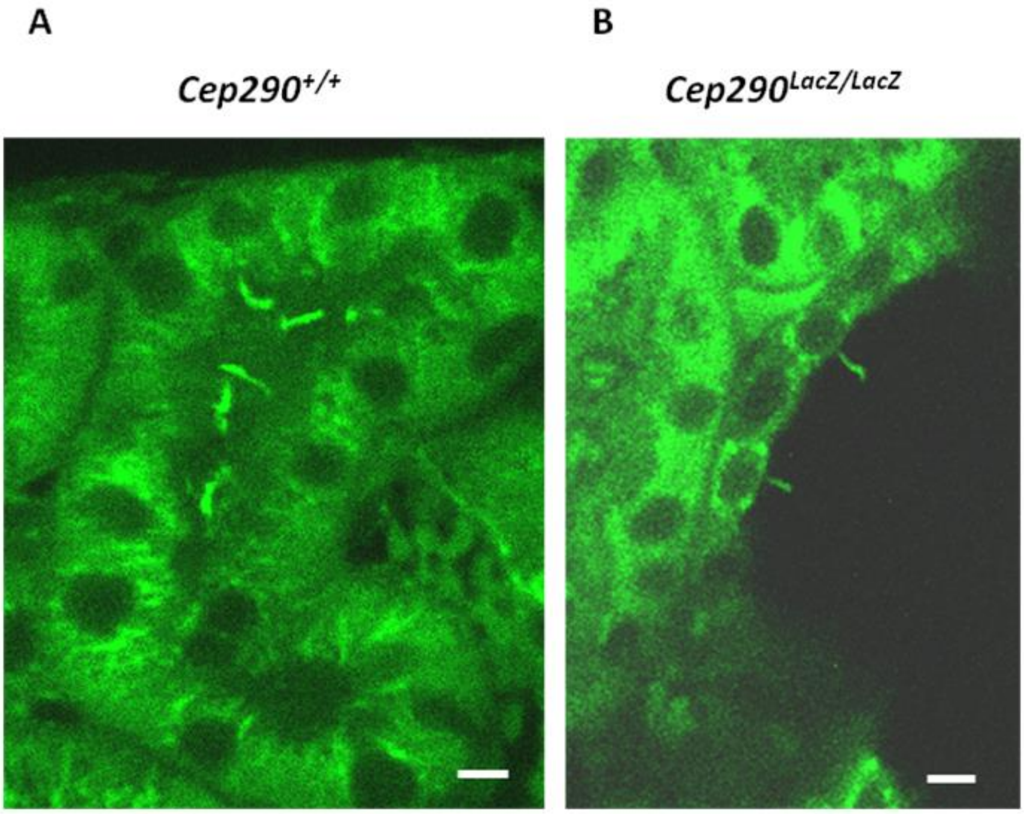

Figure 3.9 Presence of cilia is evident in *Cep290*$^{LacZ/LacZ}$ renal cystic collecting ducts.
Immunofluorescent staining of primary cilia (stained with acetylated alpha tubulin antibody) in (A) *Cep290*$^{+/+}$ collecting duct and (B) *Cep290*$^{LacZ/LacZ}$ cystic epithelium. Cilia are evident in the *Cep290*$^{LacZ/LacZ}$ collecting duct. Scale bar 5µM.

3.10 Is there structural primary cilia defects evident in renal *Cep290*$^{LacZ/LacZ}$ mice?

From figure 3.9 and figure 3.10 it is clear to see that *Cep290*$^{LacZ/LacZ}$ cystic collecting ducts have primary cilia. However not all PKD mouse models with cystic kidney disease have shown a complete loss of cilia, some have identified malformed and shortened cilia, for example the *Pkd2*$^{ws25/-}$ mouse model (Thomson, Mentone et al. 2003). The *Pkd2*$^{ws25/-}$ mouse model is a representative of the ADPKD phenotype.

The *Tg737*^{orpk} mouse model (Moyer, Lee-Tischler et al. 1994; Pazour, Dickert et al. 2000) identified shortened cilia in renal epithelial cells. The phenotype of this mouse model represents ARPKD. There have been no pathogenic mutations found in the Tg737 human orthologue (*IFT88*) in patients with ARPKD to date (McIntyre, Davis et al. 2012).

Finally the congenital polycystic kidney (*cpk*) mouse model also observed varying lengths in mutant cilia and differences in the morphology of cilia using SEM analysis (Winyard and Jenkins 2011).

To address the hypothesis of a structural cilia defect occurring in *Cep290*$^{LacZ/LacZ}$ mice after the findings observed from other PKD mouse models, *Cep290*$^{LacZ/LacZ}$ mice were analysed for malformed or shortened cilia. TEM techniques were employed to answer this question. Cilia were visible using TEM but due to the orientation of the cilia and the small number of cilia identified, cilia length could not be quantified (Figure 3.10).

2D TEM images were able to show that the cilium was protruding into the apical lumen of the cyst. Cross section images of the primary cilium were also captured, however no structural defects were evident in the cross sections. (Figure 3.10).

This study is consistent with a functional role of *Cep290* within the cilia/basal body rather than a structural role. Cep290 is likely to be a gatekeeper at the transition zone providing a platform for IFT particles to be loaded and unloaded at the base of the cilium (Craige, Tsao et al. 2010).

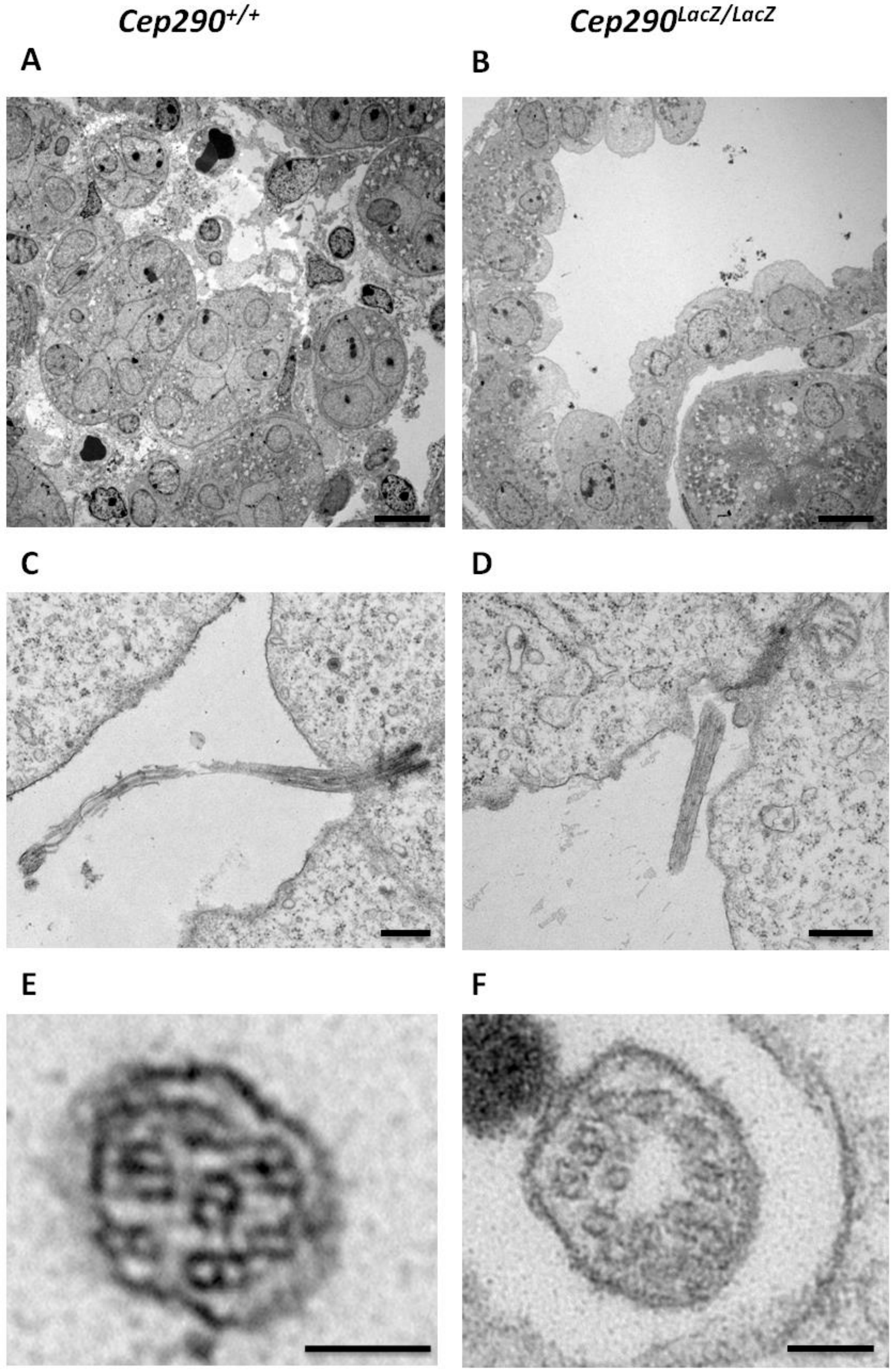

Figure 3.10 EM analysis of renal tubular epithelium in *Cep290*$^{+/+}$ and *Cep290*$^{LacZ/LacZ}$ kidneys.
TEM images of 2 week old *Cep290*$^{+/+}$ and *Cep290*$^{LacZ/LacZ}$ renal collecting ducts (Panels A+B). Scale bar 10 micron. Panels (C+D) *Cep290*$^{+/+}$ and *Cep290*$^{LacZ/LacZ}$ cilium protruding into the lumen of the collecting duct. Scale bar 500 nm. Panels (E+F) Cross sections of *Cep290*$^{+/+}$ and *Cep290*$^{LacZ/LacZ}$ cilia. Scale bar 100nm. There was no striking difference between cilia lining the cysts of *Cep290*$^{LacZ/LacZ}$ renal collecting ducts compared to *Cep290*$^{+/+}$ collecting duct cilia. Additional images would be required to identify if there was a difference between cross sections of primary cilia in *Cep290*$^{+/+}$ and *Cep290*$^{LacZ/LacZ}$ mice.

3.11 Using TEM analysis to identify other NPHP characteristics

Using Trichrome Masson staining in renal tissues we show that *Cep290*$^{LacZ/LacZ}$ mice at 2 months develop interstitial fibrosis (Figure 3.7). Cystic and non cystic collecting ducts were also visualized by TEM techniques and it was evident that collagen deposition was present in *Cep290*$^{LacZ/LacZ}$ cystic collecting ducts (asterisk on figure 3.11).

3.12 Investigating renal tubular basement membrane (TBM) morphology in *Cep290*$^{LacZ/LacZ}$ mice

Electron microscopy of TBM morphology in patients with NPHP revealed thickening and lamination of the TBM (Ashizawa, Miyazaki et al. 2005).

Abnormal thickening of the TBM was evident in *Cep290*$^{LacZ/LacZ}$ kidneys when compared to *Cep290*$^{+/+}$ controls (Figure 3.12). TBM thickness was measured in 7 different images.

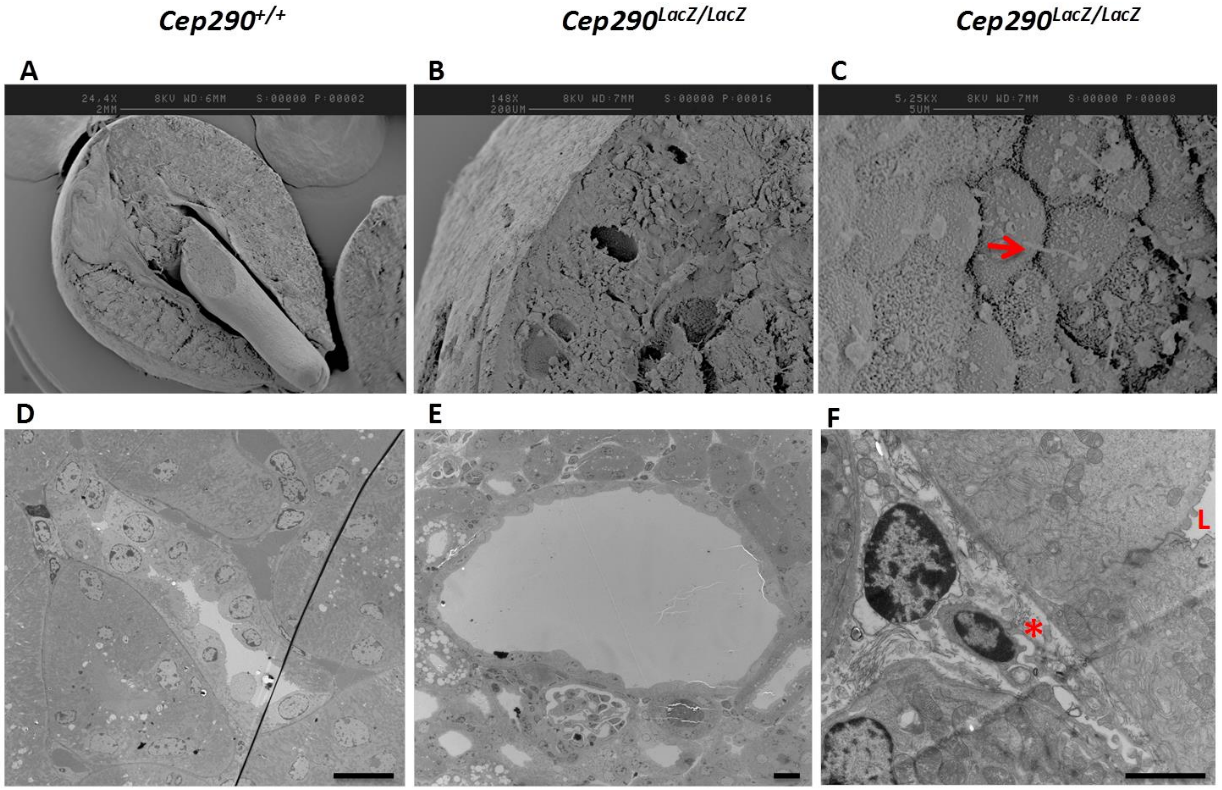

Figure 3.11 Collagen deposition is a hallmark of fibrosis and is evident in 1 month *Cep290*$^{LacZ/LacZ}$ renal collecting ducts cysts. SEM images of Wild type (A) and *Cep290*$^{LacZ/LacZ}$ kidneys (B+C) at 1 month of age. Cysts are evident in the *Cep290*$^{LacZ/LacZ}$ kidney (Panel B). Cilia are present in cysts of *Cep290*$^{LacZ/LacZ}$ kidney (Panel C) highlighted by red arrow. TEM images of wild type and *Cep290*$^{LacZ/LacZ}$ renal collecting duct cells (Panels D+E) Scale bar (D+E) 10µm. Scale bar (F) 2µm. Collagen deposition in between the tubular endothelium is evident in the *Cep290*$^{LacZ/LacZ}$ renal cysts (red asterisk), implicating that loss of Cep290 results in a loss of endothelial maintenance and integrity. (L) Lumen of collecting duct cyst

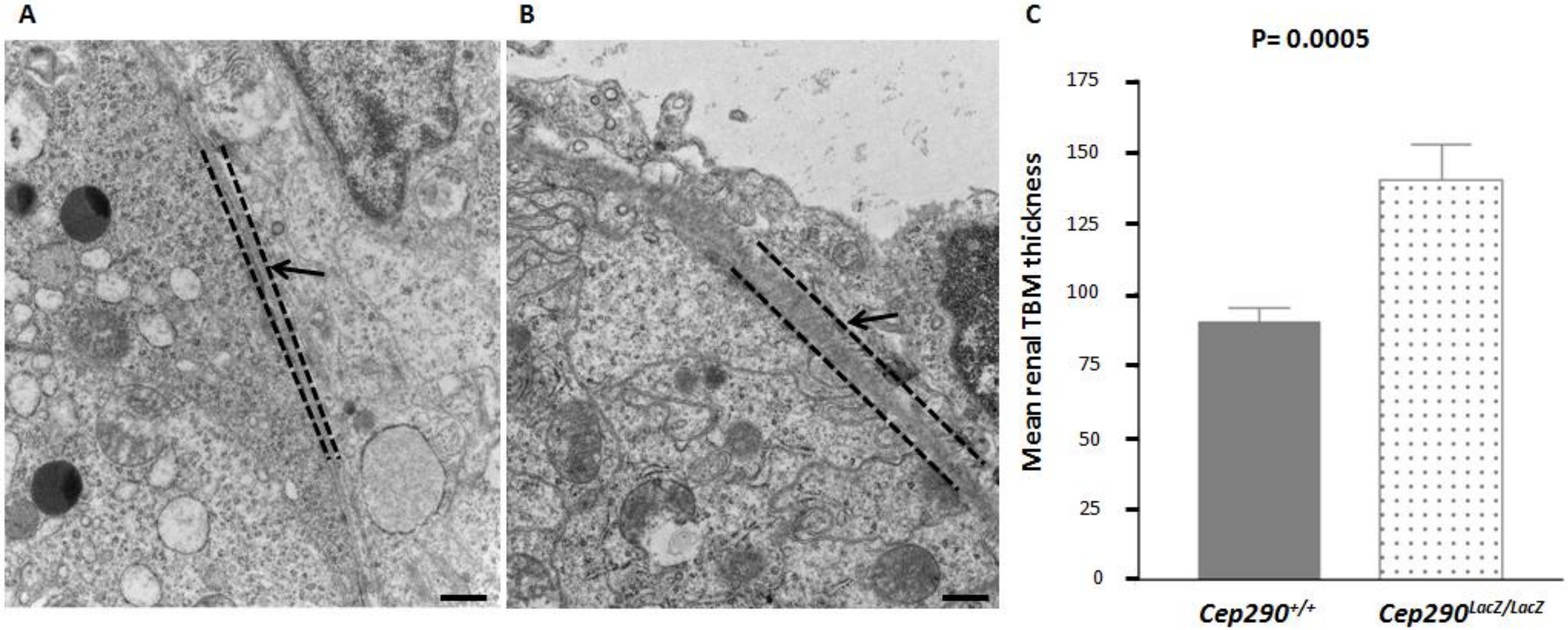

Figure 3.12 TBM defects in *Cep290*$^{LacZ/LacZ}$ mice.
TEM images of (TBM) in renal tissues of *Cep290* mice.Panel A+B) *Cep290*$^{+/+}$ and *Cep290*$^{LacZ/LacZ}$ (TBM) highlighted by dashes. Panel C) Student t test measuring the TBM thickness from 7 renal TEM images for both *Cep290*$^{+/+}$ and *Cep290*$^{LacZ/LacZ}$ mice. 20 measurements were taken in total approximately n=3 measurements per image. Scale bar 500nm. Direct Magnification for each image measured was 18500X.

3.13 Investigating the morphology of retina cell layers in *Cep290*$^{LacZ/LacZ}$ mice

Cep290 mutations are the most frequent cause of LCA, (accounting for ~15% of cases), a severe retinal dystrophy causing blindness in paediatric patients (den Hollander, Roepman et al. 2008). Retinal degeneration is due to the loss or dysfunction of the outer nuclear cell layers (ONL) of the retina specifically the photoreceptor layer (a highly ciliated layer of the retina). Retinal dystrophy affects 1:2,000 of the UK population. Currently there are no effective preventative treatments; however research is on going for various biological treatments at the Institute of Ophthalmology, London. The treatments currently being investigated include cell transplantation, gene transfection and the use of growth factors to delay cell death (http://www.ucl.ac.uk/ioo/research/bird.htm).

Possible treatment strategies for the maintenance of retinal dystrophy are currently being investigated. However mouse models are required to test treatments prior to clinical trials. An early onset of retinal degeneration occurs in children with JBTS. As stated previously *Cep290* mutations are the most frequent cause of LCA in children. Therefore novel mouse models with mutations in the *Cep290* gene are ideal model organisms used to investigate potential therapies for these children.

The *rd16;Nrl*$^{-/-}$ double mutant mice harbor an in frame deletion in the *Cep290* gene and the mice begin to present with retinal degeneration by 2 weeks of age and by 1 month of age the rod photoreceptors have completely degenerated with only a single layer of cone nuclei remains in the ONL of these mice. As the *rd16;Nrl*$^{-/-}$ mouse model showed a high loss of photoreceptors cells by 1 month of age (Cideciyan, Rachel et al. 2011), it was hypothesised that this novel *Cep290*$^{LacZ/LacZ}$ mouse model may also exhibit a retinal dystrophy phenotype.

Cep290$^{+/+}$ and *Cep290*$^{LacZ/LacZ}$ mice were examined at various time points to investigate if retinal degeneration was evident. The *Cep290*$^{LacZ/LacZ}$ mice presented with retinal degeneration which slowly progressed in severity from 2 weeks to 1 month of age. By 6 months of age all outer layers of the retina were completely degenerated (Figure 3.13). The *rd16;Nrl*$^{-/-}$ mouse model which contains a hypomorphic mutation in the *Cep290* gene confirms that this *Cep290*$^{LacZ/LacZ}$ model phenocopies an established published mouse model.

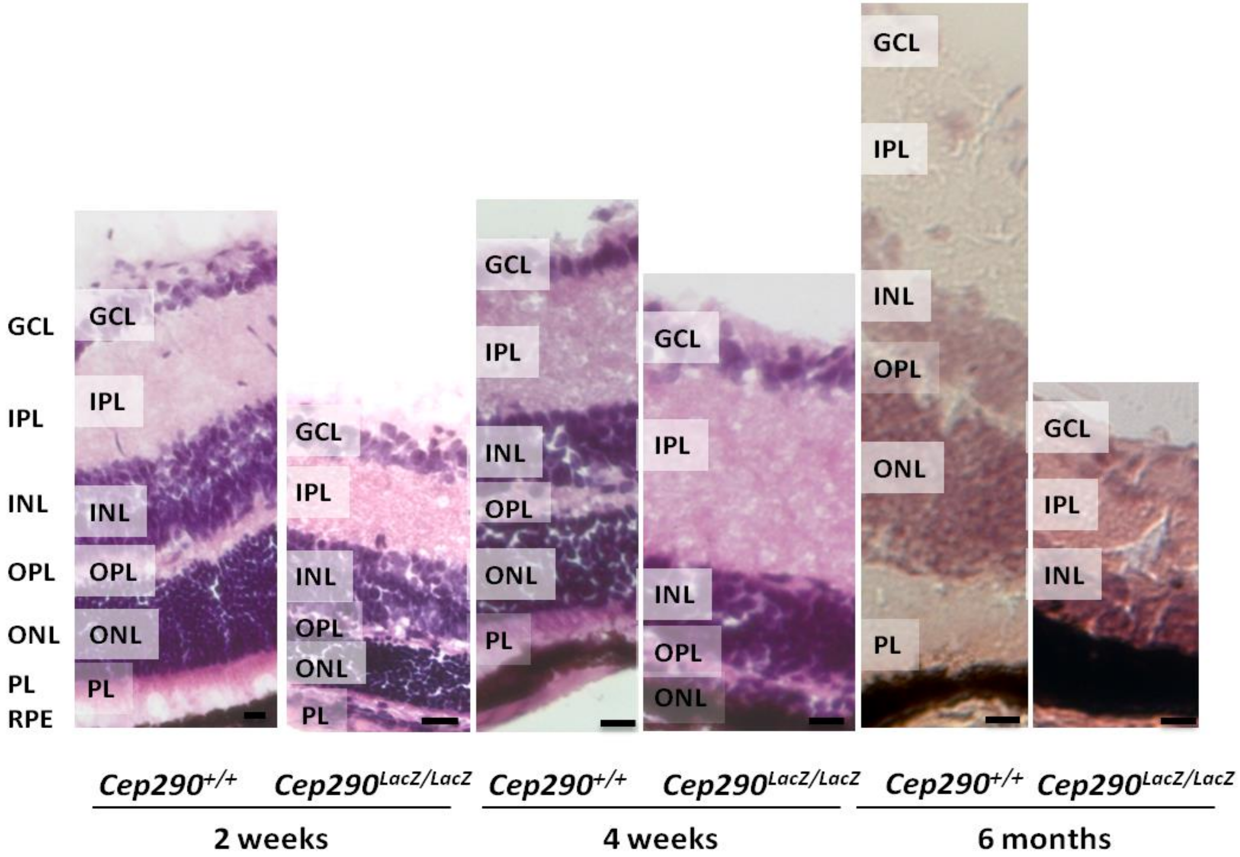

Figure 3.13 Retinal degeneration is evident in *Cep290*$^{LacZ/LacZ}$ mice on a C57BL/6J backround
Haematoxylin and Eosin staining of retina layers in 2 week, 4 week and 6 months old *Cep290*$^{+/+}$ and *Cep290*$^{LacZ/LacZ}$ mice. The outer retinal layers (ONL and PL) in *the Cep290*$^{LacZ/LacZ}$ mouse degenerate over time. By 4 weeks of age the ONL layer is reduced by half and by 6 months of age the OPL, ONL and PL are no longer evident. (GCL)-Ganglion Cell Layer, (IPL) Inner Plexiform Layer, (INL) Inner Nuclear Layer, (OPL) Outer Plexiform Layer (ONL) Outer Nuclear Layer and (PL) Photoreceptor layer, RPE (Retinal Pigmented epithelium) RPE is brown in colour in the images above. Scale bar 20µM.

3.14 Investigating the cerebellum morphology of *Cep290*$^{LacZ/LacZ}$ mice.

JBTS is a ciliopathy disease caused by malformations of the midbrain and hindbrain. Patients presenting with this disease display symptoms that include ataxia, hypotonia, developmental delay and intellectual disability (Hodgkins, Harris et al. 2004; Parisi, Doherty et al. 2007; Doherty 2009).

It has been estimated that 50% of JBTS patients have a mutation in the *CEP290* gene (Valente, Brancati et al. 2013). An investigation into the morphology of the *Cep290*$^{LacZ/LacZ}$ brain was employed by means of MRI imaging. MRI imaging identified that hydrocephaly was evident in *Cep290*$^{LacZ/LacZ}$ mice at 2 weeks of age (P14) (Figure 3.14). Hydrocephaly was also evident in the *Ahi*$^{-/-}$ mouse model of JBTS (Lancaster, Gopal et al. 2011).

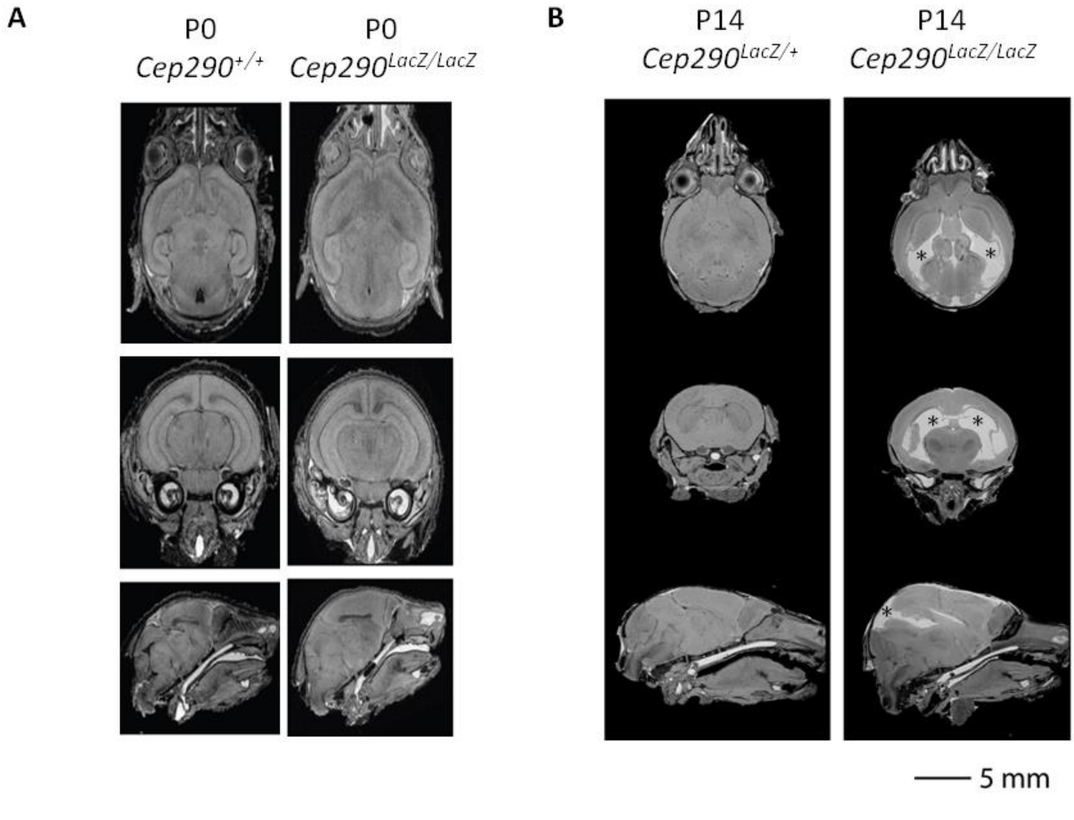

Figure 3.14 Hydrocephally is evident in *Cep290*$^{LacZ/LacZ}$ mice at 2 weeks. Brain MRI images of *Cep290*$^{+/+}$ and *Cep290*$^{LacZ/LacZ}$ at birth (Panel A) and at 2 weeks of age (Panel B). Hydrocephally is not evident at birth (n=5) however hydrocephally is visually evident from 2 weeks in *Cep290*$^{LacZ/LacZ}$ mice (highlighted by asterisks).

3.15 Embryonic lethality in *Cep290*$^{LacZ/LacZ}$ mice on the C57BL/6J background.

The phenotypes of the *Cep290*$^{LacZ/LacZ}$ mice described in figures 3.4-3.14 were from a mixed generation ($F_{2\text{-}3}$ mice) of the C57BL/6J mouse strain. Although the mice presented with hydrocephally, only 10% of the $F_{2\text{-}3}$ mice on the C57BL/6J mouse strain were viable (Table 3.1), this supports the published *Ahi1*$^{-/-}$ mouse model of JBTS where there was only a 20% survival rate noted on their C57BL/6J mixed mouse strain and the cause of lethality was unknown (Louie, Caridi et al. 2010).

The number of live births of *Cep290*$^{LacZ/LacZ}$ mice on a C57Bl/6J F_6 generation (4 out of 95 pups born) and from a mixed generation (56 out of 454) did not follow Mendelian characteristics (Table 3.1) and therefore it was hypothesised that C57Bl/6J *Cep290*$^{LacZ/LacZ}$ embryos were dying *in utero*.

To assess this possibility of embryos dying *in utero* as a consequence of the *Cep290* mutation embryos were analysed at E11.5 to ascertain the causation of the lethality (Figure 3.15). It was speculated that the embryos presented with severe brain or heart abnormalities as the embryos did not survive until birth and hence these were the organs that were investigated (Figure 3.15). A possible failure of neural groove closure was observed in the *Cep290*$^{LacZ/LacZ}$ mice. There were 24 embryos collected in total on the 6th generation C57Bl/6 mouse strain. The collective number of embryos obtained were as follows; 8 *Cep290*$^{+/+}$*,* 13 *Cep290*$^{LacZ/+}$ and 3 *Cep290*$^{LacZ/LacZ}$. Tail clippings from each embryo were gathered in order to confirm genotypes. Even though this is a small cohort and statistical methods are not employed, only 12.5% of embryos collected on the 6th generation C57BL/6J backgrounds were *Cep290*$^{LacZ/LacZ}$*.* If the *Cep290* mice on the C57Bl/6J strain were following Mendelian ratio 25% of embryos should have been *Cep290*$^{LacZ/LacZ}$.

Unfortunately, due to the lack of embryonic numbers there was no conclusive evidence for the cause of the re-absorption of *Cep290*$^{Lacz/LacZ}$ mice on the C57BL/6J strain. The main aim of this study was to analyse and assess the roles of PKD in a *Cep290*$^{LacZ/LacZ}$ mouse model. The inbred 129/Ola mice followed Mendelian characteristics (Table 3.1) and therefore this study continued investigating and assessing the phenotype of a truncated *Cep290* mutation from the 129/Ola mouse strain. There was evidence of a failure neural groove closure in the *Cep290*$^{LacZ/LacZ}$ embryos analysed on the F6 generation of C57BL/6J mice, which results in anencephaly. Anencephaly is a feature of the embryonic lethal MKS (Paetau, Salonen et al. 1985). A failure of neural groove closure of the hindbrain was also observed in the recently published *Nur12* $^{-/-}$ mouse Figure 3E (Alcaraz, Gold et al. 2006) and the *Tmem67*$^{-/-}$ JBTS-like mouse model (Figure 1 B) (Abdelhamed, Wheway et al. 2013).

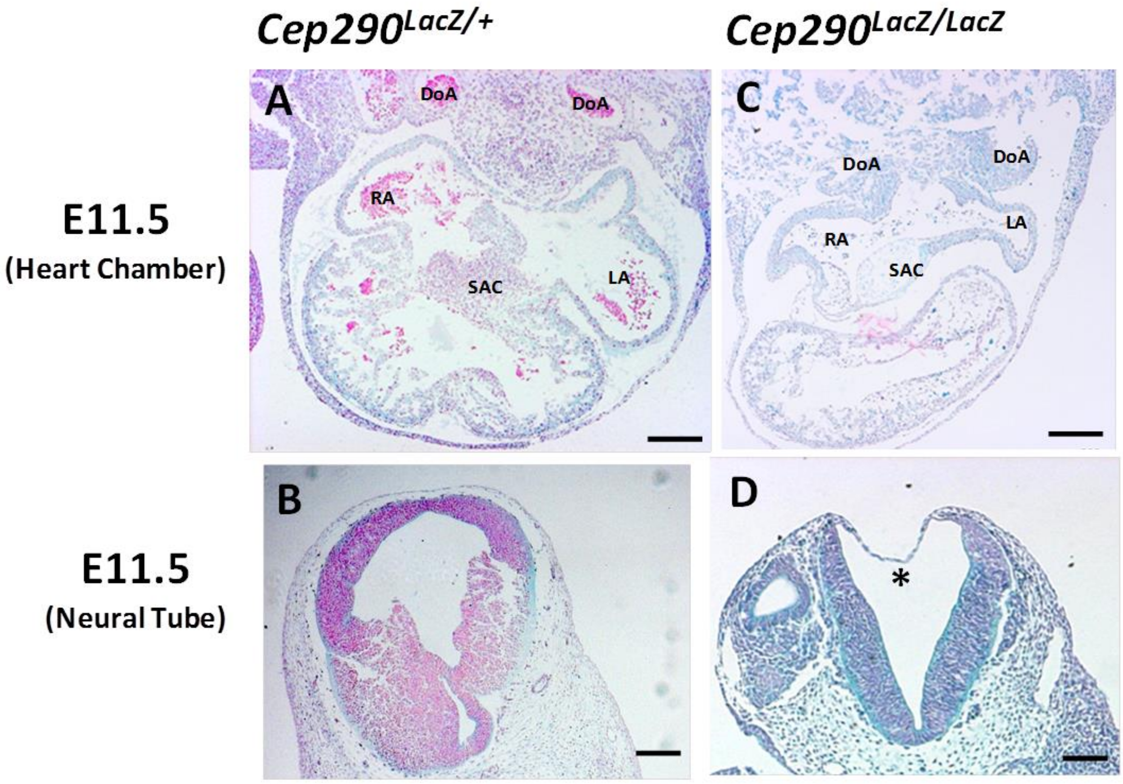

Figure 3.15 *Cep290* 6th generation C57BL/6J embryos.
Panels (A+C) Transverse sections through the hearts of *Cep290*$^{LacZ/+}$ and *Cep290*$^{LacZ/LacZ}$ embryos at approximately E11.5. The *LacZ* staining did not penetrate through to the tissues so therefore no conclusive evidence can be made as to where *Cep290* is specifically expressed in the heart. Panels (B+D) Horizontal brain sections of *Cep290*$^{LacZ/+}$ and *Cep290*$^{LacZ/LacZ}$ embryos possible failure of neural tube closure (asterisk).
Panels (A-D) Scale bars 200µm. (RA) right atrium, (LA) left atrium, (DoA) dorsal aorta, (SAC) superior atrioventricular cushion tissue.

3.16 Renal cysts in neonatal pups from *Cep290*$^{LacZ/LacZ}$ F_6 generation C57BL6/J mice.

Table 3.1 highlights the total cohort of *Cep290* mice utilised in this study. Prior to the observation that only 4% of *Cep290*$^{LacZ/LacZ}$ mice survived to gestation on the F_6 generation, *Cep290*$^{LacZ/LacZ}$ kidneys were analysed at birth (n=2) and extensive microcyst dilation was observed compared to wild-type littermates (Figure 3.16).

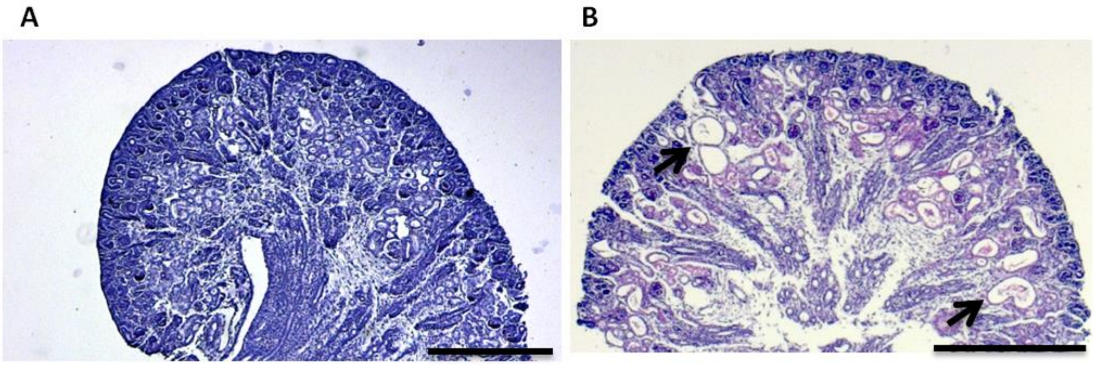

Figure 3.16 Gross cysts in newborn kidneys of 6th generation C57BL/6J *Cep290*$^{LacZ/LacZ}$.

Newborn kidneys of F_6 C57BL/6J *Cep290*$^{+/+}$ (Panel A) and *Cep290*$^{LacZ/LacZ}$ mice (Panel B), which survived to birth. At birth the kidneys were dissected and analysed for H+E histology. Note cysts were only evident in the *Cep290*$^{LacZ/LacZ}$ kidneys (n=2). There was no cysts evident in *Cep290*$^{+/+}$ or *Cep290*$^{LacZ/+}$ (n=3). Cysts (arrowed) were located in the corticomedullary region of the kidney. Scale bar 500µm.

3.17 Concluding results from the *Cep290*$^{LacZ/LacZ}$ C57BL/6J mouse colony.

In summary the *Cep290*$^{LacZ/LacZ}$ mouse model created on an inbred C57BL/6J mouse strain phenocopies a severe juvenile MKS phenotype. It should be noted that *Cep290*$^{LacZ/+}$ animals were tested alongside wild type and *Cep290*$^{LacZ/LacZ}$ littermates for the phenotypes observed. There was no evidence of renal cysts in *Cep290*$^{LacZ/+}$ mice analysed up to 1 year of age (Appendix 4, panel B). There was also no evidence of hydrocephaly (Figure 3.14) observed in *Cep290*$^{LacZ/+}$ mice.

However, as only 10% of the *Cep290*$^{LacZ/LacZ}$ mice from the $F_{2\text{-}3}$ generations were viable. Some of the mice were dying at 1 month and others surviving to a few months of age. The *Cep290* mutation was deleterious through the backcrosses of C57BL/6J mice for 6 generations. The effect of the mutation is most likely modified by modifier loci. It is presumed that the clinical variability of *CEP290* related diseases may be caused by second site modifier alleles (Coppieters, Lefever et al. 2010) and (Zhang, Seo et al. 2013).

On the F_6 generation C57BL/6J mouse strain only 4% of *Cep290*$^{LacZ/LacZ}$ mice were born. Overall it is likely that the inheritance pattern observed was due to the difference between the genetic backgrounds of the transgenic strains utilised and to the *Cep290* truncated mutation in this study.

It is common for mouse strains to show phenotypic differences over generations of breeding due to genetic drifts. In relation to the variability of phenotype observed, previous ARPKD mouse model studies have shown that disease penetrance and severity can be modulated depending on the genetic background. For example the *cpk* mutant mouse bred on the C57BL/6J strain did not present with the biliary ductal plate malformation lesions but in other mouse strains lesions were evident (Guay-Woodford, Green et al. 2000).

Another recent study with*Tmem67* knockout mice (Abdelhamed, Wheway et al. 2013) found inter-individual variation in phenotypes between *Tmem67*$^{-/-}$ littermates on a C57BL/6J inbred strain, which supports the variation in cystic phenotypes , low birth rates and varying ages of mortality rates between littermates observed in this novel C57BL/6J *Cep290* mouse model.

Following on from the results above *Cep290* 129/Ola mouse strain phenotypes and Mendelian characteristics were assessed.

3.18 *Cep290$^{LacZ/LacZ}$* 129/Ola inbred mice.

The *Cep290^{LacZ}* mutation was also placed on a pure inbred 129/0la background. On this background the gross phenotype appeared less severe with the *Cep290$^{LacZ/LacZ}$* mouse numbers being close to a Mendelian fashion (Table 3.1).

3.19 *Cep290* 129/Ola mice at 1 year.

In comparison to the cranial morphology of the *Cep290$^{LacZ/LacZ}$* mice on a C57BL/6J background (Figure 3.4 panel A) a domed head was not visible in the *Cep290$^{LacZ/LacZ}$*129/Ola mice at 1 year of age (Figure 3.17).

Unlike the *Cep290* C57BL/6J mouse strain where the *Cep290$^{LacZ/LacZ}$* mice were visibly smaller, there were no differences in the length/ size of 129/Ola *Cep290$^{LacZ/LacZ}$* mice when compared to their wild type littermates and the kidneys are not obviously smaller (Figure 3.17).

To date, reports do not indicate that patients with JBTS are smaller in height nor do they present with obvious structural cranial abnormalities. Given this observation the 129/Ola mice are anatomically similar to the patients with JBTS compared to the *Cep290$^{LacZ/LacZ}$* mice bred on a C57BL/6J background. *Cep290*$^{LacZ/LacZ}$ mice on a C57BL/6J background present with a domed head and a smaller stature compared to wild type littermates.

In ADPKD gross cysts are present within the kidney in patients/ mouse models affected with this disease. The cystic phenotype is much more subtle in patients with ARPKD, with tubular dilatations rather than huge cysts. This more subtle cystic phenotype is evident in the *Cep290$^{LacZ/LacZ}$* 129/Ola colony and the C57BL/6J mouse colony as gross cysts are not present on the extremities of the kidneys (Figures 3.17).

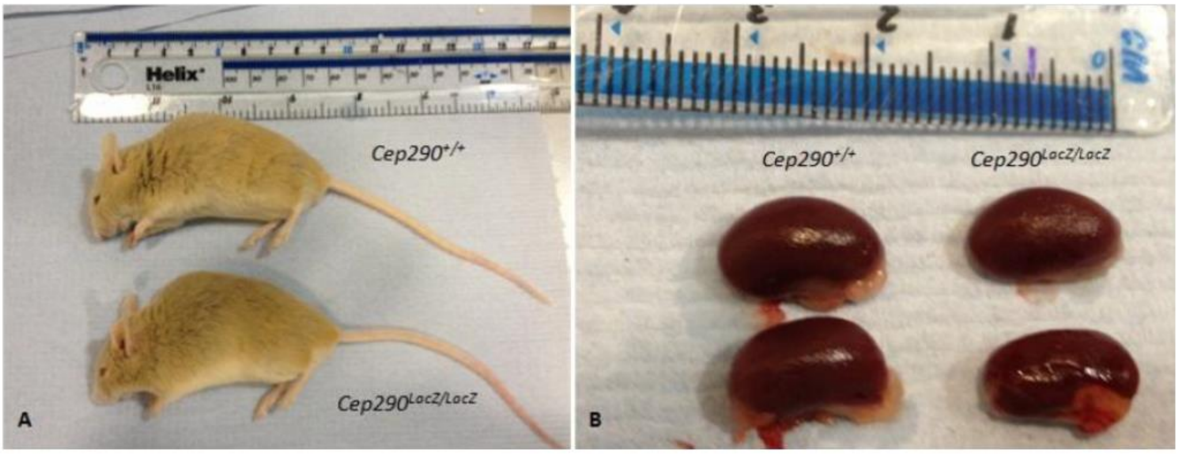

Figure 3.17 *Cep290* mice at 1 year of age.
Cep290$^{+/+}$ and *Cep290*$^{LacZ/LacZ}$ 129/Ola inbred mice at 1 year of age (Panel A). There are no differences in appearance between mice at 1 year of age unlike C57BL/6J mice where the *Cep290*$^{LacZ/LacZ}$ mouse is physically smaller. Mice from the 129/Ola background survive to 1 year of age. Wild type and *Cep290*$^{LacZ/LacZ}$ kidneys are approximately 1cm in length at 1 year of age (B). Gross cysts are not evident in the 129/Ola *Cep290* mouse model however when sectioned there are cysts evident in the cortical medullary region of the *Cep290*$^{LacZ/LacZ}$ mouse as can be seen in figures (3.18-3.19).

3.20 Comparing renal histology between *Cep290*$^{LacZ/LacZ}$ C57BL/6J mice and *Cep290*$^{LacZ/LacZ}$ 129/Ola mice at 1 month of age.

Cep290$^{LacZ/LacZ}$ 129/Ola were analysed at 1 month of age. A total of 6 mice histological phenotypes were analysed for *Cep290*$^{+/+}$ *and Cep290*$^{LacZ/LacZ}$ (Figure 3.18 for overview of three kidneys from each genotype analysed).

A comparison of the 129/Ola renal phenotype to the C57BL/6J renal phenotype at 1 month of age was addressed. It was evident that the cysts were concentrated to the corticomedullary region for both colonies; however the cysts also protruded more into the medulla in C57BL/6J mice as well as infiltrating the borders of the cortex.

At 1 month of age the *Cep290*$^{LacZ/LacZ}$ 129/Ola mouse colony cysts were similar in size and shape (Figure 3.18), unlike the C57BL/6J mice where an increase in size of cysts between individual *Cep290*$^{LacZ/LacZ}$ mice were apparent (Figure 3.7).

A steady state phenotype was observed in *Cep290*$^{LacZ/LacZ}$ 1 month old mice born on a 129/Ola background, which is ideal for studying the molecular mechanisms implicated in a constant steady inclined rate of cystogenesis in mice with NPHP. There is less variation in *Cep290*$^{LacZ/LacZ}$ 129/Ola mice compared to *Cep290*$^{LacZ/LacZ}$ C57Bl/6J which is a further indication that genetic modifiers on certain backgrounds produce some variability of phenotype

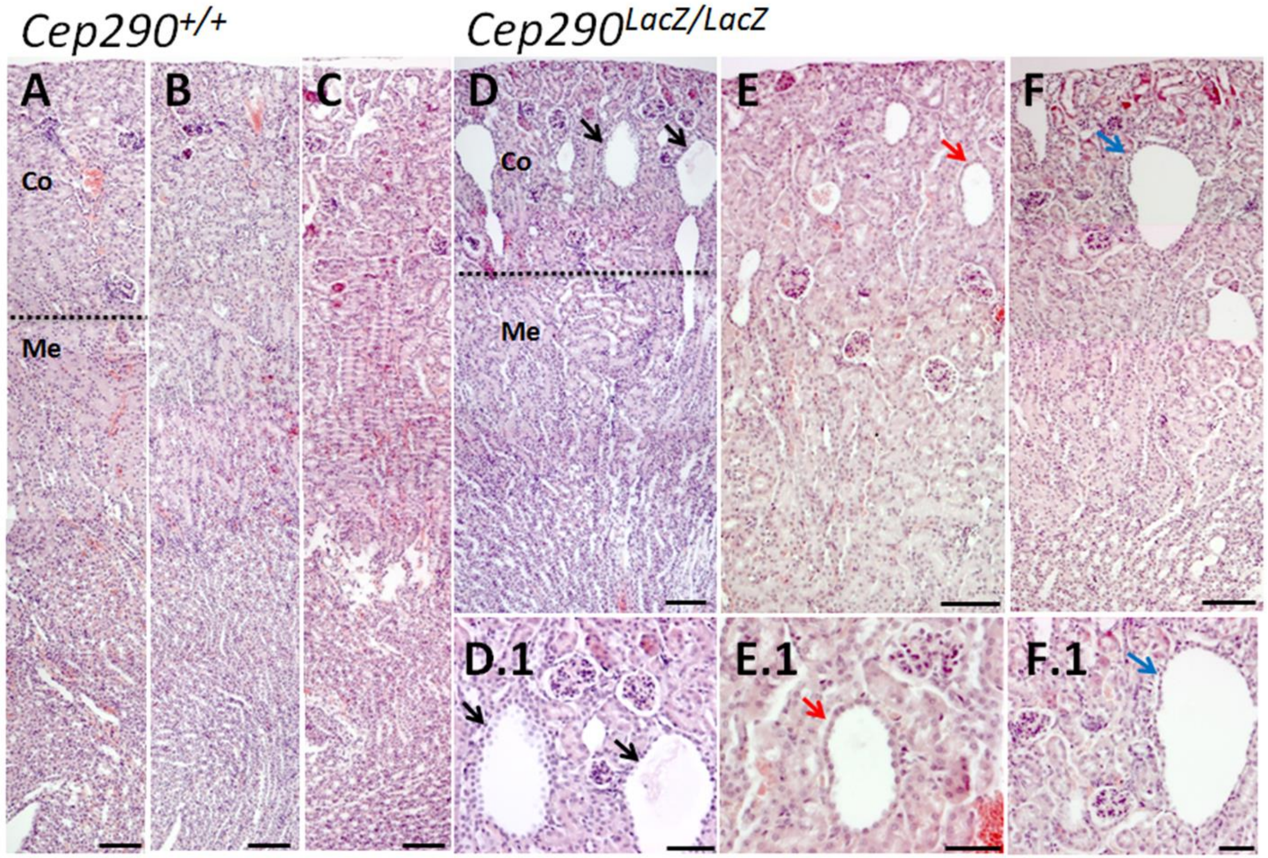

Figure 3.18 Representative features of 129/Ola *Cep290*$^{+/+}$ and *Cep290*$^{LacZ/LacZ}$ kidneys at 1 month.
Renal cysts are evident in the cortex and medulla of the kidney in *Cep290*$^{LacZ/LacZ}$ mice (Panel D-F) compared to their wild type litter mates (Panel A-C). Scale bar 100µM. Magnified images (D.1-F.1) of the *Cep290*$^{LacZ/LacZ}$ kidneys demonstrate an epithelial cell layer confirming cysts highlighted by black, red and blue arrows. Scale bars 50µM. (Co) Cortex and (Me) Medulla. Cysts vary from 50µm in width to 150µm at this time point.

3.21 Determining the renal morphology of *Cep290*$^{LacZ/LacZ}$ 129/Ola inbred mice at 1 year of age

It has been established that *Cep290*$^{LacZ/LacZ}$ 129/Ola mice survive to 1 year of age and that there is a consistent renal cystic phenotype at 1 month of age in *Cep290*$^{LacZ/LacZ}$ mice.

In order to determine the long term progression of cystic kidney phenotype and look for a fibrotic phenotype, the kidneys were examined in *Cep290*$^{+/+}$ and *Cep290*$^{LacZ/LacZ}$ mice at 1 year (n=4). Cysts were evident in the *Cep290*$^{LacZ/LacZ}$ corticomedullary renal tissues (Figure 3.18 and 3.19).

Interstitial fibrosis is one of the renal histological phenotypes associated with NPHP. Sirius Red staining was employed in order to examine the fibrotic nature of renal tissue from *Cep290*$^{LacZ/LacZ}$ 129/Ola mice at birth and at 1 year of age.

At birth in *Cep290* 129/Ola mice there was no apparent difference between *Cep290*$^{LacZ/LacZ}$ and wild type kidneys. At 1 year of age there was a substantial amount of collagen deposits in *Cep290*$^{LacZ/LacZ}$ renal tissue surrounding cysts and various parts of the corticomedullary junction confirming a fibrotic phenotype at 1 year of age in *Cep290*$^{LacZ/LacZ}$ mice (Figure 3.20).

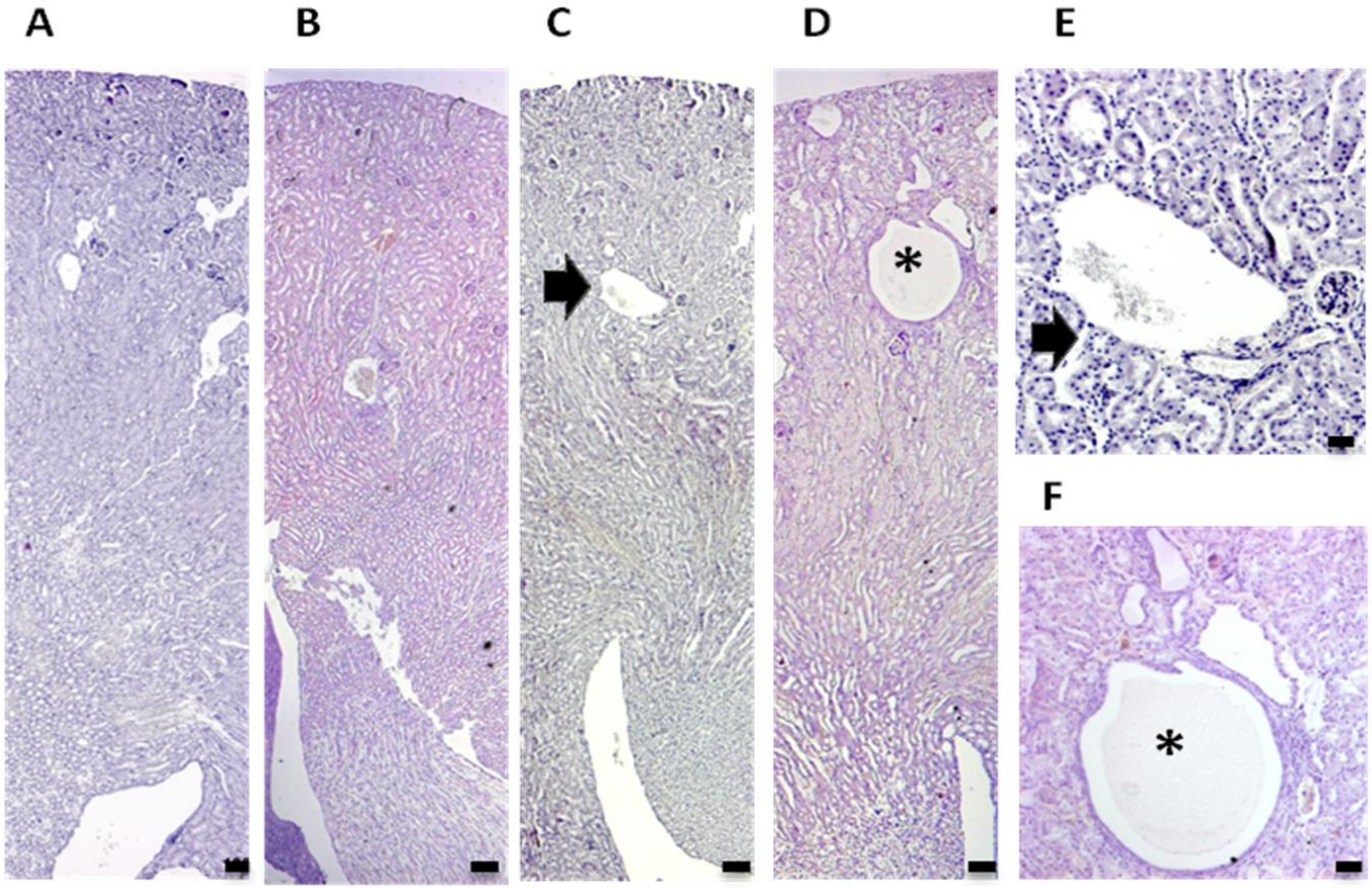

Figure 3.19 Renal cysts are prevalant in 1 year old 129/Ola *Cep290*$^{LacZ/LacZ}$ mice.
Panels (A-B) Images of *Cep290*$^{+/+}$ (C-D) *Cep290*$^{LacZ/LacZ}$ kidneys sections through the cortex, medulla and papilla. Scale bar 100µm. Panels (E-F) Magnified images of cysts in the *Cep290*$^{LacZ/LacZ}$ kidneys highlighted by a black arrow and an asterisk. Scale bar 50µm.

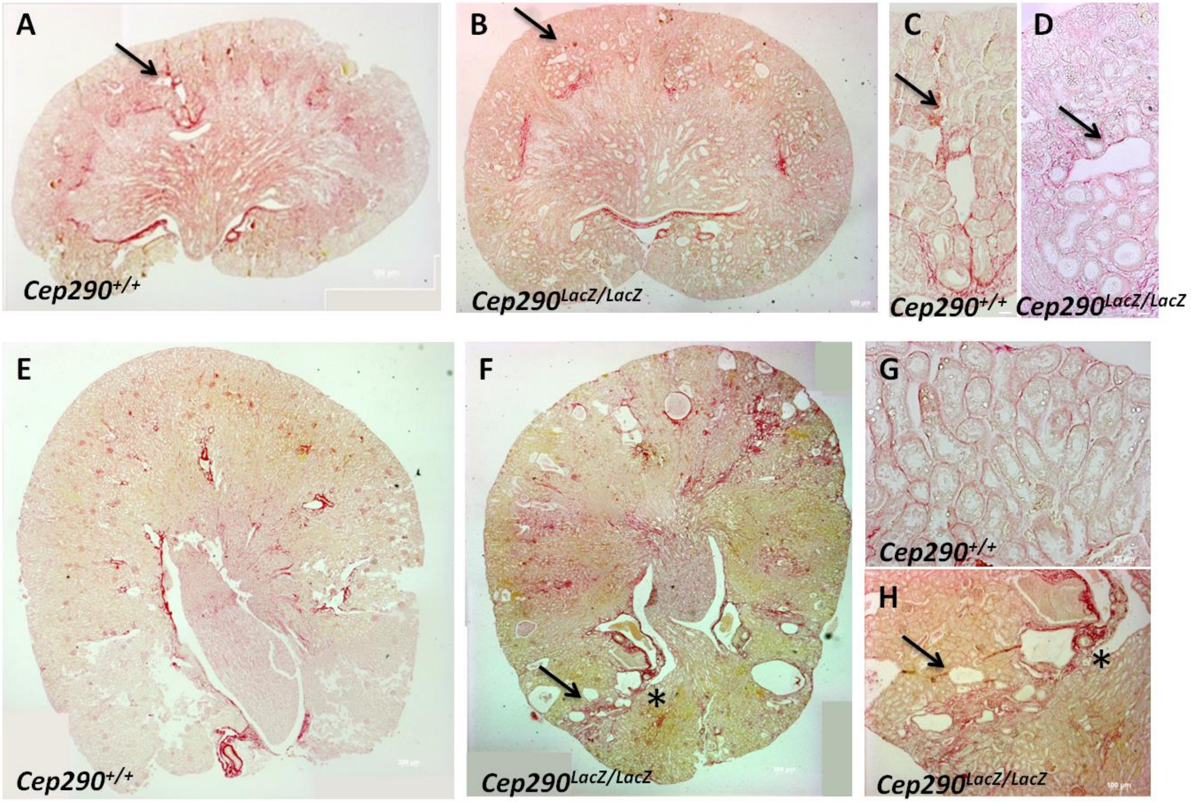

Figure 3.20 Sirius red staining to measure fibrotic changes in *Cep290* 129/Ola mice at birth and 1 year of age. Panels(A-D) Newborn *Cep290*$^{+/+}$ and *Cep290*$^{LacZ/LacZ}$ kidneys. Panels (E-H) 1 year *Cep290*$^{+/+}$ and *Cep290*$^{LacZ/LacZ}$ kidneys. Sirius red stains collagen red on a pale yellow background. In newborn kidneys for both wild type and *Cep290*$^{LacZ/LacZ}$ samples the sirius red staining are comparible. By 1 year of age there are large deposits of collagen in the *Cep290*$^{LacZ/LacZ}$ sample across the corticomedullary junctions compared to the wild type sample. The collagen deposits are also concentrated around cysts of the *Cep290*$^{LacZ/LacZ}$ kidney. Scale bar A+B 100µm. Scale bars C+D 20 µm. Scale bar E+F 200µM. Scale bar G 20µm. Scale bar H 100µm.

3.22 MRI scanning images of *Cep290*$^{LacZ/LacZ}$ mice

As seen in figure 3.14, the C57BL/6J mice (from the $F_{2\text{-}3}$ generation) presented with hydrocephaly at 2 weeks of age. MRI scans of the brains from 6 week old 129/Ola inbred mice were also obtained.

In 2010 the *Ahi1*$^{-/-}$ mouse model of Joubert syndrome identified a “mild defected cerebellar vermis foliation pattern” (Lancaster, Gopal et al. 2011). Given the observation of cerebellar vermis foliation defects in the *Ahi1*$^{-/-}$ mouse model the cerebellar vermis foliation patterns of the cerebellum in *Cep290*$^{LacZ/LacZ}$ 129/Ola mice were investigated and there was no evidence of any foliation defects (Figure 3.21).

However hydrocephaly was evident in the *Cep290*$^{LacZ/LacZ}$ 129/Ola mice at 6 weeks of age (Figure 3.21) as seen previously in this chapter for the *Cep290*$^{LacZ/LacZ}$ C57BL/6J mouse strain albeit less severe and less pronounced (Figure 3.14).

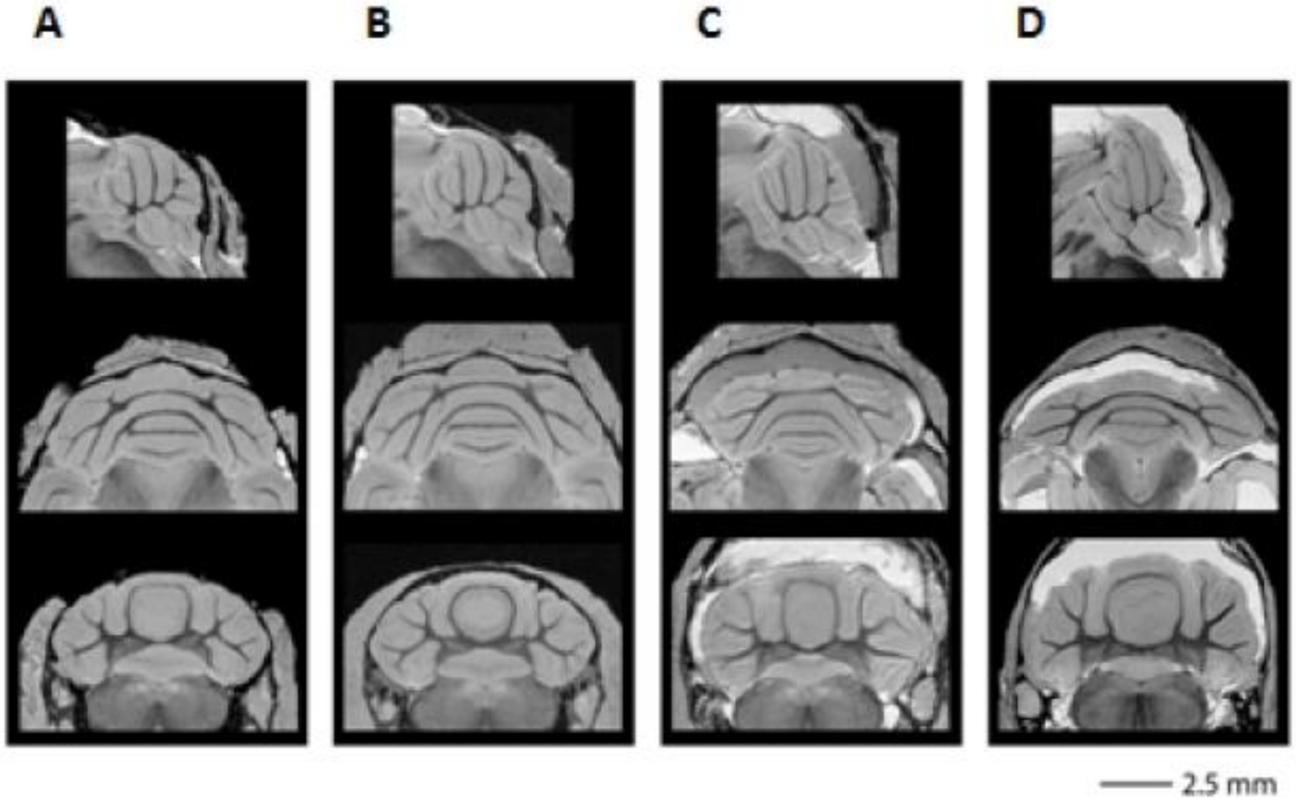

Figure 3.21 MRI imaging of *Cep290*$^{+/+}$ and *Cep290*$^{LacZ/LacZ}$ mice brains at 6 weeks of age.
Panels (A-B) Images of cerebellum foliation in *Cep290*$^{+/+}$ mice. Panels (C-D) Images of cerebellum foliation in *Cep290*$^{LacZ/LacZ}$ mice at 6 weeks. There are no extra foliations of the cerebellum observed in *Cep290*$^{LacZ/LacZ}$ mice however hydrocephaly was still evident at 6 weeks of age (Panels C-D). Scale bar 2.5mm.

3.23 Concluding remarks for *Cep290*$^{LacZ/LacZ}$ mice on an inbred 129/Ola back ground.

As shown through figures 3.18-3.21 the *Cep290*$^{LacZ/LacZ}$ mouse on an inbred 129/Ola colony present with the cystic kidney defects and brain abnormalities associated with JBTS.

An in-depth analysis into the retinal and cerebellum phenotypes of *Cep290* 129/Ola mice was not preformed as it was confirmed on the C57BL/6J background and the main aim of this section of the study was to confirm and utilise the cystic kidney nature for further experimentation in one or both colonies of *Cep290*$^{LacZ/LacZ}$ mice.

CEP290 mutations can cause a wide spectrum of diseases which have multi organ specific phenotypes ranging from embryonic lethal MKS, BBS and LCA, NPHP as well as JBTS (see chapter 1).

Extra organ specific manifestations seen in JBTS can range from polydactyly and hepatic fibrosis and/or liver cysts. This mouse study saw no evidence of cysts or fibrosis of the liver in *Cep290*$^{LacZ/LacZ}$ mice (figure 3.22) and there was no evidence of polydactyly occurring in both colonies of mice.

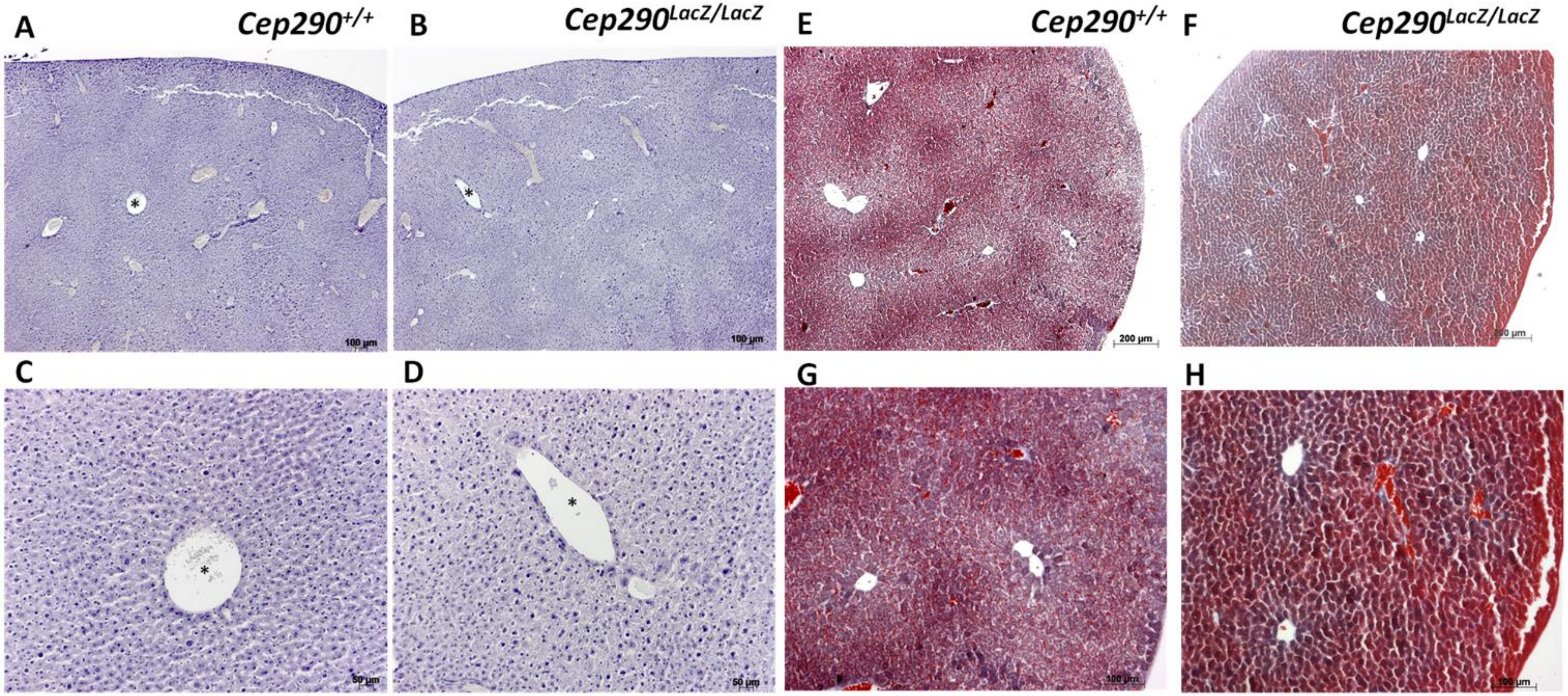

Figure 3.22 Liver phenotype in *Cep290*$^{LacZ/LacZ}$ mice.
Panels (A-D) Haematoxylin and Eosin staining of Liver samples from *Cep290*$^{+/+}$ and *Cep290*$^{LacZ/LacZ}$ mice at 1 year of age. Panels (E-H) Trichrome Masson staining of *Cep290*$^{+/+}$ and *Cep290*$^{LacZ/LacZ}$ liver samples at 1 month. No cystic or fibrotic phenotype evident in *Cep290*$^{LacZ/LacZ}$ mice. Scale bar 100µm (Panels A-B). Scale bar 50µm (Panels C-D). Panels (E-F) Scale bar 200µm. Panels (G-H) Scale bar 100µm.Asterisks highlight bile ducts which are not cystic

3.24 Discussion

In summary, the aims of this chapter were to determine the genotype and phenotype of mice with a truncated *Cep290* mutation and to investigate in detail renal phenotypes of this *Cep290*$^{LacZ/LacZ}$ model. From this analysis it was determined if this novel *Cep290* mouse model is an appropriate model of NPHP and JBTS.

As two different mouse colonies with a truncated mutation in the *Cep290* gene were utilised in this study the phenotypes of both mouse strains were assessed. It was discovered that the *Cep290*$^{LacZ/LacZ}$ mice for both inbred strains had multi-organ defects which included midbrain-hindbrain defects, retinal degeneration and renal cysts which were consistent with previous analyses carried out on patients with defects in the *CEP290* gene.

The reduced life expectancy in inbred *Cep290*$^{LacZ/LacZ}$ C57BL/6J mice is due to the strain specific variation in penetrance from the C57BL/6J back ground strain of the mice. The 129/Ola *Cep290*$^{\mathrm{LacZ/LacZ}}$ mice conformed to a normal Mendelian inheritance pattern. Unknown modifier genes which are present in C57BL/6J mice seem to affect the function of *Cep290*$^{LacZ/LacZ}$ mice consistant with variability seen in JBTS/NPHP patients.

Collecting duct cysts in *Cep290*$^{LacZ/LacZ}$ mice generated from the 129/Ola colony are specific to the corticomedullary region where as the C57BL/6J mice cysts were also found in the cortex and junction of the medulla and papilla. NPHP patient’s cysts are located specifically in the corticomedullary region. Therefore the *Cep290*$^{LacZ/LacZ}$ mouse on the 129/Ola model is an appropriate representative of the NPHP phenotype in JBTS.

Importantly the proteins mutated in cystic kidney disease are all localised to the primary cilia. Previous studies have shown that the sensory roles of the primary cilia in the kidney are required for the maintenance of fluid secretion and cellular proliferation. Polycystic kidney disease is a consequence of increased fluid secretion and cellular proliferation caused by defects in the sensory roles of the primary cilium in the kidney (Torres 2004). From these previous studies investigating the signalling mechanisms in each of the tissues affected by JBTS it is tempting to speculate that the *Cep290* truncated mutation is causing defects in the signalling mechanisms required for; maintaining the balance of CSF in the cerebellum, preventing the maintenance of photoreceptor cells in the eye and maintaining the balance of fluid secretion and cellular proliferation in the kidney.

JBTS and NPHP phenotypes are caused by mutations in the protein products of genes which are found in the primary cilium. As confirmed by SEM and TEM analysis primary cilia are present in the cysts of *Cep290*$^{LacZ/LacZ}$ kidneys. The cystic phenotypes present in *Cep290*$^{LacZ/LacZ}$ mice may therefore be due to a loss of the sensory function of the primary cilium.

In the study recently published determining the expression patterns of *CEP290* in humans, a strikingly pronounced expression of *CEP290* was observed in the developing choroid plexus in young fetal embryos, corresponding to the *LacZ* expression seen in this novel *Cep290* mouse model. Furthermore, *CEP290* human embryonic expression patterns were observed in the retinal pigment epithelium layers of the developing fetus which was also confirmed in this novel *Cep290* mouse model (Cheng, Eley et al. 2012).

It is now well established that primary cilia are present on the choroid plexus and that they act as chemosensors in maintaining the production of cerebrospinal fluid (Narita, Kawate et al. 2010). A disruption in the sensory function of the primary cilium in the choroid plexus will lead to excess cerebrospinal fluid production resulting in hydrocephaly.

Finally and most importantly for this study, the data previously published from the expression of *CEP290* in humans revealed prominent expression of *CEP290* in the developing collecting duct tubules in the human fetal embryos (Cheng, Eley et al. 2012). This *Cep290*$^{LacZ/LacZ}$ study documents the same pattern of *Cep290* expression in the brain retina and renal tissue of *Cep290*$^{LacZ/+}$ mice that was previously found in the human fetal data (Cheng, Eley et al. 2012).

Overall the phenotype of the *Cep290*$^{LacZ/LacZ}$ mouse model was consistent with the characteristics of patients with JBTS.

This *Cep290*$^{LacZ/LacZ}$ mouse model is a potentially valuable model organism which is required to dissect the pathways which are affected in NPHP. In the future this novel mouse model will be beneficial for testing targeted therapeutic treatments to prevent or to prolong the inevitable juvenile form of renal failure associated with NPHP.

This *Cep290*$^{LacZ/LacZ}$ mouse model recapitulates the cystic kidney phenotype of this human ciliopathy. The *Cep290*$^{LacZ/LacZ}$129/Ola mouse model had less variable features compared to the *Cep290*$^{LacZ/LacZ}$ C57BL/6J which manifested very variable cystic features.

Gene	Mouse model name + strain used	Phenotype			Reference
		Kidney	Brain	Eye	
Nphp1	*Nphp1*$^{del20/del20}$ (C57BL/6J)	No change	ND	ND	(Jiang, Chiou et al. 2008)
Nphp2	*Inv/Inv* (ND)	E15 collecting duct cysts	ND	ND	(Morgan, Turnpenny et al. 1998; Phillips, Miller et al. 2004)
Nphp3	(A) *Pcy* (B)*Nphp3*$^{Ko/Pcy}$ (C) *Nphp3*$^{Ko/Ko}$ (DBA/ C57BL/6J)	(A) Cysts from 2 weeks (TBM atrophy and dilation) (B) Cysts from 4 weeks old (C) NE	ND	ND	(A) (Omran, Haffner et al. 2001) (B) (Bergmann, Fliegauf et al. 2008)
Nphp4	*Nphp4*$^{nmf192/nmf192}$ (DBA+ C57BL/6J)	No change in morphology	ND	Photoreceptor Degeneration by P14	(Won, Marin de Evsikova et al. 2011)
Iqcb1	ND	ND	ND	ND	ND
Cep290	*Rd16/Rd16* (BXD-24/Ty)	No change in 6 month old mice		RD 1 month	(Chang, Khanna et al. 2006)
	Cep290$^{-/-}$ (C57BL/6J)	ND	Midline fusion defects E16.5	RD (not shown)	(Lancaster, Gopal et al. 2011)
	Rd16Nrl$^{-/-}$ (C57BL/6J)	ND	ND	Dis-functional cones	(Cideciyan, Rachel et al. 2011)
	Cep290$^{LacZ/LacZ}$ (C57BL/6J)	Collecting duct cysts at 1 month, TBM dilation, fibrosis at 1 month	Hydrocephaly	RD at 2 weeks	This study
	Cep290$^{LacZ/LacZ}$ (129/Ola)	Microscopic collecting duct cysts at birth, fibrosis not evident until after 1 month	Hydrocephaly	ND	This study
Glis2	*Glis2*$^{LacZ/LacZ}$ (C57BL/6J)	Loss of corticomedullary differentiation, small kidney resulting from reduced size in medulla over time, fibrosis by 8 weeks and TBM atrophy. Mild cystic phenotype at 8 weeks	ND	ND	(Attanasio, Uhlenhaut et al. 2007)
	Glis2^{mut} (C57BL/6J)	At 4 months reduced kidney size TBM thickening in proximal tubules, proteinuria, increased creatinine die of renal failure (NO CYSTS)	No change	ND	(Kim, Kang et al. 2008)
Rpgrip1l	*Ftm*$^{-/-}$ (Die at birth) (ND)	ND	Floor plate induction affected	Microphthalmia (reduced eye size)	(Vierkotten, Dildrop et al. 2007)
	Rpgrip1l$^{-/-}$ (Die at birth) (C3H and C57BL/6J)	E18.5 microcysts of proximal tubule	Dilated brain ventricle and cerebellar hypoplasia	Microphthalmia (reduced eye size)	(Delous, Baala et al. 2007)
	Ft/Ft (Die-midgestation) (C3H and C57BL/6J)	ND	Exencephaly	Microphthalmia (reduced eye size)	(Anselme, Laclef et al. 2007)
Nek8	*Jck-/-* (C57BL/6J)	Collecting duct cysts at 2 weeks, tubule cytoskeletal disorganisation	ND	ND	(Liu, Lu et al. 2002)
Sdccag8	ND	ND	ND	ND	ND
Tmem67	*bpck/bpck* (B6C3FeF1/J)	Death by 3 weeks from PKD	Hydrocephaly a few days after birth	ND	(Cook, Collin et al. 2009)
	Tmem67$^{-/-}$ (C57BL/6J)	Cysts at E18.5 (Die at birth but ND how)	ND	ND	(Garcia-Gonzalo, Corbit et al. 2011)
Ttc21b	*Aln*$^{-/-}$ (A/J and FVB)	ND	Delayed forebrain development	Microphthalmia (reduced eye size)	(Herron, Lu et al. 2002; Tran, Haycraft et al. 2008)

Gene	Mouse model name + (strain) used	Phenotype			Reference
		Kidney	Brain	Eye	
Wdr19	*Ift144*^{twt} (FVB/NJ)	ND	Exencephaly	Anopthalmia (Lack eyes)	(Ashe, Butterfield et al. 2012)
Wdr19	*Ift*^{dmhd} (FVB/NJ)	Die at E11.0 (Reason for death ND)			(Ashe, Butterfield et al. 2012)
Ahi1	*Ahi1*$^{-/-}$ (C57BL/6J)	Micro cysts, tubular dilation, tubular collapse, fibrosis at 1 year	Cerebellar midline fusion defects underdeveloped vermis with foliation defects	RD	(Lancaster, Louie et al. 2009)Lancaster, 2011 #35(Louie, Caridi et al. 2010)}
Atxn10	*Sca10* (FVB/N)	ND	Neuronal loss at hippocampus at 6 months vacuoles in the frontal lobe	ND	(White, Xia et al. 2012)
Znf423	*Nur12* (Mixed strains)	ND	Ataxia cerebellar vermis hypoplasia defects	ND	(Alcaraz, Gold et al. 2006)
Cep164	ND	ND	ND	ND	ND
	Han:SPRD $^{cy/+}$ *(Rat model)*	Proximal tubule cysts at P36	ND	ND	(Brown, Bihoreau et al. 2005)
Xpnpep3	ND	ND	ND	ND	ND
SLC41A1	ND	ND	ND	ND	ND
Jbts1	*Inpp5e*$^{\Delta/\Delta}$ (Mixed strains)	Multiple cysts E18.5	Exencephaly and Anencephaly	Development arrest at optic vesicle stage	(Jacoby, Cox et al. 2009)
Cors2	*Hty*$^{-/-}$ (C3H/HeN)	ND	Exencephaly	ND	(Hoover, Wynkoop et al. 2008)
Jbts3=(Ahi1), Jbts4=(Nphp1),Jbts5=(Cep290), Jbts6 =(Tmem67),Jbts7= (Rpgrip1l)					
Arl13b	*Hnn*$^{-/-}$ (C3H)	*ND*	"Open neural tube in the head"	Abnormal eye defects (E14.5)	(Caspary, Larkins et al. 2007)
Cc2d2a	*Cc2d2a*$^{-/-}$ (C57BL/6J)	ND	Forebrain failed to develop	Microphthalmia (reduced eye size)	(Garcia-Gonzalo, Corbit et al. 2011)
Ofd1	*Ofd1*$^{\Delta 4\text{-}5}$ (Mixed)	Autopsy of P0 = cystic kidneys	Exencephaly	ND	(Ferrante, Zullo et al. 2006)
Ttc21b = Nphp12					
Kif7	*Kif7*$^{-/-}$ (Mixed)	ND	Exencephaly	ND	(Cheung, Zhang et al. 2009)
	Kif7^{maki} (C57BL/6J)	ND	ND	ND	(Liem, He et al. 2009)
Tctn1	*Tctn1*$^{-/-}$ (C57BL/6J)	ND	Forebrain fails to develop	ND	(Reiter and Skarnes 2006)
Tmem237	ND	ND	ND	ND	ND
Cep41	*Cep41*$^{Gt/Gt}$ (C57BL/6J)	ND	Exencephaly lethal at E10	ND	(Lee, Silhavy et al. 2012)
Tmem138	ND	ND	ND	ND	ND
C5orf42	ND	ND	ND	ND	ND
Tctn2	*Tctn2*$^{-/-}$ (Mixed) +(C57BL/6J)	ND	(Mixed) Exencephaly E13.5	(C57BL/6J) Microphthalmia (reduced eye size)	(Sang, Miller et al. 2011)
Tctn3	ND	ND	ND	ND	ND
Tmem231	*Tmem231*$^{-/-}$ (C57BL/6J-Tyr$^{c\text{-}Brd}$)	Embryonic lethal ND			(Tang, Li et al. 2010)
Mre11	*Mre11* (Mixed)	Embryonic lethal ND			(Cherry, Adelman et al. 2007)

Table 3.2. Revised table 1.2 and 1.3 comparing Nphp/Jbts mouse models phenotypes to the *Cep290*$^{LacZ/LacZ}$ mouse model phenotype.
Not Discussed/Defined (ND) RD (Mixed= not inbred mice and mice are not bred on the one strain).

In examining the kidney phenotype alone from each of the Nphp/Jbts mouse models (Table 3.2), the *Cep290*$^{LacZ/LacZ}$ mouse model is a potentially valuable mouse model to use for targeting novel treatments for the juvenile form of NPHP.

Cep290$^{LacZ/LacZ}$ mice present with renal cysts from birth and survive until adulthood with a modest increasing cystic phenotype.

The *Nphp2, Jbts1* and *Jbts10/Ofd1* mouse models died at birth, although cystic kidneys were present in these animals it is not the juvenile form of nphp as the animals do not survive. The *Tmem67/Nphp11* mouse model is an accelerated model of nphp as the mice die from a cystic kidney phenotype at 3 weeks old hence monitoring the disease would be difficult. The *Tmem67//Nphp11* mouse reflects the infant form of NPHP rather than the juvenile form of NPHP.

The *Nphp3* mouse model has been used for treating PKD as mentioned in chapter 1 however the *Nphp3* mouse model is a slowly progressive cystic kidney disease model which mimics adolescent NPHP. Also interestingly 23/800 *pcy/pcy* mice did not have a PKD phenotype and therefore these mice were also modulated by modifier genes (Woo, Nguyen et al. 1997).

The last 2 mouse models to discuss with a cystic kidney phenotype include the *Ahi1* mouse model and the *Glis2* mouse model. The *Ahi1* mouse model only presents with a Nphp phenotype and micro cysts at 1 year of age therefore this mouse model is not suitable for comparing to the juvenile form of NPHP.

Finally the *Glis2* mouse model would be a good mouse model to use for treating juvenile NPHP however the mice only have micro cysts and are more of a fibrotic/epithelial to mesenchymal model. Hence the cystic phenotype of NPHP cannot be treated in the *Glis2* mouse model.

Chapter 4 Morphological and functional characterisation of a novel *Cep290*$^{LacZ/LacZ}$ immortal CDT cell line.

4.1 Introduction

This chapter focuses on an *in vitro* model of this *Cep290*$^{LacZ/LacZ}$ ciliopathy by generating an immortal *Cep290* CDT cell line. The *H-2Kb-tsA58* mouse line (published as the Immorto mouse (Jat, Noble et al. 1991)), was crossed with the *Cep290*$^{LacZ/LacZ}$ mouse to generate double transgenic *Cep290*$^{LacZ/LacZ}$ ::*H-2Kb-tsA58*$^{+/-}$ and *Cep290*$^{+/+}$ ::*H-2Kb-tsA58*$^{+/-}$ mice. The *Cep290* immorto mouse generated was then utilised to produce immortal CDT cells.

The *H-2Kb-tsA58* transgenic mouse strain was first described in 1991. This mouse model's genetic code is modified to contain the simian vacuolating virus (SV40) large tumour (T) antigen (Ag)- (TAg). The *H-2Kb-tsA58* transgenic mouse strain was created to conditionally immortalize many different cell types *ex vivo* (Jat, Noble et al. 1991). A modified thermo labile known as *tsA58 TAg* construct was exploited to reduce the normally high levels of proliferation and tumour genesis associated with TAg expression *in vivo* (Jat, Noble et al. 1991).

In order to ensure expression of the SV40 T antigen construct into a range of tissues, a histocompatability complex *H-2K*^{b} class I promoter was also utilized. The *H-2K*^{b} gene is active in many cells and can be induced by interferons (IFNs) thus adding an additional level of control (Wallach, Fellous et al. 1982; Israel, Kimura et al. 1986; David-Watine, Israel et al. 1990) .

The “immorto” transgene in the mice is usually dormant and can only be activated by culturing explanted cells at 33°C. At 33°C the A58 strain is activated and in the presence of IFN-γ expression the *H-2K*^{b} promoter is activated and expressed.

Cep290$^{LacZ/+}$ mice were mated with *H-2K*^{b}*-tsA58*$^{+/-}$ transgenic mice in order to isolate conditionally immortalized *Cep290*$^{+/+}$, *Cep290*$^{LacZ/+}$ and *Cep290*$^{LacZ/LacZ}$ kidney CDTs (Figure 4.1).

Immortal collecting duct cells are desirable as NPHP cysts are localised to the collecting duct epithelial cells. Mutations in *Cep290* cause NPHP and therefore CDT cells maybe a useful model study this disease at the cellular level. *Cep290*$^{LacZ/LacZ}$ mice as previously shown present with a collecting duct cystic kidney phenotype.

Unlike other cell lines derived from siRNA knockdown studies (described in further detail later in this chapter), the cells isolated in this study originated from a novel mouse model presenting with NPHP. The cysts are collecting duct in origin and therefore are the target cells at which the mutation in *Cep290* is expressed (Figure 4.2)

Importantly, CDT cells isolated from a mouse model of NPHP can be manipulated and subjected to various treatments and experiments and unlike animal models the direct affect on the cells can be easily followed.

In addition to the benefit of subjecting the cells to various treatments, CDT cells can be studied in more detail. Gene expression differences which influence a cystic phenotype in CDT's can be investigated in more precise detail compared to whole kidney tissues.

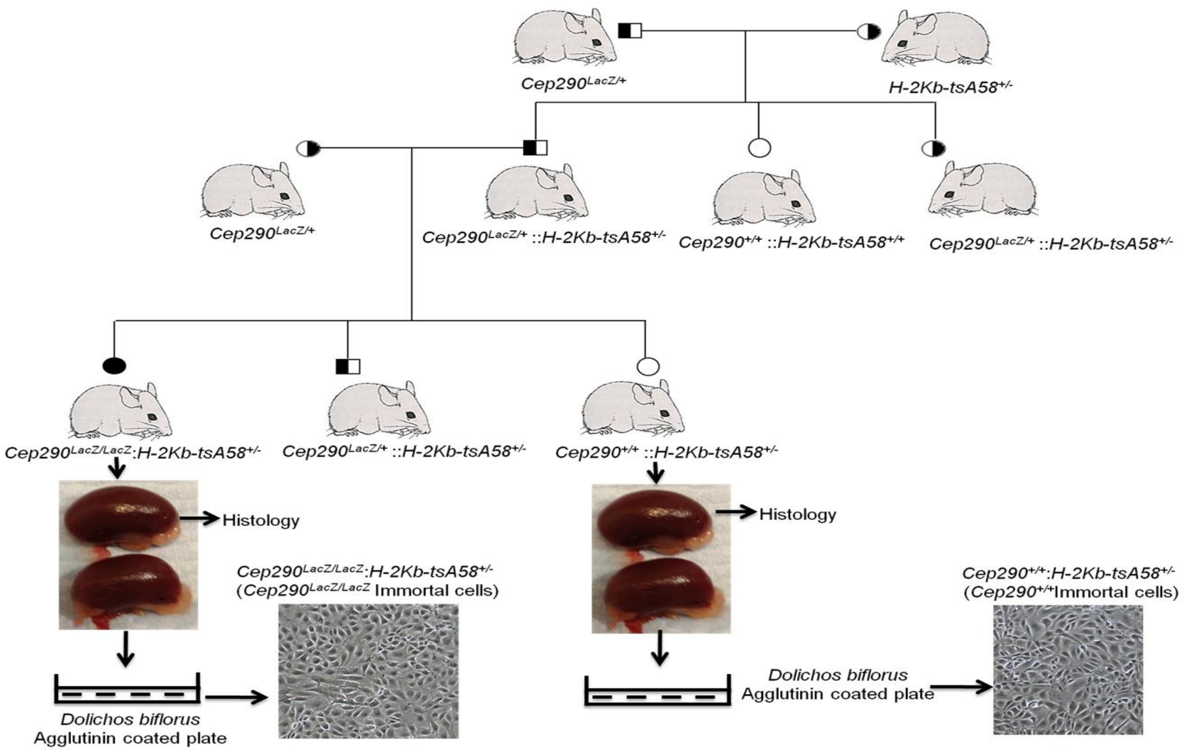

Figure 4.1 Breeding strategy for tsA58 transgenic *Cep290*$^{LacZ/LacZ}$ mice and isolation of CDT cells from these mice.
A *Cep290*$^{LacZ/+}$ male mouse was crossed with a heterozygous *H-2Kb-tsA58* transgenic female mouse to generate mice heterozygous for *Cep290* and *H-2Kb-tsA58.*These double heterozygous *Cep290:: H-2Kb-tsA58* mice were then backcrossed to a heterozygous *Cep290* mouse to generate compound mutant transgenic mice (known as the immortal *Cep290* homozygote mouse). Control mice for the immortal homozygote mouse were *Cep290*$^{+/+}$ mice with a single copy of the *H-2Kb-tsA58* transgene. When the mice were 1 month old the kidneys were dissected. One kidney was analysed for histology phenotype and the other kidney was used to generate immortal collecting duct cells. Mouse images adapted from (Strachan 2004).

4.2 Aims

A powerful tool for this study was to compare *Cep290*$^{LacZ/LacZ}$ *and Cep290*$^{+/+}$ immortal CDT cells during *in vitro* differentiation. An investigation into the morphology of the CDT cells lines generated was essential for the remainder of this chapter prior to any other experiments to ensure the cells represent a model of renal collecting duct cells.

In order to generate a *Cep290*$^{LacZ/LacZ}$ CDT cell line, the kidney phenotype of *Cep290*$^{LacZ/LacZ}$ and *Cep290*$^{+/+}$ mice bred with the *H-2K*^{b}*-tsA58*$^{+/-}$ transgenic mice needs to be assessed. Once the cystic kidney phenotype is confirmed in *Cep290*$^{LacZ/LacZ}$ mice bred with the *H-2K*^{b}*-tsA58*$^{+/-}$ mice the CDT cell line was generated from the kidneys of the double transgenic animals and the CDT cell line was characterised to confirm the cells were CDT cells. As NPHP is known as a ciliopathy related disorder the morphology of primary cilia from *Cep290*$^{LacZ/LacZ}$ CDT cell was also assessed and compared to *Cep290*$^{+/+}$ CDT cells and the results are as follows.

4.3 Generation and characterisation of CDTs.

One kidney from the offspring of the *Cep290*:: *H-2K*^{b}*-tsA58*$^{+/-}$ transgenic mice was analysed for renal morphology and a cystic phenotype (Figure 4.2). The other kidney dissected was employed for enriching CDT cells (see chapter 2 for enrichment procedure). It was confirmed that *Cep290*$^{LacZ/LacZ}$:: *H-2K*^{b}*-tsA58*$^{+/-}$ mice presented with a cystic kidney phenotype while the *Cep290*$^{+/+}$ and *Cep290*$^{LacZ/+}$ did not (Figure 4.2).

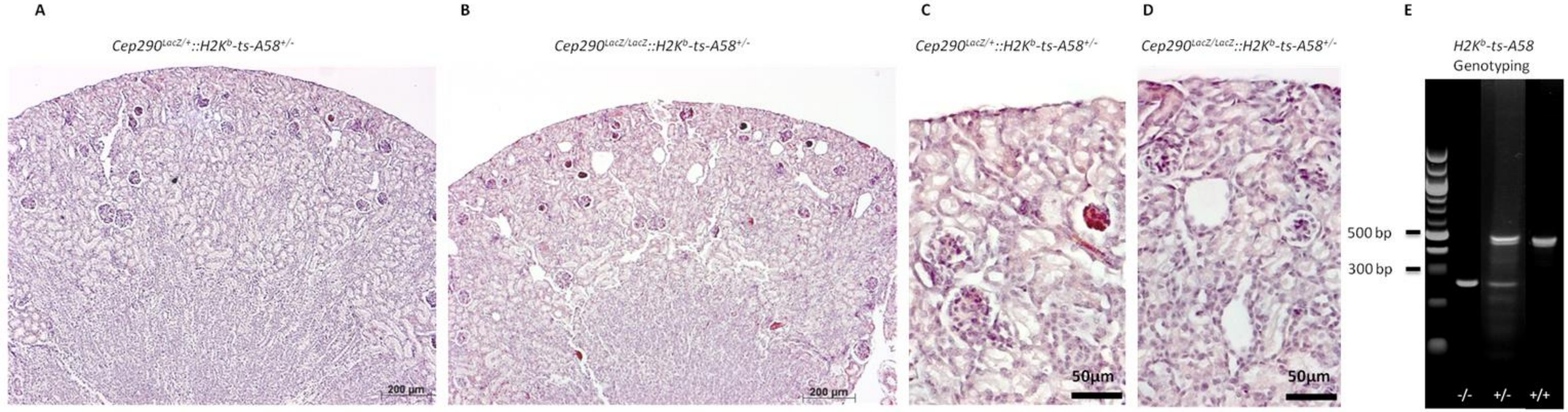

Figure 4.2 Renal phenotype of *Cep290*:: *H-2K^b-tsA58$^{+/-}$* transgenic mice and PCR confirming genotypes of *H-2K^b-tsA58* mice. Haematoxylin and Eosin staining of renal sections from *Cep290* $^{LacZ/+}$/*H-2K^b-tsA58$^{+/-}$* (A+C) and *Cep290* $^{LacZ/LacZ}$/*H-2K^b-tsA58$^{+/-}$* (B+D) transgenic mice. This figure illustrates that the heterozygous Cep290/ *H-2K^b-tsA58* mice do not express a phenotype of a cystic nature (Panel A+ C - no evidence of cysts) and thus phenocopy the heterozygote *Cep290* mouse. This figure also demonstrates that the *Cep290* $^{LacZ/LacZ}$/*H-2K^b-tsA58$^{+/-}$* (B+D) transgenic mice phenocopy the *Cep290$^{LacZ/LacZ}$* mouse presenting with cysts in the cortiex region of the kidney. Thus, these new double heterozygote/homozygote breedings phenotypically represent the *Cep290* mouse model Panel E Genotyping PCR of *H-2K^b-tsA58* mice. PCR distinguishes between wild type, heterozygous and homozygous *H-2K^b-tsA58* transgenic mice. Wild type *H-2K^b-tsA58* mice have a 500bp product and *Cep290$^{LacZ/LacZ}$* mice have a 300bp product. The wildtype and *Cep290$^{LacZ/LacZ}$* animals are clearly distinguishable and heterozygote animals have a copy of each of the products.

A single copy of the *H-2K^b-tsA58* transgene is sufficient to immortalize CDT cells. A previous study has created olignonucleotide primers identifying wild type immortal mice from heterozygous and homozygous immortal mice (Kern and Flucher 2005).

The *H-2K^b-1* transgene is located in chromosome 17 (whilst murine *Cep290* is on chromosome 18 therefore there is no risk of interfering with the *Cep290* gene) of the mouse genome with 6 coding exons. The 5' end of the *H-2K^b-1* transgene was fused to the SV40tsA58 coding sequence. The genes were fused together using the 4.2kb EcoRɪ-*Nru* ɪ fragment which contained the *H-2K^b* promoter sequence ligated to 2.7kb Bgl ɪ - *Bam*HI derived from the early region coding sequence of the tsA58 gene (Jat, Noble et al. 1991).

Before the study by Kern, G & Flucher B. E 2005, it was impossible to distinguish between heterozygote and mutant *H-2K^b-tsA58* mice, as the localization of the transgene was unknown. The mutant mice were reported to have a reduced life span compared to the heterozygous mice as the penetrance of 2 copies increase the thymic hyperplasia phenotype (Jat, Noble et al. 1991). Another report published that only 1/5th of the homozygous *H-2K^b-tsA58* females reproduced and if they did reproduce they only were able to reproduce once. It was determined that this study would focus on cells isolated from *Cep290* mice with only one copy of the *H-2K^b-tsA58* transgene (Figure 4.2 for genotyping results).

Kidney tissues were dissected from *Cep290$^{+/+}$*, *Cep290$^{LacZ/+}$* and *Cep290$^{LacZ/LacZ}$* mice heterozygous for the *H-2K^b-tsA58* gene. The method for extracting and enriching for the CDT cells has been described in the methods section and the cells were maintained as described in Chapter 2. Briefly kidney slices were digested in collagenase II digest the CDT cells were then enriched using DBA coated plates. DBA has been described as a marker of the collecting duct tubule in mammalian species including the mouse rat and rabbit (Watanabe, Muramatsu et al. 1981; Holthofer 1983; Holthofer, Schulte et al. 1987; Laitinen, Virtanen et al. 1987; Holthofer 1988; Plendl, Schoenleber et al. 1992; Kovacs, Zilahy et al. 1997; Grupp, Troche et al. 1998; Schumacher, Strehl et al. 2002).

An example of an immortalised CDT cell line from SV40 transgenic mice was first described in 1991 (Stoos, Naray-Fejes-Toth et al. 1991). This cell line exhibited some features of cortical collecting duct cells which included a typical epithelial appearance and cortical collecting duct specific antigens; however the cells lost their capability for aldosterone-stimulated Na^+ absorption via the activation of the MR (Stoos, Naray-Fejes-Toth et al. 1991).

MR expression is crucial for regulating salt water transport in the kidney. CDT's are responsible for the final regulation of maintaining sodium levels of reabsorption. Cells which exhibit aldosterone-stimulated Na^+ absorption can be easily identified using RT-PCR method to show any levels of expression of the MR.

Another important feature of CDT cells is to maintain expression of the epithelial sodium channel ENaC a membrane protein present in the apical membrane of principal cells of the cortical collecting tubule. The ENaC is responsible for apical Na^+ reabsorption in collecting duct cells (Hummler and Horisberger 1999).

In order to confirm the *Cep290* cells isolated were conditionally immortalised CDT cells (after DBA enrichment), the following parameters were examined:

1.) Bright field images of the cells at confluency were compared to published images of collecting duct tubules revealing that *Cep290*$^{+/+}$ and *Cep290*$^{LacZ/LacZ}$ CDT cells were morphologically similar to previously published images of CDT cells after every passage that has been investigated in this study (Figure 4.3 A+B).

2.) The cells were re-genotyped to confirm the presence of *Cep290* status by DNA genotyping and RT-PCR (Figure 4.3 C+D).

3.) The cells were assessed via western blotting to ensure the *Cep290*$^{LacZ/LacZ}$ cells did not express the full length *Cep290* protein product (Figure 4.3 E).

4.) To ensure cells were collecting duct in origin primers for MR and E-NaC were designed and their expression levels were tested and cells were analysed for confluent epithelial monolayers (Figure 4.3 F).

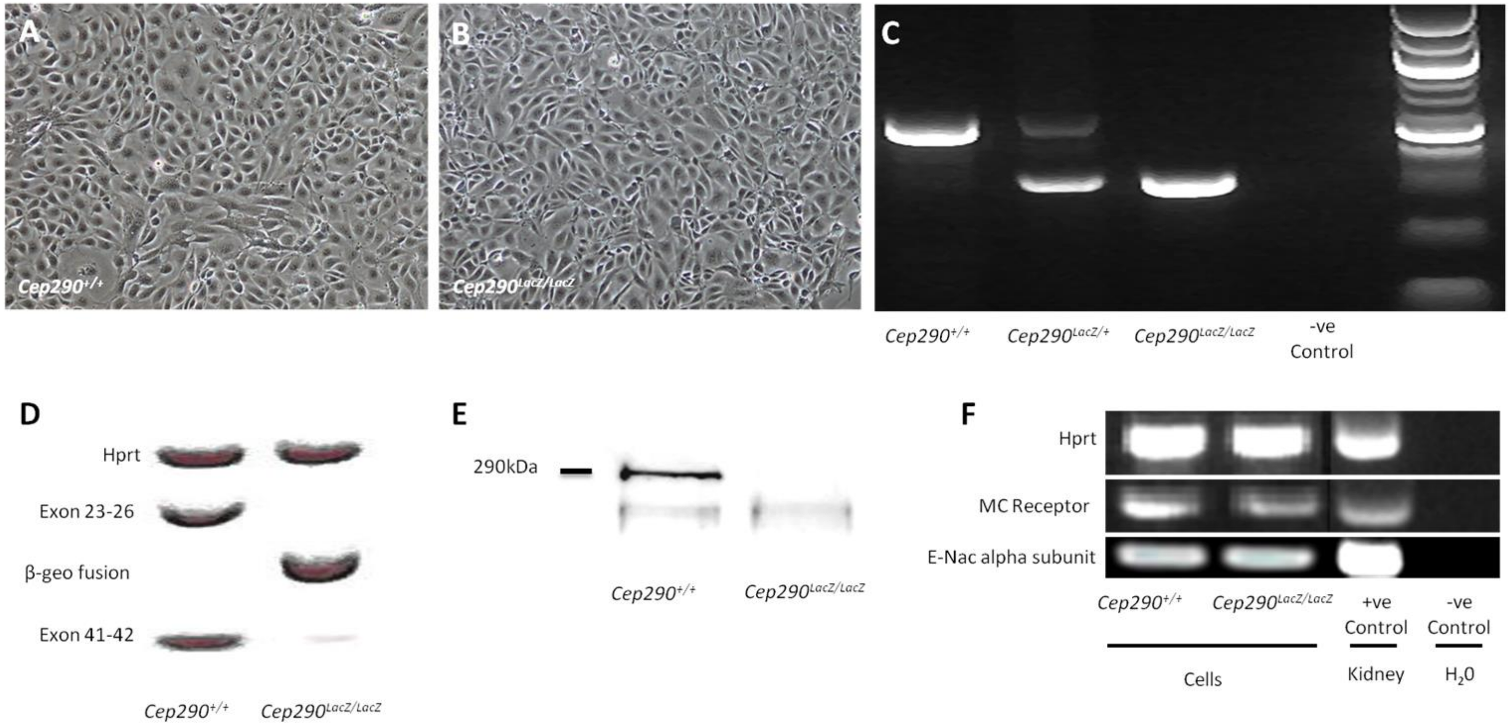

Figure 4.3 Phenotype and genotyping of *Cep290*$^{LacZ/LacZ}$ cells, heterozygote for the *H-2K*^{b}*-tsA58* gene, western blotting of whole cell protein extracts for *Cep290* and confirmation of CDT cell types.
(Panels A+B) Bright field imaging of *Cep290*$^{+/+}$ and *Cep290*$^{LacZ/LacZ}$ immortal confluent CDT cells. (Panel C) Genotyping of cells to confirm *Cep290* expression. (Panel D) RT-PCR of *HPRT* normalisation gene expression levels, expression of Exon23-26 of the *Cep290* gene only expressed in *Cep290*$^{+/+}$ cells as the gene trap truncates the Cep290 protein, Expression of β-geo only in the *Cep290*$^{LacZ/LacZ}$ sample and expression of exon 41-42 of *Cep290* gene after the gene trap. Panel E Western blot of *Cep290*$^{+/+}$ and *Cep290*$^{LacZ/LacZ}$ immorto CDT cells. The *Cep290*$^{LacZ/LacZ}$ does not express the full 290kDa *Cep290* protein product. Finally (Panel F)a RT-PCR showing the expression of MC receptor and E-NaC alpha subunit in the immortal *Cep290*$^{+/+}$ and *Cep290*$^{LacZ/LacZ}$ CDT cells, a positive control from whole kidney extract and a negative control of H_20.

In summary CDT cells for both *Cep290*$^{LacZ/LacZ}$ *and Cep290*$^{+/+}$ samples are morphologically similar to previously published studies of CDT cells. Also the gene expression levels of MR and E-NaC confirm the cells are CDT cells. Importantly figure 4.3 reveals expression of both *Cep290*$^{LacZ/LacZ}$ *and Cep290*$^{+/+}$ alleles in CDT cells.

4.4 Are there any defects in the primary cilia of cystic *Cep290*$^{LacZ/LacZ}$ CDT cells?

As discussed previously, mutations in genes encoding cilia-associated proteins have been identified in patients with NPHP. The primary cilia in renal tissue protrude from apical cells into the lumen of collecting duct tubules. Cilia with abnormal structure or function (or sometimes both) are thought to be involved in cyst formation. The mutated gene products identified in NPHP and JBTS are generally localised to the primary cilium/basal body/centrosome (Chapter 1).

Various mouse models presenting with renal cysts have shortened or malformed cilia. The *Tg737*^{orpk} mouse model presenting with an ARPKD phenotype, as an example, presents with polycystic kidneys and shortened cilia were observed on the renal epithelial cells. The *Ift20* (postnatal) mouse model presents with cystic kidneys and the kidneys have no cilia. A final example is the *Kif3α* mouse model which is embryonic lethal. The cysts lining the epithelial cells of the *Kif3a* mouse model also have no cilia. The lack of cilia in mutant kidneys is generally associated with embryonic lethal mouse models (Moyer, Lee-Tischler et al. 1994; Takeda, Yonekawa et al. 1999; Pazour, Dickert et al. 2000; Jonassen, San Agustin et al. 2008; Ko and Park 2013).

An investigation to ascertain if there were any structural cilia defects in the renal tissue of the *Cep290*$^{LacZ/LacZ}$ mice via SEM and TEM techniques was analysed in chapter 3. No conclusive evidence of structural defects in the primary cilia was found in the *Cep290*$^{LacZ/LacZ}$ kidney samples; however the data was inconclusive due to technical difficulties in orienting the images to discern the length and end of the cilium. Thus measurements of the primary cilium length and cross sections would have been inconclusive however there was subtle hint that perhaps the cilium appeared more bulbous in the *Cep290*$^{LacZ/LacZ}$ mouse collecting duct tubule compared to the *Cep290*$^{+/+}$ littermate (Chapter 3 Figure 3.10).

CDT cells provided a tool to analyse the primary cilium in greater detail than renal tissue, specifically as the CDT's are the target cells which are the source of NPHP cystic kidney disease.

In order to investigate the structure of the primary cilium at the cellular level, the assembly of the primary cilium was analysed (Figure 4.4). The protein products of the genes mutated in NPHP are located in the primary cilium. The primary cilium assembles and disassembles at different stages of the cell cycle. When the cilium is assembled ciliary signalling pathways are activated controlling multiple pathways. The primary cilium is disassembled prior to mitosis which involves the separation of daughter chromosomes and ending with cell division (cytokinesis) (Pan, Seeger-Nukpezah et al. 2012).

In Figure 4.4 the primary cilium is fully assembled at the G_0 phase when the cells are quiescent. The CDT cells of renal tissue in the adult mammalian body are consistently in quiescence.

In order to investigate in further detail the effects on the primary cilium in *Cep290*$^{LacZ/LacZ}$ CDT cells, at the cellular level, immortal *Cep290*$^{LacZ/LacZ}$ CDT confluent cells were subjected to 48h of serum starvation to induce primary cilia expression.

Serum starvation arrests the cell cycle to enter into the G_0, quiescent state.
In non dividing cells the centrioles migrate to the cell surface where the mother centriole forms a basal body that organises the formation of a cilium.
Immunofluorescent techniques were utilised in order to study the phenotype of the primary cilium in immortal *Cep290*$^{LacZ/LacZ}$ CDT cells (Figure 4.5).

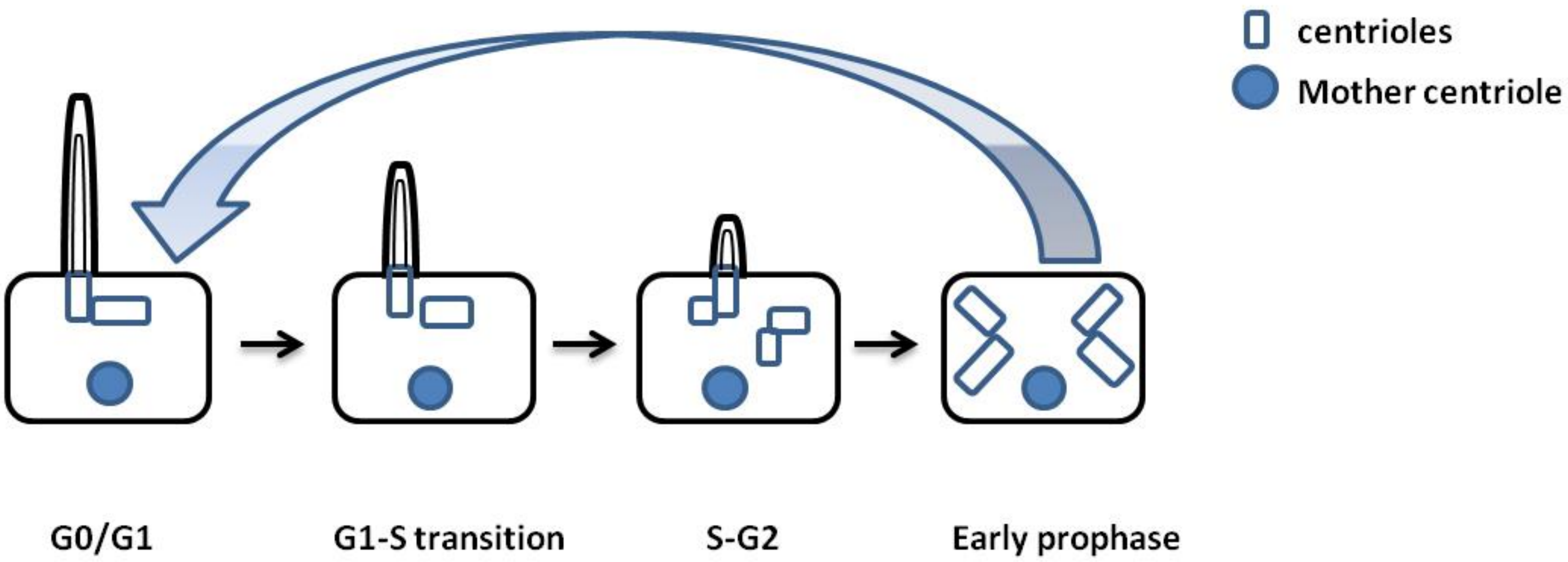

Figure 4.4 Primary cilia assembly and disassembly during the cell cycle.
The primary cilium extends from the cell surface after cytokinesis and is fully assembled at the G_0 state when the cells are in quiescence. The cilium starts to re-enter the cell at G1-S transition phase, and it is completely re-absorbed at early prophase. This process is crucial for maintaining orderly cellular division and cellular proliferation. Figure adapted from (Pan, Seeger-Nukpezah et al. 2012).

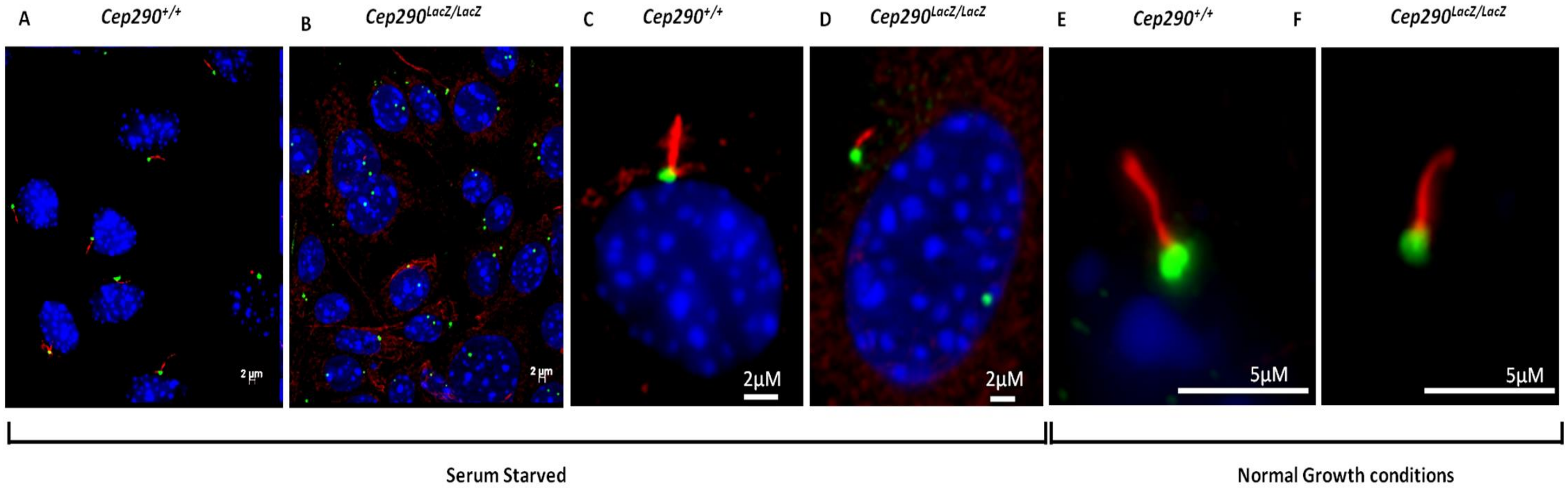

Figure 4.5 *Cep290* is required for functioning ciliogenesis in renal CDT cells.
Immunofluorescence images of confluent immortal CDT cells grown on coverslips after 48h of serum starvation. Staining with acetylated α-tubulin (red) and pericentrin (green) phenotypically shows the cilia and basal body structure in immortal *Cep290*$^{+/+}$ CDT (A+C) cells. The *Cep290*$^{LacZ/LacZ}$ CDT cells present with short stumpy cilia (Panel B+D) in serum starved cells after 48h. There was a significant reduction in cilia formation at the G0 phase in *Cep290*$^{LacZ/LacZ}$ cells compared to *Cep290*$^{+/+}$ cells (Panels A+B). It was also evident that the *Cep290*$^{LacZ/LacZ}$ cells which acquired a primary cilium were noticeably shorter than the *Cep290*$^{+/+}$ CDT cell (Panel C+D). Panel E+F Images of primary cilia from confluent CDT cells on coverslips.blue staining represent DAPI. Ki67 staining was negative after 48 h serum starvation thus confirming the cells were in quiescence (data not shown).

4.5 The primary cilium of *Cep290*$^{LacZ/LacZ}$ CDT cells

In *Cep290*$^{+/+}$ CDT cells, the cilium assembles after the cells exit mitosis (G_0 phase) and is resorbed as part of cell cycle re-entry. However in *Cep290*$^{LacZ/LacZ}$ CDT cells the primary cilium appears to be abnormal. The truncating mutation of *Cep290* resulted in both a clear reduction in ciliogenesis and aberrant stumpy cilia in the few cilia that did form when the cells were in quiescence (Figure 4.5).

A similar phenotype was observed following siRNA knockdown of centrosomal proteins which included Cep131, Cep152 and in Cep57 in serum starved cells on hTERT-RPE1 cells (Graser, Stierhof et al. 2007), suggesting that mutations in centrosomal proteins result in ciliogenesis defects.

In 2008 Kim et al., demonstrated that siRNA knockdown of *Cep290* hTERT-RPE cells revealed a similar cilium phenotype to that we have shown in *Cep290*$^{LacZ/LacZ}$ CDT cells (Figure 4.5). Kim et al., saw a loss of primary cilia in quiescent cells and found that a depletion of *Cep290* almost completely prevented primary cilium formation (Kim, Krishnaswami et al. 2008). The studies described involved the use of hTERT-RPE cells.

These studies suggest that *Cep290* is required for maintaining ciliogenesis in both the retina and the kidney epithelia.

As observed in Figure 4.5 (Panels A-B) *Cep290*$^{LacZ/LacZ}$ CDT cells when serum starved express less primary cilia. The total amount of visible cilia in serum starved CDT cells was calculated (Figure 4.6).

Over 200 cells were investigated in both *Cep290*$^{+/+}$ and *Cep290*$^{LacZ/LacZ}$ CDT cells. 55% of *Cep290*$^{+/+}$ CDT cells expressed a primary cilium. For the *Cep290*$^{+/+}$ cells; 227 cells were counted and from these cells 127 cilia were counted. However for the *Cep290*$^{LacZ/LacZ}$ CDT cells only 5% expressed a primary cilium (P<0.0001). For the *Cep290*$^{LacZ/LacZ}$ cells; 284 cells were counted and from these cells only 13 cilia were present.

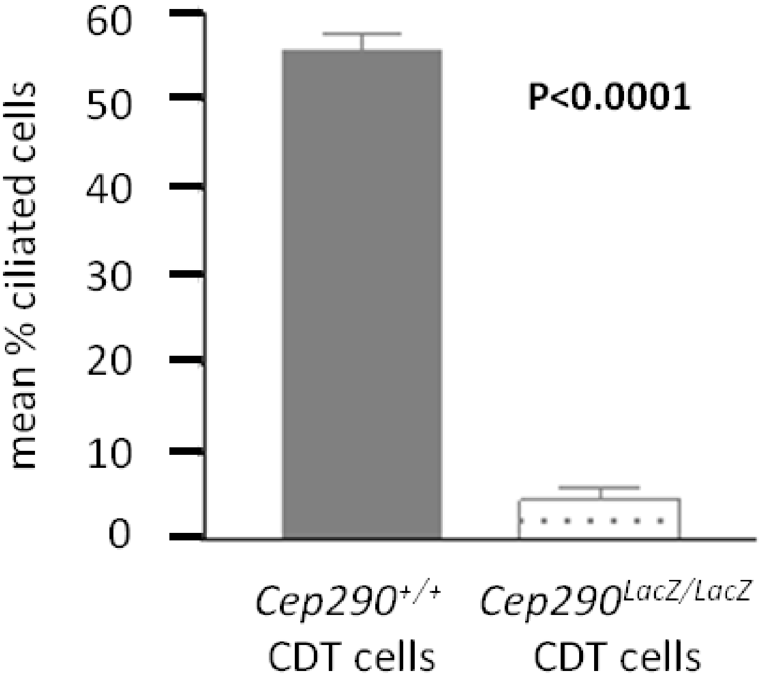

Figure 4.6 A *Cep290* truncated mutation reduced the proportion of ciliated cells in CDT cells.
Immunofluorescence images were analysed to determine the proportion of cilia present in a collection of CDT cells from *Cep290*$^{+/+}$ and *Cep290*$^{LacZ/LacZ}$ samples.

The length of primary cilia from both *Cep290*$^{+/+}$ and *Cep290*$^{LacZ/LacZ}$ CDT cells was measured. There was a statistical significant difference between *Cep290*$^{LacZ/LacZ}$ CDT cells primary cilia lengths compared to the *Cep290*$^{+/+}$ CDT cells primary cilia lengths (P=0.001) (Figure 4.7).

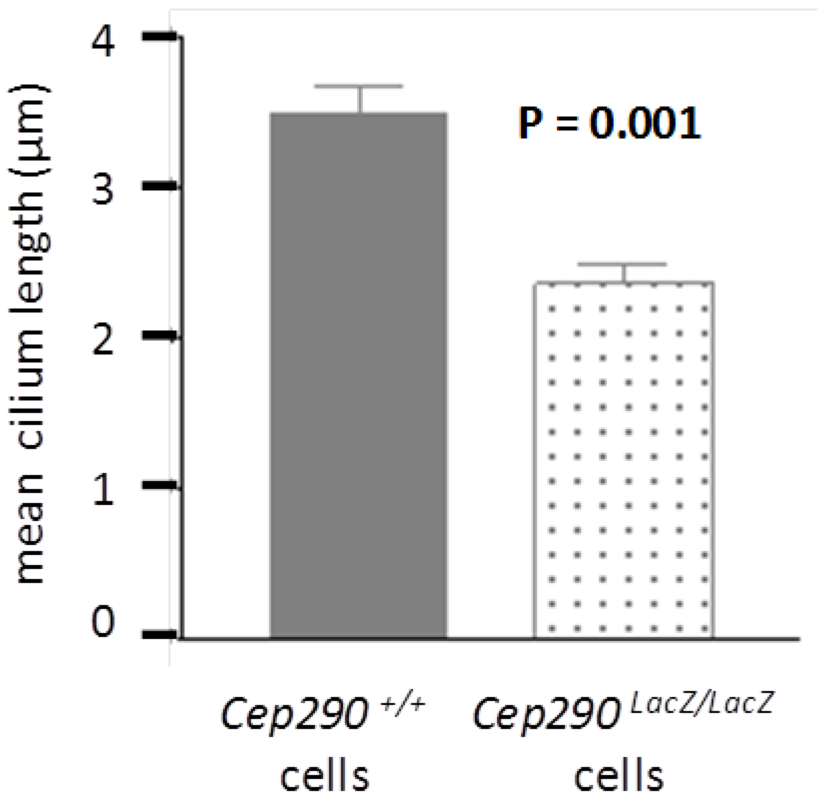

Figure 4.7 Mutations in *Cep290*$^{LacZ/LacZ}$ CDT cells present with a reduced cilium length in serum starved cells.
Immunofluorescent images were employed to determine the length of the primary cilia present in a collection of CDT cells from *Cep290*$^{+/+}$ and *Cep290*$^{LacZ/LacZ}$ CDT cells. Lengths were compared using students *t*-test.

The *Cep290*$^{+/+}$ CDT cells mean primary cilium length was 3.5µm with a standard error of the mean at 0.177, however for the *Cep290*$^{LacZ/LacZ}$ CDT cell mean primary cilium length was only 2.4µm with a standard error of the mean at 0.124. A student's *t*-test p value of the length of the primary cilium was p 0.001 determining the results are statistically significant. Cilia lengths were taken from >12 different primary cilia on *Cep290*$^{+/+}$ and *Cep290*$^{LacZ/LacZ}$ CDT renal cells serum starved for 48h. Primary cilium length was also investigated in *Cep290*$^{LacZ/LacZ}$ CDT cells when CDT cells reached confluence without serum starvation.

4.6 *Cep290* is required for ciliogenesis.

A functional primary cilium is crucial for maintaining the homeostasis of the renal CDT cell. Any defects which occur to the function of the primary cilium during ciliogenesis may cause disruption to the rest of the cell cycle in the renal CDT. Functioning ciliogenesis requires IFT machinery to move cargo towards the ciliary tip for many different cellular pathways. As observed in figure 4.6 there was a significant reduction in the percentage of ciliated *Cep290*$^{LacZ/LacZ}$ renal CDT cells when compared to their *Cep290*$^{+/+}$ controls. It was also determined that the cilia in *Cep290*$^{LacZ/LacZ}$ CDT cells were much shorter compared to *Cep290*$^{+/+}$ CDT cells (Figure 4.7).

This lack in number of cilia and the reduction of cilia length in *Cep290*$^{LacZ/LacZ}$ CDT cells suggests that signalling cascades may be altered as receptors for hedgehog, PDGF and Wnt signalling pathways are normally active along the length of the primary cilium. These receptors are also required for maintaining the structural polarity and the maintenance of the kidney CDT. In the *Cep290* mouse model this would suggest the lack of primary cilia and the reduction of cilia length in the *Cep290*$^{LacZ/LacZ}$ CDT is affiliated with the cystic kidney phenotype in the *Cep290*$^{LacZ/LacZ}$ mice.

A reduction of cilium length in quiescence was confirmed in *Cep290*$^{LacZ/LacZ}$ CDT cells (Figure 4.7) compared to normal growing conditions. In the fully formed renal CDT of mice the CDT’s are normally in quiescence.

The entire mechanism involved in the growth of the primary cilium is not known however many key proteins have been identified which are crucial in order to maintain ciliogenesis.

A previous study has identified that Cep290 is one of the key proteins for maintaining ciliogenesis. *Cep290* expression was found on both the mother and the daughter centrioles during ciliogenesis (Tsang, Bossard et al. 2008). The mother centriole during each cell cycle assembles the primary cilium and a loss of Cep290 in the mother centriole maybe influencing the improper assembly of the primary cilium. (Tsang, Bossard et al. 2008).

4.7 Determining the tubular morphology of *Cep290*$^{LacZ/LacZ}$ CDT cells

In order to determine the tubular morphology of *Cep290*$^{+/+}$ and *Cep290*$^{LacZ/LacZ}$ CDT cells, the CDT cells were cultivated in a 3D culture system consisting of a collagen I solution and a hormone HGF to provide extracellular matrix components in order to grow the cells as tubular spheroids.

Imaging 3D spheroids is a valuable tool in order to study the epithelial structure and morphogenesis of CDT cells which closely mimic their natural physiological conditions (Elia and Lippincott-Schwartz 2009). In this section the phenotype of the tubular spheroids were analysed. Spheroids were stained with DAPI to analyse the nuclear morphology of the in vivo tubules. *Cep290*$^{LacZ/LacZ}$ CDT spheroids appeared to have less cells than wild type controls (Figure 4.8). The presence of primary cilia in 3D spheroids was detected using antibodies to anti-acetylated tubulin. As observed earlier in the 2D culture systems only 5% of cilia form in the *Cep290*$^{LacZ/LacZ}$ CDT cells. The cilia that do form in *Cep290*$^{LacZ/LacZ}$ CDT cells are visually shorter than the *Cep290*$^{+/+}$ controls confirming a ciliogenesis defect. In 3D culture however there are no cilia present in *Cep290*$^{LacZ/LacZ}$ CDT cells. The lack of cilia in *Cep290*$^{LacZ/LacZ}$ CDT 3D spheroids suggests a much more severe phenotype than previously thought.

Tight junction assembly of the spheroids were analysed using an antibody to zona occludens-1 (ZO1) which is a scaffolding protein. ZO1 highlights the shape, form and location of the polarity of the spheroid. The expression of the tight junction protein ZO1 was down-regulated in *Cep290*$^{LacZ/LacZ}$ 3D spheroids and this therefore highlights a defect in the epithelial organistation of the CDT (Figure 4.8). β-catenin was employed to assess the phenotype of the adherens junctions in these 3D spheroids. β-catenin is also a key component downstream of the canonical wnt signalling pathway and therefore any visual defects found in the *Cep290*$^{LacZ/LacZ}$ 3D spheroids suggests there might be a defect in the wnt signalling pathway. The majority of β-catenin is localised to the cell membrane and is involved in the regulation of cell adhesion. Partial defects of the adherens junctions were observed in *Cep290*$^{LacZ/LacZ}$ 3D spheroids (Figure 4.8).

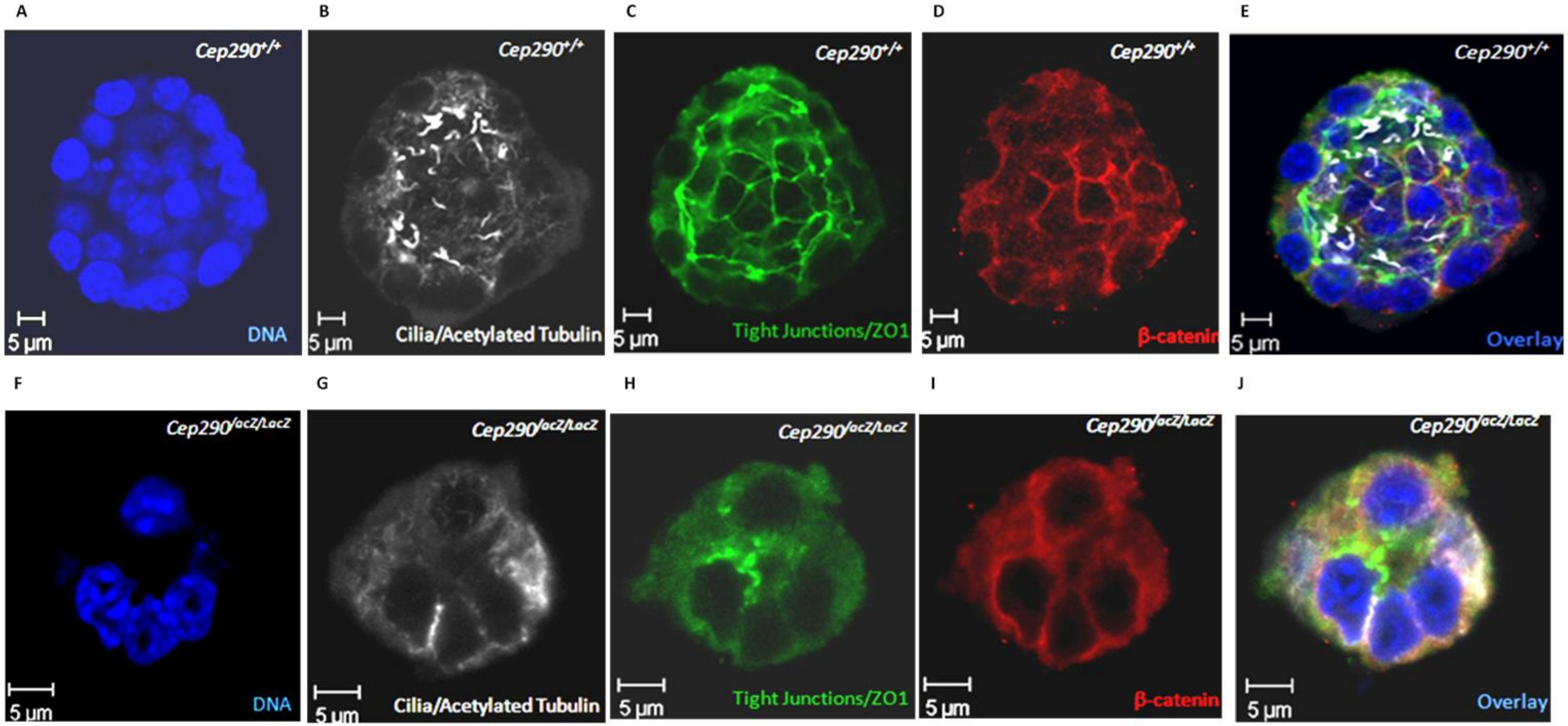

Figure 4.8 3D culture imaging of *Cep290* immortal CDT cells.
(Panels A-E) *Cep290*$^{+/+}$ immortal CDT cells and (Panels F-J) *Cep290*$^{LacZ/LacZ}$ immortal CDT cells. (Panels A+F) Dapi staining the nuclei of the spheroids, Panels B+G Anti-acetylated tubulin immunofluorescence marker staining primary cilia of the apical cells in the lumen of the spheroid. Note the *Cep290*$^{LacZ/LacZ}$ cells only seem to posses 1 primary cilium compared to the *Cep290*$^{+/+}$ cells. (Panels C+H) ZO1 staining illuminating the tight junctions of the spheroids. The tight junctions are disorganised in the *Cep290*$^{LacZ/LacZ}$ cells. (Panels D+I) stain the adherence junctions of the spheroid using β-catenin marker. (Panels E+J) merged image of DAPI, acetylated tubulin, ZO1 and β-catenin on the spheroid tubule.Tubules with misaligned nuclei were defined as abnormal. (Images collected by R Giles)

The 3D culturing system of CDT cells closely resembles the cellular nature of kidney collecting duct tubules. A previous study utilizing retroviral knockdown of *Cep290* expression IMCD3 examined the tubule structure of the *Cep290*$^{LacZ/LacZ}$ cells using a 3D culturing system. The structure of the spheroids was examined when *Cep290* was depleted. Abnormal structures of the 3D spheroids were observed and a reduction in cilia numbers was also evident (Ghosh, Hurd et al. 2012).

Microscopic investigation of the *Cep290*$^{+/+}$ 3D CDT cells identified tight epithelial junction complexes and apical microvilli which are hallmarks of a polarized epithelium. The *Cep290*$^{+/+}$ 3D CDT cells also maintained tight adherence junctions. 190 spheroids were analysed and over 50% of the cells contained a primary cilium which was as expected as 55% of cells contained a primary cilium in 2D cultures. This analysis concluded that the *Cep290*$^{+/+}$ tubule spheroids are functioning and represent a model of renal tubules.

In the *Cep290*$^{LacZ/LacZ}$ 3D CDT cells 20% of the spheroids form a tubule like structure but lack cilia. 80% of the *Cep290*$^{LacZ/LacZ}$ CDT spheroids analysed showed reduced tight junctions and reduced β-catenin staining with small lumens. Interestingly the cell number per spheroid in the *Cep290*$^{LacZ/LacZ}$ CDT cells is also reduced.

The *Cep290*$^{LacZ/LacZ}$ CDT 3D spheroids are disorganised and lack primary cilia suggesting that *Cep290* is required for the maintenance of ciliogenesis.

In order to further verify ciliogenesis defects caused by mutations in *Cep290* in patients with NPHP the 3D spheroids of *Cep290* CDT's cells (*in vitro* model) were compared with the collecting duct tubules sections isolated from *Cep290* mouse kidneys (*in vivo* model). Acetylated tubulin staining was carried out in both models to test cilia morphology. In the *Cep290*$^{LacZ/LacZ}$ mouse model primary cilia were still evident in CDT, however it was not accessible to count exactly how many cilia were evident in normal collecting duct tubules compared to cystic collecting duct tubules in the *in vivo* model. Therefore it could not be confirmed if there was a loss of cilia formation in the renal tissue of *Cep290*$^{LacZ/LacZ}$ mice. However both the 2D and the 3D cellular models of *Cep290*$^{LacZ/LacZ}$ renal CDT's demonstrated loss of cilia, suggesting that *Cep290* might possibly organise cell polarity or receptor trafficking in the absence of cilia as suggested previously by (Sang, Miller et al. 2011).

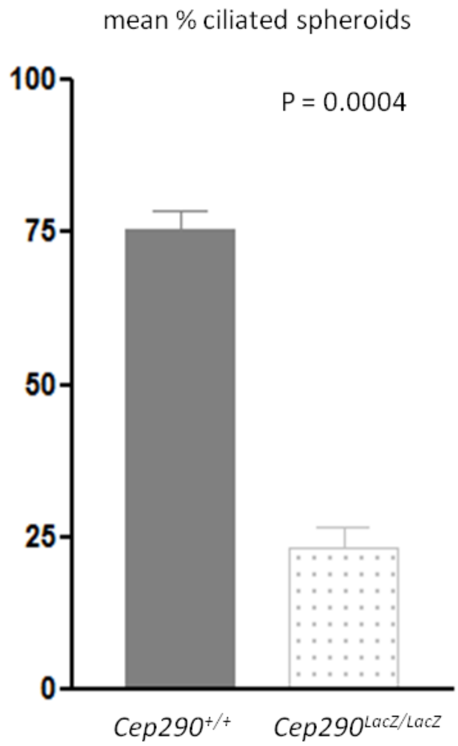

Figure 4.9 Quantifying ciliogenesis in *Cep290* 3D spheroids
Quantifying ciliogenesis in *Cep290*$^{+/+}$ and *Cep290*$^{LacZ/LacZ}$ cells from immunofluorescent images of 3D cultures . All spheroids were serum starved for 24hrs prior to staining. Lengths were compared using students *t*-test.

4.8 Discussion

The transgenic immorto mouse used in this study exhibits only modest thymic hyperplasia and does not present with tumours, suggesting that the levels of the thermolabile large T antigen are sufficiently low *in vivo* to prevent excessive cellular proliferation. The *Cep290*$^{LacZ/LacZ}$ CDT cell line is immortalised as the cells were grown under the conditions of interferon-γ (IFN-γ) which expresses the large T antigen. Over 50 passages have occurred and the cells do not lose their characteristics nor has there been a drift occurring due to the repeated use of passages. The cells have maintained the characteristics of parental cells which they have been derived from and are still maintained which also confirms cells are immortalised.

The conditionally immortalised *Cep290*$^{+/+}$ and *Cep290*$^{LacZ/LacZ}$ CDT cells express collecting duct characteristics and retain properties characteristic to renal collecting duct tubules. The characteristics were confirmed by the growth of spheroids in 3D cultures and by PCR analysis, which confirmed E-NaC and MC receptor expression in the *Cep290*$^{+/+}$ and *Cep290*$^{LacZ/LacZ}$ CDT cells.

From this study it was observed that a truncated *Cep290* mutation presents with fewer and shorter cilia in renal *Cep290*$^{LacZ/LacZ}$ CDT cells compared to *Cep290*$^{+/+}$ controls. Therefore it can be concluded that a *Cep290* truncated mutation suppresses ciliogenesis. Cilium assembly is a tightly coupled process consisting of IFT, polarized protein secretion and modification of the ciliary axonome. We found that only 5% of cells formed a primary cilium compared with 55% of *Cep290*$^{+/+}$ control cells, clearly demonstrating that *Cep290* is indispensible for primary cilia formation.

These *Cep290*$^{LacZ/LacZ}$ CDT cells have shown that ciliary assembly is affected. This *Cep290*$^{LacZ/LacZ}$ CDT system is a valuable cell system for ex vivo studies, leading the way to breakthroughs in our understanding of molecular mechanisms of NPHP. This *Cep290*$^{LacZ/LacZ}$ CDT system is also a powerful *in vitro* cell system for use in studies of renal physiology and pathophysiology associated with NPHP.

Chapter 5 Gene expression profiling in *Cep290$^{LacZ/LacZ}$* mouse renal tissue

5.1 Introduction

In chapter 3 a *Cep290$^{LacZ/LacZ}$* mouse model of NPHP was described, followed by a depiction of a defective assembly process of the primary cilia in renal CDT enriched cells isolated from this *Cep290$^{LacZ/LacZ}$* mouse (chapter 4). The next step of this study was to try to identify possible pathways which may influence NPHP.

Despite numerous genetic discoveries little is known in the literature about possible pathways influencing NPHP, other than all the protein products of the genes known to be defected in NPHP are located in or around the primary cilium (Hildebrandt, Attanasio et al. 2009; Winyard and Jenkins 2011).

Previous studies of NPHP have yet to reveal consensus pathways leading to the disease. In order to identify gene expression differences between *Cep290$^{LacZ/LacZ}$* and *Cep290$^{+/+}$* kidneys prior to an overt cystic kidney disease gene expression profiling was employed.

Illumina bead arrays were chosen because over 34,000 genes gene expression profiles are examined at once, it is highly reproducible, efficient and cost effective (http://www.lifesciences.sourcebioscience.com/genomic-services/gene-expression-/microarray-platforms.aspx) and will help to reveal unknown genes in NPHP. These unknown genes determined by the microarray may also help link possible pathways/biological processes affected in NPHP.

As discussed in the methods section (Chapter 2) newborn kidneys were isolated from inbred *Cep290$^{LacZ/LacZ}$* and *Cep290$^{+/+}$* 129/Ola mice and whole renal RNA samples were collected. Genome wide gene expression profiling of cDNA from *Cep290$^{LacZ/LacZ}$* and *Cep290$^{+/+}$* mouse kidneys was employed by the Illumina MouseWG-6 v2 Expression BeadChip (Source Bioscience). It was hypothesised that possible gene expression differences linked to NPHP would be revealed.

In order to determine genes which were involved in the development of NPHP¸ RNA from *Cep290$^{LacZ/LacZ}$* and *Cep290$^{+/+}$* mouse kidney samples were collected.

The kidney samples collected were gender selected, (all samples chosen were female; confirmed via *Sry* genotyping [data not shown]), to ensure that differences in gene expression levels were not gender specific. The *Cep290*$^{LacZ/LacZ}$ and *Cep290*$^{+/+}$ kidneys were collected between 10am and 12noon on the day of birth to rule out any artefacts which could be caused by differences in the animals' circadian rhythms. The left kidney of each mouse was collected for RNA and the right kidney was collected for histology. Recent studies have suggested that defects in the normal pattern of the circadian clock can lead to abnormalities in renal function (Stow and Gumz 2011). In ensuring that only female kidney samples were sent for microarray analysis this prevented an increase/decrease in gene expression differences occurring in sex specific genes. As both male and female *Cep290*$^{LacZ/LacZ}$ mice present with a cystic kidney phenotype either gender could have been chosen for microarray analysis. The *Cep290*$^{LacZ/LacZ}$ and *Cep290*$^{+/+}$ female mice used for microarray analysis were inbred on a 129/Ola background to prevent any strain specific variation in gene expression levels occurring from breeding with other mice. The design of this microarray experiment eliminates many variables by ensuring the animals are inbred, kidneys isolated were only from female *Cep290*$^{LacZ/LacZ}$ and *Cep290*$^{+/+}$ mice and the kidney samples are collected at the same time of day. Therefore the changes in gene expression levels are likely to be small and the changes in gene expression levels maybe primary or a secondary effect from a cystic kidney disease as whole kidney samples were isolated for the Illumina Microarray.

5.2 Aims

In order to identify other genes contributing to the beginning of cystic kidney disease when there is a known truncated mutation already found within the *Cep290* gene, global differential gene expression was employed using kidneys derived from *Cep290*$^{LacZ/LacZ}$ mice and age matched *Cep290*$^{+/+}$ controls. The list of genes generated from the Illumina Microarray will need to be confirmed via semi quantitative RT-PCR and quantitative RT-PCR (qRT-PCR).

Also in order to identify the relevance in changes found from a list of genes generated by the microarray, the biological processes of a number of genes assigned by the microarray were assessed. It was also speculated how the gene expression profile changes in the microarray might contribute to a cystic kidney phenotype.

5.3 Results

A total of 8 *Cep290*$^{+/+}$ and 5 *Cep290*$^{LacZ/LacZ}$ newborn 129/Ola kidneys were tested for quality control analysis prior to microarray analysis (See Table 5.1). The quality and concentration of total RNA was quantified using a LSN-X-013 spectrophotometer (Source Bioscience).

Genotype	Sample Name	Prior to shipping Results		Source Bioscience Results	
		Total Conc. (ng/µL)	Abs 260-280nm RNA	Total Conc. (ng/µL)	Ratio 28S/18S RNA
Cep290$^{LacZ/LacZ}$	6217	339.70	1.96	474.73	0.72
Cep290$^{LacZ/LacZ}$	6218	432.10	1.90	1627.04	N/A
Cep290$^{LacZ/LacZ}$	**D**	106.70	1.90	188.21	2.40
Cep290$^{LacZ/LacZ}$	**E**	61.80	1.81	214.85	2.19
Cep290$^{LacZ/LacZ}$	**F**	418.60	1.88	1983.00	1.95
Cep290$^{+/+}$	6222	270.40	1.91	156.24	1.33
Cep290$^{+/+}$	6223	106.70	1.91	166.35	0.93
Cep290$^{+/+}$	**A**	527.20	2.08	1557.47	1.32
Cep290$^{+/+}$	6225	385.20	2.01	653.01	1.17
Cep290$^{+/+}$	6226	101.70	1.86	44.26	N/A
Cep290$^{+/+}$	6227	377.60	2.03	2214.57	N/A
Cep290$^{+/+}$	**B**	552.30	1.94	570.74	1.70
Cep290$^{+/+}$	**C**	386.00	1.91	239.13	2.06

Table 5.1 Newborn kidney RNA QC analysis prior to shipping and QC analysis from Source Bioscience.
Cep290$^{LacZ/LacZ}$ (n=5) and *Cep290*$^{+/+}$ (n=8) newborn kidneys RNA concentration was measured. The samples chosen for microarray analysis are highlighted in yellow (n=3 for each genotype) and labelled A-F.

An electropherogram was utilised by source bioscience to separate out the components (18S, 28S) of each RNA sample and the quality of the RNA was determined (Figure 5.1). In general when the quality of RNA is acceptable for microarray analysis it is displayed on an electropherogram as follows; the 28S RNA peak would be at least twice the size of the 18S RNA peak. As observed from Table 5.1 the 28S/18S RNA ratio for the samples chosen for microarray analysis varies (1.32-2.40). The samples lower than 2 are probably due to enzymatic degradation that occurred during the RNA procedure. (The homogenisation step in RNA extraction can shear the RNA and cause degradation.

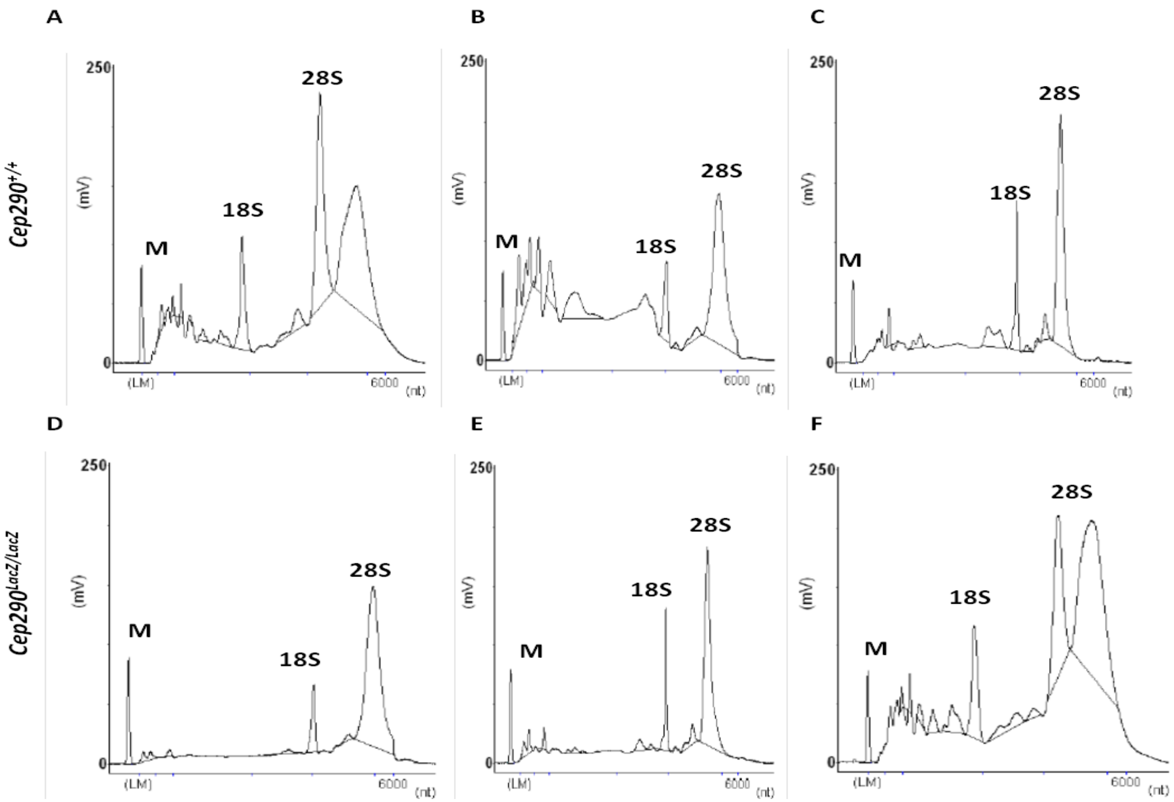

Figure 5.1 Electropherogram of the 6 samples chosen for Microarray analysis.
(Panels A-C) Newborn *Cep290*$^{+/+}$ kidney RNA samples. (Panels A+B) indicate that a small amount of RNA degradation has occurred in these 2 samples as there is no base line between the M (marker) and the 18S peak; this was confirmed by measuring the 28S/18S ratios in table 5.1. Panel C shows superior quality RNA when compared to panels A and B as the 3 peaks are clearly distinguished from the base line; also the 28S peak is twice the size of the 18S peak (confirmed in table 5.1 ratios). (Panels D-F) are newborn *Cep290*$^{LacZ/LacZ}$ kidney RNA samples. When the samples for microarray analysis were chosen they were normalised to 100ng. Qualitative and quantitative QCs were carried out on 1.5ug of RNA which was then hybridised to the mouse WG-6.v2 chip and scanned by the BeadArray Reader (LSN-X-036). (Source Bioscience).

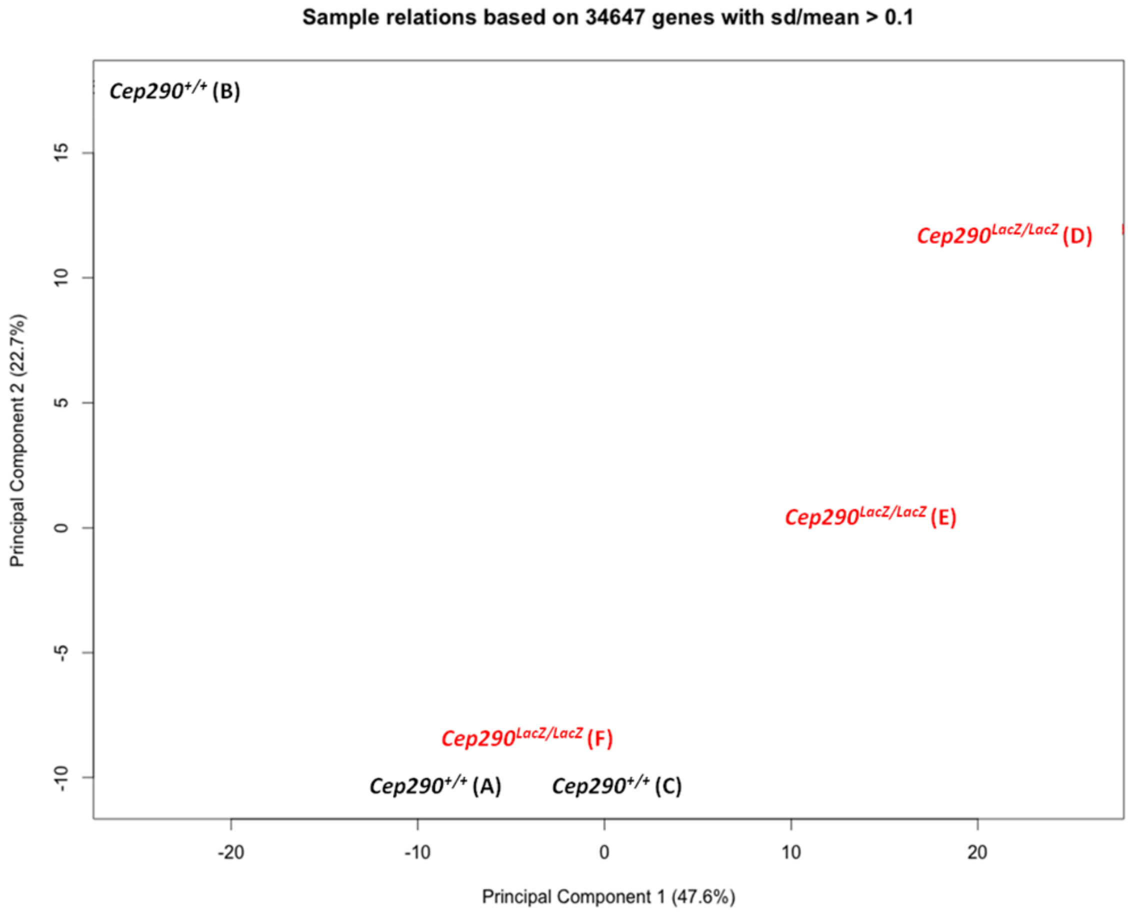

Figure 5.2 Principal component analysis (PCA) on newborn *Cep290* whole kidney microarray samples.
(A-C) *Cep290*$^{+/+}$ newborn kidney samples (highlighted in black). (D-F) *Cep290*$^{LacZ/LacZ}$ newborn kidney samples (Highlighted in red)
The samples chosen for analysing the microarray data in groups of *Cep290*$^{+/+}$ were A+C and *Cep290*$^{LacZ/LacZ}$ samples were D+E. (Image collected by Matthew Bashton, Bioinfomatics, Newcastle University) Interestingly samples D+E were from the same litter consisting of a litter of 4 newborn mice and (F) was from a litter of greater than 4 in size.

5.4 Interpreting PCA analysis

PCA is a programme that clusters samples by their similarities and the differences within a data set. The samples chosen for gene spring analysis (which determines a list of genes using a Benjamini Hochberg false discovery rate correct p-value of 0.05 and a fold change of 1.0 as cut-offs), were closely clustered samples identified by PCA.

The *Cep290*$^{+/+}$ samples chosen for Gene Spring analysis were (A+C) and the *Cep290*$^{LacZ/LacZ}$ samples chosen for gene spring analysis were (D+E). Coincidentally the samples chosen for Gene Spring analyses by the use of PCA were also the samples which showed clear concise peaks for the Electropherogram QC analysis (Figure 5.1 Sample A+C for *Cep290*$^{+/+}$ samples, Sample D+E for *Cep290*$^{LacZ/LacZ}$ samples). The PCA plot reveals one global outlier (*Cep290*$^{+/+}$ sample B) and one *Cep290*$^{LacZ/LacZ}$ sample(F) that shows similarity with two clustered *Cep290*$^{+/+}$ samples (A+C). This analysis highlights the sensitivity of the array and can be interpreted as indicating that other variables in addition to genotypes are being detected (for example perhaps stages of development).

In order to determine why the PCA analysis clustered a *Cep290*$^{LacZ/LacZ}$ sample with the *Cep290*$^{+/+}$ samples the litter sizes for each pup used in PCA analysis was analysed. Litter sizes were investigated because mice born to a litter of 6 will be much smaller in size and will be less developed compared to mice born to a litter of 2 as they will have received more nutrients from their mother during embryogenesis. *Cep290*$^{LacZ/LacZ}$ samples (D+E) were from the same litter consisting of 4 pups. *Cep290*$^{LacZ/LacZ}$ sample (F) and *Cep290*$^{+/+}$ samples C+B were also from the same litter which were greater than 4 pups suggesting that sample F may be developmentally smaller than samples D+E. However the *Cep290*$^{+/+}$ (A) sample was also from a litter of 4 therefore ruling out that perhaps the other samples are developmentally smaller. An investigation into the litter sizes did not explain why a *Cep290*$^{LacZ/LacZ}$ (sample F) clusters with the two *Cep290*$^{+/+}$ samples (A+C) therefore variations between litter sizes are not accounting for the differences observed by PCA.

The clustering from PCA is therefore not just influenced by genotype other unknown variables are affecting the clustering. The experiment set up for microarray analysis was a tight controlled experiment ensuring that the kidney samples isolated from *Cep290*$^{+/+}$ and *Cep290*$^{LacZ/LacZ}$ newborn inbred 129/Ola were female and taken at the same time of day.

The PCA analysis is a representative of all the genes on the microarray (34,647 genes) and is depicted as relative values. For this reason slight differences of unknown variables between individual newborn inbred *Cep290* mice may be highlighted. Given the similarity and care of experimental design, the contra lateral kidney for each sample (A-F) was analysed by histology.

A closer inspection of the right kidneys' histology revealed that *Cep290*$^{LacZ/LacZ}$ newborn kidneys already showed evidence of NPHP (microcysts were evident) (Figure 5.3). Sample F was an outlier as it appeared to have slightly more numbers of micro cysts evident than the other 2 samples. From the renal histology observed in *Cep290*$^{LacZ/LacZ}$ mice it was therefore hoped that the varying gene expression levels detected were primary to the cysts and not as a secondary effect of the cystic phenotype.

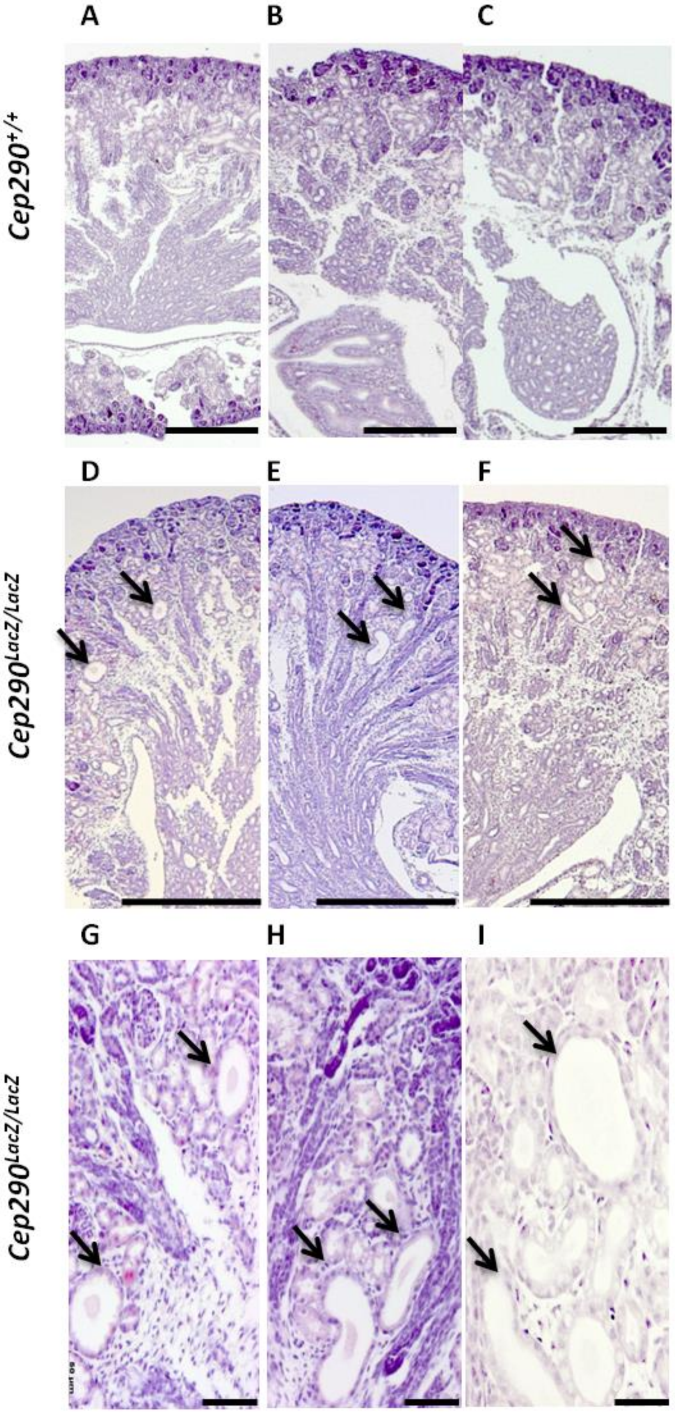

Figure 5.3 Cysts are present at birth in *Cep290$^{LacZ/LacZ}$* kidneys
(A-F) Haematoxylin and Eosin staining of paraffin embedded kidneys at birth. Haematoxylin stains the nuclei of cells blue; eosin stains cytoplasm and collagen in various shades of red and pink. (A-C) *Cep290$^{+/+}$* mice with tightly packed collecting duct tubules. (D-F) *Cep290$^{LacZ/LacZ}$* mice display early signs of nephronophthisis with cysts (black arrows). The cysts are located between the cortex and medulla (in the corticomedullary junction). Patients with nephronophthisis also display cysts in this corticomedullary region of the kidney. (G-I) Magnified images of epithelial cell layered cysts highlighted previously by black arrows in images (D-F). The width of the cysts at birth is approx 50-75µm. Scale bars (A-F) 500µm, (G-I) 50µm.Note samples A-F correspond to samples A-F in Table 5.1 and Figures 5.1 and 5.2.

Microarray analysis of genes differentially expressed in Cep290$^{LacZ/LacZ}$ kidneys		
Gene Symbol	**logFC**	**P.Value**
Miox	3.322092777	1.80E-05
Pvalb	3.312463183	7.06E-07
Ren1	3.200246146	0.000221115
Ren1	2.749052061	9.57E-06
Cyp4a14	2.371386581	0.000290118
Hmgcs2	2.360774704	0.000144394
F13b	2.16911503	4.67E-05
F13b	2.145713423	2.09E-06
Spp2	2.107803629	7.18E-06
Angptl7	1.910758685	5.85E-05
Osta	1.906892799	3.93E-05
Nphs2	1.855002711	8.68E-05
Slc13a3	1.852610118	4.02E-06
Dpep1	1.822769343	0.000111253
Apom	1.81330248	0.000117304
Slc13a3	1.795396816	0.00032081
Slc12a3	1.778359445	9.79E-06
Slc22a1	1.627703678	5.66E-05
Spp1	1.614562072	4.75E-05
Apom	1.559789151	0.000169903
BC021785	1.554266724	0.00016303
Enpp6	1.552843705	0.000110579
Gpx3	1.542743203	2.76E-05
Kl	1.519355411	2.63E-05
Defb19	1.518245641	6.57E-05
Cldn10	1.509310827	0.000138445
Acss1	1.492222958	4.65E-06
Cfi	1.465821133	0.000373538
Slc22a18	1.449181591	0.000139489
Slc22a1	1.418347414	0.000310005
0610008F07Rik	1.368965182	5.35E-05
Tcn2	1.328917107	0.00027768
Col4a3	1.317271434	0.000256134
Scn4b	1.295601612	7.81E-06
Slc12a3	1.277027112	0.000150392
Slc26a4	1.190968996	8.18E-06
Hrsp12	1.176760628	0.000338464
S100a1	1.175395011	6.14E-06
Mgst3	1.172024453	7.22E-06
Upb1	1.129406619	0.000398406
Defb1	1.121168341	0.000215491
Khk	1.108664074	4.23E-05
Ndrg1	1.10539241	0.000117825
Trpm6	1.097042623	1.36E-05
Nox4	1.083340822	0.000109711
Upb1	1.08213517	3.15E-05
C2	1.078812849	7.56E-05
Slc7a9	1.076428196	0.000192124
Acadl	1.030027916	2.94E-05
Tmem116	1.028059537	4.94E-05
Retsat	1.027799362	6.23E-05
Cyp2j9	1.023983642	3.15E-05
Ech1	1.023946424	7.36E-05
Apoa2	1.022141172	0.000336598
Myo7a	1.006352612	6.70E-05
Slc6a20b	1.001382813	0.000386685

Table 5.2 List of upregulated genes in *Cep290*$^{LacZ/LacZ}$ kidneys generated by Illumina Microarray.

A list of up regulated genes generated by the Illumina Microarray. The up regulated genes were generated when comparing *Cep290*$^{LacZ/LacZ}$ kidney mRNA with *Cep290*$^{+/+}$ kidney mRNA. In total 49 genes (excluding 7 repeats- Ren1, F13b, Slc13a3, Slc12a3, Apom, Slc22a1, Upb1) were up regulated in the *Cep290*$^{LacZ/LacZ}$ kidneys. A total of 7 genes were up regulated with a logFC of >2. The genes shaded in green expression levels were confirmed when comparing *Cep290*$^{LacZ/LacZ}$ newborn kidneys with *Cep290*$^{+/+}$ newborn kidneys via RT-PCR techniques. A list of genes was generated using a Benjamini Hochberg false discovery rate correct p-value of 0.05 and a fold change of 1.0 as cut-offs. (List generated by Matthew Bashton, Bioinformatics, Newcastle University).

A list of genes was generated using a Benjamini Hochberg false discovery rate correct p-value of 0.05 and a fold change of 1.0 as cut-offs. (List of genes was generated by Matthew Bashton, Bioinformatics, Newcastle University) Table 5.2 and Table 5.3.

Semi quantitative real time PCR (RT-PCR) and quantitative PCR (qPCR) techniques were employed to confirm the top 3 up regulated gene expression profiles found by data generated on the Illumina microarray (Highlighted in green in Table 5.2)

The microarray genes that were chosen for confirmation by semi quantitative and quantitative RT-PCR analysis were chosen due to the high log fold change in expression levels observed and or the links already established in the kidney from previous review papers.

The genes were also chosen because when the probe was (basic local assignment search tool) blasted in ensemble the gene had more than 2 exons. In order to design primers which were suitable for QPCR analysis, the gene needed to have an intron/exon boundary between at least 2 exons as this removes DNA outliers.

The genes which were on the list as duplicates were not chosen to be confirmed via semi-quantitative and qRT-PCR methods as they were already confirmed via the microarray as the microarray used a different probe to show the same up/down regulation identified previously by another probe.

Some probe sequences when blasted hit 2 genes and therefore it was decided that they would not be ideal genes to confirm.

5.5 *Cep290$^{LacZ/LacZ}$* upregulated genes identified by the Illumina microarray.

The most up-regulated gene in *Cep290$^{LacZ/LacZ}$* newborn kidneys when compared to *Cep290$^{+/+}$* newborn kidneys identified by the microarray was Myo-inositol oxygenase (*MIOX*), which is a renal specific aldo-keto reductase and catalyzes the first step of myoinositol metabolism (Arner, Prabhu et al. 2001) *MIOX* was previously identified to be confined to the cortex of the kidney (Charalampous 1959; Koller and Hoffmann-Ostenhof 1979; Hu, Chen et al. 2000; Arner, Prabhu et al. 2001).
Several published papers have shown that Myo-inositol depletion is identified in patients with diabetic nephropathy, retinopathy, neuropathy and diabetic cataracts (Greene, Chakrabarti et al. 1987; Del Monte, Rabbani et al. 1991; Lin, Reddy et al. 1991; Cohen, Wald et al. 1995; Arner, Prabhu et al. 2006) .

The exact mechanism of Myo-inositol depletion is unclear however *MIOX* catalyses the first step of the Myo-inositol pathway and therefore *MIOX* may be responsible for the depletion found in the diabetic complications above (Yang, Hodgkinson et al. 2010). There have been no reported cases of mutations in *Miox* and polycystic kidney disease to date. However an increase in *MIOX* expression may influence the fibrotic phenotype seen later in this *Cep290* model of cystic kidney disease.

In this study *Miox* expression increased by ~3 fold in *Cep290$^{LacZ/LacZ}$* newborn kidneys compared to *Cep290$^{+/+}$* littermates using data generated from an illumina microarray. The illumina microarray results were confirmed in Figure 5.3; an increase in *Miox* expression was identified in *Cep290$^{LacZ/LacZ}$* newborn kidneys using semi-RT-PCR and qPCR techniques. Semi quantitative PCR demonstrated an increased expression of *Miox* in *Cep290$^{LacZ/LacZ}$* kidneys. In order to quantify the fold change in expression in mRNA transcript levels, qPCR was carried out. In *Cep290$^{LacZ/LacZ}$* kidney mRNA transcripts there was an increase in *Miox* expression compared to *Cep290$^{+/+}$* kidney mRNA (up regulated 8-fold; $p = 0.0012$, $n=6$).

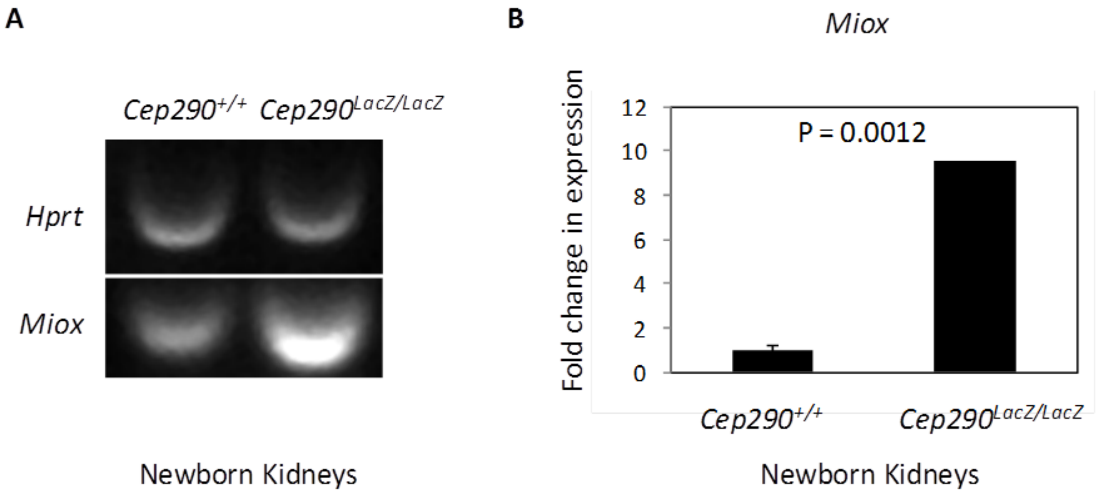

Figure 5.4 *Miox* gene expression is up regulated in *Cep290*$^{LacZ/LacZ}$ newborn kidneys.
(Panel A). Semi-quantitative RT-PCR highlighting differences in *Miox* expression in *Cep290*$^{+/+}$ and *Cep290*$^{LacZ/LacZ}$ newborn kidneys. Hypoxanthine-guanine phosphoribosyl transferase *(HPRT)* is reported as a constitutively expressed housekeeping gene in RT-PCR (de Kok, Roelofs et al. 2005) when compared with 12 other known housekeeping genes. *HPRT* is used as a reference gene against the expression level of the *Miox* gene under investigation. Semi-quantitative RT-PCR highlights an increase in expression of *Miox* in *Cep290*$^{LacZ/LacZ}$ kidney samples compared to *Cep290*$^{+/+}$ kidney samples. (Panel B) qRT-PCR of differences in *Miox* expression in *Cep290*$^{+/+}$ and *Cep290*$^{LacZ/LacZ}$ newborn kidneys. qRT-PCR identifies an increase of 8 fold change in expression of *Miox* in *Cep290*$^{LacZ/LacZ}$ kidneys compared to *Cep290*$^{+/+}$ littermates (p=0.0012, n= 6).

5.6 Parvalbumin (Pvalb)

Pvalb was the second most up regulated gene identified in newborn *Cep290*$^{LacZ/LacZ}$ mice from the illumina microarray data generated in this study. *PVALB* was previously reported to be expressed in the distal convoluted tubule in human and mouse kidneys, *Cep290* expression is found in the collecting duct tubules of the kidney, therefore this suggests that an increase in *Pvalb* may be as a result of a secondary compensatory mechanism. *PVALB* expression was also found in the brain, skeletal and heart muscles (Celio 1990; Schwaller, Dick et al. 1999; Olinger, Schwaller et al. 2012). *Pvalb* is a high affinity calcium ion binding protein. The protein product of *Pvalb* was reported to be involved in shuttling the Ca^{2+} and Mg^{2+} ions in the kidney (Ollinger, Schwaller et al., 2012). The distal nephron in the kidney plays a major role in the reabsorption of NaCl and the regulation of Ca^{2+} and Mg^{2+} excretion. Variants in *PVALB* have been described previously but the relevance to kidney function has not been investigated (Ollinger, Schwaller et al., 2012).

A knockout mouse model of *Pvalb* revealed that the mice presented with polyurea, kaliuresis and an increase in the mineralocorticoid hormone aldosterone and hypocalciuria (Belge, Gailly et al. 2007). In this study *Pvalb* expression was increased in *Cep290*$^{LacZ/LacZ}$ mice. An investigation into increased *Pvalb* expression in kidneys from previously reported microarray data from GEO profiles was carried out (http://www.ncbi.nlm.nih.gov/geoprofiles/?term=pvalb+kidneys). It was reported that over expression of the hypertension related calcium-regulated gene (*HCaRG*) in a stably transfected (Human embryonic kidney) HEK-293 cell line resulted in over expression of *Pvalb*. The study however does not confirm the over expression of *Pvalb* nor do they discuss the increased expression of *Pvalb* in their findings (El Hader, Tremblay et al. 2005). To date there are no published reports on the consequences of over expression of *Pvalb* in the kidney. As observed in Table 5.2 a 3 fold increase in expression of *Pvalb* was identified in *Cep290*$^{LacZ/LacZ}$ newborn kidneys compared to *Cep290*$^{+/+}$ kidneys. This increased expression in *Pvalb* in *Cep290*$^{LacZ/LacZ}$ kidneys was investigated using semi quantitative PCR and qPCR methods. The increase in *Pvalb* expression was confirmed using semi-quantitative RT-PCR and qRT-PCR methods (Figure 5.4). An increase in expression was observed in *Cep290*$^{LacZ/LacZ}$ kidneys compared to *Cep290*$^{+/+}$ kidneys (up regulated 65-fold; p=0.0004, n=6) (Figure 5.4).

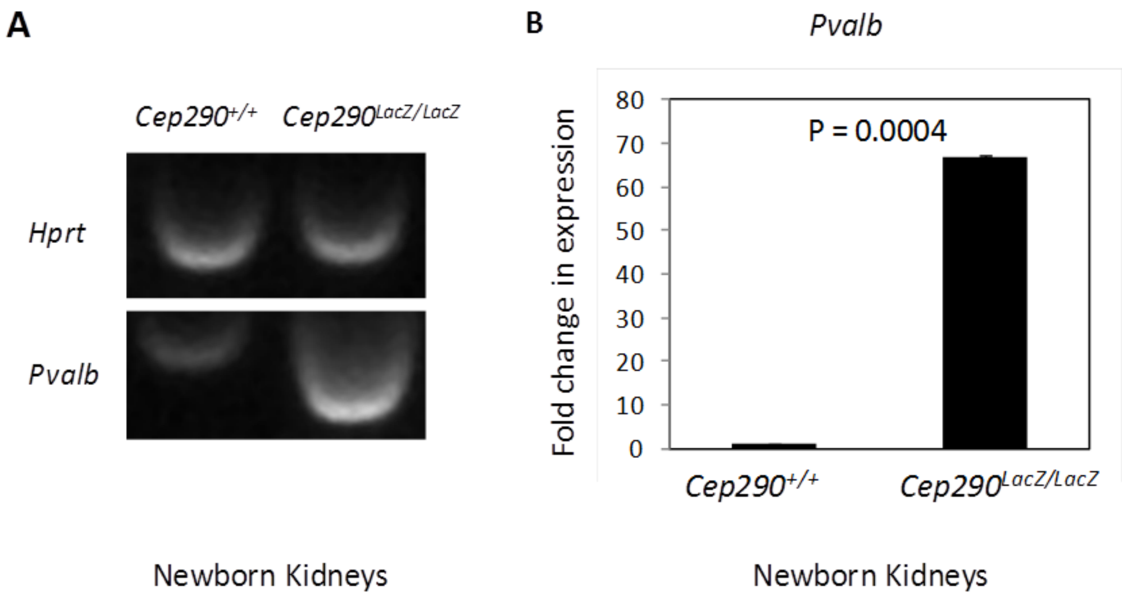

Figure 5.5 *Pvalb* gene expression is up-regulated in *Cep290*$^{LacZ/LacZ}$ newborn kidneys.
(Panel A) Semi quantitative RT-PCR of *Cep290*$^{+/+}$ and *Cep290*$^{LacZ/LacZ}$ newborn kidney mRNA transcripts levels. *Hprt* (housekeeping gene; used as a reference gene against the expression level of the *Pvalb* gene under investigation). Using semi quantitative techniques *Pvalb* expression is up-regulated in the *Cep290*$^{LacZ/LacZ}$ newborn kidney mRNA. (Panel B) qRT-PCR confirmed an increase of 65 fold change in expression of *Pvalb* in *Cep290*$^{LacZ/LacZ}$ samples compared to *Cep290*$^{+/+}$ samples (p=0.0004, n=6).

5.7 Renin (Ren1)

Ren1 was the 3rd top up regulated gene in accordance to LogFC identified by the illumina microarray in this study. *Ren1* was previously reported to be released by the juxtaglomerular cells of the kidney and catalyzes the first step in the activation of the angiotensin pathway (Pentz, Lopez et al. 2001; Sequeira-Lopez, Weatherford et al. 2010). Angiotensin is a hormone that causes vasoconstriction and a subsequent increase in blood pressure which is determined by the total amount of Na^+ in the body. The correct balance of Na^+ in the human body is controlled by the kidney (Guyton 1991). Previous studies identified that salt and water reabsorption is under tight control by the renin angiotensin system reviewed in (Eladari, Chambrey et al. 2012). *Renin* is released when serum Na^+ levels are low to try to conserve the salt water balance as referred to in a review titled “The renal renin-angiotensin system”(Harrison-Bernard 2009).

As Na^+ absorption occurs through *ENaC*, maintaining a correct balance of *ENaC* function in the kidney is crucial for Na^+ handling by the kidney (Hummler 1999; Schild and Kellenberger 2001; Stockand 2002; Hummler 2003; Schild 2004; Zaika, Mamenko et al. 2013). Therefore due to the increase of *Ren1* there is a possibility that there also might also be differences in *ENaC* expression in $Cep290^{LacZ/LacZ}$ kidneys when compared to $Cep290^{+/+}$ kidneys

In a previous ADPKD study, *Ren1* expression was increased in patients in the early stages of ADPKD, these patients also presented with hypertension and therefore the link between the renin-angiotensin pathway and cystic kidney disease was identified (Chapman, Johnson et al. 1990). Hypertension was also reported as a common trait found in ARPKD patients. In the juvenile form of ARPKD chronic renal insufficiency and hypertension have also been linked (Guay-Woodford and Desmond 2003). According to a review on NPHP, polyuria and polydypsia are related to the loss of sodium which occurs early in NPHP (Salomon, Saunier et al. 2009). It is possible that polyuria is evident in this $Cep290^{LacZ/LacZ}$ mouse model however there were not enough experimental repeats of urine samples measured in *Cep290* mice to confirm this in chapter 3.

Renin generates a cascade of events via the angiotensin II pathway which in turn exerts a negative feedback on *Renin* release. Any stimuli preventing angiotensin generation therefore increases *Renin* synthesis and release. During embryonic development Renin is expressed in the metanephric mesenchyme before vascularisation of the kidney occurs. *Renin* is also expressed later in embryonic development where it is found in the large intrarenal arteries, the glomeruli and the interstitium. Expression of *Renin* was also found in the collecting ducts of hypertensive rats (Prieto-Carrasquero, Harrison-Bernard et al. 2004; Sequeira Lopez, Pentz et al. 2004; Prieto-Carrasquero, Botros et al. 2008). As hypertension was previously described in patients with ARPKD (Guay-Woodford and Desmond 2003) and ADPKD (Chapman, Johnson et al. 1990) Increased *RENIN* expression may therefore influence the cystic kidney phenotype in PKD.

Homozygous or heterozygous mutations in *Ren1* were previously identified in patients with renal tubular dysgenesis, hyperuricemic nephropathy (Gribouval, Gonzales et al. 2005; Zivna, Hulkova et al. 2009; Gribouval, Moriniere et al. 2012). Sufficient levels of *Ren1* are therefore required to maintain homeostasis of kidney development.

According to a study using a Lewis rat model of polycystic kidney disease, renal cyst development plays a key role in the initiation of hypertension (Phillips, Hopwood et al. 2007) however another study suggests that hypertension occurs prior to cyst formation (Loghman-Adham, Soto et al. 2004). Therefore it is still unknown if increased *Renin* expression is released prior to or subsequent to cyst formation.

In this study, *Ren1* was increased by ~3 fold in newborn $Cep290^{LacZ/LacZ}$ kidneys when compared to newborn $Cep290^{+/+}$ kidneys (from the data generated by the illumina microarray). The increase in *Ren1* expression was also confirmed by semi quantitative RT-PCR and qRT-PCR techniques in newborn $Cep290^{LacZ/LacZ}$ kidneys when compared to newborn $Cep290^{+/+}$ kidneys (up regulated 14-fold; p= 0.0001, n=6) (Figure 5.5).

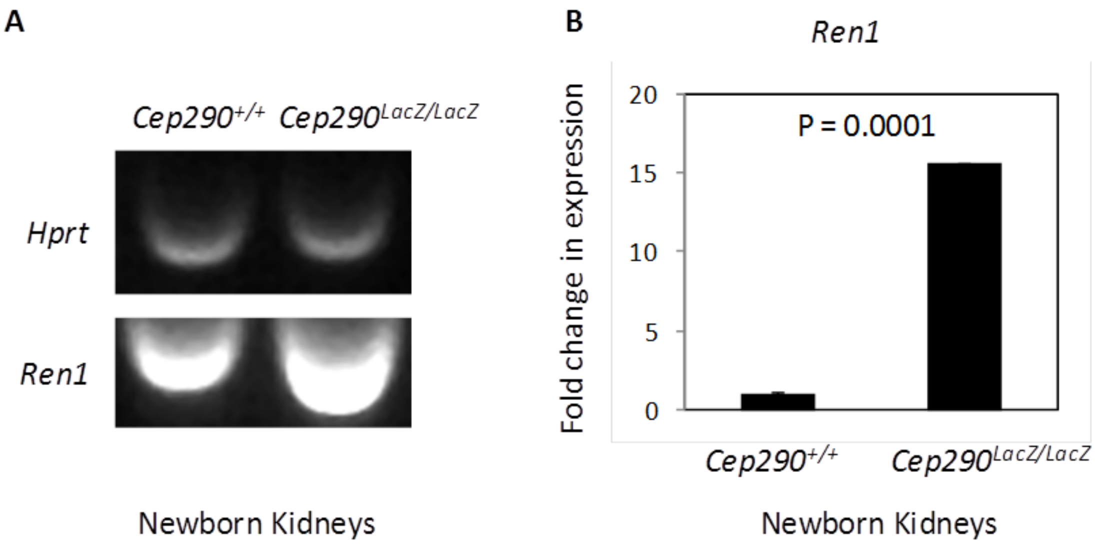

Figure 5.6 An increase in Ren1 expression in *Cep290$^{LacZ/LacZ}$* newborn kidneys was confirmed using semi quantitative RT-PCR and qPCR. (Panel A) Semi quantitative RT-PCR of the relative expression levels of *Hprt* and *Ren1* in *Cep290$^{+/+}$* and *Cep290$^{LacZ/LacZ}$* newborn kidneys. Semi quantitative RT-PCR confirms an increase in Ren1 expression in *Cep290$^{LacZ/LacZ}$* newborn kidneys. (Panel B) qRT-PCR confirmed an increase of 14 fold change in expression levels of Ren1 in *Cep290$^{LacZ/LacZ}$* newborn kidneys compared to *Cep290$^{+/+}$* newborn kidneys (p=0.0001, n=6).

Using complementary techniques, the top 3 up-regulated genes (*Miox, Pvalb* and *Ren1*) generated by the Illumina Microarray were confirmed in newborn *Cep290$^{LacZ/LacZ}$* kidneys. Miox was previously reported to be confined to the cortex of the kidney; Pvalb was previously reported to be expressed in the distal convoluted tubules of the kidney and Ren1 in the juxtaglomerular apparatus. Ren1 was also found expressed in collecting duct cells of the kidney (Prieto-Carrasquero, Harrison-Bernard et al. 2004; Prieto-Carrasquero, Botros et al. 2008; Harrison-Bernard 2009);Pentz, Lopez et al. 2001; Sequeira-Lopez, Weatherford et al. 2010.

Another interesting result regarding the list of up regulated genes identified from the illumina microarray was that 10 of the up regulated genes were solute carriers and 3 of these solute carriers (*Slc13a3*, *Slc12a3* and *Slc22a1*) were repeated twice in the list of genes. Solute carriers are extremely important for maintaining kidney homeostasis by “mediating trans-membrane movement of electrolytes, nutrients, vitamins from one cellular compartment to another

(Anderson and Thwaites 2010). The 3 repeated up regulated *SLC* genes suggests the up regulation identified is true to *Cep290*$^{LacZ/LacZ}$ renal tissue as two different probe sets confirm an up regulation in each of the *SLC* genes repeated.

The solute carrier *Slc26a4* was one of the *Slc* genes regulated in *Cep290*$^{LacZ/LacZ}$ renal tissue according to the Illumina Microarray's results. *Slc26a4* is an apical Cl^-/HCO_3^- exchanger in intercalated cells of the collecting duct tubule (Royaux, Wall et al. 2001). When *Slc26a4* is disrupted Cl^- absorption is also disrupted in the collecting duct tubule and this normally occurs in coherence with a lack of Na^+. Therefore there is a knock on effect from the increase of *Ren1* expression levels (Wall, Kim et al. 2004; Eladari, Chambrey et al. 2012). The increase of *Ren1* and *Slc* carriers therefore corroborates that there is a compensatory mechanism occurring in *Cep290*$^{LacZ/LacZ}$ kidneys due to NaCl wasting.

F13b, Apom and *Upb1* were 3 other genes which were confirmed twice as up-regulated genes in *Cep290*$^{LacZ/LacZ}$ newborn kidneys. F13b is a β subunit of the human coagulation factor protein but there are no reports for its role in the kidney (Nonaka, Matsuda et al. 1993). During human and mouse embryogenesis Apom was found exclusively expressed in kidney tissues (Zhang, Dong et al. 2003; Zhang, Jiao et al. 2004) suggesting that Apom is required for kidney morphogenesis

5.8 *Cep290$^{LacZ/LacZ}$* downregulated genes identified by the Illumina microarray.

There was also a list of down regulated genes identified in *Cep290$^{LacZ/LacZ}$* newborn kidney mRNA compared to *Cep290$^{+/+}$* newborn kidneys generated from the Illumina Microarray.

A total of 15 down regulated genes were generated with a logFC of less than -1 and a p value of 0.0003 or less. Of the 15 down regulated genes there were 3 repeats of genes (*Mest, Dlk1, Dmkn*). These 3 repeats are confirmed in addition to the previously verified genes as two different probe sets have confirmed a –Log FC in expression levels for these genes (Table 5.3).

Interestingly *Mest* was found to play a role in "mammalian metanephric development" (Kanwar, Kumar et al. 2002) as high expression of Mest was exclusively found in the metanephric mesenchyme at E13.5. Mest expression slowly decreased during kidney development with little to no expression observed in newborn kidneys (Kanwar, Kumar et al. 2002). Mest was down-regulated in *Cep290$^{LacZ/LacZ}$* newborn kidneys suggesting that there may have been a lack of *Mest* expression in *Cep290$^{LacZ/LacZ}$* kidneys during development.

Mutations in *Dlk1* have not been identified in NPHP disorders however, *Dlk1* expression was recently found in renal cell carcinomas and not in control kidney tissue of mice and humans (Chi Sabins, Taylor et al. 2013) suggesting that defective *Dlk1* expression results in unstable signalling in the normal balance of kidney homeostasis.

Dmkn expression was found in the tubular epithelium of the kidney and was found to be overexpressed in inflammatory diseases (Naso, Liang et al. 2007). In this study Dmkn was reduced in *Cep290$^{LacZ/LacZ}$* kidneys hence suggesting that reduced Dmkn expression may play a role in cystic kidney phenotype.

Two of the down regulated genes identified by the Illumina microarray data were chosen to confirm the down regulation of expression levels in *Cep290$^{LacZ/LacZ}$* newborn kidneys compared to *Cep290$^{+/+}$* newborn kidneys using semi-quantitative RT-PCR and qRT-PCR techniques.

The down regulated genes tested for gene expression levels using semi quantitative and quantitative RT-PCR methods were *Gdnf* and*Tff2*. The 15 down regulated genes had a p value of <0.0001 or less and a log fold change of -1.0 or less. A logFC of -1 is not very convincing by changes in expression levels but the p value of less than 0.05 makes this change significant.

Briefly, the genes which were confirmed were chosen because when the Illumina Microarray probe was blasted in Ensembl the gene had more than 2 exons, the genes were “top hits” according to LogFC from the Illumina Microarray and the genes were significant. The gene needed to have an intron/exon boundary between 2 exons in order to design primers which were suitable for QPCR analysis as this removes DNA outliers.

The genes which were on the hit list as duplicates were not chosen to be confirmed via semi-quantitative and qRT-PCR methods as they were already confirmed as the microarray used a different probe to show the same down regulation identified previously by another probe.

Some probe sequences when blasted hit 2 genes, suggesting non-specificity of the probe and therefore it was decided that they would not be ideal genes to confirm.

Microarray analysis of genes differentially expressed in *Cep290*$^{LacZ/LacZ}$ kidneys		
Gene Symbol	**Log FC**	**P. Value**
Csda	-1.00632	0.000111
Mest	-1.02908	1.89E-05
Crlf1	-1.0557	0.000123
Btbd11	-1.06398	1.93E-05
Gdnf	-1.07427	0.00013
Fus	-1.0749	0.000377
Dlk1	-1.10407	8.62E-06
Xlr4a	-1.11382	8.12E-06
Prrc2c	-1.11824	8.75E-05
Col2a1	-1.12927	7.69E-05
Cited1	-1.15672	9.58E-06
Tff2	-1.15967	5.32E-05
Dmkn	-1.18445	0.000193
Six2	-1.18477	1.19E-05
Dlk1	-1.22732	5.11E-06
Mest	-1.24164	6.59E-06
Dmkn	-1.24463	0.000107
Suv420h1	-1.45311	6.65E-05
Csda	-1.00632	0.000111

Table 5.3 List of downregulated genes in *Cep290*$^{LacZ/LacZ}$ kidneys generated by Illumina Microarray.
A list of down regulated genes generated by the Illumina Microarray. The down regulated genes were generated by comparing *Cep290*$^{LacZ/LacZ}$ kidney mRNA with *Cep290*$^{+/+}$ kidney mRNA. A total of 15 genes (excluding 3 repeats- *Mest, Dlk1, Dmkn*) were down regulated in the *Cep290*$^{LacZ/LacZ}$ kidneys when compared to *Cep290*$^{+/+}$ kidneys. The genes shaded in red have been confirmed in *Cep290*$^{LacZ/LacZ}$ newborn kidneys when compared to *Cep290*$^{+/+}$ newborn kidneys via RT-PCR techniques (List generated by Matthew Bashton, Bioinformatics, Newcastle University).

The down regulated genes which were on the list as duplicates (*Mest, Dlk1* and *Dmkn*) were not chosen for confirmation via semi-quantitative and qRT-PCR methods as they were already confirmed using different probes from the microarray.

Crlf1 is a signalling effector of the rearranged during transfection (RET) which has shown to play an important role in cancer (Sims-Lucas, Di Giovanni et al. 2012; Santarpia and Bottai 2013)

5.9 Glial cell derived neurotrophic factor (Gdnf)

Gdnf was the first down regulated gene (identified by the Illumina Microarray) confirmed by RT-PCR methods in this study. *Gdnf* is required for kidney morphogenesis and is expressed by the metanephric mesenchyme which promotes growth of the uteric bud branching tree that develops into the collecting duct system of the kidney (Durbec, Marcos-Gutierrez et al. 1996; Trupp, Arenas et al. 1996; Basson, Watson-Johnson et al. 2006).

Gdnf expression is found in both foetal and adult human kidney collecting duct tubules (Lee, Chan et al. 2002). Increased *Gdnf* expression was previously reported in the epithelia of collecting duct cysts of polycystic kidney patients, which suggests that increased *Gdnf* may contribute to the pathogenesis of cystic collecting ducts (Lee, Chan et al. 2002). Increased *GDNF* expression in uteric bud cultures formed cysts when cultured on 3D collagen gels confirming that increased *GDNF* expression can cause cysts (Ye, Habib et al. 2004).

Previous studies identified that the RET/GDNF signalling pathway is crucial for the correct formation of collecting ducts and also for nephrogenesis, reviewed in (Schedl and Hastie 2000). When kidneys are grown *in vitro* with excess GDNF, collecting duct branching is increased (Vega, Worby et al. 1996; Sainio, Suvanto et al. 1997; Davies and Davey 1999).

In this study *Gdnf* expression was reduced in *Cep290*$^{LacZ/LacZ}$ newborn kidneys. The correct level of GDNF expression is critical for the signalling and direction of collecting duct branching/morphogenesis and therefore a reduction in Gdnf expression in this mouse model may contribute to the cystic kidney phenotype observed in this novel *Cep290* mouse model.

Mice with mutations in *Gdnf* present with kidney aplasia and dysplasia, sympathetic ganglia defects and intestinal obstruction. Mice heterozygous for *Gdnf* occasionally display unilateral or bilateral kidney dysplasia (Pichel, Shen et al. 1996; Sanchez, Silos-Santiago et al. 1996).

Semi quantitative RT-PCR and qRT-PCR confirmed *Gdnf* expression was down-regulated in *Cep290*$^{LacZ/LacZ}$ newborn kidneys compared to kidneys isolated from *Cep290*$^{+/+}$ littermates (down regulated 0.7-fold; p <0.0001, n=6). Figure 5.7

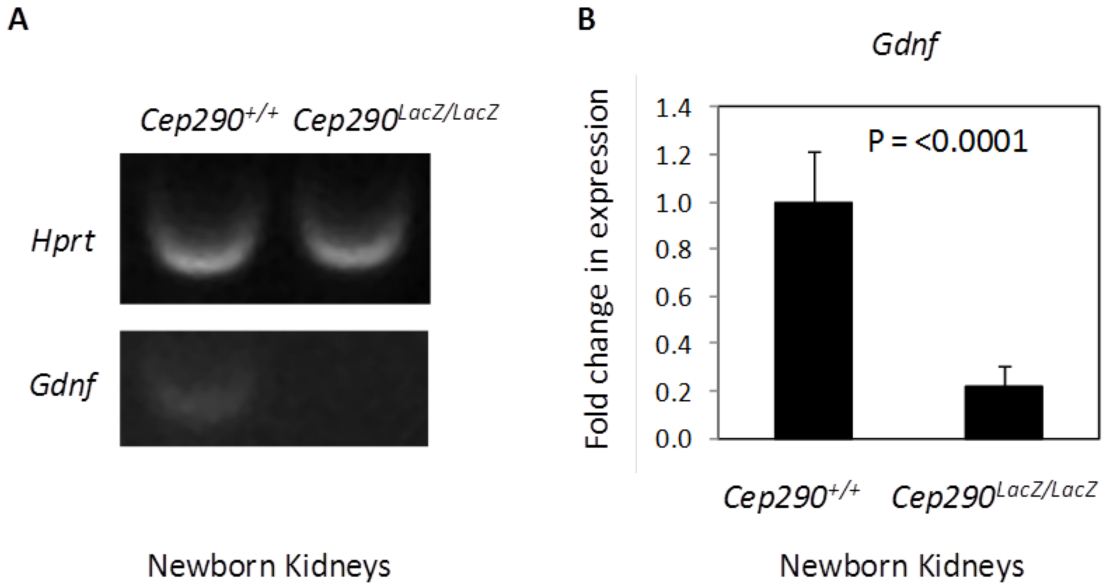

Figure 5.7 Reduced *Gdnf* expression in *Cep290*$^{LacZ/LacZ}$ newborn kidneys. Panel A) Semi quantitative RT-PCR of the expression levels of *Hprt* and *Gdnf* in *Cep290*$^{+/+}$ and *Cep290*$^{LacZ/LacZ}$ newborn kidneys. *Gdnf* expression is reduced in *Cep290*$^{LacZ/LacZ}$ newborn kidneys.
Panel B) qRT-PCR demonstrated a slight decrease in *Gdnf* expression in *Cep290*$^{LacZ/LacZ}$ newborn kidney mRNA. (p <0.0001, n=6)

5.10 Trefoil factor 2 (*Tff2)*

There is little known about the role of *Tff2* in the kidney. Previous studies have shown that *Tff2* is a secretory product of the mucous epithelia and is essential for maintaining the integrity of these epithelia (Hoffmann, Jagla et al. 2001; Hoffmann and Jagla 2002; Hertel, Chwieralski et al. 2004). As the collecting duct tubules have an epithelial cell layer lining the lumen of the collecting duct perhaps the epithelial integrity is disrupted in *Cep290*$^{LacZ/LacZ}$ mice.

Tff2 knockout mice show that *tff2* plays an important role in gastric cytoprotection and repair (Farrell, Taupin et al. 2002; Quante, Marrache et al. 2010). *Tff2* expression was found in the proximal tubules and the glomeruli of the kidney in a mouse model where a CreERT2FrtNeoFrt cassette was inserted in a bacterial artificial chromosome containing the *Tff2* gene. The expression of *Tff2* increased in these mice when epithelia were damaged (Quante, Marrache et al. 2010). From these previously published papers *Tff2* may therefore not directly affect collecting ducts but cause a secondary effect to the epithelial cells protruding into the lumen of collecting duct cells in the kidney when a cystic phenotype is beginning to occur.

In this study *Tff2* expression was down regulated in*Cep290*$^{LacZ/LacZ}$ newborn kidneys compared to *Cep290*$^{+/+}$ kidneys form data generated by the Illumina Microarray. *Tff2* was not previously identified in collecting duct cells in previous literature therefore this down regulation in expression of *Tff2* is a secondary effect of gene expression differences.

Semi-quantitative RT-PCR and qRT-PCR was employed to confirm the decrease in expression of *Tff2* in other *Cep290*$^{LacZ/LacZ}$ newborn kidney mRNA samples when compared to *Cep290*$^{+/+}$ controls (down regulated 0.5-fold; $p<0.0001$, n=6). (Figure 5.8). The fold change in expression was only decreased by 0.5 fold this therefore is not a big difference when compared to the up regulated genes which saw an average fold change in expression of >10 for each gene when confirmed by qRT-PCR.

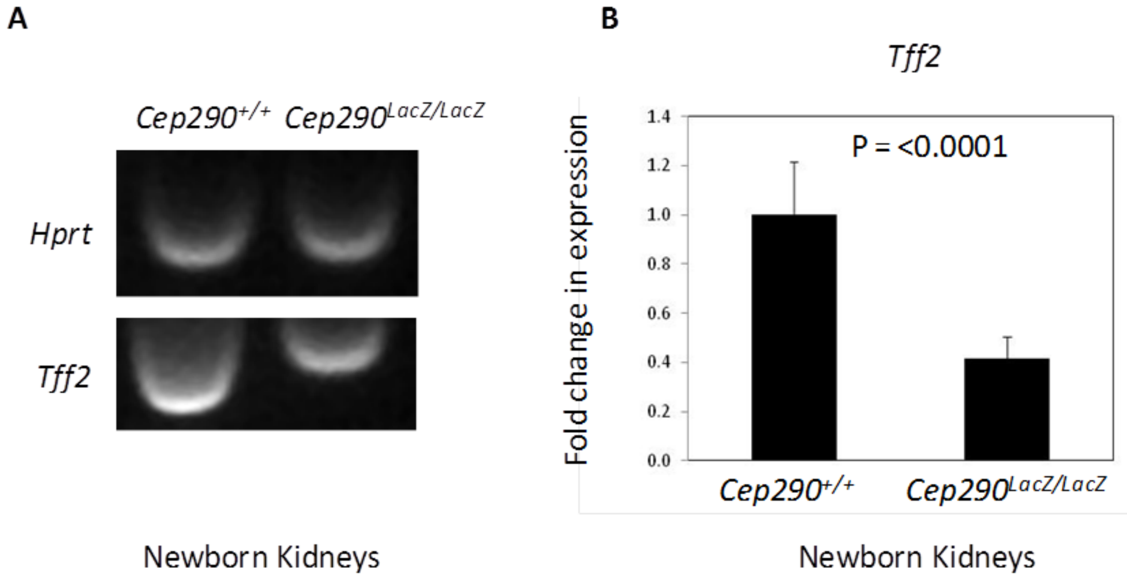

Figure 5.8 ***TFF2*** **expression is reduced in** ***Cep290$^{LacZ/LacZ}$*** **newborn kidneys.**
Panel A) Semi quantitative RT-PCR of the expression levels of *Hprt* and *Tff2* in *Cep290$^{+/+}$* and *Cep290$^{LacZ/LacZ}$* newborn kidneys. *Tff2* expression is reduced in *Cep290$^{LacZ/LacZ}$* newborn kidneys.
Panel B) qRT-PCR demonstrated a decrease of 0.5 fold in *Tff2* expression in *Cep290$^{LacZ/LacZ}$* newborn kidney mRNA when compared to *Cep290$^{+/+}$* newborn kidney mRNA ($p<0.0001$, $n= 6$).

This study identified numerous up regulated (49 up regulated genes) and only a few down regulated genes (15) in *Cep290$^{LacZ/LacZ}$* mice compared to *Cep290$^{+/+}$* mice. The increased number of up regulated genes to down regulated genes also suggests that a compensatory mechanism may be operating to counter the loss of the *Cep290* gene as many more genes are up regulated than down regulated. Also the fold changes in gene expression levels for the up regulated genes were more significant for both the microarray analysis and the qRT-PCR analysis when compared to the down regulated genes as there fold changes were 1 fold change or less.

5.11 Clustering the candidate Illumina Microarray genes into biological processes

In order to cluster the microarray genes into biological processes which may contribute to the cystic kidney phenotype of *Cep290*$^{LacZ/LacZ}$ mice, pathway analysis software was employed. A Database for Annotation, Visualisation and Integrated Discovery (DAVID) determined the link between the genes generated from the Illumina Microarray and the biological processes associated with these genes which have been previously reported in literature http://david.abcc.ncifcrf.gov/tools.jsp .

Results from the pathway analysis software programme called DAVID identified that differentially expressed genes are involved in several biological processes including signalling pathways, secreted pathways; transport pathways, ion transport pathways, oxygen reduction pathways, symport pathways and sodium transport pathways (Table 5.4).

Term	%	PValue
signal (25 genes)	35.21	1.49E-04
Secreted (19 genes)	26.76	3.98E-06
transport (16 genes)	22.54	6.96E-04
ion transport (9 genes)	12.68	0.001034
oxidoreductase (8 genes)	11.27	0.00598
Symport (6 genes)	8.45	5.94E-05
Sodium (5 genes)	7.04	6.41E-04
Sodium transport (5 genes)	7.04	8.49E-04

Table 5.4 Functional annotational chart of genes that were differentially expressed from the Illumina Microarray using a programme called DAVID. Table generated from DAVID representing the biological clustering of genes identified by the Illumina Microarray. The % was calculated using the genes involved/ total genes. A total of 74 genes were identified by the Illumina microarray. A modified Fisher Exact P-value was calculated from an EASE score of 0.1. The smaller the P-value, the more enriched. 26 genes did not make the functional annotation chart. The minimum number of genes for a corresponding term was set to 5 genes.

The top hit identified by the software programme DAVID involved a cluster of genes linked to “signalling” pathways. 25 genes clustered together were linked to “signalling” processes from data generated by the Illumina Microarray.

It is clear from many previous studies that cilia are involved in maintaining the balance of sensory signalling in the kidney and therefore an up regulation of signalling genes (22 genes of the 25 signalling genes identified were up regulated Table 5.5) also suggests that a compensatory signalling mechanism is required to try to maintain the natural balance of the kidney in *Cep290*$^{LacZ/LacZ}$ mice.

The cilia from collecting duct tubule cells isolated from this *Cep290*$^{LacZ/LacZ}$ mouse model are shorter in length and there are only 5% of cells which contain a primary cilia compared to 50% in *Cep290*$^{+/+}$ controls (Chapter 3), and therefore one could speculate that extra signalling cascades are required to try and compensate for the lack of primary cilia in both length and numbers.

Biological Process	**Clustered Gene symbols**
Signal (25 genes)	Angptl7,Apoa2, Apom,F13b, Col2a1, Col4a3, C2, Cfi, Crlf1, Defb1, Defb19, Dlk1, Dmkn,Dpep1, Enpp6, Gdnf, gpx3, Kl, Ren1, retsat, Spp1, Spp2, Scn4b, Tcn2, Tff2
Secreted (19 genes)	Angptl7, Apoa2, Apom, Col2a1, Col4a3, C2, Cfi, Crlf1, Defb1, Defb19, Dmkn, Gdnf, Gpx3, Kl, Ren1, Spp1, Spp2, Tcn2, Tff2
Transport (16 genes)	Apoa2, Apom, Bc021785, ostA, Pex13, Scn4b, Slc12a3, Slc13a3, Slc13a1, Slc22a1, Slc22a18, Slc26a4, Slc6a20b, Slc7a9, Tcn2, Trpm6
Ion Transport (9 genes)	Wnk1, Bc021785, Scn4b, Slc12a3, Slc13a3, Slc13a1, Slc22a1, Slc22a18, Slc26a4, Tcn2, Trpm6
Oxidoreductase (8 genes)	Nox4, Acadl, Cyp2j9, Cyp4a14, Gpx3, Hgd, Miox, Retsat.
Symport (6 genes)	Bc021785, Slc12a3, Slc13a3, Slc13a1, Slc22a18, Slc6a20b
Sodium+ Sodium Transport (5 genes)	Bc021785, Scn4b, Slc12a3, Slc13a3, Slc13a1

Table 5.5 Summary of the genes clustered in each biological process. Biological processes representing the genes that were differentially expressed in *Cep290*$^{LacZ/LacZ}$ newborn kidneys compared to *Cep290*$^{+/+}$ newborn kidneys using a programme called DAVID. Yellow highlights genes confirmed via semi-quantitative RT-PCR and qRT-PCR techniques. Teal represents genes which were down regulated in *Cep290*$^{LacZ/LacZ}$ newborn kidneys from the data generated by the Illumina microarray. Genes highlighted in red are all involved in the transport of sodium or organic ions into a cell membrane and are all these genes were up regulated in the *Cep290*$^{LacZ/LacZ}$ newborn kidney.

There are 2 main signalling pathways which have been recognised as defective in mouse models of NPHP/JBTS (Table1.6). The 2 main signalling pathways defective are the Shh signalling pathway or the Wnt signalling pathway.

Defective Shh signalling was investigated on human fetal samples with JBTS, it was found that the rate of proliferation in cerebellular granule cell progenitors (GCP)s and the response of GCPs to Shh, was severely disrupted in the cerebellum of JBTS patients (Aguilar, Meunier et al. 2012). GCP's proliferation rate was determined by staining fetal cerebellar sections with anti-Ki67 to label the GCPs. Shh expression was assessed in JBTS fetal samples by *in situ* hybridisation techniques on the cerebellum and from the combined results it was concluded that GCP proliferation is in harmony with active Shh signalling in the developing human cerebellum (Aguilar, Meunier et al. 2012).

The *Ahi1*$^{-/-}$ mouse model of JBTS identifies defective Wnt signalling in the developing cerebellum (Lancaster, Gopal et al. 2011). *Ahi1*$^{-/-}$ mice at E12.5 and E13.5 were treated with lithium (a wnt pathway agonist) and were assessed at E16.5. Lithium treatment reduced the midline fusion defect observed in *Ahi1*$^{-/-}$ mice therefore confirming defective wnt signalling in the developing cerebellum (Lancaster, Gopal et al. 2011). A previous study examining kidneys of *Ahi1*$^{-/-}$ mice also identified defective Wnt signalling defects in 5 month old kidneys from *Ahi1*$^{-/-}$ mice (Lancaster, Louie et al. 2009).

Disruptions in both the Wnt and Shh pathway are linked with *NPHP* mutations (Table 1.6). Chapter 6 will investigate in further detail these 2 signalling pathways and determine if they are disrupted in *Cep290*$^{LacZ/LacZ}$ kidneys.

Note *Cep290* was not on the Illumina Microarray beadchip. Only 23 genes from the 40 *NPHP/JBTS* genes listed in chapter 1, table 1.1 were on the beadchip. The 23 genes included *NPHP3, NPHP4, NPHP1, XPNPEP3, ANKS6, SLC41A1, CEP164, ATXN10, IQCB1, GLIS2, NEK8, INPP5E, TMEM216, AHI1, RPGRIP1L, ARL13B, CC2D2A, TCTN1, TMEM237, TMEM138, TCTN2, TCTN3* and *TMEM231*. The *PKD1* gene was also on the Illumina Microarray beadchip however there were no changes in gene expression levels observed for any of these genes.

5.12 Discussion

Pvalb and *Ren1* can be linked by the angiotensin pathway however the pathway analysis tool DAVID did not find a link with *Pvalb* and any other gene in the list of genes associated with the Illumina Microarray suggesting that there are still flaws in the DAVID software programme (Table 5.6 for a list of genes not linked to any other gene in the microarray list according to biological processes identified by the software programme DAVID).

Illumina ID	Gene Symbol	Log FC from microarray
ILMN_3139253	*BTBD11*	-1.063975765
ILMN_2646166	*ndrg1*	1.10539241
ILMN_1236537	*06100087F07Rik*	1.368965182
ILMN_1225602	*S100A1*	1.175395011
ILMN_2965669	*Xlr4a*	-1.113816244
ILMN_2628174	*acss1*	1.492222958
ILMN_2674979	*fus*	-1.074898405
ILMN_2610706	*Hrsp12*	1.176760628
ILMN_2725617	*khk*	1.108664074
ILMN_2615035	*Mgst3*	1.172024453
ILMN_1218223	*Pvalb*	3.312463183
ILMN_1243875	*Suv420h1*	-1.453114399
ILMN_2624031	*Tmem16*	1.028059537
ILMN_2516705, ILMN_2870788	*Upb1*	1.129406619

Table 5.6 Genes excluded from DAVID Functional annotational chart. The genes represented in this table did not make the functional annotational chart of genes generated from Figure 5.9. The cut off value of 2 (minimum number of genes for a corresponding term) excluded this list of genes from analysis.

The DAVID software programme also clustered 19 genes together under the biological process called “secretion”. Without the use of the Illumina Microarray the *Slc* (solute carriers) genes would not have been identified. Also it was identified that future studies would require monitoring the levels of Na^+ and Cl^- secretion in *Cep290*$^{LacZ/LacZ}$ urine samples as low levels are due to an increase of *Ren1* and *Slc26a4* expression. This would not have been identified without the use of the microarray data. The information gathered from the gene list identified by the Illumina Microarray aided in determining that physiological studies are required to determine the renal physiological phenotypes associated with *Cep290*$^{LacZ/LacZ}$ mutation.

A number of genes clustered together in ion/sodium transport. Each of the genes which clustered in the ion/sodium transport were up regulated in *Cep290*$^{LacZ/LacZ}$ kidneys suggesting that the *Cep290*$^{LacZ/LacZ}$ kidney is overcompensating due to excessive wasting of Na^+ and Cl^- and these physiological changes in ionic and sodium transport are contributing to a cystic kidney phenotype. As mentioned earlier *Renin* is released when Na^+ levels are low to try to conserve the salt water balance as referred to in a review article (Harrison-Bernard 2009).

An NPHP review, describes the phenotypes of polyuria and polydypsia occurring due to the loss of sodium which occurs early in NPHP (Salomon, Saunier et al. 2009). It is possible that polyuria is evident in this *Cep290*$^{LacZ/LacZ}$ mouse model however there were not enough sample numbers for urine measurement in *Cep290*$^{LacZ/LacZ}$ mice to reach statistical significance (Chapter 3).

A study briefly mentioned earlier, using a Lewis rat model of polycystic kidney disease, suggested that renal cyst development plays a key role in the initiation of hypertension (Phillips, Hopwood et al. 2007). Another study suggested that hypertension occurs prior to cyst formation (Loghman-Adham, Soto et al. 2004). From this study increased *Renin* expression occurs subsequent to micro cysts evident in *Cep290*$^{LacZ/LacZ}$ kidneys and therefore confirms the theory that renal cyst development plays a role in the initiation of hypertension (Phillips, Hopwood et al. 2007) in *Cep290*$^{LacZ/LacZ}$ kidneys.

As mentioned earlier in this chapter early onset hypertension can occur in patients with ARPKD and an increase of *Renin* leads to hypertension. *Renin* is only released when Na^+ levels are low to try to conserve the salt water balance in the kidney. In the *Cep290*$^{LacZ/LacZ}$ newborn kidneys there is an up-regulation of genes associated with sodium and sodium transport suggesting that Na^+ levels are low in *Cep290*$^{LacZ/LacZ}$ kidneys. Assuming the *Cep290*$^{LacZ/LacZ}$ mice are polyuric due to salt wasting, raised *Renin* is more than likely due to a secondary effect to try and raise blood pressure via renin-angiotensin-aldosterone axis. Defects of Na^+ handling in the collecting ducts of *Cep290*$^{LacZ/LacZ}$ mice are evident from data generated by the illumina microarray data as collecting ducts are required for efficient salt handling in the kidney.

The symport biological process involves the transport of solutes across a biological membrane in one direction. Interestingly all the proteins clustered in the symport biological processes are solute carriers and are all up regulated in *Cep290*$^{LacZ/LacZ}$ newborn kidneys once again suggesting a compensatory overall transport mechanism for the few cilia numbers identified in the cells. Some of the proteins clustered in symport are also clustered in sodium/sodium transport and transport biological processes therefore concluding that there is a lack of sodium, ions and other proteins transported around the kidney of *Cep290*$^{LacZ/LacZ}$ newborn kidneys (Table 5.5). Collecting duct cells are responsible for ion secretion and re-absorption (Taal, Chertow et al. 2011). The collecting ducts in *Cep290*$^{LacZ/LacZ}$ kidneys are not functioning normally due to the *Cep290* truncated mutation

As mentioned earlier Na^+ absorption occurs through *ENaC*, maintaining a correct balance of *ENaC* function in the kidney is crucial for Na^+ handling by the kidney (Hummler 1999; Schild and Kellenberger 2001; Stockand 2002; Hummler 2003; Schild 2004; Zaika, Mamenko et al. 2013). In the introduction to this study the *orpk* ARPKD mouse model was highlighted. The *orpk* ARPKD mouse model saw an increase in Na^+ absorption in cystic CDT cells in their mouse model (Olteanu, Yoder et al. 2006). In another study utilising a CDT cell line isolated from the *orpk* mouse model abnormal trafficking of Aqp2/V2R was identified and it was concluded that this lead to enhanced Na^+ and H_20 absorption (Saigusa, Reichert et al. 2012).

Future studies will be required to assess if *ENaC* function and/or *Aqp2* trafficking is disrupted in the *Cep290*$^{LacZ/LacZ}$ CDT cells and assess if disrupted *ENaC* and or *Aqp2* expression are involved in the cystic kidney disease phenotype associated with *Cep290* mutations. Future studies could also involve measuring the blood pressure of animals to determine if they are hypertensive. Juxtaglomerular hypertrophy can also occur in patients with severe salt wasting future studies could involve reassessing the histology of *Cep290*$^{LacZ/LacZ}$ kidneys to identify if the juxtaglomerular cells are hypertrophic.

The main challenge in any study using microarray platforms is assigning the molecular functions of the vast number of genes generated from microarrays.

Chapter 6 Investigating the possible signalling pathways disrupted in NPHP caused by a truncated Cep290 mutation.

A common feature for NPHP is that the mutated proteins are all normally located in either the primary cilium or the centrosome, hence defects to the structure or the function of cilia are linked to renal cyst development (Hildebrandt, Attanasio et al. 2009).

Ciliopathy gene products regulate signal transduction pathways and these pathways are often abnormal in cystic collecting ducts (Winyard and Jenkins 2011). The pathogenesis of NPHP is not known and therefore this *Cep290*$^{LacZ/LacZ}$ mouse model and the collecting duct cell line derived from the *Cep290*$^{LacZ/LacZ}$ mouse model will be used to help understand the signalling events which may be involved.

NPHP is a heterogenous disorder and therefore previously published NPHP review papers suggests that defects occur in a number of signalling pathways (Hildebrandt, Attanasio et al. 2009; Winyard and Jenkins 2011). Mouse models with mutations in the *Nphp*/*Jbts* genes have previously been linked to both the Wnt signalling pathway and the Shh pathway (Chapter 1, Table 1.6).

6.1 Aims

In order to determine which of these two pathways (Shh or Wnt) are affected in *Nphp* (linked with a truncated *Cep290* mutation), this chapter investigated if there were any differences in protein expression levels in known target Shh and Wnt candidate genes between newborn *Cep290*$^{LacZ/LacZ}$ renal tissue and their *Cep290*$^{+/+}$ controls.

If a change in protein expression level was identified in either of the two pathways in the renal tissue of newborn *Cep290*$^{LacZ/LacZ}$ mice when compared to wild type controls, Cep290$^{LacZ/LacZ}$ CDT cells would then be employed to examine if that particular pathway was abnormal in the CDT cells affected by cysts.

6.2 Results

The first aim of this chapter was to gain an understanding of the process of the Wnt signalling pathway (Figure.6.1).

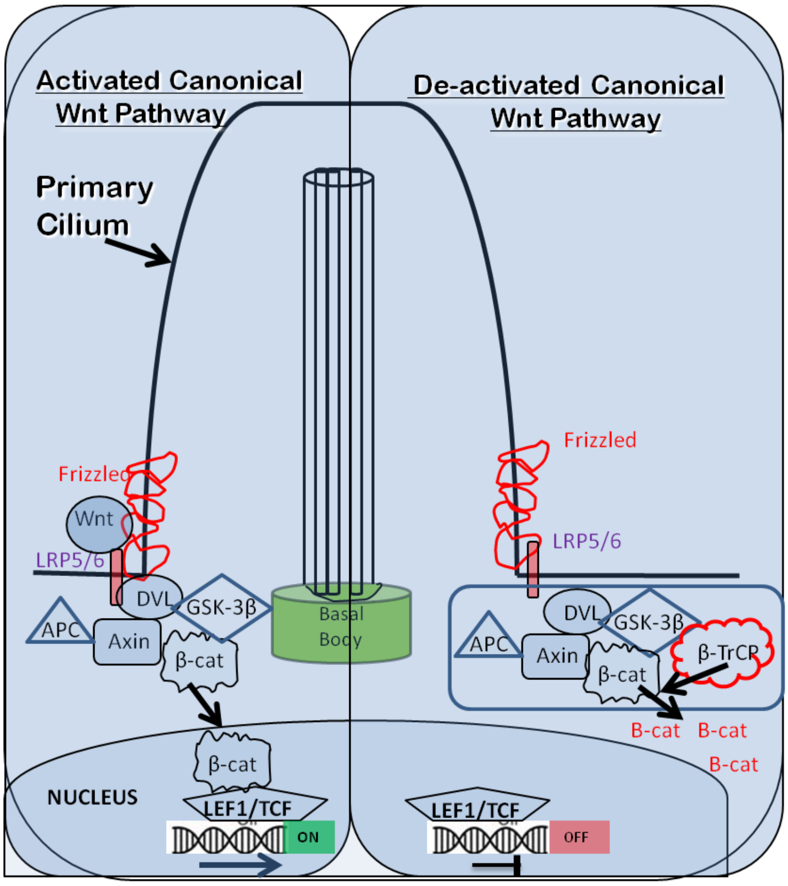

Figure 6.1 Overview of the Wnt Signalling pathway in terms of Lef1/Tcf1 processing.
The Wnt signalling pathway is activated when the Wnt ligand binds to the frizzled/low density lipoprotein receptor related protein complex (LRP5/6), activating dishevelled (*Dvl*). How *Dvl* is activated has not been fully understood in the literature but it is suggested to be partly phosphorylated by *casein kinase* 1 and 2 (*CK1* and *CK2*). *Dvl* inhibits the activity of the *β-catenin-Axin-adenomatous polyposis coli-glycogen* (*APC*) syntase kinase (multiprotein) complex which results in the accumulation of cytosolic *β-catenin*. The *β-catenin* then translocates to the nucleus where it activates/binds to the T-cell factor (*Tcf/Lef)* family of DNA binding proteins leading to transcription of wnt target genes. When wnt is absent, *Axin* recruits *CK1* to the multiprotein complex and initiates *β-catenin* phosphorylation by *GSK-3β*. Phosphorylated *β-catenin* is then degraded by the proteosome by the β-transducin repeat-containing protein (*β-TrCp*) and therefore the Lef1/Tcf proteins expression levels are reduced (adapted from (Aguilera, Munoz et al. 2007).

6.3 Is there any evidence of defective Wnt signalling in *Cep290$^{LacZ/LacZ}$* kidneys

Once a candidate Wnt gene was identified, the protein levels of expression in the Wnt candidate gene were assessed in *Cep290$^{LacZ/LacZ}$* and *Cep20$^{+/+}$* renal tissue. In order to test if there is defective Wnt signalling, the endogenous Wnt component, lymphocyte enhancer-binding factor (*Lef1*) (Filali, Cheng et al. 2002) was used to test for a defect in Wnt signalling. Lef1 expression was also examined in the *Ahi1$^{-/-}$* mouse model (Lancaster, Louie et al. 2009).

The *Ahi$^{-/-}$* mouse model identified lower expression of the Wnt responsive full-length isoform *Lef1* in *Ahi1$^{-/-}$* kidneys when compared to littermate controls at 5 months and at 1 year of age. The *Ahi1$^{-/-}$* study concluded that a Wnt signalling defect was associated with the cystic kidney phenotype occurring due to mutations in *Ahi1*. *Ahi1$^{-/-}$* mice present with a cystic kidney phenotype at ~5 months of age (Lancaster, Louie et al. 2009). The *Cep290$^{LacZ/LacZ}$* mice described in this study however have microscopic renal cysts present at birth.

Western blot analysis was employed to test if the full length isoform expression of *Lef1* was reduced in *Cep290$^{Lacz/LacZ}$* newborn, 6 months and 1 year old kidneys when compared to *Cep290$^{+/+}$* age matched controls (See figure 6.2). The expression levels of the full length Lef1 isoform between *Cep290$^{+/+}$* and *Cep290$^{LacZ/LacZ}$* littermates were comparable unlike the *Ahi$^{-/-}$* mouse model which saw a dramatic decrease in full length expression levels in the mutant mice. The short isoform of Lef1 protein begins at amino acid 116 within the full length *LEF1* sequence and is missing the *β-catenin*-binding domain and a portion of the context dependent activation domain (Hovanes, Li et al. 2001). *Lef1* transcription factor's main function is to interact with *β-catenin* and play a role as a nuclear effector of Wnt signalling. As the Lef1 short isoform is missing the β-catenin-binding domain, it is likely that the level of Lef1 short isoform expression is not as significant as the level of expression identified in the full length isoform of Lef1 seen in *Ahi1$^{-/-}$* mice.

In order to probe Wnt signalling further antibodies for another member of the Wnt pathway the T-cell factor 1 transcription factor (*Tcf1*) was utilised to determine if there was a difference in the level of *Tcf1* expression between *Cep290$^{LacZ/LacZ}$* kidneys and *Cep290$^{+/+}$* controls.

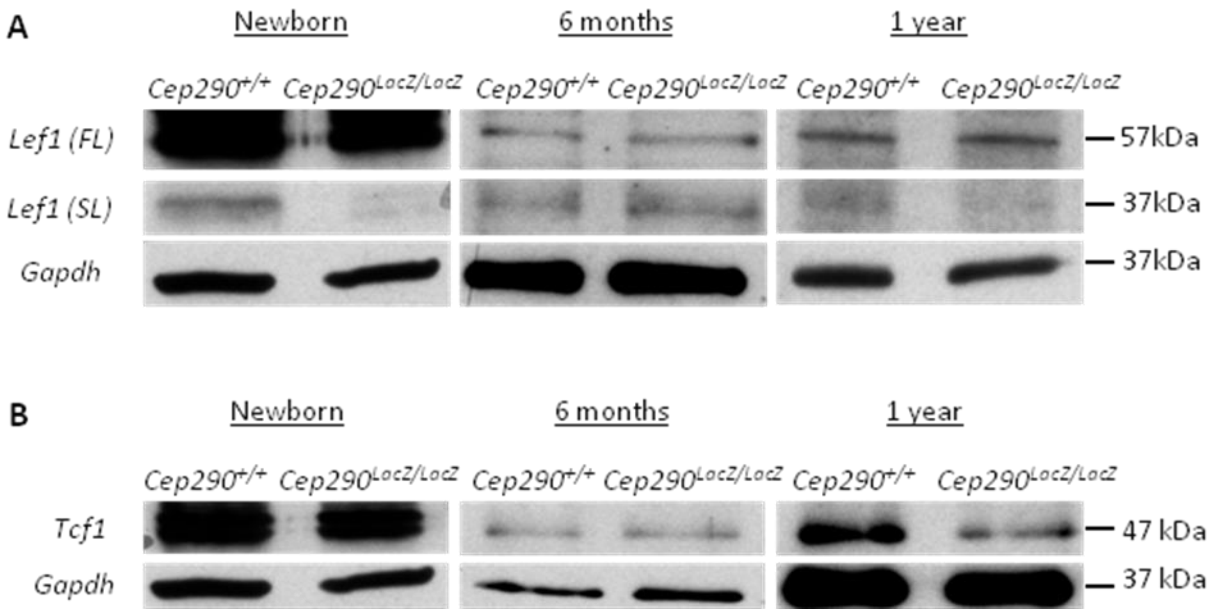

Figure 6.2 Testing differences in levels of expression between *Cep290*$^{LacZ/LacZ}$ mouse kidneys and age matched wild type controls using two transcription factors involved in wnt signalling.
Panel A) *Lef1* western blot analysis of whole kidney lysates from *Cep290*$^{+/+}$ and *Cep290*$^{LacZ/LacZ}$ littermates at birth, 6 months and 1 year of age. Panel B) *Tcf1* western blot analysis of whole kidney lysates from *Cep290*$^{+/+}$ and *Cep290*$^{LacZ/LacZ}$ littermates at birth, 6 months and 1 year of age. *Lef1*full length (FL) isoform 57kDa, *Lef1* short length (SL) isoform 37 kDa. *Tcf1* 47 kDa

Lef1/Tcf1 proteins are downstream effectors of Wnt signalling and *β-catenin* interacts with the amino acid termini of *Lef1/Tcf1* (Molenaar, van de Wetering et al. 1996; Brannon, Gomperts et al. 1997; Kengaku, Capdevila et al. 1998; Eastman and Grosschedl 1999). From these previous studies *Lef1* and *Tcf1* were good candidate Wnt target genes to measure and determine if there were any signalling defects occurring in the Wnt pathway in *Cep290*$^{LacZ/LacZ}$ kidneys.

There were no changes in the expression of *Tcf1* in *Cep290*$^{LacZ/LacZ}$ newborn kidneys when compared to *Cep290*$^{+/+}$ littermates from western blot results (Figure 6.2). Overall there were no changes in the expression levels of Wnt candidate genes in renal tissue of *Cep290*$^{+/+}$ *and Cep290*$^{LacZ/LacZ}$ mice at birth. These results therefore suggested that Wnt signalling may not be causing the micro cystic phenotype occurring at birth in *Cep290*$^{LacZ/LacZ}$ mice.

However Wnt signalling seems to be down regulated in *Cep290*$^{LacZ/LacZ}$ 1 year old kidneys consistent with *Ahi1*$^{-/-}$ mice. This suggests deregulated Wnt signalling is therefore occurring later on in the cystic kidney disease.

Cep290$^{LacZ/LacZ}$ mice at 1 year of age are fibrotic when compared to *Cep290*$^{LacZ/LacZ}$ mice at birth (See Figure 3.20). Fibrosis occurs after the cystic kidney phenotype and at a later stage of the disease in *Cep290*$^{LacZ/LacZ}$ mice. Previous review articles have linked fibrosis with defects in the Wnt signalling pathway and therefore Wnt signalling defects are secondary to the cystic and fibrotic kidney phenotype in 1 year *Cep290*$^{LacZ/LacZ}$ mice (Surendran, Schiavi et al. 2005; He, Dai et al. 2009; Kawakami, Ren et al. 2013).

As micro cysts were evident at birth in *Cep290*$^{LacZ/LacZ}$ kidneys it was therefore hypothesised that the pathway disturbed at birth may contribute to the initiating events leading to the cystic kidney phenotype associated with *Cep290* mutations. In conclusion the analysis carried out on whole kidney lysates extracted from *Cep290*$^{LacZ/LacZ}$ mice using *Lef1* and *Tcf1* as Wnt target genes suggested that there may not be defects in the Wnt signalling pathway at birth.

6.4 Is there any evidence of defective Shh signalling in *Cep290*$^{LacZ/LacZ}$ kidneys

Mutations in *KIF7, RPGRIP1L* and *INPP5E* were all identified in a subset of *JBTS/NPHP* patients and mutations in these genes have been implicated in the Shh signalling pathway (Wolf, Saunier et al. 2007; Dafinger, Liebau et al. 2011; Otto, Ramaswami et al. 2011; Travaglini, Brancati et al. 2013). *Kif7* is a ortholog of the Drosophila Costal 2 (Cos2) which is implicated in the hedgehog pathway through smoothened (Katoh and Katoh 2004). The loss of function in the *Kif7/Costal2* mouse model was previously shown to regulate sonic hedgehog signalling by preventing activation of the *Gli2* transcription factor and therefore this caused an expansion of ventral neural cell types in the neural tube because of an expanded domain of expression of Shh target genes (Liem, He et al. 2009).

The *Rpgrip1l* mouse model (known as the *Ftm* null mouse model) also showed Shh signalling defects as there was a loss of Gli3 activator to Gli3 repressor expression in *Ftm*$^{-/-}$ animals (Vierkotten, Dildrop et al. 2007).

The *Inpp5e* mouse model presented with polydactyly, exencephaly, skeletal defects, early lethality, multi cystic kidneys (including proximal tubule cysts) which are features of abnormal Shh signalling and the *JBTS/NPHP* phenotype (Jacoby, Cox et al. 2009).

TCTN3, a transition zone protein (like *Cep290*) was disrupted in *JBTS/NPHP* patients.*TCTN3* is necessary for the transduction of the Shh pathway as abnormal Gli3 processing was identified in patient fibroblast cells with mutations in *TCTN3* (Thomas, Legendre et al. 2012). Linking NPHP/JBTS candidate genes to Shh, is therefore well studied but abnormal Shh signalling has not been assessed in kidney specimens of a NPHP/JBTS model.

There are other examples of Shh deficiency in *JBTS/NPHP* cases. In a study using human fetal brain tissues detectable levels of Shh was strongly reduced in purkinje cells (Aguilar, Meunier et al. 2012). Impaired Shh signalling was also found in human brain fetal samples in three other *JBTS/NPHP* genes which include the *TMEM67/MKS3, CC2D2A* and an unidentified mutation. This suggests that Shh defects might be common in a number of ciliopathies (Aguilar, Meunier et al. 2012).

In order to determine if there was a defect in the Shh pathway in renal samples of newborn *Cep290*$^{LacZ/LacZ}$ mice when compared to *Cep290*$^{+/+}$ controls the first aim was to understand the process of the Shh signalling pathway which is outlined in Figure.6.3.

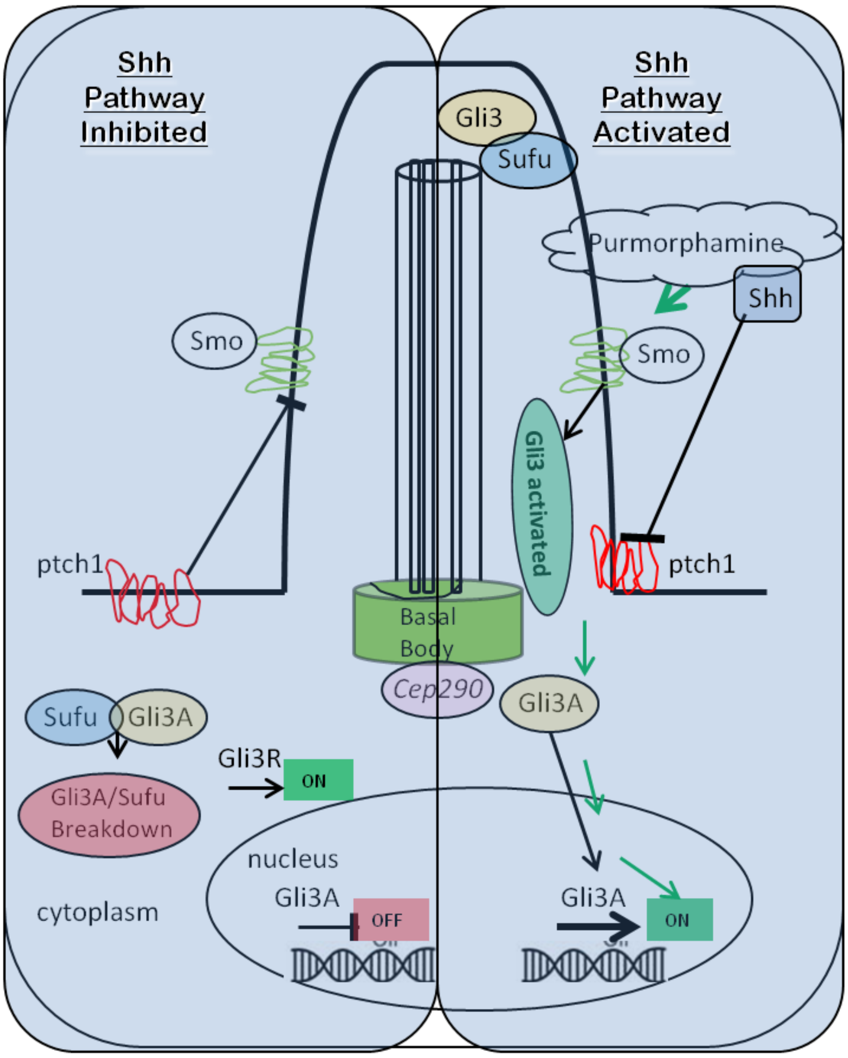

Figure 6.3 Overview of the Shh pathway when activated by purmorphamine and inhibited by patched (ptch1) in terms of Gli3 processing.
In the absense of Shh, Sufu is bound to Gli3A is phosphorylated and cleaved into a truncated peptide that represses the transcription of Shh-target genes while promoting the production of Gli3R via proteolytic cleavage of the C-terminal region of Gli3A. Gli3 processing is reduced when IFT is disrupted therefore Gli3R formation depends on cilia. Both anterograde and retrograde motors have the same effect on Hh signalling (both are required for the neural tube and for processing of Gli3. Purmorphamine treatment can activate smo. Active Smo blocks Gli3 repressor formation, allows Smo to translocate to the primary cilium and triggers Gli3/sufu dissociation and recruits them to the tip of the cilium. After Gli3A is released from Sufu, Gli3A translocates to the nucleus where it acts as a transcriptional activator of Shh target genes. (Figure and text adapted from (Huangfu and Anderson 2005; Caparros-Martin, Valencia et al. 2013).

Previous studies have examined the differences in Gli3 repressor (Gli3R) and activator (Gli3A) expression levels to measure if there were any defects in the Shh signalling pathway (Vierkotten, Dildrop et al. 2007; Caparros-Martin, Valencia et al. 2013). Gli3 expression levels determine the outcome of Shh signalling by the relative amount of Gli3R to Gli3A which leads to patterning of the neural tube (Briscoe and Ericson 2001).

In the absence of Shh signalling, an increase of Gli3R when compared to Gli3A is evident (Jacob and Briscoe 2003; Vierkotten, Dildrop et al. 2007). When Shh is absent, Sufu binds to the full length Gli3 transcription factor/Gli3A and promotes the production of the Gli3R by proteolytic cleavage of the C-terminal region of Gli3A (Wang and Li 2006; Humke, Dorn et al. 2010; Caparros-Martin, Valencia et al. 2013)

In order to determine if there was a defect in the Shh signalling pathway in whole kidney lysates isolated from *Cep290*$^{LacZ/LacZ}$ mice, the differences in expression levels of the Gli3R to Gli3A were compared to *Cep290*$^{+/+}$ whole kidney lysates.

Gli3 processing was examined in newborn *Cep290*$^{+/+}$and *Cep290*$^{LacZ/LacZ}$ whole kidney lysates via Western blot analysis, using an antibody against the N-terminus of Gli3 that interacts with both the full-length (190kDa –Gli3A) and the processed short (83 kDa-Gli3R) forms of Gli3. This antibody has been used in a recent previously published *Evc* and *Evc2* mouse model where Gli3 expression was reduced in cilia tips (Caparros-Martin, Valencia et al. 2013) (See Figure 6.4).

Maintaining the regulation of Gli3R via cleavage of Gli3A is crucial for nephrogenesis, however the exact molecular mechanism by which Gli3 controls renal embryogenesis is not known (Hu, Mo et al. 2006). *Shh*$^{-/-}$ mice have no kidneys (Hu, Mo et al. 2006), therefore from this we speculate that there will still be modest amounts of Shh signalling occurring in the *Cep290*$^{LacZ/LacZ}$ kidneys but perhaps much less than the *Cep290*$^{+/+}$ control samples.

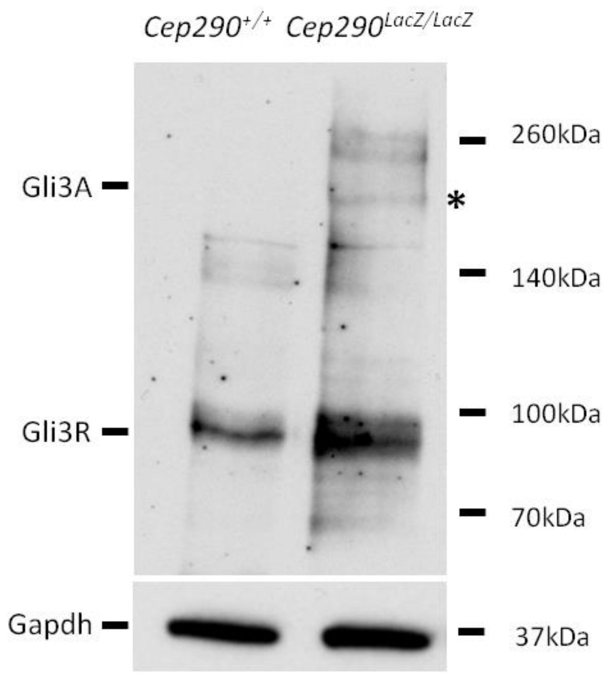

Figure 6.4 Comparing Gli3 expression in newborn kidneys of *Cep290$^{LacZ/LacZ}$* and *Cep290$^{+/+}$* mice.

Expression of Gli3 Activator (A) highlighted by an asterix and Gli3 Repressor (R) in newborn kidneys of *Cep290$^{+/+}$* and *Cep290$^{LacZ/LacZ}$* mice.

Gli3A = 190kDa and Gli3R = 83kDa. Gapdh was loaded on a 10% polyacrylamide gel. The same volume and concentration of whole kidney lysate samples were loaded on the 10% gel polyacrylamide to act as a loading control. In *Cep290$^{LacZ/LacZ}$* kidneys the Gli3R is increased compared to wild type control levels which is a indication of Shh signalling defect. At least 3 samples of each genotype have been analysed. Although there is no activator band in the *Cep290$^{+/+}$* samples the repressor band is still much stronger in the *Cep290$^{LacZ/LacZ}$* animals suggesting defective Shh signalling.

In *Cep290*$^{+/+}$ newborn renal tissue, Gli3 is efficiently processed into its repressor form (83kDa-Gli3R) Figure 6.4 panel B lane 1. From this we can only assume that this is the normal expression levels of Gli3 processing for mice at birth, as *Cep290*$^{+/+}$ animals do not have a cystic kidney phenotype and the levels of Gli3R and Gli3A protein expression levels are not known in the literature for newborn renal tissue.

By contrast however in the *Cep290*$^{LacZ/LacZ}$ homozygous mutant newborn renal tissue; Gli3 protein was present as unprocessed, full length form (190kDa-Gli3A) (Figure 6.2 panel B lane) and also had a much higher increase in level of Gli3R when compared to *Cep290*$^{+/+}$ Gli3R levels.

As a result the level of Gli3R:Gli3A expression was dramatically increased in the newborn *Cep290*$^{LacZ/LacZ}$ renal tissue. This suggests that *Cep290* acts upstream of Shh signalling (at least) partly through the regulation of Gli3 proteolytic processing and that Shh signalling is affected by a truncated *Cep290* mutation in renal tissue of newborn *Cep290*$^{LacZ/LacZ}$ mice .

6.5 Do *Cep290*$^{+/+}$ CDT cells respond to Shh treatment?

Given the results of Gli3R:A expression levels in newborn *Cep290*$^{LacZ/LacZ}$ kidney tissue, an investigation was carried out to determine Shh signalling at a functional level. *Cep290*$^{+/+}$ primary CDT cells were manipulated with a pharmacological Shh pathway agonist (Purmorphamine) and a pharmacological Shh pathway antagonist (HPI-4). The effects of the Shh agonist and antagonist manipulation on *Cep290*$^{+/+}$ primary CDT cells were then tested (See Figure 6.5).

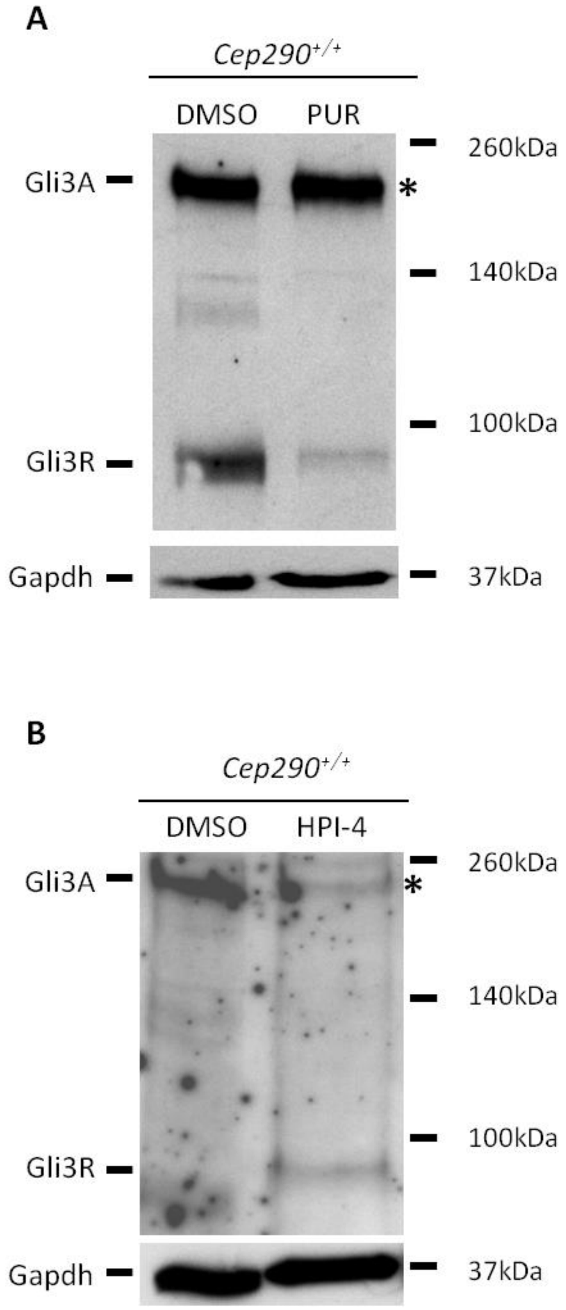

Figure 6.5 Effect of purmorphamine and HPI-4 on primary *Cep290*$^{+/+}$ CDT cells

Panel A) Gli3 expression levels in *Cep290*$^{+/+}$ CDT cells with 2µM of DMSO and 2µM of PUR. Panel B) Gli3 expression levels in *Cep290*$^{+/+}$ CDT cells with 2µM of DMSO and 2µM of HPI-4. Both Gli3A and Gli3R are decreased in *Cep290*$^{+/+}$ CDT cells treated with HPI-4. Gli3A highlighted by an asterisk.

Note *Cep290*$^{+/+}$ CDT cell were treated for 72 hours. Gapdh was loaded on a 10% polyacrylamide gel for each of the samples analysed. The same volume and concentration of *Cep290* CDT cell lysates were loaded on the 10% gel polyacrylamide to act as a loading control (n=3).

Cep290$^{+/+}$ primary CDT cells respond to Shh agonist (PUR) and antagonist (HPI-4) manipulation (See Figure 6.5).

Purmorphamine was previously described to activate the hedgehog pathway by targeting smoothened (Sinha and Chen 2006). HPI-4 was previously reported to act downstream of Sufu modulateing Gli processing, activation and trafficking. HPI-4 does not completely block Smo trafficking to the cilium but causes a decreased extent of ciliary smo accumulation in response to Shh (Hyman, Firestone et al. 2009). Purmorphamine treatment decreased Gli3R expression *Cep290*$^{+/+}$ CDT cells. Therefore purmorphamine treatment activates the Shh pathway in *Cep290*$^{+/+}$ CDT cells (See figure 6.5). HPI-4 treatment decreased overall Gli3 expression levels in *Cep290*$^{+/+}$ CDT cells confirming that *Cep290*$^{+/+}$ CDT cells respond to both the Shh agonist and the Shh antagonist.

6.6 Investigation to determine if a Shh agonist rescues tubular morphology of *Cep290*$^{LacZ/LacZ}$ CDT cells when grown in 3D cultures.

As demonstrated in Chapter 4, tubular morphology and ciliogenesis are disrupted in *Cep290*$^{LacZ/LacZ}$ CDT cells when compared to *Cep290*$^{+/+}$ CDT cells grown in a 3D culture matrix (Figure 4.8).

The 3D culturing system of CDT cells closely resembles the *in vivo* nature of the kidney collecting duct tubules unlike the 2D culturing system. The 3D culturing system of CDT cells is more representative than 2D culturing systems, as CDT cells adhere to each other rather than to the plastic on the 6 well plates, show polarity, form a lumen, producing tubular/spheroids behave more like CDT would in their natural cellular environment of the kidney.

In order to determine the effect of defective Shh signalling on the morphology of 3D cultured *Cep290*$^{LacZ/LacZ}$ CDT cells, the *Cep290*$^{LacZ/LacZ}$ CDT cells were treated with purmorphamine and their morphology was studied.

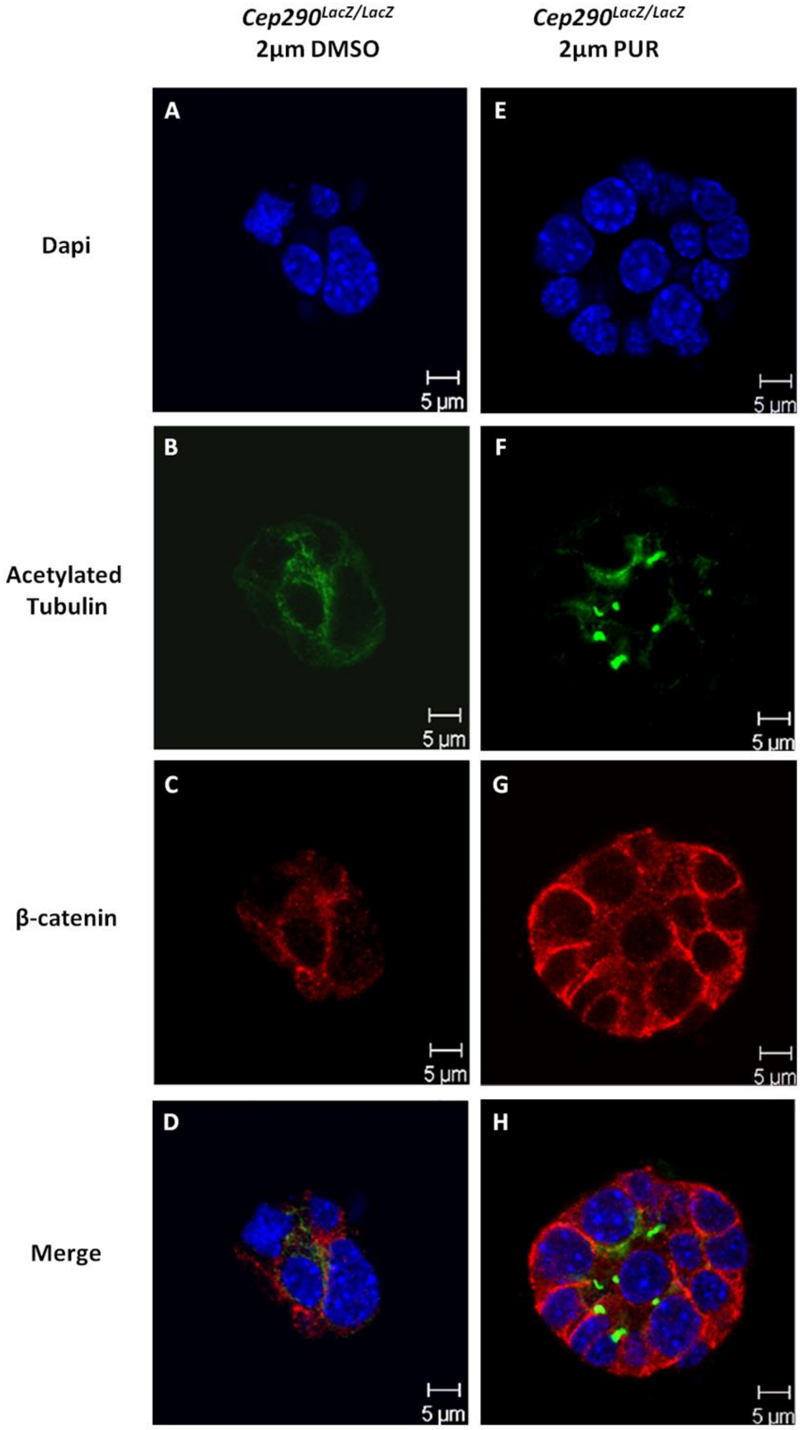

Figure 6.6 Purmorphamine treatment partically rescues ciliogenesis and tubular morphology in *Cep290*$^{LacZ/LacZ}$ CDT cells

Panels (A-D) *Cep290*$^{LacZ/LacZ}$ CDT cells treated with 2µM DMSO and Panels (E-H), *Cep290*$^{LacZ/LacZ}$ CDT cells treated with 2µM Purmorphamine(PUR). Panels (A,E) Dapi staining the nuclei of the spheroids, Panels (B,F) Acetylated tubulin immunofluorescence marker staining primary cilia of the apical cells in the lumen of the spheroid. Panels (C,G). β-catenin stains the adherence junctions of the spheroid tubules. Panels (D,H) merged images of all Dapi, A-tubulin and β-catenin (3D cultures/staining and images collected by Rachel Giles).

Purmorphamine treatment of *Cep290*$^{LacZ/LacZ}$ CDT cells partially rescues CD tubular morphology (Figure 6.6).

Larger lumens (greater than 10µm), were observed in112/150 spheroids. In *Cep290*$^{LacZ/LacZ}$ CDT cells without purmorphamine treatment virtually no lumens (22/150 spheroids) were observed *Cep290*$^{LacZ/LacZ}$ CDT cells where lumens were observed had a diameter of less than 10µm (66/150 spheroids). Increased polarity was evident in *Cep290*$^{LacZ/LacZ}$ CDT cells treated with purmorphamine.

The number of primary cilia observed in the *Cep290*$^{LacZ/LacZ}$ CDT spheroids treated with purmorphamine increased by about 25% (296/1004 nuclei) when compared to untreated *Cep290*$^{LacZ/LacZ}$ CDT spheroids (n= 880).

The reduction of Shh signalling is a functional consequence in *Cep290*$^{LacZ/LacZ}$ kidney collecting ducts and this reduction of Shh signalling is contributing to the cystic phenotype in *Cep290*$^{LacZ/LacZ}$ CDT cells, as purmorphamine can partially rescue tubular morphology and ciliogenesis in *Cep290*$^{LacZ/LacZ}$ CDT cells.

Previous studies discuss that the activation of Shh requires the translocation of smo to the primary cilium following binding of Shh ligand to the Patched receptor. If there is a loss of cilia then this process cannot occur (Corbit, Aanstad et al. 2005). Cilia numbers are reduced in 2D and in 3D cultures of *Cep290*$^{LacZ/LacZ}$ CDT cells (identified in chapter 4). Therefore this study also confirms that the expression of Shh signalling was decreased in both the CDT cells and also in newborn *Cep290*$^{LacZ/LacZ}$ kidneys compared to *Cep290*$^{+/+}$ age matched controls when testing Gli3 expression levels.

6.7 Investigation to determine if a Shh antagonist will disturb tubular morphology of *Cep290*$^{+/+}$ CDT cells when grown in 3D cultures.

From the 3D culturing results of treating *Cep290*$^{LacZ/LacZ}$ CDT cells with purmorphamine it was then decided to test *Cep290*$^{+/+}$ CDT cells treated with HPI-4 to examine the morphology of *Cep290*$^{+/+}$ CDT 3D cultures after HPI-4 treatment (Figure 6.7).

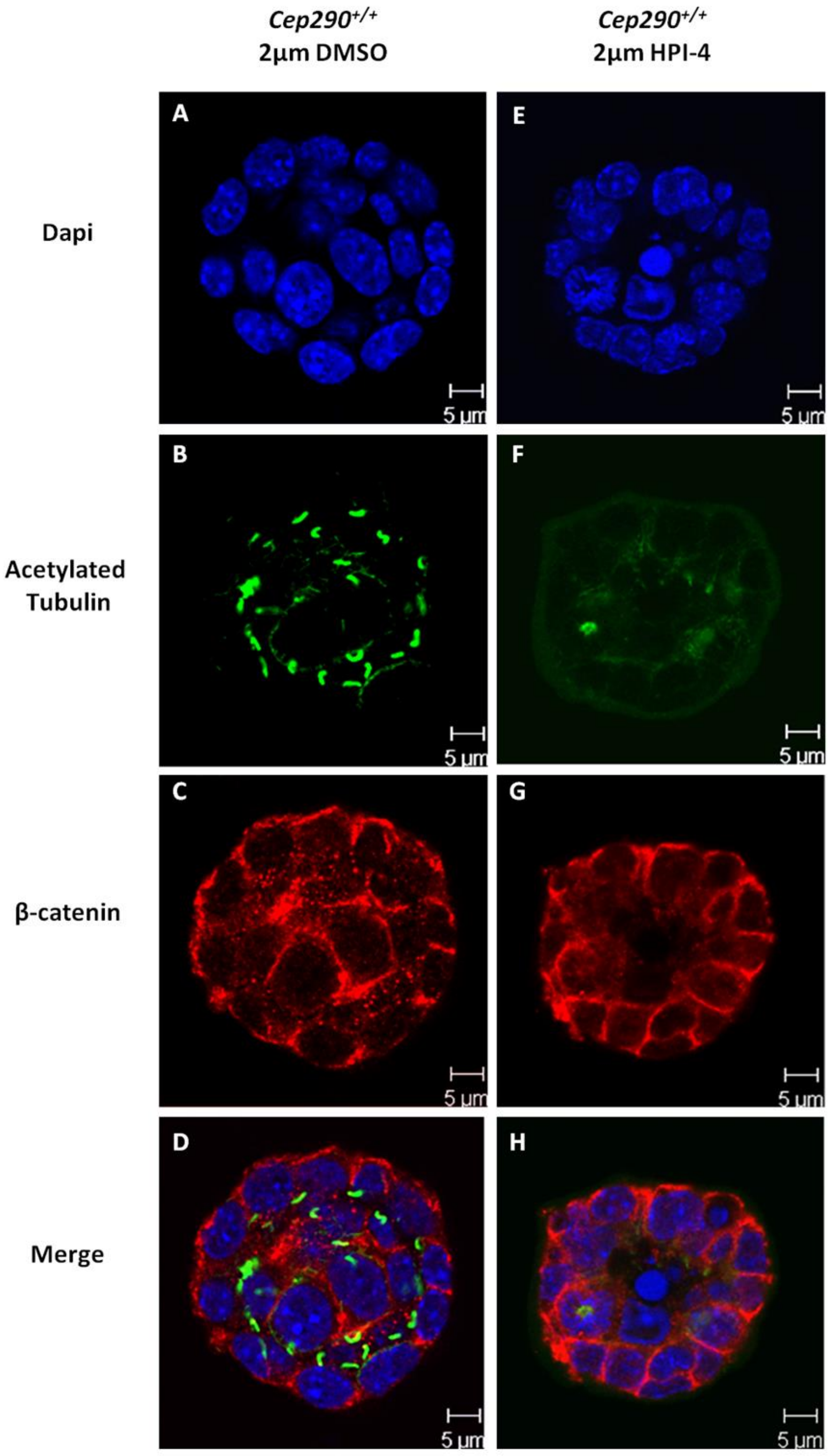

Figure 6.7 HPI-4 treatment disturbs ciliogenesis and tubular morphology in *Cep290*$^{+/+}$ CDT cells

Panels (A-D) *Cep290*$^{+/+}$ CDT cells treated with 2µM DMSO and Panels (E-H), *Cep290*$^{+/+}$ CDT cells treated with 2µMHPI-4. Panels (A,E) Dapi staining the nuclei of the spheroids, Panels (B,F) Acetylated tubulin immunofluorescence marker staining primary cilia of the apical cells in the lumen of the spheroid. Panels (C,G). β-catenin stains the adherence junctions of the spheroid tubules. Panels (D,H) merged images of all Dapi, A-tubulin and β-catenin (3D cultures/staining and Images collected by Rachel Giles).

Quantification of ciliogenesis from 3D spheroids with and without Purmorphamine and HPI-4 treatment was carried out. *Cep290*$^{LacZ/LacZ}$ cells treated with 2µM Purmorphamine for 72 h restored ciliogenesis from 24% (DMSO control) to 48% (Figure 6.8 A). Data is shown by means ± s.e.m., P = 0.0063 determined by an unpaired *t* test. *Cep290*$^{+/+}$ cells when treated with 10µM HPI-4 for 36 h showed a reduction in ciliogenesis from 75% (DMSO control) to 11%. Data is shown by means ± s.e.m., P = 0.0002 determined by an unpaired *t* test (Figure 6.8 B). This confirmed that ciliogenesis is disrupted in *Cep290*$^{LacZ/LacZ}$ cells when Shh signalling is reduced and ciliogenesis is rescued in cells stimulated with Shh.

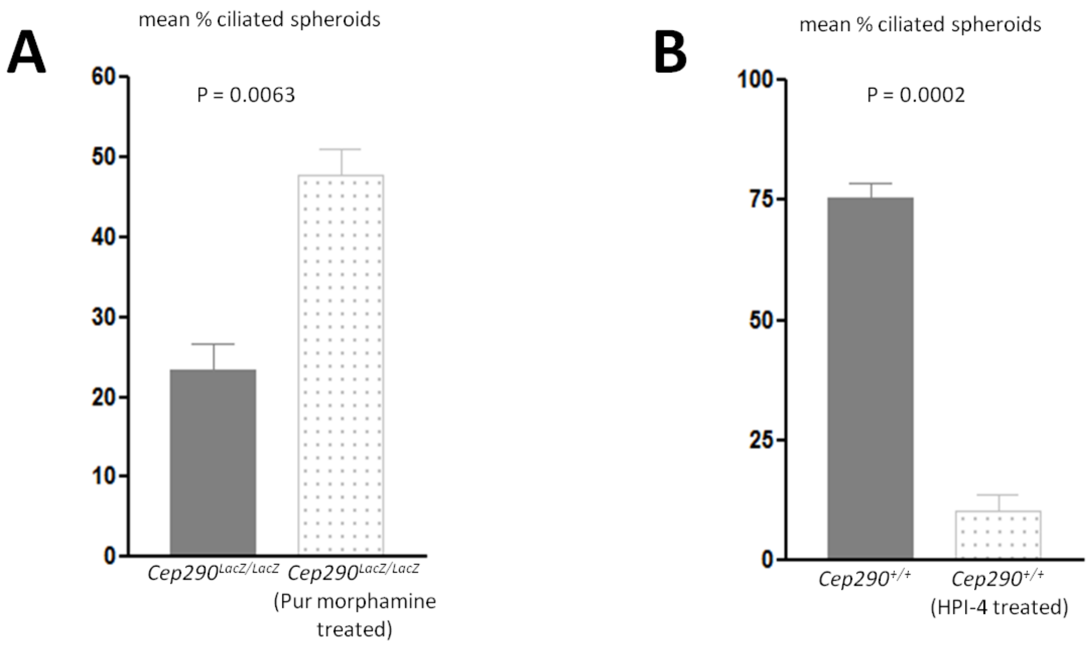

Figure 6.8 Quantifying ciliogenesis in *Cep290* 3D spheroids before and after purmorphamine and HPI-4 treatment.
Panel A Quantifying ciliogenesis in *Cep290*$^{LacZ/LacZ}$ cells without treatment (2µM DMSO) and with 2µM purmorphamine treatment after 72 h. Panel B Quantifying ciliogenesis in *Cep290*$^{+/+}$ cells without treatment (2µM DMSO) and with 10µM HPI-4 treatment after 36 h. All spheroids were serum starved for 24hrs prior to staining. Lengths were compared using students *t*-test.

6.8 Investigating the Illumina microarray's candidate gene expression levels in *Cep290*$^{LacZ/LacZ}$ CDT cells

For the remainder of this study an investigation was carried out to determine if the differences in gene expression levels observed in *Cep290*$^{LacZ/LacZ}$ whole kidney extracts from the Illumina microarray (Chapter 5) were also evident in *Cep290*$^{LacZ/LacZ}$ CDT cells. The genes previously confirmed in *Cep290*$^{LacZ/LacZ}$ whole kidney extracts via qRT-PCR techniques were *Miox*, *Ren1*, *Pvalb*, *Gdnf* and *Tff2*.

If the candidate genes expression levels in *Cep290*$^{LacZ/LacZ}$ CDTs were following the same pattern as *Cep290*$^{LacZ/LacZ}$ whole kidney mRNA, this confirms that the genes affected are likely to contributing to cystogenesis (Figure 6.9).

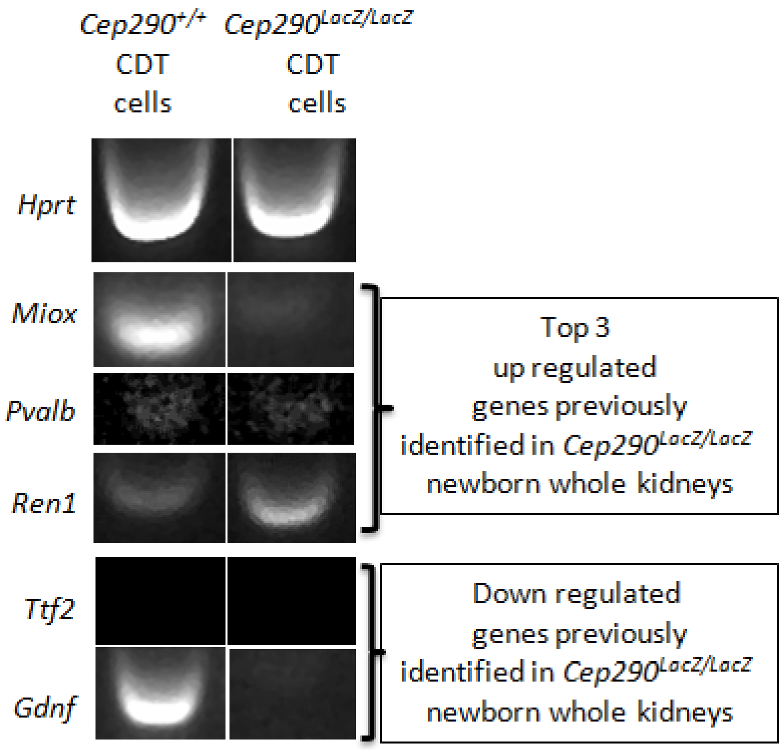

Figure 6.9 Investigating the expression levels of the genes identified from whole kidney extracts using an Illumina Microarray in *Cep290*$^{LacZ/LacZ}$ CDT cells by semi-quantitative RT-PCR.
Semi quantitative RT-PCR of *Cep290*$^{+/+}$ and *Cep290*$^{LacZ/LacZ}$ CDT cells. mRNA was used to determine if the genes identified by the Illumina Microarray in chapter 5 on *Cep290* whole newborn kidney extracts were following the same pattern of expression in *Cep290* CDT cells.

Miox, Pvalb and *Ren1* were all up regulated in *Cep290*$^{LacZ/LacZ}$ newborn kidney mRNA when compared to *Cep290*$^{+/+}$ controls (chapter 5). In CDT cells however using semi quantitative techniques *Miox* and *Pvalb* did not follow the same pattern of expression which could suggest that the changes observed in these 2 genes, in *Cep290*$^{LacZ/LacZ}$ whole kidney extracts were either secondary to the micro cysts observed or that the changes in gene expression levels were affecting other cell types of the kidney as a consequence of the micro cysts.

Miox was previously shown to be expressed in the cortex of the kidney (Charalampous 1959; Koller and Hoffmann-Ostenhof 1979; Arner, Prabhu et al. 2001), and therefore changes in *Miox* expression levels may not influence the cystic collecting ducts. *Pvalb* was previously described to be expressed in the distal convoluted tubule of the kidney (Celio 1990; Schwaller, Dick et al. 1999; Olinger, Schwaller et al. 2012). As *Pvalb* was previously expressed to be in distal convoluted tubules of the kidney and these *Cep290* cells are collecting duct in origin this confirms that the change in *Pvalb* expression is affecting another cell type of the *Cep290*$^{LacZ/LacZ}$ kidney. As previous studies have not described expression of *Pvalb* in cells of the CDT's this also confirms that these novel *Cep290* CDT cells selected by DBA are CDT cells and not expressing distal convoluted tubule markers such as *Pvalb.*

An increase in *Ren1* expression was observed in *Cep290*$^{LacZ/LacZ}$ CDT cells when compared to *Cep290*$^{+/+}$ CDT cells using semi-quantitative RT-PCR methods (See Figure 6.9). *Ren1* expression was originally found in the juxtaglomerular apparatus of the kidney but expression was also reported in CDT's (Jones, Sigmund et al. 1990; Rohrwasser, Morgan et al. 1999; Lantelme, Rohrwasser et al. 2002; Prieto-Carrasquero, Harrison-Bernard et al. 2004). A previously published murine model (known as *Apo E*$^{-/-}$ mice) with a cystic kidney phenotype also showed levels of increased *Ren1* expression. These mice were treated with Angiotensin II which induced the polycystic appearance (Kaliappan, Nagarajan et al. 2012). As mentioned in chapter 5 *Renin* catalyses the first step in the angiotensin pathway (Pentz, Lopez et al. 2001; Sequeira-Lopez, Weatherford et al. 2010). Therefore this increase in *Ren1* expression which was observed in both the *Cep290*$^{LacZ/LacZ}$ kidney and the *Cep290*$^{LacZ/LacZ}$ CDT cells and the *Apo E*$^{-/-}$ mouse model with a cystic kidney phenotype suggests that an up regulation in *Ren1* expression contribute to cystogenesis

Ttf2 and *Gdnf* expression levels were decreased in newborn *Cep290*$^{LacZ/LacZ}$ kidneys from data generated by an Illumina Microarray and by semi-quantitative RT-PCR and quantitative RT-PCR techniques. The log fold change in expression levels of these genes from the data generated by the microarray was less than 2 therefore suggesting that the changes seen in *Ttf2* and *Gdnf* were not as significant as the up regulated genes identified which had a Log FC of greater than 2. However, in chapter 5 the down regulation of both *Ttf2* and *Gdnf* gene expression levels was confirmed by semi-quantitative RT-PCR and quantitative RT-PCR.

The fold change in expression levels (confirmed by quantitative RT-PCR) for each of the down-regulated genes was all less than one when compared to the up regulated genes which showed a fold change in expression of greater than 20 for each gene (Chapter 5).

In both *Cep290*$^{+/+}$ and *Cep290*$^{LacZ/LacZ}$ CDT cells, *Ttf2* was below the threshold of detection which therefore suggests that this down regulation in expression level is also a secondary effect of cystogenesis perhaps affecting other cells of *Cep290*$^{LacZ/LacZ}$ kidneys (See Figure 6.9).

Gdnf was found to be expressed in *Cep290*$^{+/+}$ CDT cells but not in *Cep290*$^{LacZ/LacZ}$ CDT cells (Figure 6.9). *Gdnf* is required for nephrogenesis (Schedl and Hastie 2000) and *Gdnf* knockout mice present with renal agenesis therefore a reduction in *Gdnf* expression may influence a cystic collecting duct phenotype (Sanchez, Silos-Santiago et al. 1996).

Gdnf was only expressed in *Cep290*$^{+/+}$ CDT cells when compared with *Cep290*$^{LacZ/LacZ}$ CDT cells; this suggests that the changes in the level of expression of this gene may be linked to the development of the cystic kidney phenotype associated with CDT cells. *Gdnf* expression was also reduced in *Cep290*$^{LacZ/LacZ}$ whole kidney extracts. qRT-PCR methods was required to confirm if the changes in *Ren1* and *Gdnf* identified by semi quantitative methods in *Cep290* CDT cells was significant (Figure 6.9). qRT-PCR was also carried out on the other genes as it is more sensitive than semi- quantitative RT-PCR in determining if the genes are having an effect on cystogenesis.

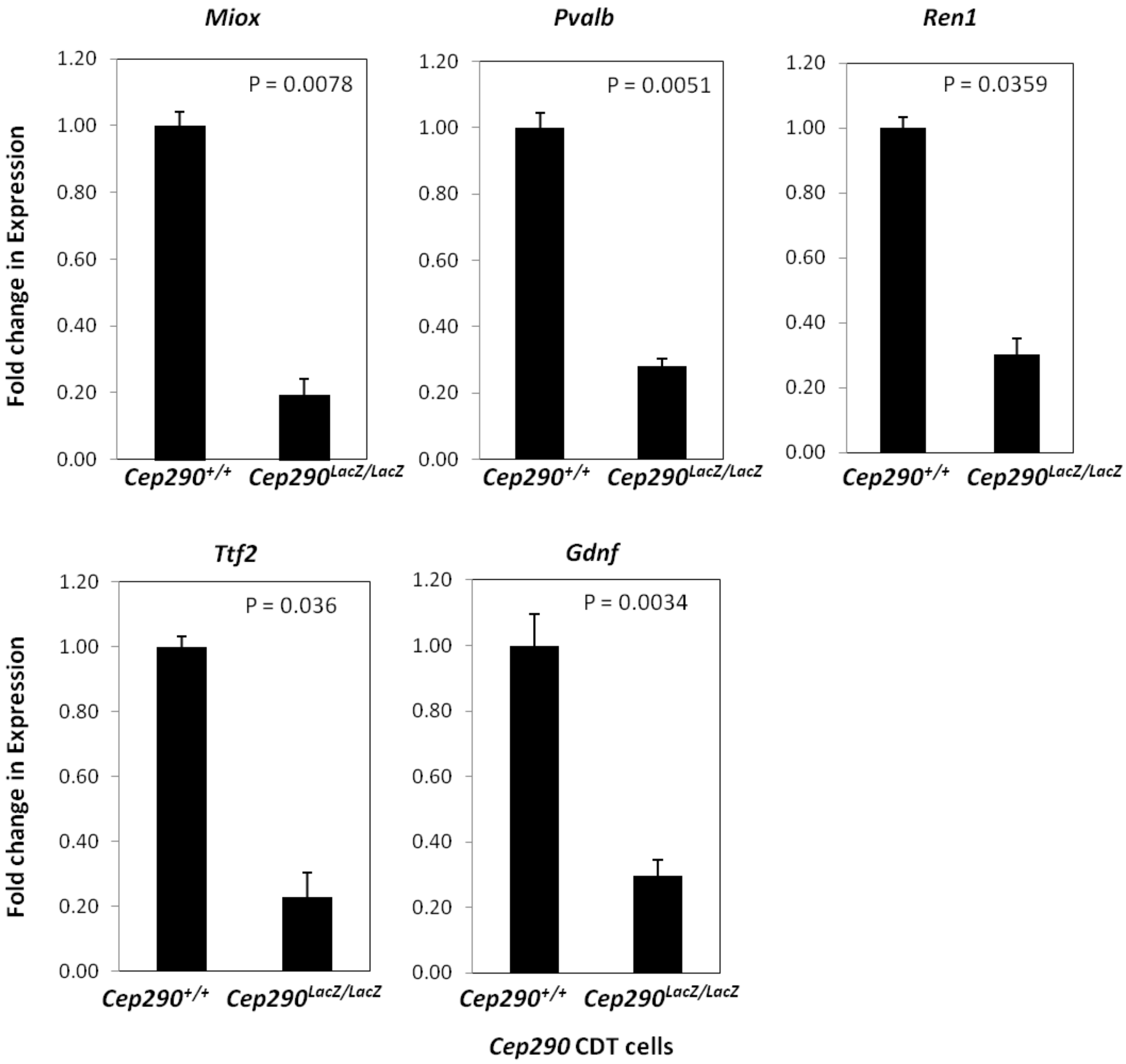

Figure 6.10 Investigating the differences in gene expression levels of 5 candidate microarray genes in *Cep290*$^{+/+}$ and *Cep290*$^{LacZ/LacZ}$ CDT cells by qRT-PCR.

qRT-PCR of *Cep290*$^{+/+}$ and *Cep290*$^{LacZ/LacZ}$ CDT cells. RNA extracted from CDT cells was used to determine if the genes identified by the Illumina Microarray in chapter 5 on whole newborn *Cep290*$^{LacZ/LacZ}$ kidney extracts were following the same pattern of expression in *Cep290*$^{LacZ/LacZ}$ CDT cells. A student's *t*-test p value was calculated for each gene determining the results are statistically significant qRT-PCR methods did not confirm the changes in level of expression found by semi-quantitative RT-PCR methods. *Ren1* was up regulated in *Cep290*$^{LacZ/LacZ}$ CDT cells by semi quantitative RT-PCR methods however via qRT-PCR methods it was not.

Gdnf expression levels were down regulated in *Cep290*$^{LacZ/LacZ}$ CDT cells by semi quantitative RT-PCR and this is the only gene which was confirmed via qRT-PCR methods in *Cep290*$^{LacZ/LacZ}$ CDT cells. Therefore these results suggest that only *Gdnf* may influence a cystic kidney phenotype and the rest of the genes expressed are a result of a secondary effect of cystogenesis.

The low level of *Gdnf* expression seen in *Cep290*$^{LacZ/LacZ}$ CDT cells mimicked the low levels of *Gdnf* gene expression levels previously observed from data generated by the Illumina Microarray using RNA extracted from *Cep290*$^{LacZ/LacZ}$ newborn kidney samples.

6.9 Discussion

In this *Cep290*$^{LacZ/LacZ}$ mouse model Shh signalling was at birth as Gli3R expression was higher in *Cep290*$^{LacZ/LacZ}$ whole kidney protein lysate when compared to *Cep290*$^{+/+}$ kidney controls.

Therefore *Cep290* is necessary for the normal process of Shh signalling pathway in kidney tissue as revealed by abnormal Gli3 processing in *Cep290*$^{LacZ/LacZ}$ renal tissue and CDT cells.

This study has shown that cilia formation and proteolytic processing of Gli3 are disrupted in *Cep290* mutants. The results generated in this study indicate that *Cep290* is required for ciliogenesis in renal tissue and that *Cep290* is required for cilium-dependent Shh signal transduction.

Renal tubular cells possess primary cilia which project into the lumen of the renal tubule, and are likely to have a sensory role (Praetorius and Leipziger 2013). Therefore one can speculate that this specific projection into the lumen is important to their function, for their ability to respond to Shh signal, or for maintaining the correct morphology of the renal tubule (Praetorius and Leipziger 2013).

Gli proteins are localised in the distal tip of the primary cilium (Haycraft, Banizs et al. 2005). The length of the primary cilium in *Cep290*$^{LacZ/LacZ}$ CDT cells was marginally shorter in 2D culturing systems. Only 5% of *Cep290*$^{LacZ/LacZ}$ CDT cells were found to have a primary cilium when compared to 55% of *Cep290*$^{+/+}$ CDT cells (Chapter 4). A disruption of Gli3 signalling was identified in *Cep290*$^{LacZ/LacZ}$ newborn kidneys and CDT cells isolated from *Cep290*$^{LacZ/LacZ}$ mice. Gli proteins may not be efficiently processed or reaching the tip of the cilium in *Cep290*$^{LacZ/LacZ}$ mice.

Interestingly homozygous *Gli3* mice (named *Xt* mice- where the *Gli3* gene is deleted), die before birth with; a midbrain exencephaly, poorly developed eyes (Dunn, Winnier et al. 1997) and the “kidneys had indentations which were previously thought to be due to the close proximity of other organs,” (Johnson 1967). Could this phenotype observed in the *Gli3* mutant kidneys be what we know today as a cystic kidney phenotype? The brain and eye phenotypes mentioned in *Gli3 /Xt* homozygote mutants were also observed in this

Cep290$^{LacZ/LacZ}$ mouse in a much milder form as inbred mice on a 129/Ola background survive to 1 year of age. This study also corroborates that a reduction of Gli3 processing perhaps may be affecting the *JBTS/NPHP* phenotype.

Intriguingly zebrafish *Cep290* knockout embryos demonstrated defects in the PCP, these fish present with renal cysts, retinitis pigmentosa and cerebellar defects (Sayer, Otto et al. 2006; Hildebrandt and Zhou 2007).

As this *Cep290*$^{LacZ/LacZ}$ mouse model has a truncated mutation and mutations in *Cep290* can cause a wide spectrum of disorders the phenotypes seen in the knockout zebrafish model may therefore be influenced by a different pathway.

Together these data indicates that the cystic nature associated with a truncated mutation in the *Cep290* gene may most likely be due to the lack of functioning cilia in *Cep290* mutants with a defect of the Shh signalling pathway.

It seems that the altered dosage of Gli3 protein expression in this *Cep290*$^{LacZ/LacZ}$ mouse model disrupts the hedgehog pathway and cell homeostasis of the kidney in *Cep290*$^{LacZ/LacZ}$ mice.

Chapter 7 Concluding remarks and final Discussion

7.1 *Cep290*$^{LacZ/LacZ}$ mice are a representative model of juvenile NPHP

Microcysts were evident in *Cep290*$^{LacZ/LacZ}$ mice inbred on the 129/Ola strain at birth, tubuar atrophy and thickened TBM was also evident in *Cep290*$^{LacZ/LacZ}$ mice. Renal fibrosis occurred at a later time point in the disease, confirming that this *Cep290*$^{LacZ/LacZ}$ mouse model recapitulates the cystic kidney phenotype of this human ciliopathy and other associated phenotypes. In comparison to the F_6 C57BL/6J newborn mice (Figure 3.16) the cystic renal phenotype is consistent in the 129/Ola colony and therefore this mouse strain is suitable for investigating NPHP (See Figure 3.17).

50% of patients with JBTS have *Cep290* mutations (Valente, Brancati et al. 2013). In this study cerebellum defects were evident in the form of hydrocephaly. Finally 15% of LCA cases are caused by *Cep290* mutations (den Hollander, Roepman et al. 2008), this study also identified retinal degeneration occurring in the *Cep290*$^{LacZ/LacZ}$ mice from 2 weeks of age. Cumulatively these results suggest that this *Cep290*$^{LacZ/LacZ}$ mouse model is a faithful model of the juvenile form of NPHP/JBTS associated disorders.

7.2 Defective Shh signalling is evident in newborn kidneys of *Cep290*$^{LacZ/LacZ}$ mice.

The *Ahi1*$^{-/-}$ mouse model is the only published NPHP mouse model where the molecular mechanisms of NPHP have been investigated and it was identified that kidneys of *Ahi1*$^{-/-}$ mice had defective Wnt signalling which was suggested to cause the NPHP phenotype. The *Ahi1*$^{-/-}$ mouse unfortunately only presents with a late onset NPHP phenotype, occurring at 5 months of age (Lancaster, Louie et al. 2009). Wnt signalling defects were investigated in this *Cep290*$^{LacZ/LacZ}$ mouse model, however no Wnt signalling defects were evident at the early and mid stages of NPHP in *Cep290*$^{LacZ/LacZ}$ mice. Shh signalling was also investigated and it was identified that Gli3 processing was disrupted in newborn kidneys of *Cep290*$^{LacZ/LacZ}$ mice. *Cep290*$^{LacZ/LacZ}$ CDT cells were employed to investigate this in further detail.

7.3 *Cep290*$^{LacZ/LacZ}$ CDT cells aid in identifying disrupted Shh signalling pathway.

The immortal *Cep290*$^{LacZ/LacZ}$ CDT cell line created from *Cep290*$^{LacZ/LacZ}$ mice (recapitulating a NPHP phenotype) is a vital cell model for studying the NPHP disease pathology at the cellular level. The *Cep290*$^{LacZ/LacZ}$ CDT cell line maintained CDT cell characteristics and the *Cep290*$^{+/+}$ CDT cell line formed large spheroids with well defined lumens and 61% of nuclei had primary cilia projecting into these lumens when grown in 3D cultures. *Cep290*$^{LacZ/LacZ}$ CDT cells on the other hand however formed fewer spheroids and the spheroids that did form had no lumen or a lumen of less than 10 microns with only 5% of the nuclei being ciliated (confirming ciliated nuclei observed using 2D culturing methods).

Stimulation of the Shh pathway restored the *Cep290*$^{LacZ/LacZ}$ CDT abnormal spheroid structural phenotype with cilia present in 26% of nuclei and the lumens were over 10 microns in size in 3D culture. This suggests that Shh signalling partly regulates ciliogenesis and the establishment of CDT spheroids in 3D cultures.

The addition of the Shh antagonist (HPI-4) resulted in disrupted *Cep290*$^{+/+}$ CDT spheroids, lumen structure and ciliogenesis in 3D cultures, hence confirming that Shh is defective in *Cep290*$^{LacZ/LacZ}$ CDT cells. The physiology of the *Cep290* CDT cells were not the focus in this study however this *Cep290*$^{LacZ/LacZ}$ CDT cell line is a potentially valuable cell model for future studies in understanding the pathophysiology of the CDT in NPHP.

Cep290 is required for the morphologic integrity and function of the kidney. This study reveals a potential new mechanism for the regulation and maintenance of collecting duct cells in cystic kidney disease

7.4 Conflicting defective signalling mechanisms identified in renal tissue of 2 NPHP mouse models.

Shh signalling was only investigated in the *Ahi1*$^{-/-}$ cerebellar granule neurons (CGNs) by the means of *N-myc* staining (a proliferative gene target of Shh signalling) where it was concluded that *Ahi1*$^{-/-}$ was not decreased in the cerebella. Western blot analysis of N-Myc and Ptch1 expression in *Ahi1*$^{-/-}$ animals in whole cerebellum lysates (at P3) concluded that N-Myc and Ptch1 expression in *Ahi1*$^{-/-}$animals was equal to wild type controls. The last set of experiments used to test for Shh signalling defects in the cerebellum of *Ahi1*$^{-/-}$ mice involved analysing qRT-PCR for 3 Shh target gene mRNAs (N-Myc, Gli and Ptch1). No differences were observed in the 3 chosen Shh target genes expression levels in the mRNAs of *Ahi1*$^{-/-}$ mice when compared to littermate controls (Lancaster, Gopal et al. 2011). From this set of results in the *Ahi1*$^{-/-}$ mouse model it was concluded that there was no Shh signalling defects occurring in the *Ahi1*$^{-/-}$ mice.

The kidney however is a different organ to the brain and it would be interesting to see if there were any Shh signalling defects occurring in *Ahi1*$^{-/-}$ mice prior to the fibrotic and cystic phenotype observed in the adult *Ahi1*$^{-/-}$ kidney.

It is well known that Shh signalling is mediated via members of the Gli transcription factors family to control cell determination, tissue patterning and organogenesis (Ingham and McMahon 2001). Until the *Ahi1*$^{-/-}$ mouse model is used to measure the differences in Gli transcription levels it cannot be truly ruled out that defective Shh signalling may be influencing the kidney phenotype observed. The *Ahi1*$^{-/-}$ study also generated a *Cep290*$^{-/-}$ mouse model (Lancaster, Gopal et al. 2011). Midline fusion defects and retinal degeneration were identified in the *Cep290*$^{-/-}$ mouse model, with no mention of a cystic kidney phenotype at E16.5. The phenotype of only 3 mice for each genotype was evaluated at E16.5. There were no RT-PCR/ qRT-PCR or Western blot results mentioned or shown to confirm if the *Cep290* protein product was knocked down (Lancaster, Gopal et al. 2011). Therefore there are still a lot of unanswered questions from the knockout *Cep290* mouse model regarding the kidney phenotype. As *CEP290* mutations cause the largest number of ciliopathies (Aguilar, Meunier et al. 2012) more mouse studies are required to understand the role of *Cep290* in NPHP.

Gene	Shh signalling	Wnt signalling	Cystic Kidneys	Lethal	Reference
JBTS1	ND	ND	ND	ND	ND
JBTS2	↓	ND	ND	Yes	(Hoover, Wynkoop et al. 2008)
JBTS3/ AHI1	No change	↓	5 months-1 year	Only 20% survived	(Lancaster, Louie et al. 2009)
JBTS4/ Nphp1	ND	ND	None	ND	(Jiang, Chiou et al. 2008)
JBTS5/ CEP290	↓	No change	NPHP at birth	Not in Ola/129 inbred mice	This study and (Aguilar, Meunier et al. 2012)
JBTS6/ NPHP11	↓	↑	Yes PKD at E18.5	Yes *Tmem67*$^{-/-}$	(Abdelhamed, Wheway et al. 2013) and (Garcia-Gonzalo, Corbit et al. 2011)
JBTS7/ NPHP8	↓	↓	Yes E18.5 cysts	Yes	(Delous, Baala et al. 2007) and (Mahuzier, Gaude et al. 2012)
JBTS8	↓	↓	ND	Yes	(Caspary, Larkins et al. 2007)
JBTS9	↓	ND	ND	Yes	(Garcia-Gonzalo, Corbit et al. 2011)
JBTS10	↓	↓	Cystic at P0	Yes	(Ferrante, Zullo et al. 2006), (Corbit, Shyer et al. 2008) and (Hunkapiller, Singla et al. 2011)
JBTS11/ NPHP12	↑	↓	ND	ND	(Stottmann, Tran et al. 2009) and (Herron, Lu et al. 2002)
JBTS12	↑	ND	ND	Yes	(Cheung, Zhang et al. 2009) and (Liem, He et al. 2009).
JBTS13	↓	ND	ND	ND	(Reiter and Skarnes 2006)
JBTS14	ND	↑	ND	ND	(Huang, Szymanska et al. 2011)
JBTS15	ND	ND	ND	ND	ND
JBTS16	ND	ND	ND	ND	ND
JBTS17	ND	ND	ND	ND	ND
TCTN2	↑	ND	ND	Yes	(Sang, Miller et al. 2011)
TCTN3 / JBTS18	↓	ND	ND	ND	(Thomas, Legendre et al. 2012)
TMEM231	↓	ND	ND	Yes	(Chih, Liu et al. 2012)
NPHP1	ND	ND	ND	ND	(Jiang, Chiou et al. 2008)
NPHP2	ND	↓ in *inv/inv* mefs and not involved in kidney (conflicting results)	E15 cysts	No	(Morgan, Turnpenny et al. 1998), (Sugiyama, Tsukiyama et al. 2011) and (Veland, Montjean et al. 2013)
NPHP3	ND	↓	Yes at 2 weeks	No	(Bergmann, Fliegauf et al. 2008), (Simons, Gloy et al. 2005) and (Omran, Haffner et al. 2001).
NPHP4	ND	↓	No change	No	(Won, Marin de Evsikova et al. 2011) and (Borgal, Habbig et al. 2012)
NPHP5	ND	ND	ND	ND	ND
NPHP6	See *JBTS5* above				
NPHP7	↓	↓	No	No	(Attanasio, Uhlenhaut et al. 2007) and (Kim, Kang et al. 2007)
NPHP8	See *JBTS7* above				
NPHP9	ND	↓	2 weeks	No	(Liu, Lu et al. 2002) and (Sabbagh, Graciolli et al. 2012)
NPHP10	ND	ND	ND	ND	ND
NPHP11	See *JBTS6* above				
NPHP12	See *JBTS11* above				
NPHP13	↑	ND	ND	Yes	(Ashe, Butterfield et al. 2012)
AHI1	See *JBTS3* above				
ATXN10, NPHP14, NPHP15, ANKS6, XPNPEP3 and *SLC41A1* currently no links to either pathway have been investigated					

Table 7.1 Revising defective Shh and Wnt signalling defects as a consequence of a *NPHP/JBTS* mutation

An increase in the expression of either the Shh or Wnt pathway is denoted by ↑. A decrease in expression of either the Shh or the Wnt pathway is highlighted by ↓. ND not defined/not determined. Yellow highlights the studies where Shh and/or Wnt signalling was investigated in kidney samples of NPHP/JBTS mice.

Only 4 studies (including this study) have investigated whether defective Wnt and/or Shh signalling is evident in the kidney samples of NPHP/JBTS mutant mice. *Ahi1*$^{-/-}$ as discussed previously confirmed a reduction in Wnt signalling in 5 month-1 year old kidney samples (Table 7.1).

The *Glis2*$^{LacZ/LacZ}$ mouse model suggests that Shh signalling is increased as *Gli1* gene is upregulated in expression levels however they also state that other known Gli targets like *Bmp4, Pax2, Sall1, Ccnd1, N-Myc* were not (Attanasio, Uhlenhaut et al. 2007). The *Glis2*$^{LacZ/LacZ}$ study also concludes their study by suggesting that "a loss of downstream effectors of Shh signalling may lead to the NPHP phenotype" (Attanasio, Uhlenhaut et al. 2007). This statement suggests reduced Shh signalling leads to the NPHP phenotype which is what we have seen in this novel *Cep290*$^{LacZ/LacZ}$ mouse model.

The *inv* mice have contrasting evidence regarding defective Wnt signalling (Sugiyama, Tsukiyama et al. 2011) and (Veland, Montjean et al. 2013). In the *inv/inv* renal study there was no evidence of defective Wnt signalling occurring in renal samples of *inv/inv* mice (Sugiyama, Tsukiyama et al. 2011). However in the *inv*$^{-/-}$ MEF study several β-catenin target genes were upregulated which is consistent with increased Wnt signalling (Veland, Montjean et al. 2013). As this study was only carried out on MEF cells therefore it cannot be determined whether or not the same increase in Wnt signalling would be evident in *inv*$^{-/-}$ kidney samples.

To date, this study of *Cep290*$^{LacZ/LacZ}$ mice is the first to identify defective Shh signalling pathway associated with NPHP. Gli3 activator and repressor isoforms were utilised in this study to measure Shh activity. It was found that there was a dramatic increase in Gli3 repressor in *Cep290*$^{LacZ/LacZ}$ newborn kidney samples which is indicative of reduced Shh signalling (Figure 6.4). Increased Gli3 repressor expression levels were also seen in patients with *TCTN3* mutations (Thomas, Legendre et al. 2012) and the embryos of E11.5 *Ftm*$^{-/-}$ mice (Vierkotten, Dildrop et al. 2007).

7.5 Gene expression profile changes will aid in identifying early stages of juvenile NPHP.

The gene expression profile changes identified by the microarray are potentially a valuable resource for identifying early changes in NPHP. Newborn *Cep290*$^{LacZ/LacZ}$ mice have micro cysts and their gene expression profiles identified a number of up regulated solute carriers.

An up regulation in expression of solute carrier genes suggests the normal physiology of the kidney is disturbed as the maintenance of the CDT cell's identity is the result of the balanced expression and repression of hundreds of genes. These changes in solute carrier gene expression levels could be assessed in renal biopsies of patients potentially thought to have NPHP to test for the first signs of cellular changes occurring in NPHP leading to an early diagnosis.

Clinical diagnosis alone of ciliopathies provides little information into possible therapeutic remedies. The varying degree of distinction of phenotypes associated with ciliopathies are often blurred therefore molecular diagnosis is required and will be valuable for clarifying pathogeneic mechanisms, (Rachel, Li et al. 2012) as it may be that not all NPHP mutations will have disrupted Shh signalling like the *Cep290*$^{LacZ/LacZ}$ mouse with a truncated mutation in the *Cep290* gene.

7.6 Impact of this work on the field of NPHP related disorders.

At present there are no therapeutic drugs offered for treating NPHP http://www.pkdcure.org/research/clinical-trials/blood-pressure . Clinical trials are only available for adults and are primarily focused on end stage renal failure or when the cystic phenotype is severe, to slow the rate of disease progression.

Hence it was crucial to study the changes in the onset of cystogenesis (performed by the Illumina microarray data in this study) in NPHP and to identify disrupted signalling pathways leading to the cystic kidney phenotype.

7.7 Limitations of the work presented in this thesis

To this day it is still unknown what causes the different combinations of the spectrum of disorders in JBTS patients. The huge clinical variability in *CEP290* mutations even within one family cannot be explained by classical Mendelian inheritance patterns with single locus allelism.

There are a few theories which suggest the explanation of the phenotypic diversity associated with NPHP/JBTS patients including; the differences in the disease causing mutation, genetic modifiers and environmental modifiers. Genetic modifiers were also suggested to influence the phenotypic variation of affected males with X-Linked retinal pigmentosa (XIRP) in one recent study (Fahim, Bowne et al. 2011).

Unidentified genetic modifier loci are perhaps influencing the JBTS phenotype seen in *Cep290*$^{LacZ/LacZ}$ mice. When comparing *Cep290*$^{LacZ/LacZ}$ inbred C57BL6/J mice with *Cep290*$^{LacZ/LacZ}$ inbred Ola/129 mice the *Cep290*$^{LacZ/LacZ}$ inbred C57BL6/J mice are embryonic lethal.

Unidentified genetic modifiers are also evident in the *Ahi1*$^{-/-}$ model as approximately 80% of the *Ahi1*$^{-/-}$ mice did not survive to adulthood (Lancaster, Louie et al. 2009). Shh signalling pathway transcription factors (Gli1-3 for example) were not investigated in the kidneys of *Ahi1*$^{-/-}$ mice (Lancaster, Louie et al. 2009) and therefore it is unknown if Shh signalling is influencing the cystic kidney phenotype observed later in development in this *Ahi1*$^{-/-}$ mouse model.

Candidate modifier loci will need to be chosen on the basis of previously demonstrated protein-protein interactions with CEP290 to determine if there is any significant association with disease severity

The *Pcy* and the *Tmem67* mouse model also recognise that modifier alleles determine the severity of the NPHP/JBTS disease between different strains of mice (Nagao, Hibino et al. 1991; Abdelhamed, Wheway et al. 2013).

7.8 Possible future directions for the study of NPHP disorders from data presented in this thesis.

As cysts are located in CDT's in patients with NPHP, gene expression differences in CDT's between wild type and *Cep290*$^{LacZ/LacZ}$ mice will aid in the confirmation of which genes are involved in the cystic phenotype rather than genes which may be involved as a consequence of a cystic nature.

Physiological studies are required in order to identify the changes in distribution patterns of transport proteins in the *Cep290*$^{LacZ/LacZ}$ CDT cells as this will aid in identifying other key signalling pathways which contribute to cystic kidney disease. The CDT is important for maintaining fluid and electrolyte balance, this balance is controlled by hormones such as aldosterone and arginine vasopressin (Canessa, Schild et al. 1994; Garty and Palmer 1997).

Given the variability of ciliopathy phenotypes, genetic modifier loci must be considered both in patients and in animal models. One simple experiment, for example, (that uses existing resources) would be to backcross the *Ahi1*$^{-/-}$ strain onto the 129/0la genetic background to see if this results in a phenocopy of the *Cep290*$^{LacZ/LacZ}$ mouse.

7.9 Appendix 1

Gene	Forward Oligonucleotide Primer	Reverse Oligonucleotide Primer
Smo	5'-GACTCGGACTCGCAGGAG-3'	5'-ACACAGCAGGGGCTGGAT-3'
Miox	5'-CCCTGGGTGCAAGAGTT-3'	5'-GTCAATCAGCCCTTGATAGT-3'
Gdnf	5'-GAAGTTATGGGATGTCGTGG-3'	5'-CATCAAACTGGTCAGGATAA-3'
Ren2	5'-AGTACGGACTACGTGCTACAG-3'	5'-CGATTGTTATGCCGATCAAACT-3'
Pvalb	5'-GATGCCAGAGACTTGTCTGCT-3'	5'-TAGAGGATGGGGGAGTAAAAA-3'
Col2a1	5'-CCCTGAAGGATGGCTGCACG-3'	5'-GTTCAGCCCCTCCAATGTCCA-3'
Tff2	5'-GTGTCATGGAAGTGTCAGCTC-3'	5'-TAAGGGTCAAGATGGTTTTA-3'
Hprt	5'-CTGGTTAAGCAGTACAGCC-3'	5'-CAACTTGCGCTCATCTTAG-3'
Lef1_S	5'-GATGGCAGGGGTGGTCAGAC-3'	5'-GACATGTACGGGTCGCTGTTC-3'
Lef1_L	5'-GAAGAGGAGGGCGACTTAGC-3'	5'-GACATGTACGGGTCGCTGTTC-3'
*Immorto _wt_*	5'-GATCTGCCTGAGGTGTTACTTG-3'	5'-GGATGGCATCACTAGTCATGAC-3'
Immorto _tsA	5'-AGTCCTCACAGTCTGTTCATGATC-3'	5'-GGATGGCATCACTAGTCATGAC-3'
Cep290 ex23_F	5'-ATGGAAGCCGAAGTCACTG-3'	
Cep290 ex26_R		5'-CTGTTTGTCATTGATTTCTTAGCC-3'
B-geo_ fus_Rev		5'-CGACGGGATCCTCTAGAGTC-3'
ENAC	5'-GTGTGCATTCACTCCTGCTT-3'	5'-AGAAGGCAGCCTGCAGTTTA-3'

cDNA mouse primers

7.10 Appendix 2

Primary Antibody	Species raised in:	Dilution required	Incubation period	Secondary Antibody	Dilution required	Incubation period
Acetylated Tubulin. **Sigma T6793**	**Mouse**	**1:1,000**	**1h room temperature**	**Anti-mouse Alexa Fluor 594. Invitrogen A21203**	**1:200**	**1h room temperature**
Anti-Pericentrin	**Rabbit**	**1:1,000**	**1h room temperature**	**Anti rabbit FITC Jackson 111-095-114**	**1:200**	**1h room temperature**
AQP2 **Santa Cruz sc-28629**	**Rabbit**	**1:200**	**1h room temperature**	**Anti rabbit FITC Invitrogen A21206**	**1:200**	**1h room temperature**
ATP6VOA4 **Gift from Fiona Karet**	**Rabbit**	**1:3,000**	**1h room temperature**	**Anti rabbit CY3 Sigma C-2306**	**1:200**	**1h room temperature**
Smo **Gift from Jeremy Reiter**	**Rabbit**	**1:200**	**O/N at 4°C**	**Anti rabbit FITC Jackson 111-095-114**	**1:200**	**1h room temperature**

List of immunofluorescent primary and secondary antibodies.
O/N (overnight).

7.11 Appendix 3

Primary Antibody	Species raised in:	Dilution required	Incubation period	Secondary Antibody	Dilution required	Incubation period
Gapdh **Cell Signalling (14C10)**	**Rabbit**	**1:15,000**	**1h room temperature**	**Anti- Rabbit HRP Dako P0399**	**1:2,000**	**1h room temperature**
Cep290 **Covalab**	**Rabbit**	**1:100**	**1h room temperature**	**Anti- Rabbit HRP Dako P0399**	**1:2,000**	**1h room temperature**
Gli3 **(R&D Systems AF3690)**	**Goat**	**1:3,000**	**2h room temperature**	**Anti- Rabbit HRP Jackson**	**1:2,000**	**1h room temperature**
Lef1 **Cell Signalling (C12A5)**	**Rabbit**	**1:1,000**	**1h room temperature**	**Anti- Rabbit HRP Jackson**	**1:2,000**	**1h room temperature**
Tcf1 **Cell Signalling (C63D9)**	**Rabbit**	**1:1,000**	**1h room temperature**	**Anti- Rabbit HRP Jackson**	**1:2,000**	**1h room temperature**

List of western blot primary and secondary antibodies.

**Cep290* Coval antibody is directed towards murine *Cep290* and was custom made (CovalAb, Cambridge), targeting the antigenic sequence a the C-terminus of the Cep290 protien. The Peptide (2427-2440): C-DLKYNYKEEVKKNI-coNH2, whose sequence is conserved between mus and human was used to generate a rabbit polyclonal antibody.

7.12 Appendix 4

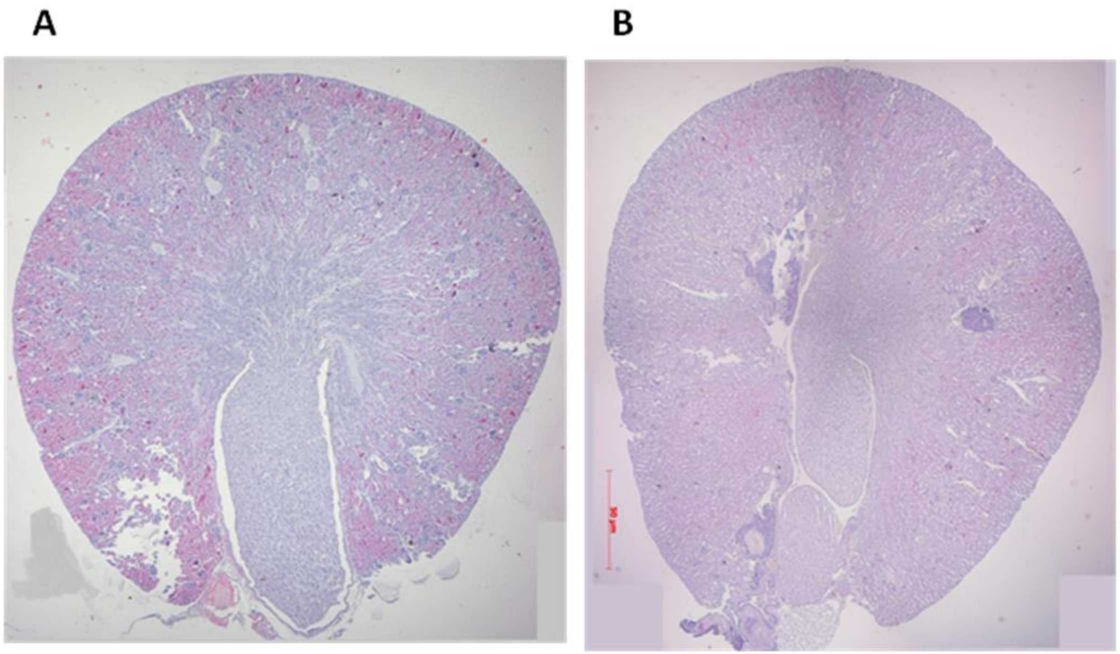

H+E image of kidneys isolated from *Cep290*$^{LacZ/LacZ}$ and *Cep290*$^{LacZ/+}$ mice

Panel A Overview of kidney isolated from the homozygote mouse which exhibited polyuria (50mls in 24h). Panel B Overview of 1 year old *Cep290*$^{LacZ/+}$ kidney. The morphology of each of the kidneys (A+B) appears healthy, as there are no extra deposits of collagen which occur in fibrotic kidneys and there is no evidence of cysts in the corticomedullary region of the kidney (See figure 3.7 for comparison of wild type and *Cep290*$^{LacZ/LacZ}$ kidneys which present with cysts).

Abdelhamed, Z. A., G. Wheway, et al. (2013). "Variable expressivity of ciliopathy neurological phenotypes that encompass Meckel-Gruber syndrome and Joubert syndrome is caused by complex de-regulated ciliogenesis, Shh and Wnt signalling defects." Hum Mol Genet **22**(7): 1358-1372.

Adams, M., R. J. Simms, et al. (2012). "A meckelin-filamin A interaction mediates ciliogenesis." Hum Mol Genet **21**(6): 1272-1286.

Aguilar, A., A. Meunier, et al. (2012). "Analysis of human samples reveals impaired SHH-dependent cerebellar development in Joubert syndrome/Meckel syndrome." Proc Natl Acad Sci U S A **109**(42): 16951-16956.

Aguilera, O., A. Munoz, et al. (2007). "Epigenetic alterations of the Wnt/beta-catenin pathway in human disease." Endocr Metab Immune Disord Drug Targets **7**(1): 13-21.

Alcaraz, W. A., D. A. Gold, et al. (2006). "Zfp423 controls proliferation and differentiation of neural precursors in cerebellar vermis formation." Proc Natl Acad Sci U S A **103**(51): 19424-19429.

Andersen, J. S., C. J. Wilkinson, et al. (2003). "Proteomic characterization of the human centrosome by protein correlation profiling." Nature **426**(6966): 570-574.

Anderson, C. M. and D. T. Thwaites (2010). "Hijacking solute carriers for proton-coupled drug transport." Physiology (Bethesda) **25**(6): 364-377.

Anselme, I., C. Laclef, et al. (2007). "Defects in brain patterning and head morphogenesis in the mouse mutant Fused toes." Dev Biol **304**(1): 208-220.

Arner, R. J., K. S. Prabhu, et al. (2006). "Expression of myo-inositol oxygenase in tissues susceptible to diabetic complications." Biochem Biophys Res Commun **339**(3): 816-820.

Arner, R. J., K. S. Prabhu, et al. (2001). "myo-Inositol oxygenase: molecular cloning and expression of a unique enzyme that oxidizes myo-inositol and D-chiro-inositol." Biochem J **360**(Pt 2): 313-320.

Arts, H. H., D. Doherty, et al. (2007). "Mutations in the gene encoding the basal body protein RPGRIP1L, a nephrocystin-4 interactor, cause Joubert syndrome." Nat Genet **39**(7): 882-888.

Ashe, A., N. C. Butterfield, et al. (2012). "Mutations in mouse Ift144 model the craniofacial, limb and rib defects in skeletal ciliopathies." Hum Mol Genet **21**(8): 1808-1823.

Ashizawa, M., M. Miyazaki, et al. (2005). "Nephronophthisis in two siblings." Clin Exp Nephrol **9**(4): 320-325.

Attanasio, M., N. H. Uhlenhaut, et al. (2007). "Loss of GLIS2 causes nephronophthisis in humans and mice by increased apoptosis and fibrosis." Nat Genet **39**(8): 1018-1024.

Baala, L., S. Romano, et al. (2007). "The Meckel-Gruber syndrome gene, MKS3, is mutated in Joubert syndrome." Am J Hum Genet **80**(1): 186-194.

Basson, M. A., J. Watson-Johnson, et al. (2006). "Branching morphogenesis of the ureteric epithelium during kidney development is coordinated by the opposing functions of GDNF and Sprouty1." Dev Biol **299**(2): 466-477.

Belge, H., P. Gailly, et al. (2007). "Renal expression of parvalbumin is critical for NaCl handling and response to diuretics." Proc Natl Acad Sci U S A **104**(37): 14849-14854.

Bens, M., V. Vallet, et al. (1999). "Corticosteroid-dependent sodium transport in a novel immortalized mouse collecting duct principal cell line." J Am Soc Nephrol **10**(5): 923-934.
Berbari, N. F., A. K. O'Connor, et al. (2009). "The primary cilium as a complex signaling center." Curr Biol **19**(13): R526-535.
Bergmann, C. (2012). "Educational paper: ciliopathies." Eur J Pediatr **171**(9): 1285-1300.
Bergmann, C., M. Fliegauf, et al. (2008). "Loss of nephrocystin-3 function can cause embryonic lethality, Meckel-Gruber-like syndrome, situs inversus, and renal-hepatic-pancreatic dysplasia." Am J Hum Genet **82**(4): 959-970.
Bergmann, C., J. Senderek, et al. (2004). "PKHD1 mutations in autosomal recessive polycystic kidney disease (ARPKD)." Hum Mutat **23**(5): 453-463.
Bielas, S. L., J. L. Silhavy, et al. (2009). "Mutations in INPP5E, encoding inositol polyphosphate-5-phosphatase E, link phosphatidyl inositol signaling to the ciliopathies." Nat Genet **41**(9): 1032-1036.
Bisgrove, B. W. and H. J. Yost (2006). "The roles of cilia in developmental disorders and disease." Development **133**(21): 4131-4143.
Blyth, H. and B. G. Ockenden (1971). "Polycystic disease of kidney and liver presenting in childhood." J Med Genet **8**(3): 257-284.
Borgal, L., S. Habbig, et al. (2012). "The ciliary protein nephrocystin-4 translocates the canonical Wnt regulator Jade-1 to the nucleus to negatively regulate beta-catenin signaling." J Biol Chem **287**(30): 25370-25380.
Brancati, F., B. Dallapiccola, et al. (2010). "Joubert Syndrome and related disorders." Orphanet J Rare Dis **5**: 20.
Brannon, M., M. Gomperts, et al. (1997). "A beta-catenin/XTcf-3 complex binds to the siamois promoter to regulate dorsal axis specification in Xenopus." Genes Dev **11**(18): 2359-2370.
Bredrup, C., S. Saunier, et al. (2011). "Ciliopathies with skeletal anomalies and renal insufficiency due to mutations in the IFT-A gene WDR19." Am J Hum Genet **89**(5): 634-643.
Briscoe, J. and J. Ericson (2001). "Specification of neuronal fates in the ventral neural tube." Curr Opin Neurobiol **11**(1): 43-49.
Brown, J. H., M. T. Bihoreau, et al. (2005). "Missense mutation in sterile alpha motif of novel protein SamCystin is associated with polycystic kidney disease in (cy/+) rat." J Am Soc Nephrol **16**(12): 3517-3526.
Burckle, C., H. M. Gaude, et al. (2011). "Control of the Wnt pathways by nephrocystin-4 is required for morphogenesis of the zebrafish pronephros." Hum Mol Genet **20**(13): 2611-2627.
Bustin, S. A., J. F. Beaulieu, et al. (2010). "MIQE precis: Practical implementation of minimum standard guidelines for fluorescence-based quantitative real-time PCR experiments." BMC Mol Biol **11**: 74.
Bustin, S. A., V. Benes, et al. (2009). "The MIQE guidelines: minimum information for publication of quantitative real-time PCR experiments." Clin Chem **55**(4): 611-622.
Bustin, S. A., V. Benes, et al. (2011). "Primer sequence disclosure: a clarification of the MIQE guidelines." Clin Chem **57**(6): 919-921.
Byrne, C., R. Steenkamp, et al. (2010). "UK Renal Registry 12th Annual Report (December 2009): chapter 4: UK ESRD prevalent rates in 2008: national and centre-specific analyses." Nephron Clin Pract **115 Suppl 1**: c41-67.

Cadnapaphornchai, M. A., D. M. George, et al. (2011). "Effect of statin therapy on disease progression in pediatric ADPKD: design and baseline characteristics of participants." Contemp Clin Trials **32**(3): 437-445.

Calvet, J. P. and J. J. Grantham (2001). "The genetics and physiology of polycystic kidney disease." Semin Nephrol **21**(2): 107-123.

Canessa, C. M., L. Schild, et al. (1994). "Amiloride-sensitive epithelial Na+ channel is made of three homologous subunits." Nature **367**(6462): 463-467.

Cantagrel, V., J. L. Silhavy, et al. (2008). "Mutations in the cilia gene ARL13B lead to the classical form of Joubert syndrome." Am J Hum Genet **83**(2): 170-179.

Caparros-Martin, J. A., M. Valencia, et al. (2013). "The ciliary Evc/Evc2 complex interacts with Smo and controls Hedgehog pathway activity in chondrocytes by regulating Sufu/Gli3 dissociation and Gli3 trafficking in primary cilia." Hum Mol Genet **22**(1): 124-139.

Caridi, G., L. Murer, et al. (1998). "Renal-retinal syndromes: association of retinal anomalies and recessive nephronophthisis in patients with homozygous deletion of the NPH1 locus." Am J Kidney Dis **32**(6): 1059-1062.

Caspary, T., C. E. Larkins, et al. (2007). "The graded response to Sonic Hedgehog depends on cilia architecture." Dev Cell **12**(5): 767-778.

Celio, M. R. (1990). "Calbindin D-28k and parvalbumin in the rat nervous system." Neuroscience **35**(2): 375-475.

Chaki, M., R. Airik, et al. (2012). "Exome capture reveals ZNF423 and CEP164 mutations, linking renal ciliopathies to DNA damage response signaling." Cell **150**(3): 533-548.

Chang, B., H. Khanna, et al. (2006). "In-frame deletion in a novel centrosomal/ciliary protein CEP290/NPHP6 perturbs its interaction with RPGR and results in early-onset retinal degeneration in the rd16 mouse." Hum Mol Genet **15**(11): 1847-1857.

Chang, M. Y. and A. C. Ong (2013). "New treatments for autosomal dominant polycystic kidney disease." Br J Clin Pharmacol.

Chapman, A. B. (2008). "Approaches to testing new treatments in autosomal dominant polycystic kidney disease: insights from the CRISP and HALT-PKD studies." Clin J Am Soc Nephrol **3**(4): 1197-1204.

Chapman, A. B., A. Johnson, et al. (1990). "The renin-angiotensin-aldosterone system and autosomal dominant polycystic kidney disease." N Engl J Med **323**(16): 1091-1096.

Charalampous, F. C. (1959). "Biochemical studies on inositol. V. Purification and properties of the enzyme that cleaves inositol to D-glucuronic acid." J Biol Chem **234**(2): 220-227.

Cheng, Y. Z., L. Eley, et al. (2012). "Investigating embryonic expression patterns and evolution of AHI1 and CEP290 genes, implicated in Joubert syndrome." PLoS One **7**(9): e44975.

Cherry, S. M., C. A. Adelman, et al. (2007). "The Mre11 complex influences DNA repair, synapsis, and crossing over in murine meiosis." Curr Biol **17**(4): 373-378.

Cheung, H. O., X. Zhang, et al. (2009). "The kinesin protein Kif7 is a critical regulator of Gli transcription factors in mammalian hedgehog signaling." Sci Signal **2**(76): ra29.

Chi Sabins, N., J. L. Taylor, et al. (2013). "DLK1: A Novel Target for Immunotherapeutic Remodeling of the Tumor Blood Vasculature." Mol Ther.

Chih, B., P. Liu, et al. (2012). "A ciliopathy complex at the transition zone protects the cilia as a privileged membrane domain." Nat Cell Biol **14**(1): 61-72.

Cideciyan, A. V., R. A. Rachel, et al. (2011). "Cone photoreceptors are the main targets for gene therapy of NPHP5 (IQCB1) or NPHP6 (CEP290) blindness: generation of an all-cone Nphp6 hypomorph mouse that mimics the human retinal ciliopathy." Hum Mol Genet **20**(7): 1411-1423.

Coene, K. L., R. Roepman, et al. (2009). "OFD1 is mutated in X-linked Joubert syndrome and interacts with LCA5-encoded lebercilin." Am J Hum Genet **85**(4): 465-481.

Cohen, A. M., H. Wald, et al. (1995). "Effect of myo-inositol supplementation on the development of renal pathological changes in the Cohen diabetic (type 2) rat." Diabetologia **38**(8): 899-905.

Cook, S. A., G. B. Collin, et al. (2009). "A mouse model for Meckel syndrome type 3." J Am Soc Nephrol **20**(4): 753-764.

Coppieters, F., S. Lefever, et al. (2010). "CEP290, a gene with many faces: mutation overview and presentation of CEP290base." Hum Mutat **31**(10): 1097-1108.

Corbit, K. C., P. Aanstad, et al. (2005). "Vertebrate Smoothened functions at the primary cilium." Nature **437**(7061): 1018-1021.

Corbit, K. C., A. E. Shyer, et al. (2008). "Kif3a constrains beta-catenin-dependent Wnt signalling through dual ciliary and non-ciliary mechanisms." Nat Cell Biol **10**(1): 70-76.

Craige, B., C. C. Tsao, et al. (2010). "CEP290 tethers flagellar transition zone microtubules to the membrane and regulates flagellar protein content." J Cell Biol **190**(5): 927-940.

D'Angelo, A., A. De Angelis, et al. (2012). "Ofd1 controls dorso-ventral patterning and axoneme elongation during embryonic brain development." PLoS One **7**(12): e52937.

Dafinger, C., M. C. Liebau, et al. (2011). "Mutations in KIF7 link Joubert syndrome with Sonic Hedgehog signaling and microtubule dynamics." J Clin Invest **121**(7): 2662-2667.

David-Watine, B., A. Israel, et al. (1990). "The regulation and expression of MHC class I genes." Immunol Today **11**(8): 286-292.

Davies, J. A. and M. G. Davey (1999). "Collecting duct morphogenesis." Pediatr Nephrol **13**(6): 535-541.

Davis, E. E., Q. Zhang, et al. (2011). "TTC21B contributes both causal and modifying alleles across the ciliopathy spectrum." Nat Genet **43**(3): 189-196.

de Kok, J. B., R. W. Roelofs, et al. (2005). "Normalization of gene expression measurements in tumor tissues: comparison of 13 endogenous control genes." Lab Invest **85**(1): 154-159.

Del Monte, M. A., R. Rabbani, et al. (1991). "Sorbitol, myo-inositol, and rod outer segment phagocytosis in cultured hRPE cells exposed to glucose. In vitro model of myo-inositol depletion hypothesis of diabetic complications." Diabetes **40**(10): 1335-1345.

Dell, K. M. (2011). "The spectrum of polycystic kidney disease in children." Adv Chronic Kidney Dis **18**(5): 339-347.

Delous, M., L. Baala, et al. (2007). "The ciliary gene RPGRIP1L is mutated in cerebello-oculo-renal syndrome (Joubert syndrome type B) and Meckel syndrome." Nat Genet **39**(7): 875-881.
den Hollander, A. I., R. Roepman, et al. (2008). "Leber congenital amaurosis: genes, proteins and disease mechanisms." Prog Retin Eye Res **27**(4): 391-419.
Devuyst, O., C. R. Burrow, et al. (1996). "Expression of aquaporins-1 and -2 during nephrogenesis and in autosomal dominant polycystic kidney disease." Am J Physiol **271**(1 Pt 2): F169-183.
Dixon-Salazar, T., J. L. Silhavy, et al. (2004). "Mutations in the AHI1 gene, encoding jouberin, cause Joubert syndrome with cortical polymicrogyria." Am J Hum Genet **75**(6): 979-987.
Doherty, D. (2009). "Joubert syndrome: insights into brain development, cilium biology, and complex disease." Semin Pediatr Neurol **16**(3): 143-154.
Dunn, N. R., G. E. Winnier, et al. (1997). "Haploinsufficient phenotypes in Bmp4 heterozygous null mice and modification by mutations in Gli3 and Alx4." Dev Biol **188**(2): 235-247.
Durbec, P., C. V. Marcos-Gutierrez, et al. (1996). "GDNF signalling through the Ret receptor tyrosine kinase." Nature **381**(6585): 789-793.
Eastman, Q. and R. Grosschedl (1999). "Regulation of LEF-1/TCF transcription factors by Wnt and other signals." Curr Opin Cell Biol **11**(2): 233-240.
Efimenko, E., O. E. Blacque, et al. (2006). "Caenorhabditis elegans DYF-2, an orthologue of human WDR19, is a component of the intraflagellar transport machinery in sensory cilia." Mol Biol Cell **17**(11): 4801-4811.
El Hader, C., S. Tremblay, et al. (2005). "HCaRG increases renal cell migration by a TGF-alpha autocrine loop mechanism." Am J Physiol Renal Physiol **289**(6): F1273-1280.
Eladari, D., R. Chambrey, et al. (2012). "A new look at electrolyte transport in the distal tubule." Annu Rev Physiol **74**: 325-349.
Elia, N. and J. Lippincott-Schwartz (2009). "Culturing MDCK cells in three dimensions for analyzing intracellular dynamics." Curr Protoc Cell Biol **Chapter 4**: Unit 4 22.
Fahim, A. T., S. J. Bowne, et al. (2011). "Allelic heterogeneity and genetic modifier loci contribute to clinical variation in males with X-linked retinitis pigmentosa due to RPGR mutations." PLoS One **6**(8): e23021.
Farrell, J. J., D. Taupin, et al. (2002). "TFF2/SP-deficient mice show decreased gastric proliferation, increased acid secretion, and increased susceptibility to NSAID injury." J Clin Invest **109**(2): 193-204.
Ferland, R. J., W. Eyaid, et al. (2004). "Abnormal cerebellar development and axonal decussation due to mutations in AHI1 in Joubert syndrome." Nat Genet **36**(9): 1008-1013.
Ferrante, M. I., A. Zullo, et al. (2006). "Oral-facial-digital type I protein is required for primary cilia formation and left-right axis specification." Nat Genet **38**(1): 112-117.
Filali, M., N. Cheng, et al. (2002). "Wnt-3A/beta-catenin signaling induces transcription from the LEF-1 promoter." J Biol Chem **277**(36): 33398-33410.
Fliegauf, M., J. Horvath, et al. (2006). "Nephrocystin specifically localizes to the transition zone of renal and respiratory cilia and photoreceptor connecting cilia." J Am Soc Nephrol **17**(9): 2424-2433.
Flurkey, K. C., J. M. Harrison, D. E. (2007). The mouse in aging research. American College of Laboratory Animal Medicine, Burlington, MA.

Frank, V., S. Habbig, et al. (2013). "Mutations in NEK8 link multiple organ dysplasia with altered Hippo signalling and increased c-MYC expression." Hum Mol Genet **22**(11): 2177-2185.
Fushimi, K., S. Uchida, et al. (1993). "Cloning and expression of apical membrane water channel of rat kidney collecting tubule." Nature **361**(6412): 549-552.
Garcia-Gonzalo, F. R., K. C. Corbit, et al. (2011). "A transition zone complex regulates mammalian ciliogenesis and ciliary membrane composition." Nat Genet **43**(8): 776-784.
Garty, H. and L. G. Palmer (1997). "Epithelial sodium channels: function, structure, and regulation." Physiol Rev **77**(2): 359-396.
Gattone, V. H., 2nd, X. Wang, et al. (2003). "Inhibition of renal cystic disease development and progression by a vasopressin V2 receptor antagonist." Nat Med **9**(10): 1323-1326.
Ghosh, A. K., T. Hurd, et al. (2012). "3D spheroid defects in NPHP knockdown cells are rescued by the somatostatin receptor agonist octreotide." Am J Physiol Renal Physiol **303**(8): F1225-1229.
Goetz, S. C. and K. V. Anderson (2010). "The primary cilium: a signalling centre during vertebrate development." Nat Rev Genet **11**(5): 331-344.
Gorden, N. T., H. H. Arts, et al. (2008). "CC2D2A is mutated in Joubert syndrome and interacts with the ciliopathy-associated basal body protein CEP290." Am J Hum Genet **83**(5): 559-571.
Graser, S., Y. D. Stierhof, et al. (2007). "Cep164, a novel centriole appendage protein required for primary cilium formation." J Cell Biol **179**(2): 321-330.
Greene, D. A., S. Chakrabarti, et al. (1987). "Role of sorbitol accumulation and myo-inositol depletion in paranodal swelling of large myelinated nerve fibers in the insulin-deficient spontaneously diabetic bio-breeding rat. Reversal by insulin replacement, an aldose reductase inhibitor, and myo-inositol." J Clin Invest **79**(5): 1479-1485.
Gribouval, O., M. Gonzales, et al. (2005). "Mutations in genes in the renin-angiotensin system are associated with autosomal recessive renal tubular dysgenesis." Nat Genet **37**(9): 964-968.
Gribouval, O., V. Moriniere, et al. (2012). "Spectrum of mutations in the renin-angiotensin system genes in autosomal recessive renal tubular dysgenesis." Hum Mutat **33**(2): 316-326.
Grupp, C., I. Troche, et al. (1998). "Highly specific separation of heterogeneous cell populations by lectin-coated beads: application for the isolation of inner medullary collecting duct cells." Exp Nephrol **6**(6): 542-550.
Guay-Woodford, L. M. and R. A. Desmond (2003). "Autosomal recessive polycystic kidney disease: the clinical experience in North America." Pediatrics **111**(5 Pt 1): 1072-1080.
Guay-Woodford, L. M., W. J. Green, et al. (2000). "Germline and somatic loss of function of the mouse cpk gene causes biliary ductal pathology that is genetically modulated." Hum Mol Genet **9**(5): 769-778.
Gusmano, R., G. M. Ghiggeri, et al. (1998). "Nephronophthisis-medullary cystic disease: clinical and genetic aspects." J Nephrol **11**(5): 224-228.
Guyton, A. C. (1991). "Blood pressure control--special role of the kidneys and body fluids." Science **252**(5014): 1813-1816.
Habbig, S., M. P. Bartram, et al. (2012). "The ciliopathy disease protein NPHP9 promotes nuclear delivery and activation of the oncogenic transcriptional regulator TAZ." Hum Mol Genet **21**(26): 5528-5538.

Halbritter, J., J. D. Porath, et al. (2013). "Identification of 99 novel mutations in a worldwide cohort of 1,056 patients with a nephronophthisis-related ciliopathy." Hum Genet.
Halvorson, C. R., M. S. Bremmer, et al. (2010). "Polycystic kidney disease: inheritance, pathophysiology, prognosis, and treatment." Int J Nephrol Renovasc Dis **3**: 69-83.
Harris, P. C. and S. Rossetti (2004). "Molecular genetics of autosomal recessive polycystic kidney disease." Mol Genet Metab **81**(2): 75-85.
Harris, P. C. and V. E. Torres (2009). "Polycystic kidney disease." Annu Rev Med **60**: 321-337.
Harrison-Bernard, L. M. (2009). "The renal renin-angiotensin system." Adv Physiol Educ **33**(4): 270-274.
Haycraft, C. J., B. Banizs, et al. (2005). "Gli2 and Gli3 localize to cilia and require the intraflagellar transport protein polaris for processing and function." PLoS Genet **1**(4): e53.
He, W., C. Dai, et al. (2009). "Wnt/beta-catenin signaling promotes renal interstitial fibrosis." J Am Soc Nephrol **20**(4): 765-776.
Herron, B. J., W. Lu, et al. (2002). "Efficient generation and mapping of recessive developmental mutations using ENU mutagenesis." Nat Genet **30**(2): 185-189.
Hertel, S. C., C. E. Chwieralski, et al. (2004). "Profiling trefoil factor family (TFF) expression in the mouse: identification of an antisense TFF1-related transcript in the kidney and liver." Peptides **25**(5): 755-762.
Hildebrandt, F., M. Attanasio, et al. (2009). "Nephronophthisis: disease mechanisms of a ciliopathy." J Am Soc Nephrol **20**(1): 23-35.
Hildebrandt, F. and E. Otto (2000). "Molecular genetics of nephronophthisis and medullary cystic kidney disease." J Am Soc Nephrol **11**(9): 1753-1761.
Hildebrandt, F. and E. Otto (2005). "Cilia and centrosomes: a unifying pathogenic concept for cystic kidney disease?" Nat Rev Genet **6**(12): 928-940.
Hildebrandt, F., E. Otto, et al. (1997). "A novel gene encoding an SH3 domain protein is mutated in nephronophthisis type 1." Nat Genet **17**(2): 149-153.
Hildebrandt, F. and W. Zhou (2007). "Nephronophthisis-associated ciliopathies." J Am Soc Nephrol **18**(6): 1855-1871.
Hodgkins, P. R., C. M. Harris, et al. (2004). "Joubert syndrome: long-term follow-up." Dev Med Child Neurol **46**(10): 694-699.
Hoff, S., J. Halbritter, et al. (2013). "ANKS6 is a central component of a nephronophthisis module linking NEK8 to INVS and NPHP3." Nat Genet.
Hoffmann, W. and W. Jagla (2002). "Cell type specific expression of secretory TFF peptides: colocalization with mucins and synthesis in the brain." Int Rev Cytol **213**: 147-181.
Hoffmann, W., W. Jagla, et al. (2001). "Molecular medicine of TFF-peptides: from gut to brain." Histol Histopathol **16**(1): 319-334.
Hogan, M. C., T. V. Masyuk, et al. (2010). "Randomized clinical trial of long-acting somatostatin for autosomal dominant polycystic kidney and liver disease." J Am Soc Nephrol **21**(6): 1052-1061.
Holthofer, H. (1983). "Lectin binding sites in kidney. A comparative study of 14 animal species." J Histochem Cytochem **31**(4): 531-537.
Holthofer, H. (1988). "Cell type-specific glycoconjugates of collecting duct cells during maturation of the rat kidney." Cell Tissue Res **253**(2): 305-309.

Holthofer, H., B. A. Schulte, et al. (1987). "Expression of binding sites for Dolichos biflorus agglutinin at the apical aspect of collecting duct cells in rat kidney." Cell Tissue Res **249**(3): 481-485.

Hoover, A. N., A. Wynkoop, et al. (2008). "C2cd3 is required for cilia formation and Hedgehog signaling in mouse." Development **135**(24): 4049-4058.

Hovanes, K., T. W. Li, et al. (2001). "Beta-catenin-sensitive isoforms of lymphoid enhancer factor-1 are selectively expressed in colon cancer." Nat Genet **28**(1): 53-57.

Hsiao, Y. C., Z. J. Tong, et al. (2009). "Ahi1, whose human ortholog is mutated in Joubert syndrome, is required for Rab8a localization, ciliogenesis and vesicle trafficking." Hum Mol Genet **18**(20): 3926-3941.

Hu, E., Z. Chen, et al. (2000). "Identification of a novel kidney-specific gene downregulated in acute ischemic renal failure." Am J Physiol Renal Physiol **279**(3): F426-439.

Hu, M. C., R. Mo, et al. (2006). "GLI3-dependent transcriptional repression of Gli1, Gli2 and kidney patterning genes disrupts renal morphogenesis." Development **133**(3): 569-578.

Huang, L., K. Szymanska, et al. (2011). "TMEM237 is mutated in individuals with a Joubert syndrome related disorder and expands the role of the TMEM family at the ciliary transition zone." Am J Hum Genet **89**(6): 713-730.

Huangfu, D. and K. V. Anderson (2005). "Cilia and Hedgehog responsiveness in the mouse." Proc Natl Acad Sci U S A **102**(32): 11325-11330.

Humke, E. W., K. V. Dorn, et al. (2010). "The output of Hedgehog signaling is controlled by the dynamic association between Suppressor of Fused and the Gli proteins." Genes Dev **24**(7): 670-682.

Hummler, E. (1999). "Implication of ENaC in salt-sensitive hypertension." J Steroid Biochem Mol Biol **69**(1-6): 385-390.

Hummler, E. (2003). "Epithelial sodium channel, salt intake, and hypertension." Curr Hypertens Rep **5**(1): 11-18.

Hummler, E. and J. D. Horisberger (1999). "Genetic disorders of membrane transport. V. The epithelial sodium channel and its implication in human diseases." Am J Physiol **276**(3 Pt 1): G567-571.

Hunkapiller, J., V. Singla, et al. (2011). "The ciliogenic protein Oral-Facial-Digital 1 regulates the neuronal differentiation of embryonic stem cells." Stem Cells Dev **20**(5): 831-841.

Hurd, T. W. and F. Hildebrandt (2011). "Mechanisms of nephronophthisis and related ciliopathies." Nephron Exp Nephrol **118**(1): e9-14.

Hurd, T. W., E. A. Otto, et al. (2013). "Mutation of the Mg2+ Transporter SLC41A1 Results in a Nephronophthisis-Like Phenotype." J Am Soc Nephrol **24**(6): 967-977.

Hyman, J. M., A. J. Firestone, et al. (2009). "Small-molecule inhibitors reveal multiple strategies for Hedgehog pathway blockade." Proc Natl Acad Sci U S A **106**(33): 14132-14137.

Ingham, P. W. and A. P. McMahon (2001). "Hedgehog signaling in animal development: paradigms and principles." Genes Dev **15**(23): 3059-3087.

Ishikawa, H. and W. F. Marshall (2011). "Ciliogenesis: building the cell's antenna." Nat Rev Mol Cell Biol **12**(4): 222-234.

Israel, A., A. Kimura, et al. (1986). "Interferon response sequence potentiates activity of an enhancer in the promoter region of a mouse H-2 gene." Nature **322**(6081): 743-746.

Jacob, J. and J. Briscoe (2003). "Gli proteins and the control of spinal-cord patterning." EMBO Rep **4**(8): 761-765.
Jacoby, M., J. J. Cox, et al. (2009). "INPP5E mutations cause primary cilium signaling defects, ciliary instability and ciliopathies in human and mouse." Nat Genet **41**(9): 1027-1031.
Jat, P. S., M. D. Noble, et al. (1991). "Direct derivation of conditionally immortal cell lines from an H-2Kb-tsA58 transgenic mouse." Proc Natl Acad Sci U S A **88**(12): 5096-5100.
Jiang, S. T., Y. Y. Chiou, et al. (2008). "Targeted disruption of Nphp1 causes male infertility due to defects in the later steps of sperm morphogenesis in mice." Hum Mol Genet **17**(21): 3368-3379.
Johnson, D. R. (1967). "Extra-toes: anew mutant gene causing multiple abnormalities in the mouse." J Embryol Exp Morphol **17**(3): 543-581.
Jonassen, J. A., J. San Agustin, et al. (2008). "Deletion of IFT20 in the mouse kidney causes misorientation of the mitotic spindle and cystic kidney disease." J Cell Biol **183**(3): 377-384.
Jones, C. A., C. D. Sigmund, et al. (1990). "Expression of murine renin genes during fetal development." Mol Endocrinol **4**(3): 375-383.
Joubert, M., J. J. Eisenring, et al. (1968). "Familial dysgenesis of the vermis: a syndrome of hyperventilation, abnormal eye movements and retardation." Neurology **18**(3): 302-303.
Kaliappan, G., P. Nagarajan, et al. (2012). "Ang II induce kidney damage by recruiting inflammatory cells and up regulates PPAR gamma and Renin 1 gene: effect of beta carotene on chronic renal damage." J Thromb Thrombolysis.
Kanwar, Y. S., A. Kumar, et al. (2002). "Identification of developmentally regulated mesodermal-specific transcript in mouse embryonic metanephros." Am J Physiol Renal Physiol **282**(5): F953-965.
Katoh, Y. and M. Katoh (2004). "KIF27 is one of orthologs for Drosophila Costal-2." Int J Oncol **25**(6): 1875-1880.
Kawakami, T., S. Ren, et al. (2013). "Wnt signalling in kidney diseases: dual roles in renal injury and repair." J Pathol **229**(2): 221-231.
Kengaku, M., J. Capdevila, et al. (1998). "Distinct WNT pathways regulating AER formation and dorsoventral polarity in the chick limb bud." Science **280**(5367): 1274-1277.
Kern, G. and B. E. Flucher (2005). "Localization of transgenes and genotyping of H-2kb-tsA58 transgenic mice." Biotechniques **38**(1): 38, 40, 42.
Kim, J., S. R. Krishnaswami, et al. (2008). "CEP290 interacts with the centriolar satellite component PCM-1 and is required for Rab8 localization to the primary cilium." Hum Mol Genet **17**(23): 3796-3805.
Kim, S. and B. D. Dynlacht (2013). "Assembling a primary cilium." Curr Opin Cell Biol **25**(4): 506-511.
Kim, Y. S., H. S. Kang, et al. (2008). "Kruppel-like zinc finger protein Glis2 is essential for the maintenance of normal renal functions." Mol Cell Biol **28**(7): 2358-2367.
Kim, Y. S., H. S. Kang, et al. (2007). "The Kruppel-like zinc finger protein Glis2 functions as a negative modulator of the Wnt/beta-catenin signaling pathway." FEBS Lett **581**(5): 858-864.
Ko, J. Y. and J. H. Park (2013). "Mouse models of polycystic kidney disease induced by defects of ciliary proteins." BMB Rep **46**(2): 73-79.
Kolisek, M., A. Nestler, et al. (2012). "Human gene SLC41A1 encodes for the Na+/Mg(2)+ exchanger." Am J Physiol Cell Physiol **302**(1): C318-326.

Koller, F. and O. Hoffmann-Ostenhof (1979). "myo-Inositol oxygenase from rat kidneys. I: Purification by affinity chromatography; physical and catalytic properties." Hoppe Seylers Z Physiol Chem **360**(4): 507-513.
Kovacs, J., M. Zilahy, et al. (1997). "Morphology of cystic renal lesions. Lectin and immuno-histochemical study." Acta Chir Hung **36**(1-4): 176-178.
Kroes, H. Y., P. H. van Zon, et al. (2008). "DNA analysis of AHI1, NPHP1 and CYCLIN D1 in Joubert syndrome patients from the Netherlands." Eur J Med Genet **51**(1): 24-34.
Kumar, S., M. Adeva, et al. (2006). "Duodenal diverticulosis in autosomal dominant polycystic kidney disease." Nephrol Dial Transplant **21**(12): 3576-3578.
Lagier-Tourenne, C., E. Boltshauser, et al. (2004). "Homozygosity mapping of a third Joubert syndrome locus to 6q23." J Med Genet **41**(4): 273-277.
Laitinen, L., I. Virtanen, et al. (1987). "Changes in the glycosylation pattern during embryonic development of mouse kidney as revealed with lectin conjugates." J Histochem Cytochem **35**(1): 55-65.
Lancaster, M. A., D. J. Gopal, et al. (2011). "Defective Wnt-dependent cerebellar midline fusion in a mouse model of Joubert syndrome." Nat Med **17**(6): 726-731.
Lancaster, M. A., C. M. Louie, et al. (2009). "Impaired Wnt-beta-catenin signaling disrupts adult renal homeostasis and leads to cystic kidney ciliopathy." Nat Med **15**(9): 1046-1054.
Lantelme, P., A. Rohrwasser, et al. (2002). "Effects of dietary sodium and genetic background on angiotensinogen and Renin in mouse." Hypertension **39**(5): 1007-1014.
Larkins, C. E., G. D. Aviles, et al. (2011). "Arl13b regulates ciliogenesis and the dynamic localization of Shh signaling proteins." Mol Biol Cell **22**(23): 4694-4703.
Lee, D. C., K. W. Chan, et al. (2002). "RET receptor tyrosine kinase isoforms in kidney function and disease." Oncogene **21**(36): 5582-5592.
Lee, J. E., J. L. Silhavy, et al. (2012). "CEP41 is mutated in Joubert syndrome and is required for tubulin glutamylation at the cilium." Nat Genet **44**(2): 193-199.
Lee, J. H. and J. G. Gleeson (2010). "The role of primary cilia in neuronal function." Neurobiol Dis **38**(2): 167-172.
Lee, J. H., J. L. Silhavy, et al. (2012). "Evolutionarily assembled cis-regulatory module at a human ciliopathy locus." Science **335**(6071): 966-969.
Leitch, C. C., N. A. Zaghloul, et al. (2008). "Hypomorphic mutations in syndromic encephalocele genes are associated with Bardet-Biedl syndrome." Nat Genet **40**(4): 443-448.
Li, B., A. A. Rauhauser, et al. (2011). "Increased hedgehog signaling in postnatal kidney results in aberrant activation of nephron developmental programs." Hum Mol Genet **20**(21): 4155-4166.
Li, J. B., J. M. Gerdes, et al. (2004). "Comparative genomics identifies a flagellar and basal body proteome that includes the BBS5 human disease gene." Cell **117**(4): 541-552.
Liem, K. F., Jr., M. He, et al. (2009). "Mouse Kif7/Costal2 is a cilia-associated protein that regulates Sonic hedgehog signaling." Proc Natl Acad Sci U S A **106**(32): 13377-13382.
Lin, F., T. Hiesberger, et al. (2003). "Kidney-specific inactivation of the KIF3A subunit of kinesin-II inhibits renal ciliogenesis and produces polycystic kidney disease." Proc Natl Acad Sci U S A **100**(9): 5286-5291.

Lin, L. R., V. N. Reddy, et al. (1991). "Polyol accumulation in cultured human lens epithelial cells." Exp Eye Res **52**(1): 93-100.
Lindvall, M. and C. Owman (1981). "Autonomic nerves in the mammalian choroid plexus and their influence on the formation of cerebrospinal fluid." J Cereb Blood Flow Metab **1**(3): 245-266.
Liu, S., W. Lu, et al. (2002). "A defect in a novel Nek-family kinase causes cystic kidney disease in the mouse and in zebrafish." Development **129**(24): 5839-5846.
Locascio, L. E. and D. J. Donoghue (2013). "KIDs rule: regulatory phosphorylation of RTKs." Trends Biochem Sci **38**(2): 75-84.
Loghman-Adham, M., C. E. Soto, et al. (2004). "The intrarenal renin-angiotensin system in autosomal dominant polycystic kidney disease." Am J Physiol Renal Physiol **287**(4): F775-788.
Louie, C. M., G. Caridi, et al. (2010). "AHI1 is required for photoreceptor outer segment development and is a modifier for retinal degeneration in nephronophthisis." Nat Genet **42**(2): 175-180.
Mahuzier, A., H. M. Gaude, et al. (2012). "Dishevelled stabilization by the ciliopathy protein Rpgrip1l is essential for planar cell polarity." J Cell Biol **198**(5): 927-940.
Mandell, J., W. K. Koch, et al. (1983). "Congenital polycystic kidney disease. Genetically transmitted infantile polycystic kidney disease in C57BL/6J mice." Am J Pathol **113**(1): 112-114.
Manning, D. K., M. Sergeev, et al. (2013). "Loss of the ciliary kinase Nek8 causes left-right asymmetry defects." J Am Soc Nephrol **24**(1): 100-112.
Maria, B. L., K. B. Hoang, et al. (1997). ""Joubert syndrome" revisited: key ocular motor signs with magnetic resonance imaging correlation." J Child Neurol **12**(7): 423-430.
Masyuk, T. V., A. I. Masyuk, et al. (2007). "Octreotide inhibits hepatic cystogenesis in a rodent model of polycystic liver disease by reducing cholangiocyte adenosine 3',5'-cyclic monophosphate." Gastroenterology **132**(3): 1104-1116.
McEwen, D. P., R. K. Koenekoop, et al. (2007). "Hypomorphic CEP290/NPHP6 mutations result in anosmia caused by the selective loss of G proteins in cilia of olfactory sensory neurons." Proc Natl Acad Sci U S A **104**(40): 15917-15922.
McIntyre, J. C., E. E. Davis, et al. (2012). "Gene therapy rescues cilia defects and restores olfactory function in a mammalian ciliopathy model." Nat Med **18**(9): 1423-1428.
Mears, A. J., M. Kondo, et al. (2001). "Nrl is required for rod photoreceptor development." Nat Genet **29**(4): 447-452.
Mochizuki, T., K. Tsuchiya, et al. (2013). "Autosomal dominant polycystic kidney disease: recent advances in pathogenesis and potential therapies." Clin Exp Nephrol **17**(3): 317-326.
Molenaar, M., M. van de Wetering, et al. (1996). "XTcf-3 transcription factor mediates beta-catenin-induced axis formation in Xenopus embryos." Cell **86**(3): 391-399.
Mollet, G., R. Salomon, et al. (2002). "The gene mutated in juvenile nephronophthisis type 4 encodes a novel protein that interacts with nephrocystin." Nat Genet **32**(2): 300-305.
Mollet, G., F. Silbermann, et al. (2005). "Characterization of the nephrocystin/nephrocystin-4 complex and subcellular localization of

nephrocystin-4 to primary cilia and centrosomes." Hum Mol Genet **14**(5): 645-656.
Morgan, D., L. Eley, et al. (2002). "Expression analyses and interaction with the anaphase promoting complex protein Apc2 suggest a role for inversin in primary cilia and involvement in the cell cycle." Hum Mol Genet **11**(26): 3345-3350.
Morgan, D., L. Turnpenny, et al. (1998). "Inversin, a novel gene in the vertebrate left-right axis pathway, is partially deleted in the inv mouse." Nat Genet **20**(2): 149-156.
Moyer, J. H., M. J. Lee-Tischler, et al. (1994). "Candidate gene associated with a mutation causing recessive polycystic kidney disease in mice." Science **264**(5163): 1329-1333.
Nagao, S., T. Hibino, et al. (1991). "Strain difference in expression of the adult-type polycystic kidney disease gene, pcy, in the mouse." Jikken Dobutsu **40**(1): 45-53.
Nagao, S., M. Kugita, et al. (2012). "Animal models for human polycystic kidney disease." Exp Anim **61**(5): 477-488.
Nagao, S., K. Nishii, et al. (2006). "Increased water intake decreases progression of polycystic kidney disease in the PCK rat." J Am Soc Nephrol **17**(8): 2220-2227.
Nagao, S. and T. Yamaguchi (2012). "PPAR-gamma agonists in polycystic kidney disease with frequent development of cardiovascular disorders." Curr Mol Pharmacol **5**(2): 292-300.
Nagao, S., T. Yamaguchi, et al. (2003). "Renal activation of extracellular signal-regulated kinase in rats with autosomal-dominant polycystic kidney disease." Kidney Int **63**(2): 427-437.
Narita, K., T. Kawate, et al. (2010). "Multiple primary cilia modulate the fluid transcytosis in choroid plexus epithelium." Traffic **11**(2): 287-301.
Nasmyth, K. and C. H. Haering (2005). "The structure and function of SMC and kleisin complexes." Annu Rev Biochem **74**: 595-648.
Naso, M. F., B. Liang, et al. (2007). "Dermokine: an extensively differentially spliced gene expressed in epithelial cells." J Invest Dermatol **127**(7): 1622-1631.
Nauli, S. M., F. J. Alenghat, et al. (2003). "Polycystins 1 and 2 mediate mechanosensation in the primary cilium of kidney cells." Nat Genet **33**(2): 129-137.
Nauta, J., Y. Ozawa, et al. (1993). "Renal and biliary abnormalities in a new murine model of autosomal recessive polycystic kidney disease." Pediatr Nephrol **7**(2): 163-172.
Nonaka, M., Y. Matsuda, et al. (1993). "Molecular cloning of the b subunit of mouse coagulation factor XIII and assignment of the gene to chromosome 1: close evolutionary relationship to complement factor H." Genomics **15**(3): 535-542.
Noor, A., C. Windpassinger, et al. (2008). "CC2D2A, encoding a coiled-coil and C2 domain protein, causes autosomal-recessive mental retardation with retinitis pigmentosa." Am J Hum Genet **82**(4): 1011-1018.
Nurnberger, J., R. L. Bacallao, et al. (2002). "Inversin forms a complex with catenins and N-cadherin in polarized epithelial cells." Mol Biol Cell **13**(9): 3096-3106.
O'Toole, J. F., Y. Liu, et al. (2010). "Individuals with mutations in XPNPEP3, which encodes a mitochondrial protein, develop a nephronophthisis-like nephropathy." J Clin Invest **120**(3): 791-802.

Olbrich, H., M. Fliegauf, et al. (2003). "Mutations in a novel gene, NPHP3, cause adolescent nephronophthisis, tapeto-retinal degeneration and hepatic fibrosis." Nat Genet **34**(4): 455-459.
Olinger, E., B. Schwaller, et al. (2012). "Parvalbumin: calcium and magnesium buffering in the distal nephron." Nephrol Dial Transplant **27**(11): 3988-3994.
Olteanu, D., B. K. Yoder, et al. (2006). "Heightened epithelial Na+ channel-mediated Na+ absorption in a murine polycystic kidney disease model epithelium lacking apical monocilia." Am J Physiol Cell Physiol **290**(4): C952-963.
Omori, S., M. Hida, et al. (2006). "Extracellular signal-regulated kinase inhibition slows disease progression in mice with polycystic kidney disease." J Am Soc Nephrol **17**(6): 1604-1614.
Omran, H., K. Haffner, et al. (2001). "Human adolescent nephronophthisis: gene locus synteny with polycystic kidney disease in pcy mice." J Am Soc Nephrol **12**(1): 107-113.
Omran, H., G. Sasmaz, et al. (2002). "Identification of a gene locus for Senior-Loken syndrome in the region of the nephronophthisis type 3 gene." J Am Soc Nephrol **13**(1): 75-79.
Onuchic, L. F., L. Furu, et al. (2002). "PKHD1, the polycystic kidney and hepatic disease 1 gene, encodes a novel large protein containing multiple immunoglobulin-like plexin-transcription-factor domains and parallel beta-helix 1 repeats." Am J Hum Genet **70**(5): 1305-1317.
Otto, E., J. Hoefele, et al. (2002). "A gene mutated in nephronophthisis and retinitis pigmentosa encodes a novel protein, nephroretinin, conserved in evolution." Am J Hum Genet **71**(5): 1161-1167.
Otto, E. A., T. W. Hurd, et al. (2010). "Candidate exome capture identifies mutation of SDCCAG8 as the cause of a retinal-renal ciliopathy." Nat Genet **42**(10): 840-850.
Otto, E. A., B. Loeys, et al. (2005). "Nephrocystin-5, a ciliary IQ domain protein, is mutated in Senior-Loken syndrome and interacts with RPGR and calmodulin." Nat Genet **37**(3): 282-288.
Otto, E. A., G. Ramaswami, et al. (2011). "Mutation analysis of 18 nephronophthisis associated ciliopathy disease genes using a DNA pooling and next generation sequencing strategy." J Med Genet **48**(2): 105-116.
Otto, E. A., B. Schermer, et al. (2003). "Mutations in INVS encoding inversin cause nephronophthisis type 2, linking renal cystic disease to the function of primary cilia and left-right axis determination." Nat Genet **34**(4): 413-420.
Otto, E. A., K. Tory, et al. (2009). "Hypomorphic mutations in meckelin (MKS3/TMEM67) cause nephronophthisis with liver fibrosis (NPHP11)." J Med Genet **46**(10): 663-670.
Otto, E. A., M. L. Trapp, et al. (2008). "NEK8 mutations affect ciliary and centrosomal localization and may cause nephronophthisis." J Am Soc Nephrol **19**(3): 587-592.
Paetau, A., R. Salonen, et al. (1985). "Brain pathology in the Meckel syndrome: a study of 59 cases." Clin Neuropathol **4**(2): 56-62.
Pan, J., T. Seeger-Nukpezah, et al. (2012). "The role of the cilium in normal and abnormal cell cycles: emphasis on renal cystic pathologies." Cell Mol Life Sci.

Parisi, M. A., C. L. Bennett, et al. (2004). "The NPHP1 gene deletion associated with juvenile nephronophthisis is present in a subset of individuals with Joubert syndrome." Am J Hum Genet **75**(1): 82-91.
Parisi, M. A., D. Doherty, et al. (2007). "Joubert syndrome (and related disorders) (OMIM 213300)." Eur J Hum Genet **15**(5): 511-521.
Pazour, G. J., B. L. Dickert, et al. (2000). "Chlamydomonas IFT88 and its mouse homologue, polycystic kidney disease gene tg737, are required for assembly of cilia and flagella." J Cell Biol **151**(3): 709-718.
Pazour, G. J. and J. L. Rosenbaum (2002). "Intraflagellar transport and cilia-dependent diseases." Trends Cell Biol **12**(12): 551-555.
Pentz, E. S., M. L. Lopez, et al. (2001). "Ren1d and Ren2 cooperate to preserve homeostasis: evidence from mice expressing GFP in place of Ren1d." Physiol Genomics **6**(1): 45-55.
Perico, N., L. Antiga, et al. (2010). "Sirolimus therapy to halt the progression of ADPKD." J Am Soc Nephrol **21**(6): 1031-1040.
Phillips, C. L., K. J. Miller, et al. (2004). "Renal cysts of inv/inv mice resemble early infantile nephronophthisis." J Am Soc Nephrol **15**(7): 1744-1755.
Phillips, J. K., D. Hopwood, et al. (2007). "Temporal relationship between renal cyst development, hypertension and cardiac hypertrophy in a new rat model of autosomal recessive polycystic kidney disease." Kidney Blood Press Res **30**(3): 129-144.
Pichel, J. G., L. Shen, et al. (1996). "Defects in enteric innervation and kidney development in mice lacking GDNF." Nature **382**(6586): 73-76.
Piperno, G. and M. T. Fuller (1985). "Monoclonal antibodies specific for an acetylated form of alpha-tubulin recognize the antigen in cilia and flagella from a variety of organisms." J Cell Biol **101**(6): 2085-2094.
Pirson, Y. (2010). "Extrarenal manifestations of autosomal dominant polycystic kidney disease." Adv Chronic Kidney Dis **17**(2): 173-180.
Plendl, J., B. Schoenleber, et al. (1992). "Sexual dimorphism of the kidney in the NMRI mouse as shown by Dolichos biflorus agglutinin labelling." Anat Histol Embryol **21**(2): 118-126.
Praetorius, H. A. and J. Leipziger (2013). "Primary cilium-dependent sensing of urinary flow and paracrine purinergic signaling." Semin Cell Dev Biol **24**(1): 3-10.
Prieto-Carrasquero, M. C., F. T. Botros, et al. (2008). "Collecting duct renin is upregulated in both kidneys of 2-kidney, 1-clip goldblatt hypertensive rats." Hypertension **51**(6): 1590-1596.
Prieto-Carrasquero, M. C., L. M. Harrison-Bernard, et al. (2004). "Enhancement of collecting duct renin in angiotensin II-dependent hypertensive rats." Hypertension **44**(2): 223-229.
Quante, M., F. Marrache, et al. (2010). "TFF2 mRNA transcript expression marks a gland progenitor cell of the gastric oxyntic mucosa." Gastroenterology **139**(6): 2018-2027 e2012.
Rachel, R. A., T. Li, et al. (2012). "Photoreceptor sensory cilia and ciliopathies: focus on CEP290, RPGR and their interacting proteins." Cilia **1**(1): 22.
Rakkolainen, A., S. Ala-Mello, et al. (2002). "Four novel mutations in the OFD1 (Cxorf5) gene in Finnish patients with oral-facial-digital syndrome 1." J Med Genet **39**(4): 292-296.
Reiter, J. F. and W. C. Skarnes (2006). "Tectonic, a novel regulator of the Hedgehog pathway required for both activation and inhibition." Genes Dev **20**(1): 22-27.

Richards, W. G., W. E. Sweeney, et al. (1998). "Epidermal growth factor receptor activity mediates renal cyst formation in polycystic kidney disease." J Clin Invest **101**(5): 935-939.
Rodat-Despoix, L. and P. Delmas (2009). "Ciliar functions in the nephron." Pflugers Arch **458**(1): 179-187.
Rohatgi, R., A. Greenberg, et al. (2003). "Na transport in autosomal recessive polycystic kidney disease (ARPKD) cyst lining epithelial cells." J Am Soc Nephrol **14**(4): 827-836.
Rohrwasser, A., T. Morgan, et al. (1999). "Elements of a paracrine tubular renin-angiotensin system along the entire nephron." Hypertension **34**(6): 1265-1274.
Romio, L., V. Wright, et al. (2003). "OFD1, the gene mutated in oral-facial-digital syndrome type 1, is expressed in the metanephros and in human embryonic renal mesenchymal cells." J Am Soc Nephrol **14**(3): 680-689.
Rossetti, S. and P. C. Harris (2007). "Genotype-phenotype correlations in autosomal dominant and autosomal recessive polycystic kidney disease." J Am Soc Nephrol **18**(5): 1374-1380.
Royaux, I. E., S. M. Wall, et al. (2001). "Pendrin, encoded by the Pendred syndrome gene, resides in the apical region of renal intercalated cells and mediates bicarbonate secretion." Proc Natl Acad Sci U S A **98**(7): 4221-4226.
Ruiz i Altaba, A. (1997). "Catching a Gli-mpse of Hedgehog." Cell **90**(2): 193-196.
Saar, K., L. Al-Gazali, et al. (1999). "Homozygosity mapping in families with Joubert syndrome identifies a locus on chromosome 9q34.3 and evidence for genetic heterogeneity." Am J Hum Genet **65**(6): 1666-1671.
Sabbagh, Y., F. G. Graciolli, et al. (2012). "Repression of osteocyte Wnt/beta-catenin signaling is an early event in the progression of renal osteodystrophy." J Bone Miner Res **27**(8): 1757-1772.
Sabers, C. J., M. M. Martin, et al. (1995). "Isolation of a protein target of the FKBP12-rapamycin complex in mammalian cells." J Biol Chem **270**(2): 815-822.
Saigusa, T., R. Reichert, et al. (2012). "Collecting duct cells that lack normal cilia have mislocalized vasopressin-2 receptors." Am J Physiol Renal Physiol **302**(7): F801-808.
Sainio, K., P. Suvanto, et al. (1997). "Glial-cell-line-derived neurotrophic factor is required for bud initiation from ureteric epithelium." Development **124**(20): 4077-4087.
Salomon, R., S. Saunier, et al. (2009). "Nephronophthisis." Pediatr Nephrol **24**(12): 2333-2344.
Sanchez, M. P., I. Silos-Santiago, et al. (1996). "Renal agenesis and the absence of enteric neurons in mice lacking GDNF." Nature **382**(6586): 70-73.
Sands, J. M., M. Naruse, et al. (1997). "Apical extracellular calcium/polyvalent cation-sensing receptor regulates vasopressin-elicited water permeability in rat kidney inner medullary collecting duct." J Clin Invest **99**(6): 1399-1405.
Sang, L., J. J. Miller, et al. (2011). "Mapping the NPHP-JBTS-MKS protein network reveals ciliopathy disease genes and pathways." Cell **145**(4): 513-528.

Santarpia, L. and G. Bottai (2013). "Inhibition of RET activated pathways: novel strategies for therapeutic intervention in human cancers." Curr Pharm Des **19**(5): 864-882.
Satir, P., L. B. Pedersen, et al. (2010). "The primary cilium at a glance." J Cell Sci **123**(Pt 4): 499-503.
Satlin, L. M. (1999). "Regulation of potassium transport in the maturing kidney." Semin Nephrol **19**(2): 155-165.
Sattar, S. and J. G. Gleeson (2011). "The ciliopathies in neuronal development: a clinical approach to investigation of Joubert syndrome and Joubert syndrome-related disorders." Dev Med Child Neurol **53**(9): 793-798.
Saunier, S., J. Calado, et al. (1997). "A novel gene that encodes a protein with a putative src homology 3 domain is a candidate gene for familial juvenile nephronophthisis." Hum Mol Genet **6**(13): 2317-2323.
Sayer, J. A., E. A. Otto, et al. (2006). "The centrosomal protein nephrocystin-6 is mutated in Joubert syndrome and activates transcription factor ATF4." Nat Genet **38**(6): 674-681.
Schafer, T., M. Putz, et al. (2008). "Genetic and physical interaction between the NPHP5 and NPHP6 gene products." Hum Mol Genet **17**(23): 3655-3662.
Schedl, A. and N. D. Hastie (2000). "Cross-talk in kidney development." Curr Opin Genet Dev **10**(5): 543-549.
Schild, L. (2004). "The epithelial sodium channel: from molecule to disease." Rev Physiol Biochem Pharmacol **151**: 93-107.
Schild, L. and S. Kellenberger (2001). "Structure function relationships of ENaC and its role in sodium handling." Adv Exp Med Biol **502**: 305-314.
Schumacher, K., R. Strehl, et al. (2002). "Detection of glycosylated sites in embryonic rabbit kidney by lectin chemistry." Histochem Cell Biol **118**(1): 79-87.
Schwaller, B., J. Dick, et al. (1999). "Prolonged contraction-relaxation cycle of fast-twitch muscles in parvalbumin knockout mice." Am J Physiol **276**(2 Pt 1): C395-403.
Sequeira-Lopez, M. L., E. T. Weatherford, et al. (2010). "The microRNA-processing enzyme dicer maintains juxtaglomerular cells." J Am Soc Nephrol **21**(3): 460-467.
Sequeira Lopez, M. L., E. S. Pentz, et al. (2004). "Renin cells are precursors for multiple cell types that switch to the renin phenotype when homeostasis is threatened." Dev Cell **6**(5): 719-728.
Serra, A. L., D. Poster, et al. (2010). "Sirolimus and kidney growth in autosomal dominant polycystic kidney disease." N Engl J Med **363**(9): 820-829.
Shiba, D., D. K. Manning, et al. (2010). "Inv acts as a molecular anchor for Nphp3 and Nek8 in the proximal segment of primary cilia." Cytoskeleton (Hoboken) **67**(2): 112-119.
Shiba, D., Y. Yamaoka, et al. (2009). "Localization of Inv in a distinctive intraciliary compartment requires the C-terminal ninein-homolog-containing region." J Cell Sci **122**(Pt 1): 44-54.
Shiba, D. and T. Yokoyama (2012). "The ciliary transitional zone and nephrocystins." Differentiation **83**(2): S91-96.
Shillingford, J. M., N. S. Murcia, et al. (2006). "The mTOR pathway is regulated by polycystin-1, and its inhibition reverses renal cystogenesis in polycystic kidney disease." Proc Natl Acad Sci U S A **103**(14): 5466-5471.

Sievers, F., A. Wilm, et al. (2011). "Fast, scalable generation of high-quality protein multiple sequence alignments using Clustal Omega." Mol Syst Biol **7**: 539.
Simms, R. J., L. Eley, et al. (2009). "Nephronophthisis." Eur J Hum Genet **17**(4): 406-416.
Simons, M., J. Gloy, et al. (2005). "Inversin, the gene product mutated in nephronophthisis type II, functions as a molecular switch between Wnt signaling pathways." Nat Genet **37**(5): 537-543.
Sims-Lucas, S., V. Di Giovanni, et al. (2012). "Ureteric morphogenesis requires Fgfr1 and Fgfr2/Frs2alpha signaling in the metanephric mesenchyme." J Am Soc Nephrol **23**(4): 607-617.
Sinha, S. and J. K. Chen (2006). "Purmorphamine activates the Hedgehog pathway by targeting Smoothened." Nat Chem Biol **2**(1): 29-30.
Smith, L. A., N. O. Bukanov, et al. (2006). "Development of polycystic kidney disease in juvenile cystic kidney mice: insights into pathogenesis, ciliary abnormalities, and common features with human disease." J Am Soc Nephrol **17**(10): 2821-2831.
Spektor, A., W. Y. Tsang, et al. (2007). "Cep97 and CP110 suppress a cilia assembly program." Cell **130**(4): 678-690.
Srour, M., F. F. Hamdan, et al. (2012). "Mutations in TMEM231 cause Joubert syndrome in French Canadians." J Med Genet **49**(10): 636-641.
Srour, M., J. Schwartzentruber, et al. (2012). "Mutations in C5ORF42 cause Joubert syndrome in the French Canadian population." Am J Hum Genet **90**(4): 693-700.
Stallone, G., B. Infante, et al. (2012). "Rapamycin for treatment of type I autosomal dominant polycystic kidney disease (RAPYD-study): a randomized, controlled study." Nephrol Dial Transplant **27**(9): 3560-3567.
Stockand, J. D. (2002). "New ideas about aldosterone signaling in epithelia." Am J Physiol Renal Physiol **282**(4): F559-576.
Stoos, B. A., A. Naray-Fejes-Toth, et al. (1991). "Characterization of a mouse cortical collecting duct cell line." Kidney Int **39**(6): 1168-1175.
Stottmann, R. W., P. V. Tran, et al. (2009). "Ttc21b is required to restrict sonic hedgehog activity in the developing mouse forebrain." Dev Biol **335**(1): 166-178.
Stow, L. R. and M. L. Gumz (2011). "The circadian clock in the kidney." J Am Soc Nephrol **22**(4): 598-604.
Strachan, T. (2004). Human Molecular Genetics 3, Garland Publishing.
Sugiyama, N., T. Tsukiyama, et al. (2011). "The canonical Wnt signaling pathway is not involved in renal cyst development in the kidneys of inv mutant mice." Kidney Int **79**(9): 957-965.
Surendran, K., S. Schiavi, et al. (2005). "Wnt-dependent beta-catenin signaling is activated after unilateral ureteral obstruction, and recombinant secreted frizzled-related protein 4 alters the progression of renal fibrosis." J Am Soc Nephrol **16**(8): 2373-2384.
Sweeney, W. E., Y. Chen, et al. (2000). "Treatment of polycystic kidney disease with a novel tyrosine kinase inhibitor." Kidney Int **57**(1): 33-40.
Sweeney, W. E., Jr. and E. D. Avner (2006). "Molecular and cellular pathophysiology of autosomal recessive polycystic kidney disease (ARPKD)." Cell Tissue Res **326**(3): 671-685.
Taal, M. W., G. M. Chertow, et al. (2011). Brenner and Rector's The Kidney Saunders.

Takeda, S., Y. Yonekawa, et al. (1999). "Left-right asymmetry and kinesin superfamily protein KIF3A: new insights in determination of laterality and mesoderm induction by kif3A-/- mice analysis." J Cell Biol **145**(4): 825-836.

Tallila, J., E. Jakkula, et al. (2008). "Identification of CC2D2A as a Meckel syndrome gene adds an important piece to the ciliopathy puzzle." Am J Hum Genet **82**(6): 1361-1367.

Tang, T., L. Li, et al. (2010). "A mouse knockout library for secreted and transmembrane proteins." Nat Biotechnol **28**(7): 749-755.

Tao, Y., J. Kim, et al. (2005). "Rapamycin markedly slows disease progression in a rat model of polycystic kidney disease." J Am Soc Nephrol **16**(1): 46-51.

Thomas, S., M. Legendre, et al. (2012). "TCTN3 mutations cause Mohr-Majewski syndrome." Am J Hum Genet **91**(2): 372-378.

Thomson, R. B., S. Mentone, et al. (2003). "Histopathological analysis of renal cystic epithelia in the Pkd2WS25/- mouse model of ADPKD." Am J Physiol Renal Physiol **285**(5): F870-880.

Torres, V. E. (2004). "Therapies to slow polycystic kidney disease." Nephron Exp Nephrol **98**(1): e1-7.

Torres, V. E., A. B. Chapman, et al. (2012). "Tolvaptan in patients with autosomal dominant polycystic kidney disease." N Engl J Med **367**(25): 2407-2418.

Torres, V. E. and P. C. Harris (2009). "Autosomal dominant polycystic kidney disease: the last 3 years." Kidney Int **76**(2): 149-168.

Torres, V. E., W. E. Sweeney, Jr., et al. (2003). "EGF receptor tyrosine kinase inhibition attenuates the development of PKD in Han:SPRD rats." Kidney Int **64**(5): 1573-1579.

Torres, V. E., X. Wang, et al. (2004). "Effective treatment of an orthologous model of autosomal dominant polycystic kidney disease." Nat Med **10**(4): 363-364.

Tory, K., C. Rousset-Rouviere, et al. (2009). "Mutations of NPHP2 and NPHP3 in infantile nephronophthisis." Kidney Int **75**(8): 839-847.

Tran, P. V., C. J. Haycraft, et al. (2008). "THM1 negatively modulates mouse sonic hedgehog signal transduction and affects retrograde intraflagellar transport in cilia." Nat Genet **40**(4): 403-410.

Travaglini, L., F. Brancati, et al. (2013). "Phenotypic spectrum and prevalence of INPP5E mutations in Joubert syndrome and related disorders." Eur J Hum Genet.

Trupp, M., E. Arenas, et al. (1996). "Functional receptor for GDNF encoded by the c-ret proto-oncogene." Nature **381**(6585): 785-789.

Tsang, W. Y., C. Bossard, et al. (2008). "CP110 suppresses primary cilia formation through its interaction with CEP290, a protein deficient in human ciliary disease." Dev Cell **15**(2): 187-197.

Tsang, W. Y., A. Spektor, et al. (2009). "Cep76, a centrosomal protein that specifically restrains centriole reduplication." Dev Cell **16**(5): 649-660.

Utsch, B., J. A. Sayer, et al. (2006). "Identification of the first AHI1 gene mutations in nephronophthisis-associated Joubert syndrome." Pediatr Nephrol **21**(1): 32-35.

Valente, E. M., F. Brancati, et al. (2013). "Clinical utility gene card for: Joubert syndrome - update 2013." Eur J Hum Genet.

Valente, E. M., C. V. Logan, et al. (2010). "Mutations in TMEM216 perturb ciliogenesis and cause Joubert, Meckel and related syndromes." Nat Genet **42**(7): 619-625.
Valente, E. M., D. C. Salpietro, et al. (2003). "Description, nomenclature, and mapping of a novel cerebello-renal syndrome with the molar tooth malformation." Am J Hum Genet **73**(3): 663-670.
Valente, E. M., J. L. Silhavy, et al. (2006). "Mutations in CEP290, which encodes a centrosomal protein, cause pleiotropic forms of Joubert syndrome." Nat Genet **38**(6): 623-625.
Vega, Q. C., C. A. Worby, et al. (1996). "Glial cell line-derived neurotrophic factor activates the receptor tyrosine kinase RET and promotes kidney morphogenesis." Proc Natl Acad Sci U S A **93**(20): 10657-10661.
Veland, I. R., R. Montjean, et al. (2013). "Inversin/Nephrocystin-2 is required for fibroblast polarity and directional cell migration." PLoS One **8**(4): e60193.
Vierkotten, J., R. Dildrop, et al. (2007). "Ftm is a novel basal body protein of cilia involved in Shh signalling." Development **134**(14): 2569-2577.
Wahl, P. R., A. L. Serra, et al. (2006). "Inhibition of mTOR with sirolimus slows disease progression in Han:SPRD rats with autosomal dominant polycystic kidney disease (ADPKD)." Nephrol Dial Transplant **21**(3): 598-604.
Waldherr, R., T. Lennert, et al. (1982). "The nephronophthisis complex. A clinicopathologic study in children." Virchows Arch A Pathol Anat Histol **394**(3): 235-254.
Wall, S. M., Y. H. Kim, et al. (2004). "NaCl restriction upregulates renal Slc26a4 through subcellular redistribution: role in Cl- conservation." Hypertension **44**(6): 982-987.
Wallach, D., M. Fellous, et al. (1982). "Preferential effect of gamma interferon on the synthesis of HLA antigens and their mRNAs in human cells." Nature **299**(5886): 833-836.
Walz, G., K. Budde, et al. (2010). "Everolimus in patients with autosomal dominant polycystic kidney disease." N Engl J Med **363**(9): 830-840.
Wang, B. and Y. Li (2006). "Evidence for the direct involvement of {beta}TrCP in Gli3 protein processing." Proc Natl Acad Sci U S A **103**(1): 33-38.
Wang, C. J., C. Creed, et al. (2011). "Water prescription in autosomal dominant polycystic kidney disease: a pilot study." Clin J Am Soc Nephrol **6**(1): 192-197.
Wang, X., V. Gattone, 2nd, et al. (2005). "Effectiveness of vasopressin V2 receptor antagonists OPC-31260 and OPC-41061 on polycystic kidney disease development in the PCK rat." J Am Soc Nephrol **16**(4): 846-851.
Ward, C. J., M. C. Hogan, et al. (2002). "The gene mutated in autosomal recessive polycystic kidney disease encodes a large, receptor-like protein." Nat Genet **30**(3): 259-269.
Watanabe, M., T. Muramatsu, et al. (1981). "Discrete Distribution of binding sites for Dolichos biflorus agglutinin (DBA) and for peanut agglutinin (PNA) in mouse organ tissues." J Histochem Cytochem **29**(7): 779-780.
White, M., G. Xia, et al. (2012). "Transgenic mice with SCA10 pentanucleotide repeats show motor phenotype and susceptibility to seizure: a toxic RNA gain-of-function model." J Neurosci Res **90**(3): 706-714.
Wilson, P. D. (1997). "Epithelial cell polarity and disease." Am J Physiol **272**(4 Pt 2): F434-442.

Winkelbauer, M. E., J. C. Schafer, et al. (2005). "The C. elegans homologs of nephrocystin-1 and nephrocystin-4 are cilia transition zone proteins involved in chemosensory perception." J Cell Sci **118**(Pt 23): 5575-5587.

Winyard, P. and D. Jenkins (2011). "Putative roles of cilia in polycystic kidney disease." Biochim Biophys Acta **1812**(10): 1256-1262.

Wolf, M. T. and F. Hildebrandt (2011). "Nephronophthisis." Pediatr Nephrol **26**(2): 181-194.

Wolf, M. T., S. Saunier, et al. (2007). "Mutational analysis of the RPGRIP1L gene in patients with Joubert syndrome and nephronophthisis." Kidney Int **72**(12): 1520-1526.

Won, J., C. Marin de Evsikova, et al. (2011). "NPHP4 is necessary for normal photoreceptor ribbon synapse maintenance and outer segment formation, and for sperm development." Hum Mol Genet **20**(3): 482-496.

Woo, D. D., D. K. Nguyen, et al. (1997). "Genetic identification of two major modifier loci of polycystic kidney disease progression in pcy mice." J Clin Invest **100**(8): 1934-1940.

Wu, M., P. R. Wahl, et al. (2007). "Everolimus retards cyst growth and preserves kidney function in a rodent model for polycystic kidney disease." Kidney Blood Press Res **30**(4): 253-259.

Wu, X., J. Walker, et al. (2004). "Purmorphamine induces osteogenesis by activation of the hedgehog signaling pathway." Chem Biol **11**(9): 1229-1238.

Yang, B., A. Hodgkinson, et al. (2010). "Polymorphisms of myo-inositol oxygenase gene are associated with Type 1 diabetes mellitus." J Diabetes Complications **24**(6): 404-408.

Ye, P., S. L. Habib, et al. (2004). "Fibronectin induces ureteric bud cells branching and cellular cord and tubule formation." Kidney Int **66**(4): 1356-1364.

Yoshihara, D., M. Kugita, et al. (2012). "Global Gene Expression Profiling in PPAR-gamma Agonist-Treated Kidneys in an Orthologous Rat Model of Human Autosomal Recessive Polycystic Kidney Disease." PPAR Res **2012**: 695898.

Yoshihara, D., H. Kurahashi, et al. (2011). "PPAR-gamma agonist ameliorates kidney and liver disease in an orthologous rat model of human autosomal recessive polycystic kidney disease." Am J Physiol Renal Physiol **300**(2): F465-474.

Yoshimura, S., J. Egerer, et al. (2007). "Functional dissection of Rab GTPases involved in primary cilium formation." J Cell Biol **178**(3): 363-369.

Zaika, O., M. Mamenko, et al. (2013). "Direct activation of ENaC by angiotensin II: recent advances and new insights." Curr Hypertens Rep **15**(1): 17-24.

Zerres, K., G. Mucher, et al. (1994). "Mapping of the gene for autosomal recessive polycystic kidney disease (ARPKD) to chromosome 6p21-cen." Nat Genet **7**(3): 429-432.

Zhang, X. Y., X. Dong, et al. (2003). "Specific tissue expression and cellular localization of human apolipoprotein M as determined by in situ hybridization." Acta Histochem **105**(1): 67-72.

Zhang, X. Y., G. Q. Jiao, et al. (2004). "Expression pattern of apolipoprotein M during mouse and human embryogenesis." Acta Histochem **106**(2): 123-128.

Zhang, Y., S. Seo, et al. (2013). "BBS mutations modify phenotypic expression of CEP290-related ciliopathies." Hum Mol Genet.

Zheleznova, N. N., P. D. Wilson, et al. (2011). "Epidermal growth factor-mediated proliferation and sodium transport in normal and PKD epithelial cells." Biochim Biophys Acta **1812**(10): 1301-1313.

Zivna, M., H. Hulkova, et al. (2009). "Dominant renin gene mutations associated with early-onset hyperuricemia, anemia, and chronic kidney failure." Am J Hum Genet **85**(2): 204-213.

Zollinger, H. U., M. J. Mihatsch, et al. (1980). "Nephronophthisis (medullary cystic disease of the kidney). A study using electron microscopy, immunofluorescence, and a review of the morphological findings." Helv Paediatr Acta **35**(6): 509-530.